Corrosion Chemistry

George R. Brubaker, EDITOR
Illinois Institute of Technology

P. Beverley P. Phipps, EDITOR
IBM Corporation

Based on a 1976 lecture series sponsored by the Chicago Sections of the American Chemical Society and the Electrochemical Society.

ACS SYMPOSIUM SERIES 89

AMERICAN CHEMICAL SOCIETY
WASHINGTON, D. C. 1979

Library of Congress CIP Data

Corrosion chemistry.
(ACS symposium series; 89) ISSN 0087-6156

Includes bibliographical references and index.

1. Corrosion and anti-corrosives—Addresses, essays, lectures.
I. Brubaker, George R., 1939– . II. Phipps, Peter Beverley, 1936– . III. American Chemical Society, Chicago Section. IV. Electrochemical Society. Chicago Section. V. Series.

TA418.74.C595 620.1'6'23 78-25554
ISBN 0-8412-0471-3 ASCMC 8 89 1-424 1979

PRINTED IN THE UNITED STATES OF AMERICA

ACS Symposium Series

Robert F. Gould, *Editor*

Advisory Board

In Corrosion Chemistry; Brubaker, G., et al.;
ACS Symposium Series; American Chemical Society: Washington, DC, 1979.

FOREWORD

The ACS SYMPOSIUM SERIES was founded in 1974 to provide a medium for publishing symposia quickly in book form. The format of the SERIES parallels that of the continuing ADVANCES IN CHEMISTRY SERIES except that in order to save time the papers are not typeset but are reproduced as they are submitted by the authors in camera-ready form. As a further means of saving time, the papers are not edited or reviewed except by the symposium chairman, who becomes editor of the book. Papers published in the ACS SYMPOSIUM SERIES are original contributions not published elsewhere in whole or major part and include reports of research as well as reviews since symposia may embrace both types of presentation.

PREFACE

This volume records the proceedings of a twelve lecture short course jointly sponsored by the Chicago Sections of the American Chemical Society and the Electrochemical Society. The lectures covered several aspects of current work in corrosion; they were addressed to physical chemists and chemical engineers as well as to corrosion specialists and surface scientists. Readers from each of these disciplines will find several parts of the work described here challenging and informative.

The study of corrosion has undergone substantial expansion in the past decade in response to new techniques of study and to demands for new materials to withstand hostile environments. New techniques include expanded applications of electrochemistry, and recently developed methods for more-or-less routine surface analysis. Examples in which consideration of corrosion has had a major impact on the development of new materials include high temperature turbines, airframe structures, electronic applications of thin metal films, and energy development programs such as coal gasification. This volume contains chapters related to applications and reviews of fundamental research. The impact of new electrochemical and surface characterization methodology is seen throughout the text. Sections on electrochemistry and high temperature corrosion will introduce those unfamiliar with these areas to new concepts. This volume clearly illustrates the empirical foundations of corrosion chemistry, yet applications of solid state theory—to ionic and electronic conduction in solids, for example—emerge in several chapters.

The editors thank the author of each chapter for his or her work, which in many cases involved substantial rewriting of the oral presentation; Rudolph H. Hausler for organizing the lecture series; Ms. Dorothy Huber for taped transcripts of the proceedings; the staff of the Chicago Section for management of the lecture series; and the institutions for which we work for allowing us the opportunity to bring this volume together.

Illinois Institute of Technology
Chicago, Illinois

GEORGE BRUBAKER

IBM Corporation
San Jose, California

BEVERLEY PHIPPS

September, 1978

Corrosion: The Most General Problem of Materials Science

DONALD TUOMI

Solid State Physics, Roy C. Ingersoll Research Center, Borg-Warner Corp., Des Plaines, IL 60016

The following chapters systematically address varied aspects of the field known as corrosion.[1] In this introductory overview, an effort will be made to touch only lightly the breadth and depth of corrosion - the most general problem of materials science.

For the first step to developing an overview, a meaning to the word corrosion needs expression. To my wife, corrosion means that there is a dirty brown splotch on the side of the car which means it is worn out and time to trade in is here. They don't make them as well as before! This brings our attention to the classic meaning of corrosion as being a loss in value for some solid object which has been suffering from chemical attack at the surface. I suspect that for many this feeling of decreased value through corrosion leads to a negative feeling towards the topic. Corrosion, in general, is used to describe degradation in value of useful objects.

An alternative perspective is present in corrosion engineer anecdotes. "Nope, we don't have any corrosion problems in this plant. The pumps wear out every six weeks and we replace them." Or alternatively, "We just dump the scrap here and as soon as we can fill a railroad car we haul it to a hole a hundred miles away and bury it. Some day when the corrosion finishes the junk off, we'll build condominiums on the land." Or yet another one - "Hey, would you believe that with six months' data they want me to warrant that tank for 50 years of radioactive waste storage?" Yes, these do represent some famous last words. Enough for the anecdotal description; we are not gathered here to be entertained.

Corrosion is a serious, costly materials science problem. In the years ahead as our resources are increasingly utilized to the limits of practicality,

0-8412-0471-3/79/47-089-001$08.50/0

and conservation and recycling are watchwords, not catchwords; the corrosion engineer will be at the forefront.

May I emphasize again the title, "Corrosion: The Most General Problem of Materials Science." So many I encounter speak in a disparaging voice about corrosion problems - that it's just a black art - without supportive science. Just go in there and do your thing - don't bother me with the facts. As a matter of fact, however, there is so much science in this show that a constipation of words readily sets in before the constipation of ideas is even approached.

For the next 90 minutes or so let us explore this field - CORROSION. We shall travel in two distinct ways. One is to bring your attention to arrays of key words and concepts. The other is to formulate a pattern of solid state surface structural chemistry which may be useful as a framework for remembering complex options and for exploring new options. The latter will be within two areas: (1) exchange current descriptions of corrosion potentials and (2) the nature of corroding surfaces.

The empiricism that appears to follow the corrosion engineer arises from the multi-factor, multi-component situations which are present within all common articles of commerce, be they made from iron, aluminum, or more exotic material combinations. The variables are continually interacting in increasingly complex ways so we can become engrossed for even a lifetime with just one problem in performance such as airfoil stress corrosion cracking, boiler feed water stabilizations, or corrosion inhibiting paints, and many more. But does this mean the work lacks for glamour and excitement?

Well, the materials engineer is frequently caught with orders to select materials combinations in a practical situation giving desired property balances with adequate performance designed to first or to life costs. Alternatively, he selects model Mark II materials to cover model Mark I mistakes. More important today, material selections must avoid warranty payouts capable of corporate bankruptcy as well as extended personal liability. How indeed are R & D data predicting field reliability? What is a valid test?

The corrosion engineer is frequently the pragmatist - so what is the problem - get rid of the offending material. Another approach is "Hey, what can we add to, introduce to, or otherwise coat the system with so the problem will disappear long enough to keep the customers adequately happy? Or at least not

In Corrosion Chemistry; Brubaker, G., et al.;
ACS Symposium Series; American Chemical Society: Washington, DC, 1979.

seriously disappointed in the value received? We can't sell many gold-plated Cadillacs." Or the customer asks how can I cheaply save money in the long run without paying the factory? Ziebart it!

Well, enough commercials - who is this corrosion engineer and what is he like? How many years has he spent in the ivory towers? Or has he ever visited them?

Well, if I had my druthers, I would see to it that the corrosion engineer had a bit of flavoring from materials science as shown in Figure 1. In these days of specialization, it would be nice to train some generalists. As an expert responsible for the future behaviors of most of our solid materials, surely a mastery of the full range covered by chemistry, physics metallurgy, and just a few other incidental fields would be consistent with assigned responsibilities. If he feels a bit short, clearly recourse will be taken to the consultants and the colleagues forming his supportive technical society.

What, you think the survey is facetious and out of place? Let's take a look at a corrosion smörgåsbord of terminology in Figure 2. The experiences of a corrosion engineer are represented by the term array. Sampling them at random, it seems to be a jumble. However, it is an overview.

Who, then, is the corrosion engineer? For many here, he has an exciting, responsible way of doing complex materials science in service to our society. This individual may never have deliberately planned the career which developed. Rather as a civil engineer, a mechanical engineer, a chemist, a physicist, an analyst, one day suddenly he has a responsibility thrust on him relating to materials reliability, to materials performance or just to solve that problem before we are broke.

Thus, many routes lead to a corrosion engineer's responsibility as is reflected in Figure 3. He contributes to A Priori Problem Solving but economics of first costs frequently lead to Post-Factum Problem Solving. For, too often, corrosion is tied directly to systems' weakest link variables. Much of the needed knowledge is absorbed almost by an osmosis process because there just aren't simple valid descriptions of general use. All quickly become specific.

Ladies and gentlemen - if you were to examine the agenda for the next few weeks, quickly a recognition would develop that the key-words have touched on the program exposures each will experience - can you see the beauty of the toughest materials science problems emerging through the program?

In Corrosion Chemistry; Brubaker, G., et al.;
ACS Symposium Series; American Chemical Society: Washington, DC, 1979.

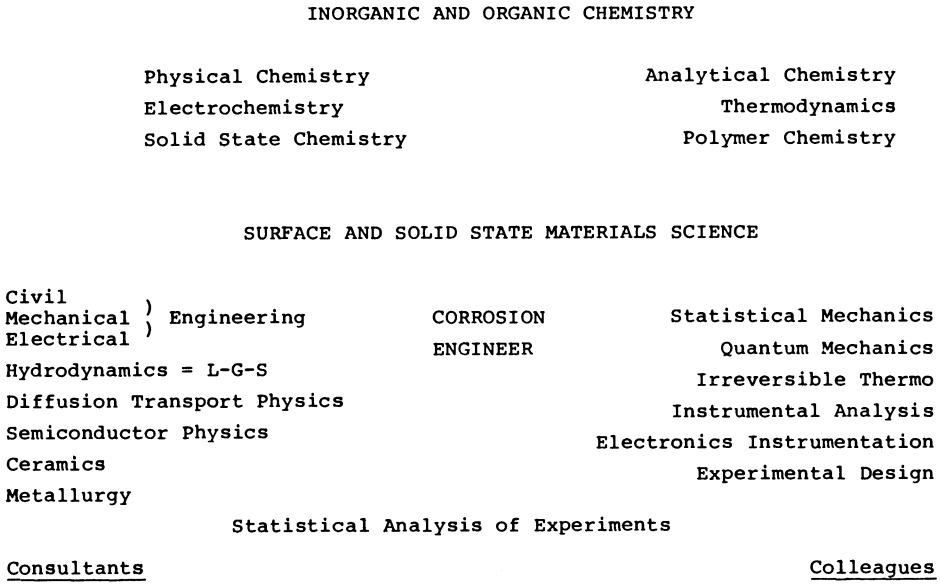

Figure 1. Corrosion engineer

In Corrosion Chemistry; Brubaker, G., et al.;
ACS Symposium Series; American Chemical Society: Washington, DC, 1979.

Figure 2. Corrosion term smorgasbord

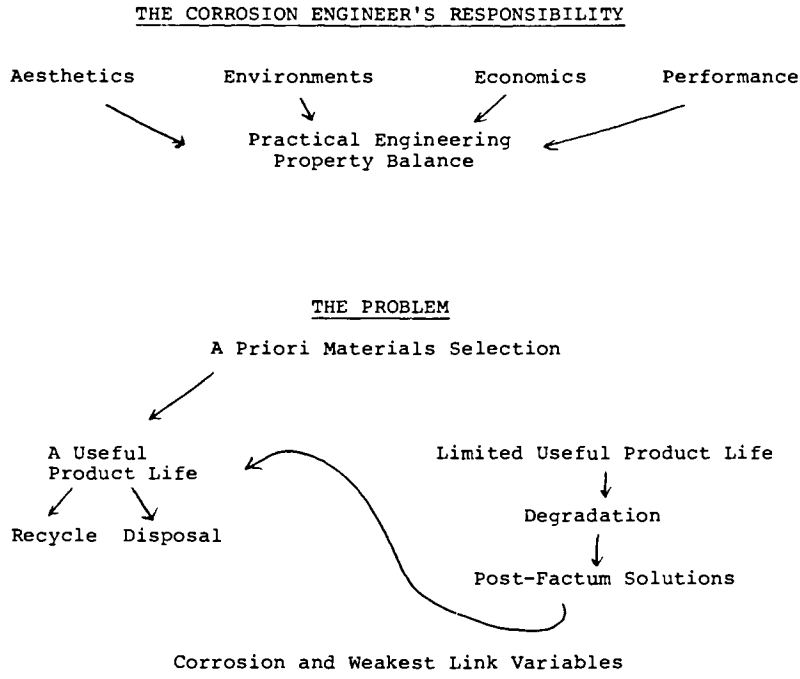

Figure 3. Corrosion engineer's responsibility

Let us look at another pair of smörgåsbord figures on corrosion. The first, Figure 4, focusses largely on surface phenomena from a physical chemist - electrochemist or surface chemist context. Do the words have a familiar meaning? Should I define a few or perhaps we should look at another, Figure 5, which outlines another set of, probably less familiar to most, key words. These are related to the description of solid state structures which are encountered on the solid side of the electrical double layer. It is the disturbing phenomena proceeding within the solid surface side that gives rise to the diverse experiences of the corrosion engineer.

For an overview we clearly could spend much time on each word, learning what meaning was experienced by each of us. Each would be surprised what a range could be revealed by the dialogue. This is why so much of the management end of the talent spectrum is inclined to say, please practice your art without fully recognizing or experiencing the complex beauty present. For it is only art to the beholder - let us continue sketching the canvas.

Did you ever stop to contrast the conceptualization of chemists' common models, or for that matter, most descriptions of solid material behaviors? In Figure 6 we are examining the phenomenological situation over which we spend so much time puzzling. The mental images usually do not assign detailed structure to the solid phase. We can clearly see it before us - it is so obvious.

The model we are usually speaking about is shown in the lower left corner - a structureless solid behaving in an environment of liquid, or gas, more rarely an imperfect, impure vacuum. The latter environment has the spatial extent.

More truly as in the lower right corner the solid is defined by x-y-z coordinates which define what is actually happening where as a function of time in an experiment.

Still more precisely, the solid in the experiment is being space averaged to produce the data in the figures above.

The solid is best described generally for the corrosion engineer's purposes as a

> "polyphase inhomogeneous solid containing heterogeneity homogeneously dispersed."

The description is rather precise according to Webster's Unabridged Dictionary. This reference can be cited if the statement requires substantiation.

Goodness, with this complexity where do we go from

Figure 4. Corrosion smorgasbord (continued)

In Corrosion Chemistry; Brubaker, G., et al.;
ACS Symposium Series; American Chemical Society: Washington, DC, 1979.

Figure 5. Corrosion smorgasbord (continued)

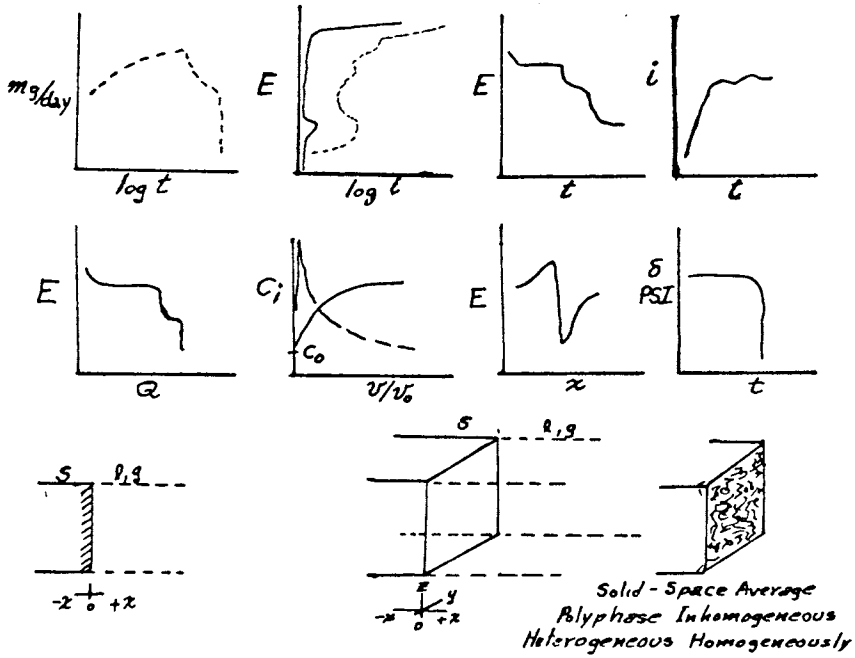

Figure 6. Phenomenological view of a one-dimensional solid contrasts with the three-dimensional reality of most solid systems.

here? Well, let's just acknowledge that this has always been the stage on which most of us are acting out our professional lives.

Thus, in Figure 7, Solids are described as being ideally perfect versus ideally imperfect with most being in the latter category. A sharp consequence was taught to me many years ago by Leroy Dunham of the Edison Primary Battery. When I smartly described a statistical quantum-mechanics model of charge transfer catalysis of oxygen reduction on an electrode surface, he smiled as if he was enjoying himself. He had been forced to leave school at the eighth grade level.

Later in the day as he and I strolled through the production plant making his electrodes, he quietly said, "Don, I enjoyed your comments so very much. Back in the '30's when I was doing the development work many confusing results came from experiments. In the evenings I have enjoyed reading the Encyclopedia Britannica. One day it dawned on me that the distribution of people in the United States versus other areas resembled the charge transfer behavior. To change things the people must move around, get into and out of cars, trains, planes.

What a memorable moment - the theory did not have to be absolutely right to be useful in guiding experiments.

Why have I taken such a circumspect path to reach this point? Well, I wish to present a conceptualization of the problems which has been useful to me. It has helped to bridge the chasm separating different experimental situations.

The following Figure 8 indicates that the lectures could be placed in a variety of categories. First, the familiar metal-electrolyte system with gas evolution potentially present. Second, the systems involving metals separated from the liquid by a covering film structure, and third the metal separated from a gas by an intermediate phase layer. There is some ambiguity evident in this description; however, in the next few minutes perhaps some new perspectives for thought organization can emerge.

In a more general sense surface corrosion processes can be described in terms of the phases present as shown in Figure 9. Here the solid is not identified simply as a metal but a more general term S is being used with L representing liquid phase and G gas phase. The systems locally present can be represented by the notations S-L, S-L-G, S-G or, if a covering chemically altered layer exists on the surface, then S_1-S_2 is present with S_1 the starting material.

In Corrosion Chemistry; Brubaker, G., et al.;
ACS Symposium Series; American Chemical Society: Washington, DC, 1979.

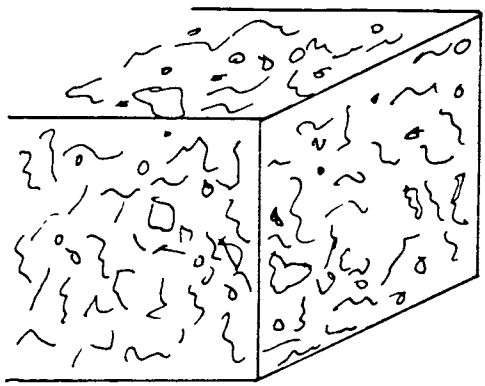

Solids

Ideally Perfect Reality → Ideally Imperfect

THEORY:

if it leads to experiments
does not need to be

RIGHT

to be very valuable.

Figure 7. Modeling

In Corrosion Chemistry; Brubaker, G., et al.;
ACS Symposium Series; American Chemical Society: Washington, DC, 1979.

Metal-Electrolyte-Gas

Corrosion Electrochemistry
Iron Dissolution Mechanisms
Corrosion Inhibition and Inhibitors
Stress Corrosion Cracking

Metal-Solid-Liquid

Solid Electrolyte-Ionic Electronic Transport
Iron Passivation
Valve Metals Dielectric Layers
Industrial Problem: Cooling Waters and Treatments

LECTURE SERIES

CORROSION

Metal-Solid-Gas

High-Temperature Corrosion
Low-Temperature Atmospheric Corrosion
Corrosion Phenomena Novel Energy Conversion Processes
Iron Passivation

Figure 8. Corrosion lecture classifications

In Corrosion Chemistry; Brubaker, G., et al.;
ACS Symposium Series; American Chemical Society: Washington, DC, 1979.

The perspective of simple phases and phase equilibria is adequate for many corrosion problems. This is particularly true for the cases where thermodynamic free energy data really describe what phases are present.

Let us examine this for a few minutes from the viewpoint of everyday experience. We will utilize the key device which was responsible for our arrival at the lecture - the black box called

THE LEAD-ACID STORAGE BATTERY.

This system permits brief descriptions of some key concepts encountered in corrosion phenomena: electrode potentials, exchange currents, mixed potentials, corrosion potentials, passive films, as well as leading to thermodynamic descriptions of systems.[2]

The redox systems of the battery are simply presented as:

Negative:

$$Pb_{(s)} + SO_4^{=} \underset{\text{Cathodic}}{\overset{\text{Anodic}}{\rightleftharpoons}} PbSO_{4(s)} + 2e \qquad +0.335$$

Positive:

$$PbO_{2(s)} + 4H^{+} + SO_4^{=} + 2e \underset{\text{Anodic}}{\overset{\text{Cathodic}}{\rightleftharpoons}} PbSO_4 + 2H_2O \qquad +1.685$$

$$Pb_{(s)} + PbO_{2(s)} + 2H_2SO_4 \rightleftharpoons PbSO_{4(s)} + 2H_2O \qquad \sim 2\ v$$

At the negative lead is oxidized to lead sulfate during discharge while at the positive lead dioxide is reduced to lead sulfate. The functioning of the battery for many cycles depends upon maintaining the reactions isolated to their respective electrodes, to having the electrons flowing through an external circuit, and only ionic currents flowing in the internal electrolyte circuit.

If the potential-current (E-i) characteristics of the individual reactions were measured, the reactions could be readily modeled as electrochemical reactions with the battery at open circuit as indicated by the processes in Figure 10. If dynamic electrode potential-current relationships were determined, the electrode is expected to show the classic Tafel slope behaviors as the exchange current of the anodic-cathodic equilibrium is shifted into either direction. From the Tafel curves a value for the E_o and i_o of the electrode could be defined.

In Corrosion Chemistry; Brubaker, G., et al.;
ACS Symposium Series; American Chemical Society: Washington, DC, 1979.

LOCAL REGION SOLID SURFACE TRANSFORMATIONS

Solid-Liquid S-L	Solid-Liquid-Gas S-L-G	Solid Gas SG
Solid 1-Solid 2-L	Solid 1-Solid 2-L-G	Solid 1-Solid 2-G
S_1- S_2- L	S_1- S_2- L - G	S_1- S_2- G

Figure 9. Corrosion system

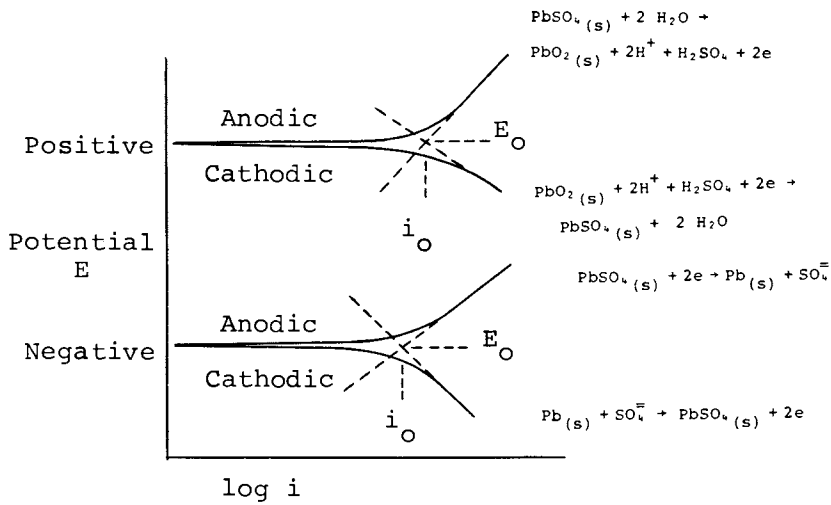

Figure 10. Model battery anodic–cathodic reactions

In Corrosion Chemistry; Brubaker, G., et al.;
ACS Symposium Series; American Chemical Society: Washington, DC, 1979.

If the two electrodes are short-circuited together, the cathodic process of the positive combines with the anodic process of the negative as shown in Figure 11. The battery now has a singular potential - the short circuited potential. This clearly is a mixed potential or could be viewed as a corrosion potential of the system.

Looking at Figure 12, a sketch of a single cell shows that the positive is a paste of PbO_2 in a lead grid. This electrode in the electrolyte clearly must have a mixed potential since metallic lead in the presence of lead dioxide and sulfuric acid is thermodynamically unstable. At the negative the lead grid contains pasted lead! This is also unstable with respect to charging the battery. Both electrodes represent a corrosion control problem!

Really, this is a little too simple, because if the electrodes are fully charged, the voltage may be increased so oxygen and hydrogen are evolved at the positive and negative, respectively. This is indicated by the potential-log current lines in Figure 13. These reactions convert the battery into a potential explosive by the H_2-O_2 recombination to form water if a match is used to aid in seeing how much water needs to be added. If the O_2 reduction could be made to proceed on the negative surface as a local corrosion current, and if the H_2 could be made to undergo oxidation on the positive surface, a hermetically sealed cell could be made. These electrochemical reactions, however, represent forms of local cell reactions familiar to corroding systems.

As any of these reactions proceed at the electrode surface, the surface chemistry is continuously changing. The composition of the local electrolyte in contact with the solids is changing. Thus, the simple chemistry implied by the reaction

$$Pb + PbO_2 + 2\ H_2SO_4 \rightarrow PbSO_4 + 2\ H_4O$$

really does not exist. There are numerous changes of a complex form proceeding on the metal surfaces, on the metallic heavily-doped oxide PbO_2, on the $PbSO_4$ crystallites, on the Pb particulates in the negative grid, as well as in systems of grain boundaries which are present.

Suddenly, as we peer beyond the casual solution chemistry equation, rather complex solid state chemistry is interacting with solution and gas phases processes.

In Corrosion Chemistry; Brubaker, G., et al.;
ACS Symposium Series; American Chemical Society: Washington, DC, 1979.

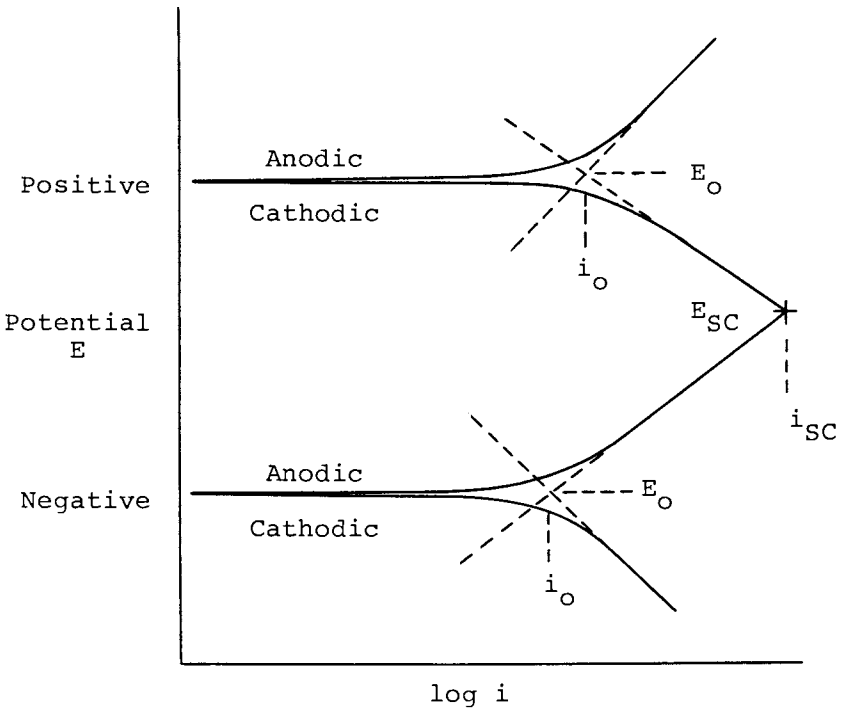

Figure 11. Short circuit of battery terminals creates characteristic short circuit potential (E_{sc}) and short circuit current (i_{sc}).

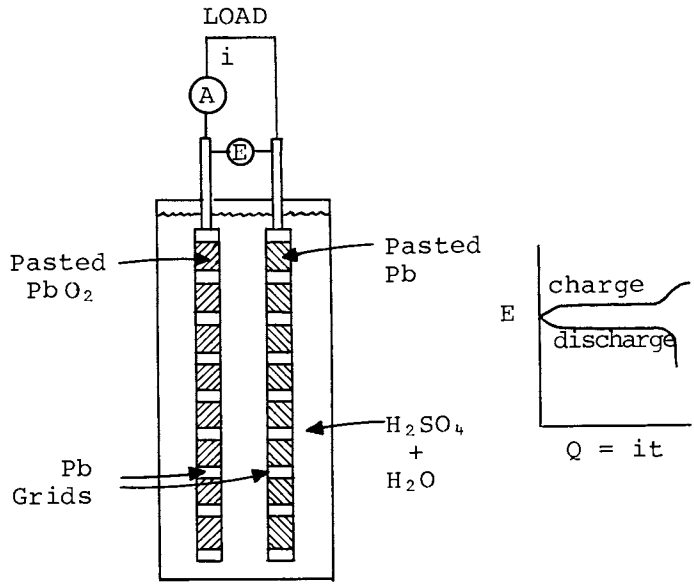

Figure 12. Simple cell in a lead–acid battery

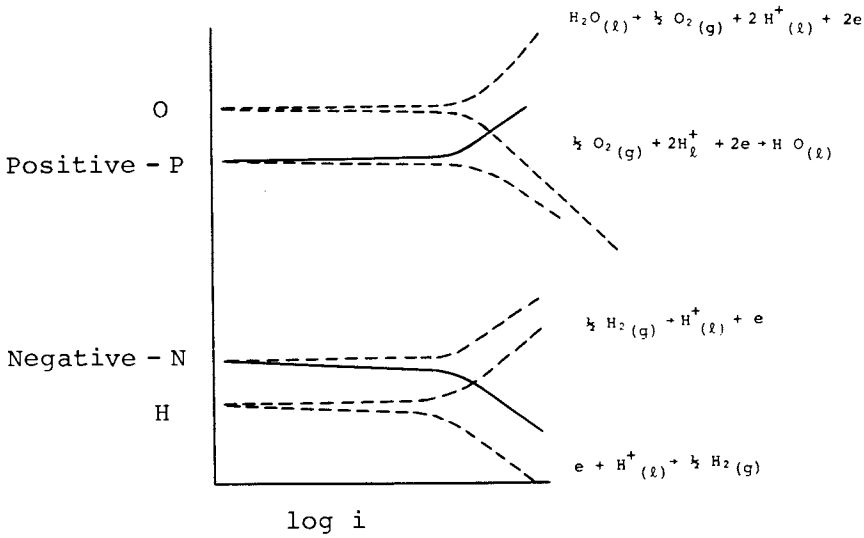

Figure 13. Hydrogen and oxygen evolution reactions at the battery electrode

In Corrosion Chemistry; Brubaker, G., et al.;
ACS Symposium Series; American Chemical Society: Washington, DC, 1979.

Clearly the system has electrochemical-chemical exchange currents at the positives and negatives which define the potentials observed. The metal grid must show combinations of $PbSO_4$ film, PbO_2 film, as well as hydride film phenomena. Isn't corrosion chemistry exciting in that black box under the hood?

The battery electrode mixed potential brings attention to the corrosion engineer's problem of controlling either the cathodic or anodic process to minimize the corrosion current. The problems of surface passivation, the question of identifying the distinctive spatial locations of the reaction processes are frequently present in practical situations - what is cathodic to an anodic region or vice versa, what are useful ways to modify the surface processes?

Thus, when attention is given to detail, what appeared as a simple problem initially has with a little thought become complex.

For a few moments let's drop the key words and turn to creating a skeleton for the corrosion engineer's interphase transport processes. We need all the tools possible to bring the materials science resources to our aid. How can we express questions so aid can come from other experts?

Part II

This phase of the discussion is concerned with concepts of solid state chemistry rather than a detailed analysis of a particular case. The objective is to bring attention to a variety of surface chemistry perspectives. This variety can be helpful because the number of ways we can scavenge information from related materials science areas becomes expanded. Further, a variety of seemingly unconnected phenomena can be brought into related ballgames. The multidisciplinary character of real material science is its real richness.

Earlier attention was brought to the corrosion processes of liquid-solid systems. Let's start with a metal contacting an electrolyte as do all electrochemistry texts.

The simplest model of the electrical double layer between a metal and an electrolyte is the simple capacitor visualized by Helmholtz[3] as shown in Figure 14. The diffuse ion distribution in the liquid phase was recognized by Gouy and Chapman[4,5] to form a space charge region adjacent to the electrode surface.

Stern[6] in 1924 combined the structures to form a compact double layer at the electrode surface with a

In Corrosion Chemistry; Brubaker, G., et al.;
ACS Symposium Series; American Chemical Society: Washington, DC, 1979.

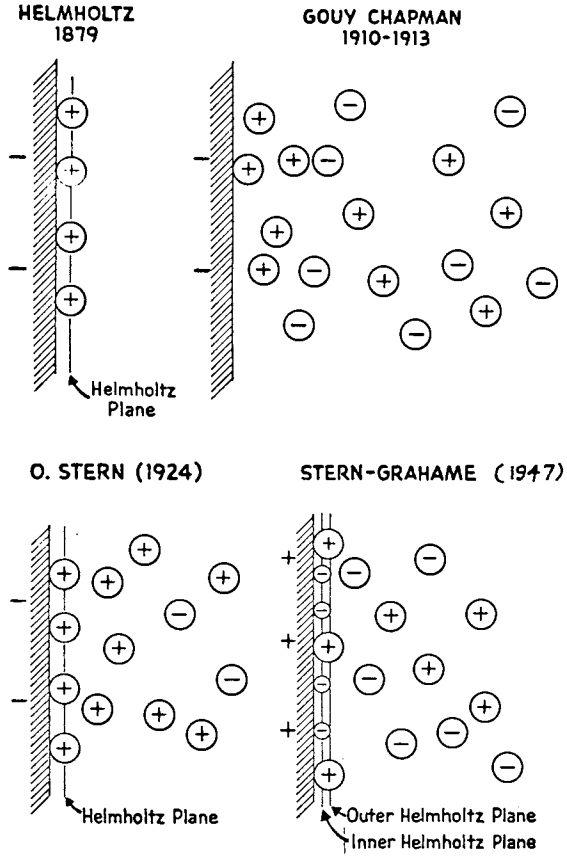

Figure 14. Models for the electrical double layer at a metal surface

diffuse space charge. In 1947 David Grahame[7] added to this the specific adsorption of ions forming an inner and outer Helmholtz plane with hydrated cations not approaching as closely as the anions at the ideal metal substrate surface. In this ideal polarizable electrode model perspective, no charge transfer occurs between metal and liquid phase - i.e., no Faradaic processes are present. It is important to visualize this surface region as formed of atoms, molecules, and ions having significant thermal vibrational, rotational and translational energy. The sketched structures are for only a moment in time but are averaging over space adjacent to the electrode surface when measurements are being made.

A subsequent description by Bockris and associates[8] drew attention to further complexities as shown in Figure 15. The metal surface now is covered by combinations of oriented structured water dipoles, specifically adsorbed anions, followed by secondary water dipoles along with the hydrated cation structures. This model serves to bring attention to the dynamic situation in which changes in potential involve sequential as well as simultaneous responses of molecular and atomic systems at and near an electrode surface. Changes in potential distribution involve interactions extending from atom polarizability, through dipole orientation, to ion movements. The electrical field effects are complex in this ideal polarized electrode model.

The models clearly have not assigned any atomic structure to the metal side. With a metallic substrate Rice, in 1928,[9] showed the electric field penetration was indeed slight. Consequently, this model was adequate for the ideal polarizable electrode without Faradaic charge transfer.

A further complication is introduced in Figure 16 where the presence of surface adatoms is indicated as well as metal lattice vacancies in the substrate surface. Within the system attention now can be drawn to Faradaic processes involving the substrate structure. The transfer of an atom to the surface can be expressed by the equation

$$M/\square_M + \square_S \rightleftarrows M / \square_S + \square_M$$

where $M/\square_S$, the surface adatom, is further potentially involved in the exchange process

$$M/\square_S + n\ H_2O \rightarrow M^+ (H_2O)_n + e + \square_S$$

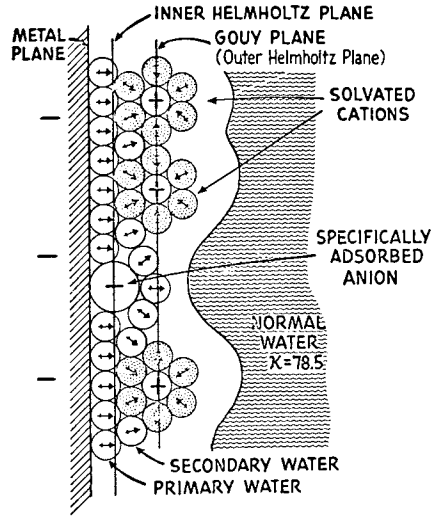

Proceedings of the Royal Society of London

Figure 15. Structures of the electrical double layer, ideal polarizable electrode (8)

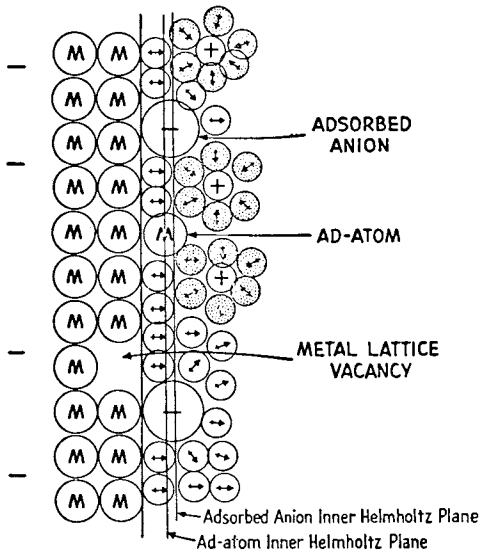

Figure 16. Electrical double layer with structure introduced on the metal side

This suggests that attention needs to be given to interphase exchange currents which involve not only electron transfer from the metal surface, but may involve atom exchanges from the bulk to the surface region. The plane metal surface associated with studying the model ideal polarized electrode behavior now becomes part of an interphase system separating metal from an electrolyte or a gas phase system.

The evolution of semiconductor electronics depended upon developing a detailed materials science, first for germanium and then for silicon. This confronted the electrochemist with a further refinement of the electrical double layer systems model. At the surface of a silicon semiconductor crystal the electronic process now is no longer simply an electron transfer from a metal but involves two distinct reactants, electrons or holes. Thus, the following two reactions are not equivalent at the surface of a semiconductor, S:[10]

$$S + OH^- \rightarrow SOH + e$$

$$S + OH^- + p \rightarrow SOH$$

A further complication arises when attention is focussed on the electron density distribution within the semiconductor solid. This, in contrast to the metal case, now is able to vary from a low to a high concentration level as electrons in a conduction band or as holes in a valence band. The electric field on the solid side of the electrical double layer now has spatial extent - a diffuse double layer character exists within the solid. The conventional electric field effects previously associated with ion motion and ion distributions in the electrolyte have a counterpart within the solid phase.

A further complication is brought to the forefront by silicon-electrolyte electrochemical studies. This is the phenomena of surface states at the solid-electrolyte interface. These become critically involved in charge transfer reactions involving complex reactants at the surface. Thus simple electric field distributions are not present except in particular model cases.

On the other hand, rather than having a semiconductor replacing the metal, the actual situation may involve growth of semiconductor layers on a metal surface, or a dielectric film, or more generally a compound MX separating the base metal from the corrosion media. A new phase separates the corroding base from the reactants.

In Corrosion Chemistry; Brubaker, G., et al.;
ACS Symposium Series; American Chemical Society: Washington, DC, 1979.

The examination of the material MX as a model two-dimensional lattice solid phase, AB, in Figure 17 is revealing. The material can have a variety of lattice imperfection structures[11] including

interstitial A and B atoms	A/Δ, B/Δ
improper site A and B atoms	A/⊟, B/⊞
lattice vacancies for A and B sites	⊞ , ⊟
associated A and B vacancies	⊞⊟

as readily described by a simplified symbolism. In real systems attention must be given to defining at least conceptually the nature of the phases present. Frequently, under ordinary conditions the solid does not fit any simple stoichiometry or electrical neutrality compound model but is a structure unique to the actual system under study. Thus, useful results may come from unorthodox approaches to real systems.

If attention is given to the combination of a metal M becoming covered with MX the model as shown in Figure 18, several observations can be made as to interphase systems and the growth of the film layer. At the exterior surface a particular combination of interphase exchange currents for solid phase growth can be formulated depending on the detailed character of the solid phase, the surface states, the allowed electronic processes. Similarly, a set of interphase exchange currents can be formulated at the boundary of the metal and the MX layer again subject to constraints defined by the mass transport processes permissible in the covering layer and in the metal.

The situation is illustrated in greater detail in the following model situations where attention is given to the interphase boundary exchange currents injecting the lattice imperfections which are responsible for atom transport through the compound MX.[12]

Thus in Figure 19 lattice vacancy with a trapped hole is injected at the compound electrolyte interface, the imperfection at the metal-compound interface reacts to release a vacancy into the metal. Alternatively, in Figure 20 the exchange process injects a lattice vacancy on the cation lattice which appears at the metal compound interphase to release an electron and transfer a metal ion into the surface region.

Transport models such as these have been created to bring attention to the possibility of the boundary exchange currents injecting imperfection into a crystalline phase during an anodic process. In fact, they may determine the solid phase structures formed. Furthermore, the metal with a solid phase covering film

In Corrosion Chemistry; Brubaker, G., et al.;
ACS Symposium Series; American Chemical Society: Washington, DC, 1979.

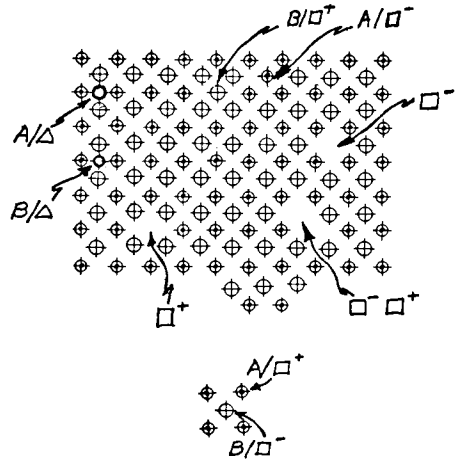

Journal of the Electrochemical Society

Figure 17. A model two-dimensional AB compound lattice illustrating simple imperfection structures expected as a systems variable (12)

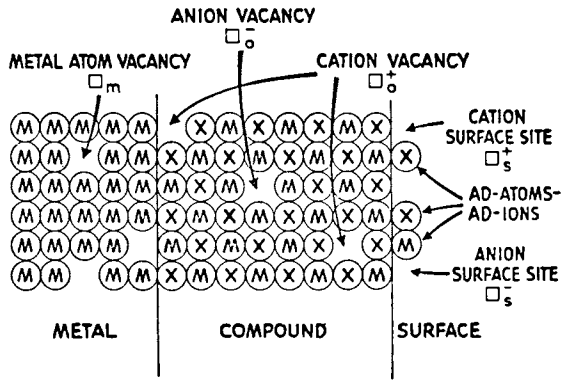

Journal of the Electrochemical Society

Figure 18. Model situation where metal, M, is separated from corroding medium by covering-layer compound (MX) containing imperfection structures (12)

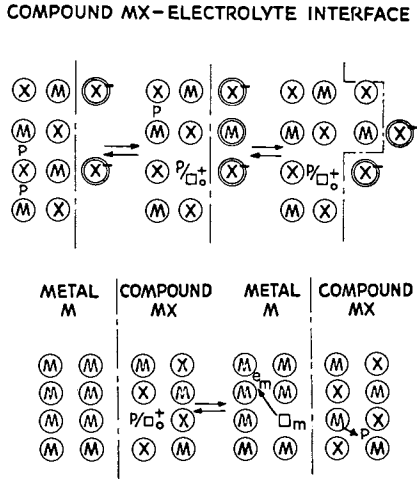

Journal of the Electrochemical Society

Figure 19. Model boundary interphase exchange currents involving the injection of a lattice vacancy with trapped hole at compound–electrolyte interface and vacancy release into the metal with a hole and metal ion in the compound (12)

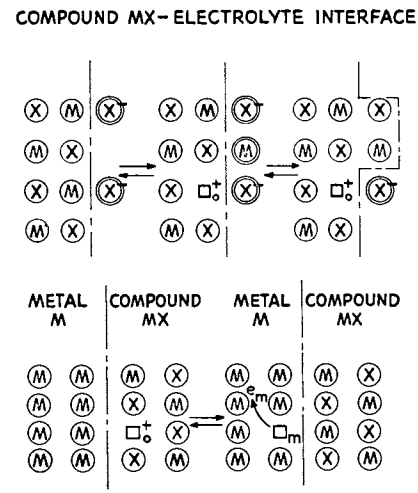

Journal of the Electrochemical Society

Figure 20. Model boundary interphase exchange currents involving lattice vacancy injection at the compound–electrolyte interface and vacancy exchange into the metal releasing an electron and transferring a metal ion into the compound layer (12)

can be in reversible equilibrium with an electrolyte without having exposed metal necessarily in contact with an electrolyte. In such a model, an increase in the driving currents may increase the mass transport rates (alter solid phase structures) within limits so the rapid phase transformations (M to MX) can occur without necessarily involving ion-solution and precipitation reactions in the ordinary sense.

This discussion has brought attention to the potential presence of two classes of interphase transport conditions in solid state systems. Let us examine these for a moment from the perspective of forming solid phases under model conditions.

For the single interphase exchange process of solid phase P_2 interactions with P_1 shown in Figure 21, a series of model conditions are illustrated. For each a set of interphase atom exchange reactions can be formulated which have both thermodynamic and kinetic interpretations. The first is the local deposition of metallic titanium by the thermal decomposition of $TiCl_4$ gas on a hot wire. This vapor plating technique can be performed to grow a varied crystallite structure of a relatively pure titanium on the hot filament. More generally, vapor plating techniques of many complex forms are used to grow epitaxial silicon layers of controlled impurity content onto silicon substrates. The careful control of conditions results in an amazingly homogeneous film growth of high semiconductor quality. The imperfection structure in a composition and structural sense depends on technique details.

The second example is electrolytic plating of copper films. Contrary to some expectations growth close to equilibrium potential conditions does not result in the highest quality deposit. In general, the composition and structure of the deposit depends on the detailed combination of transport processes towards and away from the electrode surface. Adding the local hydrodynamic variables provides the system with an extremely broad structural chemical range.

The third example involves growth of a crystalline salt phase from the saturated solution. The thermodynamic description again is inadequate for describing the detailed states of the solid. The relatively anhydrous chloride ion readily deposits into the surface lattice but the sodium ion must be dehydrated to form NaCl. This means that water must be diffused away from the surface during solidification. The white cast of salt, termed veiling, involves solution incorporation during growth with a subsequent diffusion of the solvent out of the crystal.

In Corrosion Chemistry; Brubaker, G., et al.;
ACS Symposium Series; American Chemical Society: Washington, DC, 1979.

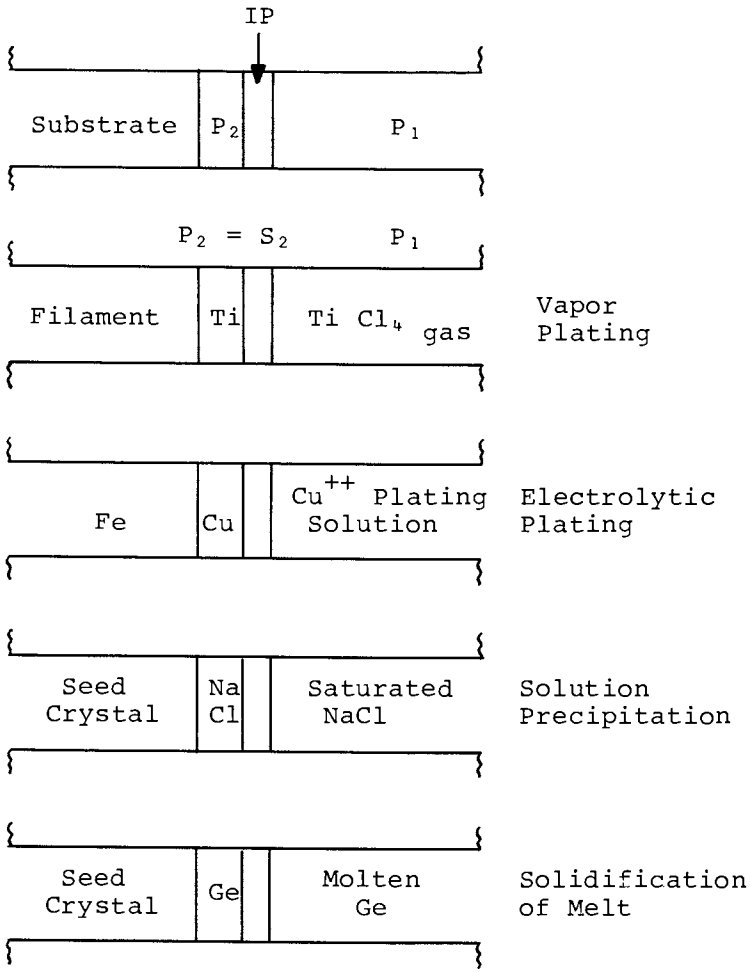

Figure 21. Single interphase exchange current model for solid-phase formation (P_2) through interphase reactions with second phase (P_1)

In Corrosion Chemistry; Brubaker, G., et al.;
ACS Symposium Series; American Chemical Society: Washington, DC, 1979.

The fourth example is the controlled solidification of germanium (or silicon) to produce semiconductor grade materials. The solid phase structure and composition depend strongly upon the interphase exchange processes which can enhance incorporation into the solid or into the liquid depending upon ??? This example implicitly includes the production of most of the metallic structural materials.

The metal alloy systems generally have both controlled and uncontrolled impurities being deposited and redistributed within the solid as a result of complex liquid hydrodynamic interphase region processes as well as secondary solid state diffusion and transformation processes. This materials science is familiar to all corrosion engineers who become involved with commercial systems.

The second interphase transport model incorporates the dynamic interaction of three phases with two interphase exchange currents at the separated boundaries as indicated in Figure 22 where a solid phase P_2 is formed by interactions involving the separated phases P_3 and P_1.

The classic oxidation of aluminum to form a passive surface is the first illustration. While the second model is the anodic oxidation of aluminum, the interphase transport phenomena here can be distributed within more complex contexts as a result of the boundary layer composition changes in the electrolyte. This model is a particularly fascinating one because several decades ago it was clear that the large negatively charged oxygen anion could not migrate in such oxidation processes - the metal ion +3 aluminum was small and of course had to transport all the current through the film. Famous last words that created a crisis when good transport number experiments were performed which showed both atoms move in the film-forming process.[13]

The silver tarnishing reaction involving hydrogen sulfide is a classic of solid state materials science literature, and the zinc oxidation is yet another example of a more complex protective layer corrosion problem for which wide ranges of data exist relating to purity, to kinetic conditions, etc.

This interphase exchange current modeling of the solid phase formation process serves to emphasize the varied perspectives from which useful information can be drawn to aid in describing and understanding corrosion processes in varied systems. Rarely are the real systems simple and many pieces of data are examined before the models do incorporate the full ranges of

In Corrosion Chemistry; Brubaker, G., et al.;
ACS Symposium Series; American Chemical Society: Washington, DC, 1979.

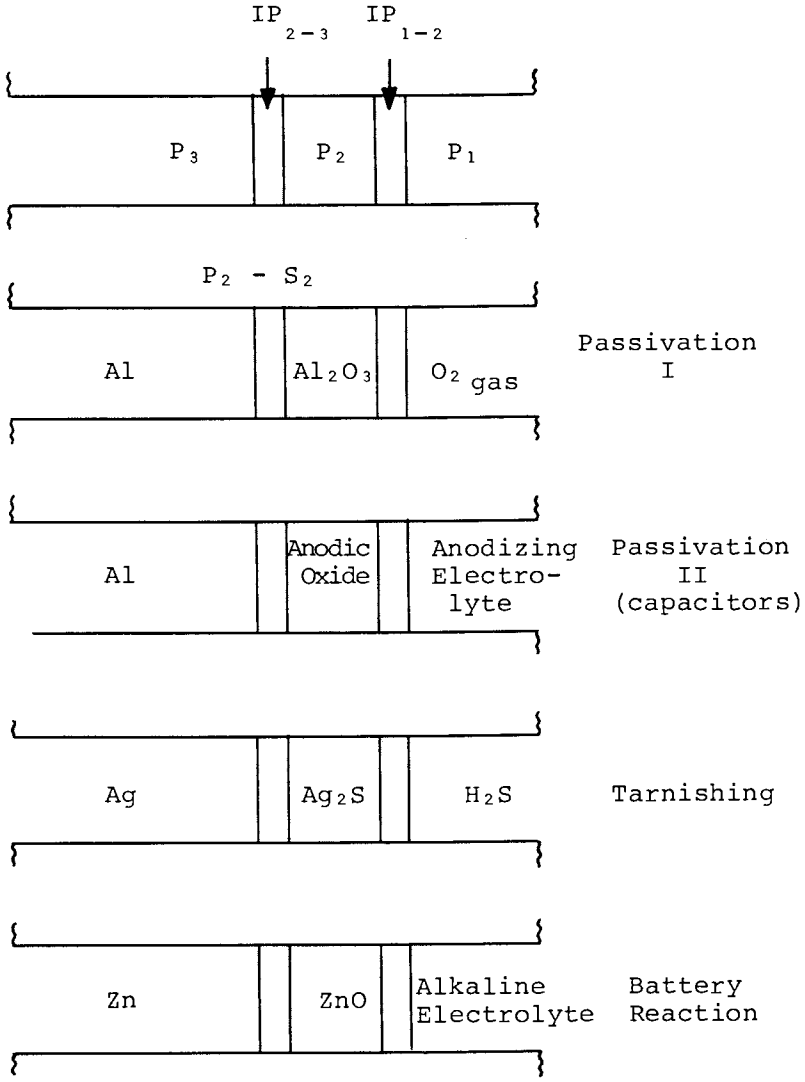

Figure 22. Double interphase exchange current model for solid-phase formation (P_2) through interphase reactions (IP) at P_2–P_3 and P_2–P_1 boundaries

In Corrosion Chemistry; Brubaker, G., et al.;
ACS Symposium Series; American Chemical Society: Washington, DC, 1979.

variables present.

The corrosion engineer's experiences exist in a complex synergistic relationship to the varied interphase exchange current relationships present within systems of practical concern. It is indeed rare that his problems are expressed within any model materials science contexts. He must necessarily work with the economically feasible materials for the practical applications. As the production engineers work with steadily increasing labor costs in assembly, the materials engineer - corrosion engineer - wear engineer become increasingly on the spot to extract the required values from cheaper materials. It is no joke that the contract went to the lowest bidder.

What does this mean to all of us assembled here?

First, a recognition needs to exist that in all practical situations materials science is a tough ball game - it cannot remain a phenomenological art if we are expected to warranty the performance.

Second, a recognition needs to exist that, though the problems are complex, many new tools and skills are increasingly available to clarify directly the character of the problems present. The articles which follow bring attention to this.

Third, a recognition needs to exist that organized knowledge on solid state chemistry is becoming increasingly available to us. This is illustrated by N. B. Hannay's multi-volume Treatise on Solid State Chemistry.[14] As noted by Hannay in his foreword,

> "... Yet even though the role of chemistry in the solid state sciences has been a vital one and the solid state sciences have, in turn, made enormous contributions to chemical thought, solid state chemistry has not been recognized by the general body of chemists as a major subfield of chemistry ... Solid state chemistry has many facets, and one of the purposes of this treatise is to help define the field."

If chemists are to be the atomic-molecular domain custodians of solid state materials science, a serious concern will need to exist for acquiring useful backgrounds in this area. A significant related publication is the recent appearance of F. A. Kröger's second edition of the Chemistry of Imperfect Crystals[15] in three volumes. The defect chemistry concepts from this area need to be incorporated more generally into the new surface science which relates to the environmental

In Corrosion Chemistry; Brubaker, G., et al.;
ACS Symposium Series; American Chemical Society: Washington, DC, 1979.

stability of materials.

Fourth and last, but not least, a growing recognition needs to exist that the application of the new complex instrumental techniques can clarify the surface chemistry speculations previously necessary. So frequently our conceptualizations of the real problem are wrong. I personally accept the hypothesis that the first six models when tested in detail will prove wrong. However, as the real model emerges in its complex beauty, the number of paths to optimizations have multiplied and science is no longer dead ended.

The complex instrumentations include LEED, low energy electron diffraction, which is revealing a complex model for surface structure when apparent multilayer adsorption of oxygen proceeds on clean metal surfaces.

It also includes ESCA, electron spectroscopy for chemical analysis, or x-ray photoelectron spectroscopy that can prove that the postulated covering film, by golly, is not covering, and what's the surface composition? Ever try to deal with nine surface components at once? Well, you can seriously explore that distribution for electroless nickel films being deposited on a catalyzed substrate.

It also includes Auger electron spectroscopy microprobe identification of the surface crud in the pit, or definition of the surface composition gradient previously omitted from the speculation on atom transport processes.

The scanning electron microscope provides us neophytes with a realistic look at surface structure as encountered in the system. When teamed with Auger or ESCA a confrontation can be created with self, trying to rationalize the old comfortable models that did not have to acknowledge that surface chemical structure really existed on the "polyphase inhomogeneous solid containing heterogeneity homogeneously dispersed."

Corrosion is here to stay. The wedding to materials science is implicitly reviewed in the first five figures. It is a clearly important complex materials science drawing on all the other disciplines. As the surface science of interphase mass and charge transport phenomena on solids continues to evolve then more clearly, defined new routes for product optimizations will be evident.

Would you agree that corrosion is the most general problem of materials science?

May all have fun exploring the new vistas of our physical world through the following chapters. For

In Corrosion Chemistry; Brubaker, G., et al.;
ACS Symposium Series; American Chemical Society: Washington, DC, 1979.

indeed we are all stewards of the utilization of materials on this scene in service to all. May the mastery of corrosion extend the resources available to all those who will celebrate the tricentennial, for few of us will have this privilege.

Acknowledgements

I would like to specifically acknowledge the challenge provided by Dr. Rudolph Hausler when he indicated that preparing the overview would be an easy task. It wasn't, but it did provide an opportunity to survey corrosion literature and to recognize more fully the title of this article: Corrosion (is) the Most General Problem of Materials Science.

General References

1. Tedmon, Craig S., editor, "Corrosion Problems in Energy Conversion and Generation," Corrosion Division, Electrochemical Society (1974).
2. Evans, U. R., "Corrosion and Oxidation of Metals: Scientific Principles and Practical Applications," Arnold, London (1960).
3. Fontana, M. G., Greene, N. D., "Corrosion Engineering," McGraw-Hill, New York (1967).
4. Hauffe, K., "Oxidation of Metals," Plenum Press, New York (1965).
5. Hamner, N. E., compiler, "Corrosion Data Survey: Metals and Non-Metals," Fifth Edition, National Association of Corrosion Engineers, Houston, Texas (1974).
6. Nathan, C. C., editor, "Corrosion Inhibitors," National Association of Corrosion Engineers, Houston, Texas (1973).
7. Pourbaix, M., "Lectures on Electrochemical Corrosion," Plenum Press, New York (1973).
8. Uhlig, H. H., "Corrosion and Corrosion Control: An Introduction to Corrosion Science and Engineering," John Wiley, New York (1963).
9. Uhlig, H. H., et. al., "Corrosion Handbook," Wiley, New York, (1948).
10. "Corrosion, the Journal of Science and Engineering," published monthly by the National Association of Corrosion Engineers, Houston, Texas.

Literature Cited

1. General References 1 - 10.
2. Stern, M., et. al., J. Electrochem. Soc. (1957) 104 pp. 56-63, 559-63, 645-50.
3. Helmholtz, H., Wiss Abhandlphysik. Tech. Reichenstalt I (1879) p. 925.
4. Gouy, G., J. Phys. (1910) 9 p. 457.
5. Chapman, D. L., Phil. Mag. (1913) 25 (6) p. 475.
6. Stern, O., Z. Electrochem. (1924) 30 p. 508.
7. Grahame, D. C., Chem. Rev. (1947) 41 p. 441.
8. Bockris, J. O'M., et. al., Proc. Roy. Soc. (1963) A274 pp. 55-79.
9. Rice, O. K., Phys. Rev. (1928) 31 p. 1051, MacDonald, J. R., J. Appl. Phys. (1964) 35 (10) p. 3053.
10. See, for example H. Gerischer, 177-204, H. Gatos, 381-408, "The Surface Chemistry of Metals and Semiconductors," H. C. Gatos, editor, John Wiley, New York (1960).
11. Rees, A. L. G., "Chemistry of the Defect Solid State," John Wiley, New York (1954).
12. Croft, G. T., and Tuomi, D., J. Electrochem. Soc. (1961) 108 p. 915.
13. Davies, J. A., et. al., J. Electrochem. Soc. (1965) 112 p. 675.
14. Hannay, N. B., editor, "Treatise on Solid State Chemistry," Volumes 1-7, Plenum Press, New York (1974).
15. Kröger, F. A., "Chemistry of Imperfect Crystals - Volume 1, Preparation, Purification, Crystal Growth, and Phase Theory; Volume 2, Imperfection Chemistry of Crystalline Solids; Volume 3, Applications of Imperfection Chemistry: Solid State Reactions and Electrochemistry," North Holland-American Elsevier, New York (1974).

RECEIVED September 1, 1978.

2

Electrochemical Techniques in Corrosion Studies

FRANCIS M. DONAHUE

Department of Chemical Engineering, University of Michigan, Ann Arbor, MI 48109

Corrosion may be defined as the spontaneous deterioration of a structure or part of a structure due to the action of the total environment or individual environmental agents. For the purposes of this chapter, the structure is assumed to be metallic and the environment is assumed to be aqueous. Using this definition and the constraints noted, this chapter will outline the electrochemical techniques used to develop criteria of corrosion and those used in the study of corrosion kinetics.

Chemical Criterion of Corrosion

Free Enthalpy Change.

In the definition of corrosion given above, the word "spontaneous" was used in the thermodynamic sense, i.e., a chemical reaction for which the free enthalpy change, ΔG, is negative. Therefore, one can ascertain whether a postulated corrosion reaction can lead to corrosion by determining the sign of the free enthalpy change of the reaction.

The free enthalpy change for a chemical reaction at a temperature, T, is given by

$$\Delta G_T = \Delta G_T^\circ + RT \ln(\Pi(a_Y)^{\nu_Y}) \quad (1)$$

where ΔG_T° is the standard free enthalpy change for the reaction at the prescribed temperature, Π is the multiplication operator, a_Y and ν_Y are the activity (fugacity, for gaseous species) and stoichiometric coefficient, respectively, for a species, Y, in the chemical reaction and R is the gas constant. By convention,

0-8412-0471-3/79/47-089-035$10.25/0

stoichiometric coefficients for reactants are negative while those for products are positive.

The standard free enthalpy change for a chemical reaction can be calculated from tabulated values of various thermodynamic functions (1-3). For aqueous chemical reactions at 25°C, the standard free enthalpy change is computed from

$$\Delta G^{\circ}_{298} = \Sigma \nu_Y \mu^{\circ}_Y \qquad (2)$$

where Σ is the summation operator and μ°_Y is the standard chemical potential of a species, Y, at 25°C. Pourbaix (1) has tabulated the standard chemical potentials of most species of interest in corrosion studies. At other temperatures, the standard free enthalpy change is

$$\Delta G^{\circ}_T = \Sigma(\nu_Y \Delta H^{\circ}_{fY,298}) + T\Sigma\nu_Y((G^{\circ}_T - H^{\circ}_{298})/T)_Y \qquad (3)$$

where $H^{\circ}_{fY,298}$ is the standard enthalpy of formation of a species, Y, at 25°C and $((G^{\circ}_T - H^{\circ}_{298})/T)_Y$ is a thermodynamic function which depends on the species, Y, and the temperature, T. These thermodynamic quantities are tabulated in some reference books (2,3).

Equation 1 is useful as a criterion of corrosion for postulated corrosion reactions. Its main utility is that it permits one to ascertain whether a particular environmental agent (dissolved species) or the solvent can interact chemically with the metallic structure to cause corrosion of the structure. If the computed free enthalpy change is positive, it indicates that corrosion cannot occur by the postulated reaction. However, it does not mean that corrosion cannot occur due to the action of another environmental agent. Therefore, computations of this sort should be exhaustive and account for all environmental agents. If the computed free enthalpy change is negative, it indicates that corrosion by the postulated reaction is possible. The computation provides no information about the rate of the corrosion reaction.

Many corrosion processes, e.g., stress corrosion cracking and other corrosion-fracture processes, cannot be described completely by a chemical reaction. These processes are complex interactions among chemistry, physical properties of the metal and mechanical stress. Therefore, the corrosion tendency of the metal-environment interaction cannot be evaluated using Equation 1. At the present time, empirical criteria (which are beyond the scope of this chapter) are used.

In Corrosion Chemistry; Brubaker, G., et al.;
ACS Symposium Series; American Chemical Society: Washington, DC, 1979.

Illustration 1. Chemical Criterion of Corrosion. Copper metal is in contact with a strong acid solution at 25°C.

a) If the only information available are the activities of hydrogen ion (10^{-2}) and cupric ion (10^{-4}), can corrosion occur?
b) If oxygen at a fugacity of 0.2 is in equilibrium with the solution in part "a", can corrosion occur?
c) If ferrous ($a=10^{-6}$) and ferric ($a=10^{-7}$) ions are contaminants of the solution in part "a", can corrosion occur?

Solutions:

a) Assume a corrosion reaction,

$$Cu + 2H^+ \rightarrow Cu^{2+} + H_2$$

From Pourbaix (1) and inspection of the chemical reaction,

Species	μ_Y° (kcal/mole)	ν_Y
Cu	0	-1
H^+	0	-2
Cu^{2+}	15.53	+1
H_2	0	+1

Using Equations 1 and 2 and the available data (assuming unit fugacity for hydrogen gas),

$$\Delta G = (-1)(0) + (-2)(0) + (1)(15530) + (1)(0) + (1.987)(298)\ \ell n((10^{-4})/(10^{-2})^2)$$

$$= +1.553 \times 10^4 \text{ cal/mole of Cu}$$

Therefore, corrosion cannot occur by the postulated reaction.

b) Assume a corrosion reaction,

$$2Cu + 4H^+ + O_2 \rightarrow 2Cu^{2+} + 2H_2O$$

From Pourbaix (1) and inspection of the chemical reaction,

Species	μ_Y° (kcal/mole)	ν_Y
Cu	0	-2
H^+	0	-4
O_2	0	-1
Cu^{2+}	15.53	+2
H_2O	-56.69	+2

In Corrosion Chemistry; Brubaker, G., et al.;
ACS Symposium Series; American Chemical Society: Washington, DC, 1979.

Using Equations 1 and 2 and the available data (assuming unit activity for water),

$\Delta G = (-2)(0) + (-4)(0) + (-1)(0) + (2)(15530) + (2)(-56690) + (1.987)(298)\ \ln((10^{-4})^2/(10^{-2})^4(0.2))$

$= -8.14 \times 10^4$ cal/ 2 mole of Cu

Therefore, corrosion can occur as a result of the postulated reaction.

c) Assume a corrosion reaction,

$Cu + 2Fe^{3+} \rightarrow Cu^{2+} + 2Fe^{2+}$

From Pourbaix (1) and inspection of the chemical reaction,

Species	μ_Y° (kcal/mole)	ν_Y
Cu	0	-1
Fe^{3+}	-2.53	-2
Cu^{2+}	15.53	+1
Fe^{2+}	-20.30	+2

Using Equations 1 and 2 and the available data,

$\Delta G = (-1)(0) + (-2)(-2530) + (1)(15530) + (2)(-20300) + (1.987)(298)\ \ln(10^{-2})$

$= -2.27 \times 10^4$ cal/mole of Cu

Therefore, corrosion can occur by the postulated reaction.

Electrochemical Thermodynamics

Electrode Potential Measurements.

Electrochemical reactions can be written in the general form

$$Red = Ox + ne^- \qquad (4)$$

where Red represents the reduced form of a chemical species (and any other species with which it reacts in the electrochemical reaction), Ox represents the oxidized form of the same chemical species (and any other species with which it reacts) and n is the stoichiometric coefficient of the electron, e^-. Electrochemical reactions take place at the interface between a metal (or other electrically conductive substrate) and a solution. An electric field exists across this metal-solution interface due to the nature of the reaction

In Corrosion Chemistry; Brubaker, G., et al.;
ACS Symposium Series; American Chemical Society: Washington, DC, 1979.

and the disposition of ionic and dipolar species on the solution side of the interface. Although this electric field is present, it cannot be measured directly. Instead, a relative measurement is made which provides useful information.

The circuit used in this measurement is shown in Figure 1. The electrode under investigation, TE, is connected to a second electrode, RE, by means of a voltage-measuring device, E. Since it is necessary to make these measurements in the virtual absence of a current flowing in the circuit, the voltage-measuring device should possess a large ($>10^9$ ohms) input impedance. In addition, it is usually necessary to make measurements over the range of ±2.0V with an accuracy on the order of ±1mV.

The reference electrode, RE, should possess a stable, known electrode potential, i.e., a measure of the electric field at its metal-solution interface. Since all electrode potential measurements are relative, it is convenient to have an "ultimate reference point". By convention, the electrode potential of the hydrogen-hydrogen ion electrochemical reaction, i.e.,

$$H_2 = 2H^+ + 2e^- \qquad (5)$$

is assumed to have a value of 0.000V when hydrogen gas is at unit fugacity and the hydrogen ion is at unit activity. This is the so-called standard hydrogen electrode (SHE). The electrode potentials of some common reference electrodes (relative to the electrode potential of SHE) are given in Table I.

The electrode potential of the test electrode, TE, shown in Figure 1 is the voltage measured on the device, E, and is reported as "x.xxxV vs. RE". If it is necessary to convert the value of the electrode potential of a test electrode from one reference electrode scale to another, this is accomplished by

$$\phi_2 = \phi_1 + \phi_{RE1,2} \qquad (6)$$

where ϕ_2 is the electrode potential relative to the second reference electrode (the desired quantity), ϕ_1 is the electrode potential relative to the first reference electrode (the measured quantity) and $\phi_{RE1,2}$ is the electrode potential of the first reference electrode relative to the second reference electrode.

In Corrosion Chemistry; Brubaker, G., et al.;
ACS Symposium Series; American Chemical Society: Washington, DC, 1979.

Table I. Electrode potentials of some common reference electrodes at 25°C. (4)

Electrode Reaction/ Name of Reference Electrode	Electrolyte	Electrode Potential (V vs. SHE)
$2Hg + 2Cl^- = Hg_2Cl_2 + 2e^-$ / Calomel	0.01 M KCl	0.389
	0.10 M "	0.333
	1.0 M "	0.280
	Satd. "	0.241
$Cu = Cu^{2+} + 2e^-$ / Copper-Copper Sulfate	0.1 M $CuSO_4$	0.284
	0.5 M "	0.294
	Satd. "	0.298
$Ag + Cl^- = AgCl + e^-$ Silver-Silver Chloride	0.001 M KCl	0.400
	0.01 M "	0.343
	0.1 M "	0.288
	1.0 M "	0.234

Illustration 2. Conversion of Reference Electrode Scale.
If the electrode potential of an iron electrode is -0.528 V vs. saturated calomel reference electrode (SCE), what is its value relative to SHE?
Solution:
Inserting the measured electrode potential and the electrode potential of the reference electrode from Table I ($\phi_{Rel,2}$ = 0.241 V vs. SHE) in Equation 6,
ϕ_2 = -0.287 V vs. SHE.

Equilibrium Electrode Potentials.

The condition for equilibrium for the electrochemical reaction given in Equation 4 is

$$\nu_e \mu_{eo} + \Sigma \nu_Y \mu_Y = 0 \qquad (7)$$

where the "chemical" potential of the electron at equilibrium, μ_{eo}, is related to the equilibrium electrode potential of the reaction, ϕ_o, by

$$\mu_{eo} = -F\phi_o \qquad (8)$$

where F is the Faraday constant. The chemical potential of a species, Y, is

In Corrosion Chemistry; Brubaker, G., et al.;
ACS Symposium Series; American Chemical Society: Washington, DC, 1979.

$$\mu_Y = \mu_Y^\circ + RT \ln a_Y \quad (9)$$

Inserting Equations 8 and 9 in 7 and rearranging

$$\phi_o = (1/\nu_e F)\Sigma\nu_Y\mu_Y^\circ + (RT/\nu_e F)\ln(\Pi(a_Y)^{\nu_Y}) \quad (10)$$

It can be shown that

$$\phi^\circ = (1/\nu_e F)\Sigma\nu_Y\mu_Y^\circ \quad (11)$$

where ϕ° is the standard electrode potential of the reaction. Tabulated values of standard electrode potentials relative to SHE for many electrochemical reactions of interest in corrosion are available (4). Inserting Equation 11 in 10

$$\phi_o = \phi^\circ + (RT/\nu_e F)\ln(\Pi(a_Y)^{\nu_Y}) \quad (12)$$

Equation 12 may be used to compute equilibrium electrode potentials for electrochemical reactions. In order for such calculations to be consistent with respect to the sign of the potential, the standard electrode potentials should have signs consistent with those of de Bethune (4) and the stoichiometric coefficients should be inserted consistent with Equation 4 as written.

Activities and/or activity coefficients are not available for ionic species in most corrosion solutions. Therefore, as a practical expedient, the concentrations of the species are used in place of the respective activities when computing equilibrium electrode potentials.

Pourbaix Diagrams.

If an electrochemical reaction is perturbed from the equilibrium state, the relative stabilities of the species in the reaction are changed. The manifestation of the perturbation is the measured electrode potential, which differs from the equilibrium electrode potential for the reaction. If the measured electrode potential is positive with respect to the equilibrium potential, the reaction given by Equation 4 proceeds irreversibly from left to right, i.e., the reduced form of the chemical species is unstable while the oxidized form of the species is stable. The converse is true when the

In Corrosion Chemistry; Brubaker, G., et al.;
ACS Symposium Series; American Chemical Society: Washington, DC, 1979.

measured potential is negative with respect to the equilibrium potential.

Water is an electrochemically active chemical species. The electrochemical reactions in which water is the primary reactant or product are

$$2H_2O = 4H^+ + O_2 + 4e^- \quad (13)$$

and

$$H_2 + 2OH^- = 2H_2O + 2e^- \quad (14)$$

For solutions where the activity of water is unity and the fugacities of oxygen and hydrogen gases are unity, the equilibrium electrode potentials for the reactions given by Equations 13 and 14 at 25°C are, respectively,

$$\phi_{o,H_2O/O_2} = +1.23 - 0.059pH \quad (15)$$

and

$$\phi_{o,H_2/H_2O} = -0.059pH \quad (16)$$

where these electrode potentials are V vs. SHE.

Pourbaix (1) has shown that plotting electrode potentials of electrochemical reactions against solution pH is useful in delineating regions of stability of various chemical species in and in contact with aqueous solutions. These plots are commonly called Pourbaix Diagrams. The utility of this approach will become evident in the subsequent presentation.

The Pourbaix Diagram for the system, H_2O-H_2-O_2-H^+-OH^-, is given in Figure 2. The lines "15" and "16" represent plots of the data for Equations 15 and 16, respectively. Inspection of Equation 13 and line "15", in conjunction with the previous discussion of species stability, indicates that the solvent, water, is stable (with respect to Equation 13) at electrode potentials below this line while water is unstable at potentials above this line. Similarly, inspection of Equation 14 and line "16" indicates that water is stable at electrode potentials above line "16" and unstable below the line. Figure 2 is analogous to a phase diagram; it represents a form of electrochemical phase diagram. Similar to a phase diagram, the region where a species is stable is identified with the chemical symbol for the species.

The Pourbaix Diagram is particularly useful in determining the stable species for metallic systems in

In Corrosion Chemistry; Brubaker, G., et al.;
ACS Symposium Series; American Chemical Society: Washington, DC, 1979.

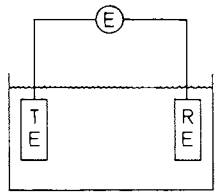

Figure 1. Schematic of a circuit to measure the electrode potential of a test electrode

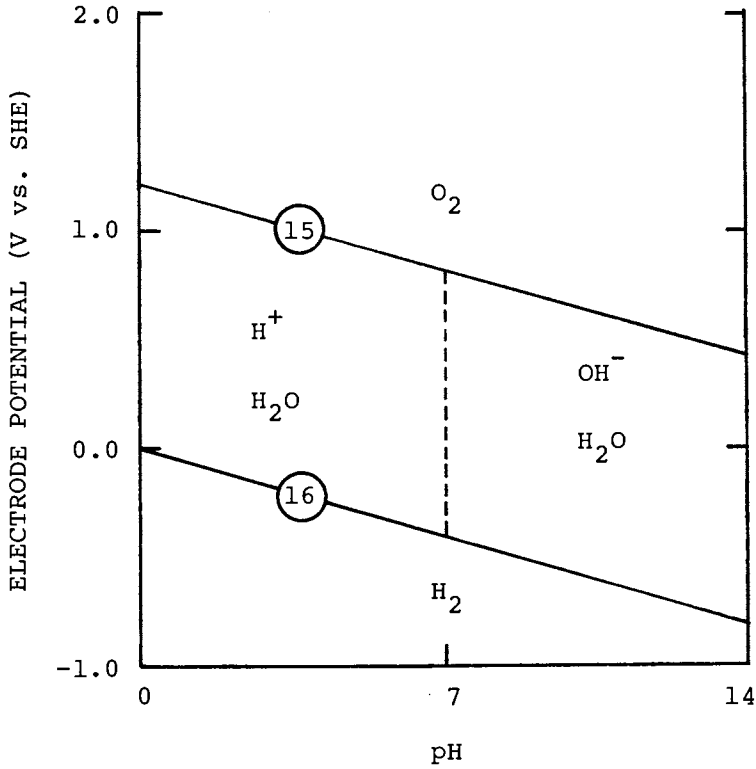

Figure 2. Pourbaix diagram for the system H_2O–H_2–O_2–H^+–OH^-. Activity of water is unity; fugacities of hydrogen and oxygen are unity. Temperature is 25°C.

In Corrosion Chemistry; Brubaker, G., et al.;
ACS Symposium Series; American Chemical Society: Washington, DC, 1979.

contact with aqueous solutions. Two general classes of metals are found when Figure 2 and the Pourbaix Diagram for a metal are superimposed. This classification is based on the relationship between the metal-metallion equilibrium reaction and the region of stability of water. In the first case, the metal-metallion equilibrium potential falls within the region of stability of water. In these instances, it is possible to measure the equilibrium electrode potential of the metal-metallion reaction in aqueous solutions and to devise a means whereby the kinetic properties of this reaction may be obtained with minimal kinetic complexity. The second class of metals has metal-metallion equilibrium electrode potentials which fall below the region of stability of water. Since these metals form mixed potential systems with the solvent (see below), the equilibrium electrode potential of the metal-metallion reaction cannot be measured in aqueous solution, and the kinetics of the complete reaction can be determined only with great difficulty. Copper and iron are examples of these two classes of metals and will be discussed below.

Figure 3 is the Pourbaix Diagram for copper and some of its ionic species and compounds in contact with water at 25°C. The equilibrium electrode potential for the copper-cupric ion reaction is located within the region of water stability (dashed lines). Therefore, the measurement of the equilibrium potential is possible, and the kinetics of the copper-cupric ion system can be studied without interference from reactions involving decomposition of the solvent. With the exception of Equation 21, which is a chemical reaction involving the hydrolysis of cupric ion (reactions which are purely chemical, since they bear no relation to electrochemical reactions, *per se*, appear as vertical lines on Pourbaix Diagrams), all of the reactions considered in Figure 3 are electrochemical and may be studied using the techniques outlined in this chapter. If the measured electrode potential (with respect to SHE) and the solution pH are known, Figure 3 may be used to determine the stable form of copper or its compounds which can be expected under those conditions.

Figure 4 is the Pourbaix Diagram for iron and some of its ionic species and compounds in contact with water at 25°C. The equilibrium potential of the iron-ferrous ion reaction falls outside the region of stability of water (dashed lines). Therefore, any attempt to measure the equilibrium potential will fail since the solvent will undergo electrochemical reduc-

In Corrosion Chemistry; Brubaker, G., et al.;
ACS Symposium Series; American Chemical Society: Washington, DC, 1979.

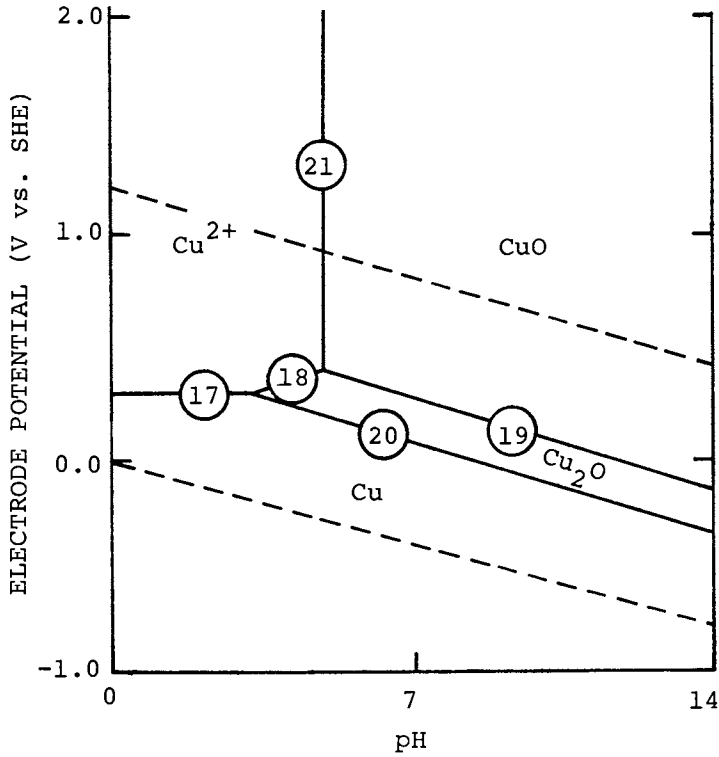

Figure 3. Pourbaix diagram for the system $Cu–Cu^{2+}–Cu_2O–H_2O$. Activity of cupric ion is assumed to be 0.01. The dashed lines denote the stability range of water. Temperature is 25°C. The reactions considered:

$$Cu = Cu^{2+} + 2e^- \quad (17)$$

$$Cu_2O + 2H^+ = 2Cu^{2+} + H_2O + 2e^- \quad (18)$$

$$Cu_2O + H_2O = 2CuO + 2H^+ + 2e^- \quad (19)$$

$$2Cu + H_2O = Cu_2O + 2H^+ + 2e^- \quad (20)$$

$$Cu^{2+} + H_2O = CuO + 2H^+ \quad (21)$$

In Corrosion Chemistry; Brubaker, G., et al.;
ACS Symposium Series; American Chemical Society: Washington, DC, 1979.

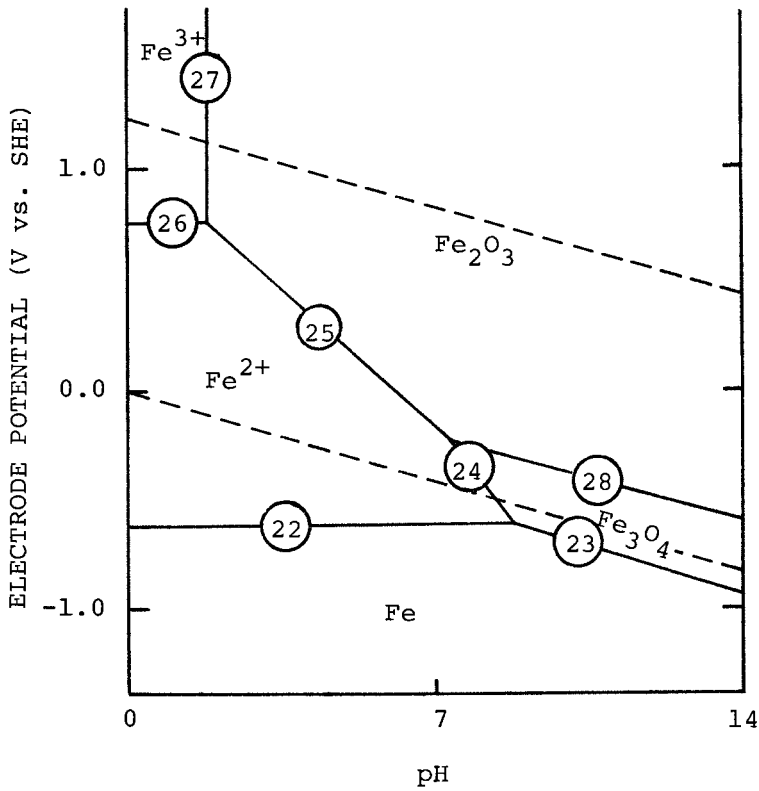

Figure 4. Pourbaix diagram for the system Fe–Fe^{2+}–Fe^{3+}–Fe_3O_4–Fe_2O_3. Activities of ferrous and ferric ions are 10^{-6}. Temperature is 25°C. The reactions considered:

$$Fe = Fe^{2+} + 2e^- \quad (22)$$

$$3Fe + 4H_2O = Fe_3O_4 + 8H^+ + 8e^- \quad (23)$$

$$3Fe^{2+} + 4H_2O = Fe_3O_4 + 8H^+ + 2e^- \quad (24)$$

$$2Fe^{2+} + 3H_2O = Fe_2O_3 + 6H^+ + 2e^- \quad (25)$$

$$Fe^{2+} = Fe^{3+} + e^- \quad (26)$$

$$2Fe^{3+} + 3H_2O = Fe_2O_3 + 6H^+ \quad (27)$$

$$2Fe_3O_4 + H_2O = 3Fe_2O_3 + 2H^+ + 2e^- \quad (28)$$

tion while the iron will undergo electrochemical oxidation. This type of process is a form of corrosion and is the basis for an electrochemical model of corrosion called the theory of mixed potentials (to be discussed below).

In the potential-pH region where iron metal is the stable species, corrosion - defined as dissolution or oxidation - cannot occur since these reactions are not favored thermodynamically. Pourbaix (1) has designated these regions as "immune" to corrosion. However, in the broader sense of corrosion (see definition of corrosion at the beginning of this chapter) this region may be quite conducive to iron deterioration. For example, in this region hydrogen gas is stable (see Figure 2). Some iron alloys are susceptible to fracture in the presence of hydrogen (5). Therefore, it is not sufficient for a structure to be chemically "immune" in order for it to be free of corrosion.

When a chemically stable oxide (or salt) film is present on the surface of a metal (see the iron oxide stable regions of Figure 4), that metal may be free of subsequent corrosion. The conditions for this form of corrosion mitigation are that the underlying film is adherent, coherent and pore-free. In essence, these conditions merely stipulate that the film must be an effective barrier between the metal and the environment. This condition is called passivity and is characterized by measured electrode potentials in the regions where the film is stable. Iron and its alloys have been shown to exhibit passive behavior (6).

Figure 5 is a simplified representation of the Pourbaix Diagram for iron. It delineates the regions where immunity, corrosion and passivity can be expected. Similar diagrams (as well as the more chemically-oriented diagrams) are available in the monograph by Pourbaix (1).

Illustration 3. Use of Pourbaix Diagrams.
Identify the stable species and whether corrosion is possible in the following situations:

a) copper metal at +0.150 V vs. SCE in an aqueous solution with a pH of 2.5 and a cupric ion activity of 0.01 at 25°C.
b) iron metal at -0.750 V vs. SCE in an aqueous solution with a pH of 5.0 and a ferrous ion activity of 10^{-6} at 25°C.

Solutions:

a) the electrode potential (vs. SHE) is computed using Equation 6 and Table I, i.e., $\phi = 0.391$ V

vs. SHE. Referring to Figures 2 and 3, the stable species are Cu^{2+}, H^{+} and H_2O. Corrosion is possible under these conditions.

b) the electrode potential (vs. SHE) is computed using Equation 6 and Table I, i.e., $\phi = -0.509$ V vs. SHE. Referring to Figures 2 and 4, the stable species are ferrous ions and H_2. Corrosion is possible under these conditions.

Electrochemical Kinetics

Properties of Electrode Reactions.

Electrochemical (electrode) reactions are inherently heterogeneous. The electron transfer reaction occurs at a metal (or other electrically conducting substrate)-solution interface. However, prior to and following the electron transfer reaction, transport of chemical species between the bulk of the solution and the interface also takes place. Figure 6 is a representation of these processes which constitute the totality of the electrochemical reaction.

The three steps associated with electrochemical reactions, i.e., transport of reactant(s) to the interface, the electron transfer (surface) reaction and transport of product(s) from the interface, are sequential. Therefore, the overall rate of reaction is controlled by the slowest of the three steps. When the transport processes are capable of operating at high rates relative to the electron transfer reaction, the rate of the overall reaction can be described by equations of electrodekinetics. These types of electrode reactions are said to be "under activation control". On the other hand, when the electrode reaction is capable of operating at high rates relative to the transport process(es), the rate of the overall reaction can be described by equations of convective mass transport. These types of electrode reactions are said to be "under transport control". In the discussion to follow, the equations of electrodekinetics and convective mass transport will be presented with the conditions under which the respective equations apply. Readers wishing a more detailed presentation than is possible here should refer to the monograph by Vetter (7).

The rate of an electrochemical reaction is usually measured by a current, I, flowing in an external electrical circuit (see below). This current is related to the flux of a reacting species, N_J, and the flux of a

In Corrosion Chemistry; Brubaker, G., et al.;
ACS Symposium Series; American Chemical Society: Washington, DC, 1979.

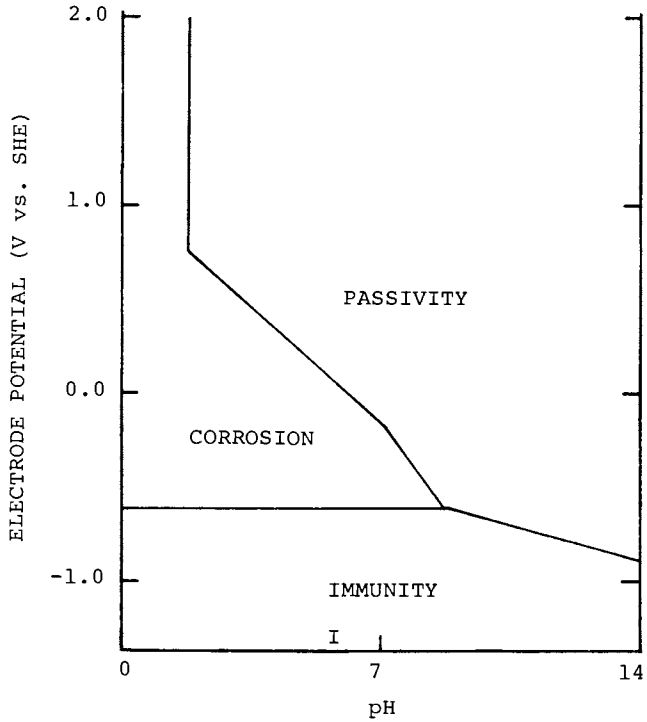

Figure 5. Pourbaix diagram for iron in terms of corrosion, passivity, and immunity

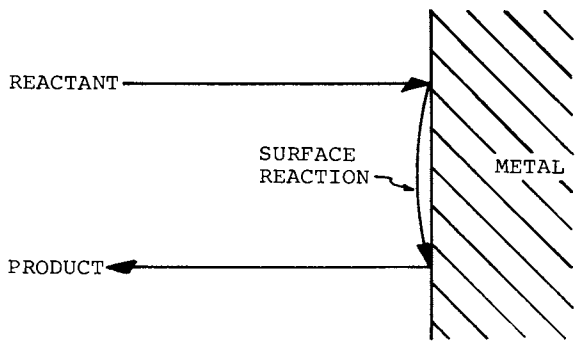

Figure 6. Representation of transport and kinetic processes in electrode reactions

product species, N_K, and the rate of the surface reaction (based on the reacting species), r_J, by

$$I/nFA = N_J = \nu_J N_K/\nu_K = r_J \quad (29)$$

where n is the number of electrons transferred in the in the electrochemical reaction, A is the surface area of the metal substrate in contact with the solution and ν_J and ν_K are the stoichiometric coefficients of the reactant and product species, respectively.

The sign of the current is dependent on the sense of the electrochemical reaction. For example, when Equation 4 operates from left to right, i.e.,

$$Red \rightarrow Ox + ne^- \quad (4a)$$

an electrochemical oxidation takes place. Electrochemical oxidations are often called anodic reactions. In the convention used in this chapter, anodic reactions are associated with positive currents. When the direction of the reaction is reversed, i.e.,

$$Ox + ne^- \rightarrow Red \quad (4b)$$

an electrochemical reduction (cathodic reaction) occurs. Cathodic reactions are associated with negative currents. The signs of the rate and flux terms in Equation 29 should be adjusted to accomodate this sign convention.

The rate (current) of an electrochemical reaction is described by the sum of the rates (currents) of the anodic and cathodic reactions which constitute the electrode reaction. The anodic and cathodic currents, representing "parts" of the overall current (rate), are called partial currents.

Activation Controlled Electrode Reactions.

At equilibrium, the rates of the anodic and cathodic partial reactions are equal, i.e., there is no net change of the inventory of Red and Ox. When the system is perturbed such that the electrode potential is positive with respect to the equilibrium potential, the rate of the anodic partial reaction is greater than that of the cathodic partial reaction. The electrode reaction exhibits a net anodic (oxidation) current. Likewise, for perturbations negative to the equilibrium potential, the electrode reaction exhibits

In Corrosion Chemistry; Brubaker, G., et al.;
ACS Symposium Series; American Chemical Society: Washington, DC, 1979.

a net cathodic (reduction) current.

The equation which has been found to describe the current-electrode potential behavior of activation controlled reactions is

$$I/A = i = i_o[\exp(\eta/\beta_a)-\exp(-\eta/\beta_c)] \quad (30)$$

where i is the net current density (I/A), i_o is the exchange current density, η is the overpotential and β_a and β_c are so-called Tafel constants (slopes).

The exchange current density is a measure of the intrinsic reactivity of the electrode reaction, i.e., the rates of the anodic and cathodic partial reactions at the equilibrium potential. The empirical equation which often describes the exchange current density is

$$i_o = nFk^\circ[\text{Red}]^\rho[\text{Ox}]^\omega[\text{Cat}]^\gamma \quad (31)$$

where k° is a specific rate constant, [Red] and [Ox] are the concentrations of the oxidized and reduced forms of the chemical species, [Cat] is the concentration of a catalytic species and ρ, ω and γ are reaction orders.

The overpotential is defined by

$$\eta = \phi_i - \phi_o \quad (32)$$

where ϕ_i is the perturbed electrode potential associated with a net current density, i. Overpotentials for anodic reactions are positive while those for cathodic reactions are negative.

At large anodic overpotentials, Equation 30 becomes

$$i = i_o\exp[\eta/\beta_a] \quad (33)$$

or

$$\eta = \beta_a \ell n(i/i_o) \quad (34)$$

where β_a is the anodic Tafel constant or slope (see above). Equation 34 indicates that ϕ-ℓn i data for an electrode reaction are linear over a specified range. This linear region provides access to two important empirical parameters in Equation 30, viz., the anodic Tafel slope and the exchange current density. The former is the slope of the line in this linear region. The exchange current density is obtained by extrapolating

In Corrosion Chemistry; Brubaker, G., et al.;
ACS Symposium Series; American Chemical Society: Washington, DC, 1979.

the line for the linear region data to the equilibrium potential, i.e., $\eta=0$. Inspection of Equation 34 shows that the current density obtained by this extrapolation is numerically equal to the exchange current density.

At large (negative) cathodic overpotentials, Equation 30 becomes

$$i = -i_o \exp[-\eta/\beta_c] \quad (35)$$

or

$$\eta = -\beta_c \ell n(-i/i_o) \quad (36)$$

where β_c is the cathodic Tafel constant or slope. The utility of Equation 36 for the analysis of empirical kinetic parameters for cathodic partial reactions is identical to that for Equation 34 for anodic partial reactions.

When electrochemical rate data, i.e., electrode potential-current density data, are plotted, it is often done on semi-logarithmic paper. Since the logarithmic scale of this paper is usually "base 10", the Tafel slopes which are measured are related to the Tafel constants in Equation 30 by

$$\beta = b/2.30 \quad (37)$$

where b is the slope measured on "base 10" paper.

Illustration 4. Analysis of Electrochemical Rate Data for Activation Controlled Reactions. Estimate the exchange current density and Tafel slopes for an electrode reaction from the data given below.

ϕ mV vs. SCE	i mA/cm^2	ϕ mV vs. SCE	i mA/cm^2	ϕ mV vs. SCE	i mA/cm^2
280	100	210	0.96	150	- 2.6
270	57	205	0.42	140	- 3.1
260	32	200	0.00	130	- 3.9
250	18	195	-0.35	110	- 4.6
245	13	190	-0.64	110	- 5.6
240	9.5	185	-0.90	100	- 6.8
235	7.2	180	-1.15	80	-10
230	5.1	175	-1.37	60	-15
225	3.8	170	-1.60	40	-21
220	2.5	165	-1.80	20	-32
215	1.76	160	-2.10	0	-47
		155	-2.30		

In Corrosion Chemistry; Brubaker, G., et al.;
ACS Symposium Series; American Chemical Society: Washington, DC, 1979.

Solution:
The data are plotted in Figure 7. The anodic and cathodic Tafel slopes ("base 10") are 40 and 120 mV, respectively, and the exchange current density is 1.0 mA/cm^2. Therefore, the current density-electrode potential behavior of this activation controlled electrode reaction is described by

$$i = 1.0[\exp(\eta/17.4)-\exp(-\eta/52.2)]$$

where the current density is in mA/cm^2 and the overpotential is in mV.

Transport Controlled Electrode Reactions.

As noted above, the transport of material to and from the surface is involved in any electrochemical reaction. The convective mass transport equations which describe this material flux (in terms of current density and consistent with the sign convention proposed in this chapter) are

$$i = (n/|\nu_{Red}|)Fk_c([Red]_b-[Red]_s) \quad (38)$$

and

$$i = -(n/|\nu_{Ox}|)Fk_c([Ox]_b-[Ox]_s) \quad (39)$$

where k_c is the mass transfer coefficient and the subscripts b and s represent the bulk and interfacial concentrations, respectively. To the extent that the bulk and interfacial concentrations are approximately the same order of magnitude, the kinetics of the electrode reaction are adequately described by Equation 30. However, when these concentrations differ by an order of magnitude or more, the rate of the electrode reaction is controlled by the rate of mass transport.

Figure 8 shows the electrode potential-current density behavior of a cathodic partial process demonstrating activation control, transport control and the transition region between them. The dashed line represents the extension of the Tafel line, i.e., Equation 36. This dashed line predicts current densities which exceed the rate of mass transport - an impossibility. The vertical (electrode potential independent) line represents the limiting current density for the process. Although mathematical relationships have been proposed for the transition region, their utility is minimal since the limiting cases of activation and

In Corrosion Chemistry; Brubaker, G., et al.;
ACS Symposium Series; American Chemical Society: Washington, DC, 1979.

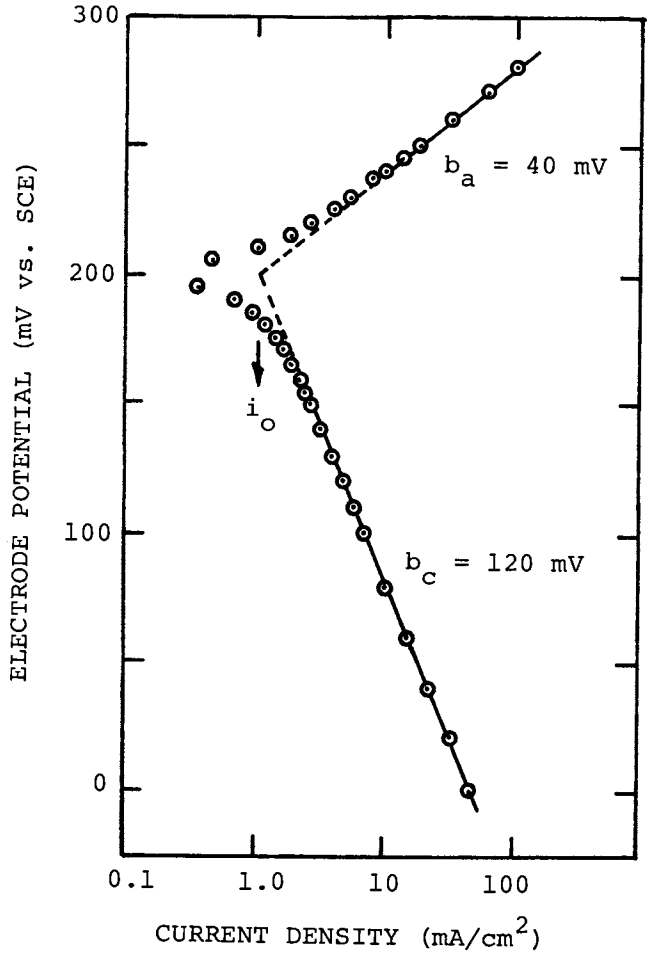

Figure 7. Plot of data for Figure 4

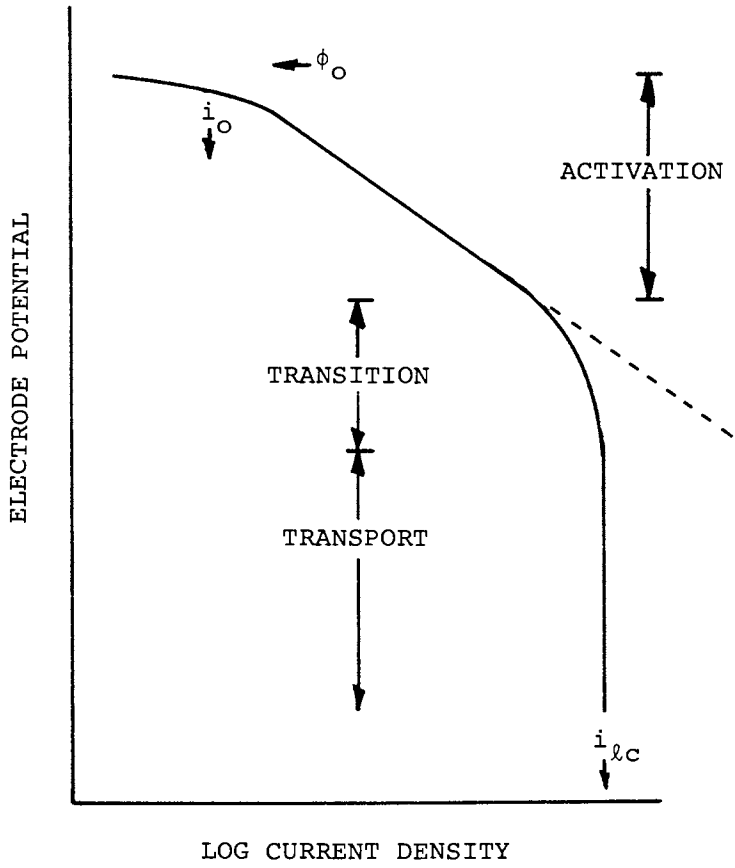

Figure 8. Electrode potential–current density behavior of a cathodic partial process showing regions of activation control, transport control, and the transition between them

transport control represent the properties of the vast majority of electrode reactions.

Mass transport control of electrode reactions can be caused by one of two physical processes. In the first case, the interfacial concentration of the reactant drops to zero, i.e., the electron transfer reaction consumes the species as quickly as it arrives at the interface. In the second case, the interfacial concentration of the product reaches saturation. When these conditions prevail, the rate of mass transport is at its limiting (maximum) value. Limiting current densities, $i_{\ell a}$ and $i_{\ell c}$, for anodic and cathodic partial reactions, respectively, are

$$i_{\ell a} = (n/|\nu_{Red}|)Fk_c[Red]_b \quad (40)$$

$$i_{\ell a} = (n/|\nu_{Ox}|)Fk_c([Ox]_{satn}-[Ox]_b) \quad (41)$$

$$i_{\ell c} = -(n/|\nu_{Ox}|)Fk_c[Ox]_b \quad (42)$$

$$i_{\ell c} = -(n/|\nu_{Red}|)Fk_c([Red]_{satn}-[Red]_b) \quad (43)$$

The value of the mass transfer coefficient depends on the physical system, the transporting species, physicochemical properties of the fluid and the fluid flow rate. Methods of estimating mass transfer coefficients are given elsewhere (8-10).

Illustration 5. Estimation of Limiting Current Density.

Estimate the limiting current density for the reduction of oxygen (concentration, $[Ox]_b \simeq 10^{-7}$ mole/cm^3; diffusivity, D, $\simeq 10^{-5}$ cm^2/sec) to a rotating cylinder (rotation speed, ω, = 95 sec^{-1}; radius, r, = 1.27 cm) if the kinematic viscosity, ν, of the solution is approximately 10^{-3} cm^2/sec.

Solution:

The mass transport correlation for a rotating cylinder is (9)

$$Sh = 0.0627\ Re^{2/3}Sc^{1/3}$$

where, in this case,

Sh = Sherwood Number = $k_c r/D$

Re = Reynolds Number = $\omega r^2/\nu$

Sc = Schmidt Number = ν/D
Then,
$k_c = 0.0627(D/r)(\omega r^2/\nu)^{2/3}(\nu/D)^{1/3}$
$= 6.58X10^{-3}$ cm/sec.
The electrochemical reaction for oxygen reduction is
$O_2 + 4H^+ + 4e^- \rightarrow 2H_2O$
Then, the limiting current density, i.e., Equation 42, is
$i_{\ell c} = -4Fk_c[Ox]_b$
$= (-4 \text{ equiv/mole})(9.65X10^4 \text{ A-sec/equiv})$
$(6.58X10^{-3} \text{ cm/sec})(10^{-7} \text{ mole/cm}^3)$
$= -2.54X10^{-4} \text{ A/cm}^2.$

Criteria for Control of Electrode Reactions.

It is useful to be able to ascertain a priori which type of control operates for an electrode reaction. In order to demonstrate how this may be achieved, consider a cathodic partial reaction. The key element in ascertaining control is the ratio of the hypothetical activation controlled current density, Equation 35, to the limiting current density, e.g., Equation 42. This ratio is

$$i/i_\ell = (|\nu_{Ox}| i_o/nFk_c[Ox]_b)\exp(-\eta/\beta_c) \qquad (44)$$

For electrode reactions where this ratio is 0.3 or less, activation control operates. When the ratio is 1.0 or greater, the electrode reaction is under transport control.

Inspection of Equation 44 underlines the relative importance of various parameters in the study of electrode reactions. It is evident that the analysis of activation controlled electrochemical data for reactions with large exchange current densities is restricted to a small range of overpotential unless the mass transfer coefficient is large. The mass transfer coefficient is generally large for experimental arrangements like rotating disks, rotating cylinders and other systems capable of achieving high fluid velocity rates (9). On the other hand, if one wants to study the region of mass transport control, it is necessary to operate at large (negative, in the case of cathodic reactions) overpotentials and low concentrations of the reactant species. However, this

approach is not without its difficulties (9), e.g., the appearance of a second electrode reaction may influence the data.

Electrochemical Kinetics of Corrosion Processes

Mixed Potential Model of Corrosion.

Metallic corrosion processes which are chemical in nature (see above) can be written in the following general form

$$M + Ox_{env} \rightarrow M^{z+} + Red_{env} \quad (45)$$

where M represents the metal, M^{z+} represents an oxidized form of the metal (for convenience, it is written as a metallic ion), Ox_{env} represents the species in the aqueous solution which reacts with the metal in the corrosion reaction and Red_{env} is the modified form of that species. Inspection of Equation 45 shows that it is composed of two electrochemical partial reactions, i.e.,

$$M \rightarrow M^{z+} + ze^- \quad (46)$$

and

$$Ox_{env} + ze^- \rightarrow Red_{env} \quad (47)$$

The anodic partial process, Equation 46, generates the electrons which are used in the cathodic partial process, Equation 47. This model of corrosion processes is based on the theory of mixed potentials (11) and is shown schematically in Figure 9. The original theory of mixed potentials was based on the "superposition" of polarization curves for the respective partial processes (11-13). However, since many mixed potential systems (particularly corrosion processes) involve interactions among the reactants, the presentation of mixed potentials given here will consider the more recent approach considering these interactions (14).

Metals where corrosion processes take place are usually isolated, i.e., not in contact with an external electrical circuit. Charge conservation is the necessary condition for a mixed potential process to lead to corrosion on an isolated metal, i.e.,

$$\Sigma A_j i_j(\phi_{corr}) = 0 \quad (48)$$

In Corrosion Chemistry; Brubaker, G., et al.;
ACS Symposium Series; American Chemical Society: Washington, DC, 1979.

where A_j is the surface area where the "jth" partial process operates, $i_j(\phi_{corr})$ is the current density of the "jth" partial process at the electrode potential for the isolated electrode, i.e., corrosion potential, ϕ_{corr}. Equation 48 represents an operational definition of the corrosion potential, i.e., that electrode potential where the sum of the partial currents in a corrosion process is zero. This definition is similar to that for an equilibrium potential. However, the essential difference between equilibrium and mixed potentials is that of inventory of the reactant and product species - mixed potential systems necessarily involve changes in this inventory.

For uniform corrosion, i.e., the entire surface is accessible to the metal oxidation reaction and the environmental reaction(s), Equation 48 becomes

$$\Sigma i_j(\phi_{corr}) = 0 \qquad (49)$$

Equation 49 will be used subsequently to develop expressions for the corrosion current density for specific examples of corrosion systems.

When a metal electrode is made part of an electrical circuit (see below), the net current density, i.e., i=I/A, at a perturbed potential, ϕ_i, in uniform corrosion is

$$i = \Sigma i_j(\phi_i) \qquad (50)$$

Equation 50 will be used subsequently to develop electrochemical rate equations for specific examples of corrosion systems.

Two Activation Controlled Partial Processes.

When there are two partial process in a mixed potential system and both are under activation control, the most probable forms of the current densities of the anodic and cathodic partial processes are Equations 33 and 35, respectively. For an isolated metal, the overpotential (since the corrosion potential represents the perturbed electrode potential in this case) is

$$\eta = \phi_{corr} - \phi_o \qquad (51)$$

Substituting the appropriate forms of the respective current densities for the partial processes and this definition in Equation 49, one obtains

In Corrosion Chemistry; Brubaker, G., et al.;
ACS Symposium Series; American Chemical Society: Washington, DC, 1979.

$$i_{oa}\exp((\phi_{corr}-\phi_{oa})/\beta_{aa}) - i_{oc}\exp((\phi_{oc}-\phi_{corr})/\beta_{cc}) = 0 \quad (52)$$

where the additional subscripts, a and c, denote the properties of the respective partial processes. The exchange current densities in Equation 52 have mathematical forms similar to Equation 31. If interactions among the reactants are present (14), the interacting species behave like catalysts.

The first term in Equation 52 is proportional to the rate of metal dissolution at the corrosion potential, i.e., the corrosion rate. Therefore, a measure of the corrosion rate is the corrosion current density, i_{corr}, which is defined for this case as

$$i_{corr} = i_{oa}\exp((\phi_{corr}-\phi_{oa})/\beta_{aa}) = i_{oc}\exp((\phi_{oc}-\phi_{corr})/\beta_{cc}) \quad (53)$$

A mathematical relationship similar to Equation 31 can usually be obtained experimentally for the corrosion current density.

For a corroding metal which is connected to an electrical circuit (in order to study its electrode potential-current density properties - see below), the overpotential is

$$\eta = \phi_i-\phi_o = (\phi_i-\phi_{corr})+(\phi_{corr}-\phi_o) \quad (54)$$

Substituting the appropriate forms of the respective current densities and this definition in Equation 50, one obtains

$$i = i_{oa}\exp((\phi_{corr}-\phi_{oa})/\beta_{aa})\exp((\phi_i-\phi_{corr})/\beta_{aa}) - i_{oc}\exp((\phi_{oc}-\phi_{corr})/\beta_{cc})\exp((\phi_{corr}-\phi_i)/\beta_{cc}) \quad (55)$$

Noting the definition of corrosion current density, i.e., Equation 53, Equation 55 becomes

$$i = i_{corr}[\exp((\phi_i-\phi_{corr})/\beta_{aa}) - \exp((\phi_{corr}-\phi_i)/\beta_{cc})] \quad (56)$$

For convenience, one may define a parameter called polarization, ε, as

$$\varepsilon = \phi_i-\phi_{corr} \quad (57)$$

In Corrosion Chemistry; Brubaker, G., et al.;
ACS Symposium Series; American Chemical Society: Washington, DC, 1979.

which is the mixed potential analog of overpotential. Inserting Equation 57 in 56 yields

$$i = i_{corr}[\exp(\varepsilon/\beta_{aa}) - \exp(-\varepsilon/\beta_{cc})] \quad (58)$$

Since Equation 58 is identical in form to Equation 30, the analysis of data for mixed potential systems is the same as that for simple electrode reactions.

In studies of reaction mechanisms of the partial processes, the following form of Equation 50 is useful (15)

$$i = nF\{k_a^\circ[\text{Red}]^{\rho_a}[\text{Ox}]^{\omega_a}\exp((\phi_i - \phi_a^\circ)/\beta_{aa}) - k_c^\circ[\text{Red}]^{\rho_c}[\text{Ox}]^{\omega_c}\exp((\phi_c^\circ - \phi_i)/\beta_{cc})\} \quad (59)$$

When data are taken at fixed potential(s) in the respective linear region(s) (the so-called Tafel region) of electrode potential-current density experiments (so-called polarization experiments) with appropriate variation of concentration of one or more of the species, the reaction order(s) of the species may be computed, e.g., for cathodic data,

$$\left(\frac{\partial \ln i}{\partial \ln[\text{Ox}]}\right)_{\phi_i,[\text{Red}],T} = \omega_c \quad (60)$$

With judicious choice of experimental conditions and appropriate analysis of the data, the parameters in Equation 59 can be obtained with relative ease. Once these parameters are specified, the elucidation of the reaction mechanism(s) can be attempted. However, no discussion of reaction mechanisms or the methods used to develop them will be given here.

Illustration 6. Analysis of Activation Controlled Mixed Potential Data.
The data given in the accompanying tables are for iron in sulfuric acid. Determine:
a) the corrosion potentials and the corrosion current densities for the three systems;
b) the specific rate constant and the reaction order for hydrogen ion for free corrosion;
c) the specific rate constants and the reaction orders for hydrogen ion for the partial

processes.

System	$[H^+]$ M	Symbol
A	0.055	○
B	0.100	□
C	0.250	△

ϕ mV vs. SHE	CURRENT DENSITY (A/cm^2) System A	System B	System C
-300	$6.88X10^{-2}$	$3.78X10^{-2}$	$1.51X10^{-2}$
-325	$1.58X10^{-2}$	$8.65X10^{-3}$	$3.35X10^{-3}$
-350	$3.59X10^{-3}$	$1.91X10^{-3}$	$5.89X10^{-4}$
-375	$7.60X10^{-4}$	$3.23X10^{-4}$	$-1.56X10^{-4}$
-400	$7.09X10^{-5}$	$-1.14X10^{-4}$	$-5.08X10^{-4}$
-425	$-1.52X10^{-4}$	$-3.31X10^{-4}$	$-8.80X10^{-4}$
-450	$-3.06X10^{-4}$	$-5.70X10^{-4}$	$-1.44X10^{-3}$
-500	$-8.27X10^{-4}$	$-1.50X10^{-3}$	$-3.76X10^{-3}$
-550	$-2.16X10^{-3}$	$-3.94X10^{-3}$	$-9.84X10^{-3}$
-600	$-5.66X10^{-3}$	$-1.03X10^{-2}$	$-2.57X10^{-2}$

Solutions:

a) The data are plotted in Figure 10. Extrapolation of the Tafel region data to the respective intersections yields:

System	ϕ_{corr}	i_{corr}
A	-406	$1.33X10^{-4}$
B	-390	$1.79X10^{-4}$
C	-367	$2.85X10^{-4}$

where the corrosion potentials are mV vs. SHE_2 and the corrosion current densities are A/cm^2.

b) In order to determine the reaction order of hydrogen ion for free corrosion, plot log i_{corr} vs. log (hydrogen ion concentration) ,i.e., the lowest line in Figure 11. The slope of the line, 0.5, is the reaction order for hydrogen ion under these conditions. To compute the specific rate constant, one notes that

$k°=i_{corr}/nF[H^+]^{0.5}$

where n=2 and $F=9.65X10^4$ A-sec/equiv and k° "contains" the terms associated with "Red".

In Corrosion Chemistry; Brubaker, G., et al.;
ACS Symposium Series; American Chemical Society: Washington, DC, 1979.

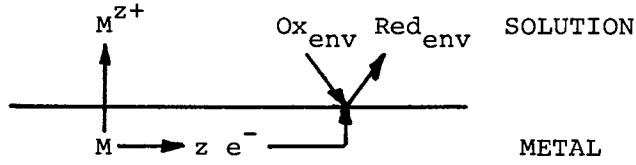

Figure 9. Schematic of corrosion as a mixed potential process

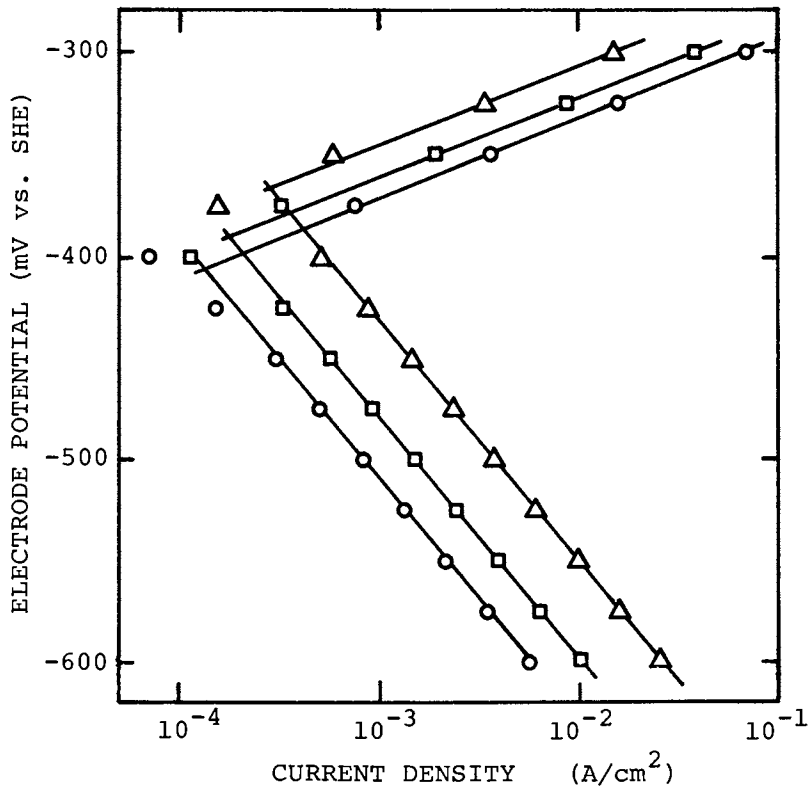

Figure 10. Polarization diagram for data in Figure 6

In Corrosion Chemistry; Brubaker, G., et al.;
ACS Symposium Series; American Chemical Society: Washington, DC, 1979.

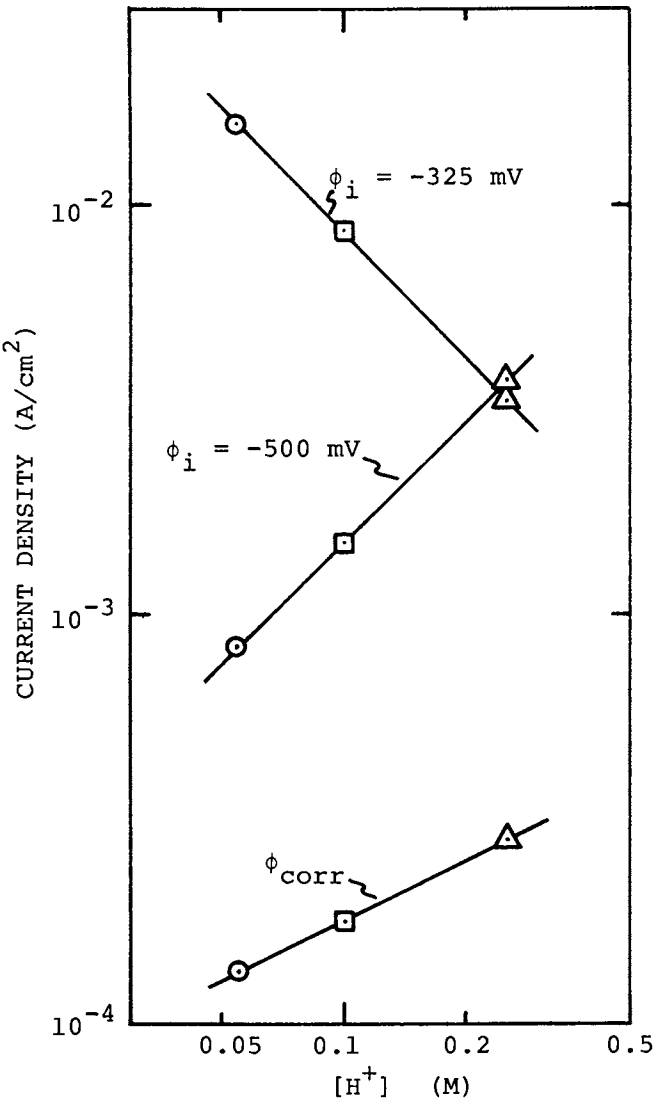

Figure 11. Analysis of data from Figure 10

In Corrosion Chemistry; Brubaker, G., et al.;
ACS Symposium Series; American Chemical Society: Washington, DC, 1979.

Then,

System	k°
A	2.94×10^{-9}
B	2.93×10^{-9}
C	2.95×10^{-9}
mean value=	2.94×10^{-9}

c) In order to determine the reaction orders for hydrogen ion for the partial processes, choose ϕ_i=-325 mV for the anodic partial process data and ϕ_i=-500 mV for the cathodic partial process data. Plot the log $i(\phi_i)$ vs. log$[H^+]$, i.e., the upper pair of lines in Figure 11. The slopes of these lines are the respective reaction orders, i.e., ω_a=-1.0 and ω_c=+1.0. The specific rate constants are computed from (see de Bethune (4) for the standard electrode potentials and Tafel slopes are from Figure 10)

$$k_a^\circ = i_a [H^+]/nF \exp((-325-(-440))/17)$$

and

$$k_c^\circ = -i_c/nF[H^+] \exp((0-(-500))/51)$$

The data for these analyses:

System	i_a A/cm^2	k_a°	$-i_c$ A/cm^2	k_c°
A	1.58×10^{-2}	5.46×10^{-11}	8.27×10^{-4}	4.30×10^{-12}
B	8.65×10^{-3}	5.44×10^{-11}	1.50×10^{-3}	4.29×10^{-12}
C	3.35×10^{-3}	5.27×10^{-11}	3.76×10^{-3}	4.30×10^{-12}

The mean values of the constants are:

$k_a^\circ = 5.39 \times 10^{-11}$ and $k_c^\circ = 4.30 \times 10^{-12}$.

Two Partial Processes - One Under Transport Control.

Mixed potential systems with the cathodic partial process under transport control and the anodic partial process under activation control is typical of many corrosion systems. For the cathodic partial process to be under transport control, Equation 44 must be unity or larger. This occurs when the absolute value of the difference between the equilibrium electrode potential of the cathodic partial process and the corrosion is on the order of one volt. This condition prevails for most metals of interest in corrosion studies if oxygen

In Corrosion Chemistry; Brubaker, G., et al.;
ACS Symposium Series; American Chemical Society: Washington, DC, 1979.

is present in the solution and for many metals when contaminants like ferric and cupric ions are present.

The corrosion current density for this class of corrosion sytems (assuming that the limiting current density for the cathodic partial process is given by Equation 42) is

$$i_{corr} = i_{oa}\exp((\phi_{corr}-\phi_{oa})/\beta_{aa}) = (n/|\nu_{Ox}|)Fk_c[Ox]_b \quad (61)$$

Equation 61 demonstrates that the corrosion rate for this class of systems is controlled uniquely by the by the rate of mass transport. Comparing Equation 61 with Equation 53 reveals that the corrosion potential is defined by the natures of the anodic and cathodic partial processes for Equation 53 while, in the case at hand, the corrosion potential is influenced by the magnitude of the mass transfer coefficient - a property of the convective mass transport condition.

The electrode potential-current density behavior of this type of corrosion system is

$$i = i_{corr}[\exp(\varepsilon/\beta_{aa})-1] \quad (62)$$

Equation 62 predicts Tafel behavior only for anodic (positive) polarization. Cathodic polarization is predicted to be potential independent at large negative polarizations. However, for most corrosion systems, this region of potential independence is small due to the presence of other cathodic partial processes, e.g., solvent decomposition to form hydrogen gas. While these other cathodic partial processes usually do not participate in the corrosion system *per se*, they are manifested in the experimental data and can cause difficulty in analyzing the data. Methods of compensating for these effects have been employed with success (16, 17).

Illustration 7. Evaluation of Mass Transport Controlled Data.

The data given below are for cathodic polarization of iron in 0.01 M sulfuric acid in the presence of 0.53 M ferric ion. Estimate the limiting current density and mass transfer coefficient for the reduction of ferric ion under these conditions.

In Corrosion Chemistry; Brubaker, G., et al.;
ACS Symposium Series; American Chemical Society: Washington, DC, 1979.

$-\phi$ mV vs. SHE	$-i$ mA/cm^2
360	0
380	1.30
400	4.54
450	4.89
500	5.37
550	5.96
600	7.57
650	11.6
700	22.0

Solution:
The data are plotted in Figure 12. Although there is no unequivocally potential independent region, the data between -400 and -550 mV approximate that behavior. The mean value of the current density over this range, 5.2 mA/cm^2, is assumed to be the best estimate of the limiting current density.
The electrode reaction for ferric ion reduction is

$$Fe^{3+} + e^- \rightarrow Fe^{2+}$$

Then, the mass transfer coefficient is

$$k_c = i_{\ell c}/F[Fe^{3+}]_b$$
$$= (5.2X10^{-3})/(9,65X10^4)(5.3X10^{-4}\ mole/cm^3)$$
$$= 1.02X10^{-4}\ cm/sec$$

Multiple Partial Process Corrosion Systems.

Although most corrosion systems can be described by the limiting models presented above, there are instances where control of the corrosion system is a combination of both types, viz., activation controlled anodic partial process with two cathodic partial processes - one under activation control and another under transport control. Examples are iron corrosion in acid solution with inorganic contaminants (16, 18) and oxygen (17). The corrosion current density in such systems is

$$i_{corr} = i_{oa}\exp((\phi_{corr}-\phi_{oa})/\beta_{aa})$$
$$= i_{oc}\exp((\phi_{oc}-\phi_{corr})/\beta_{cc})$$
$$+ (n/|\nu_{Ox}|)Fk_c[Ox]_b \qquad (63)$$

where $[Ox]_b$ is the bulk concentration of the "contam-

In Corrosion Chemistry; Brubaker, G., et al.;
ACS Symposium Series; American Chemical Society: Washington, DC, 1979.

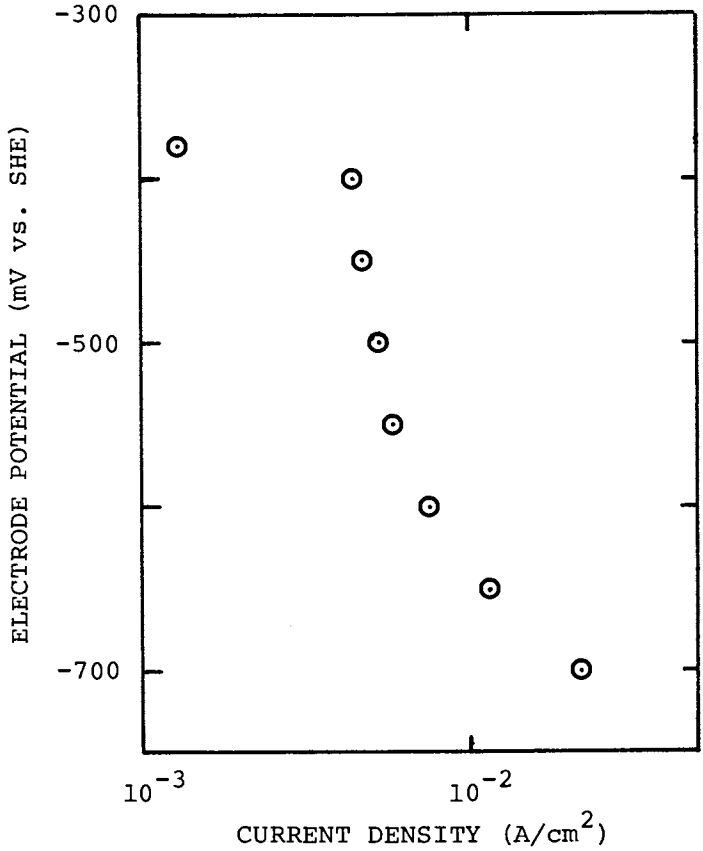

Figure 12. Polarization diagram for data in Figure 7

In Corrosion Chemistry; Brubaker, G., et al.;
ACS Symposium Series; American Chemical Society: Washington, DC, 1979.

inant". It is evident from Equation 63 that such multiple control is a fortuitous combination of properties of the respective cathodic partial processes and, while observed, probably represents a "special case" of the other types of corrosion systems.

Experimental Techniques

Although the other authors in this monograph have described their experimental systems in detail, it is worthwhile to outline the essential features of the experimental electrochemical techniques which are used to measure and evaluate the various parameters discussed in this chapter.

Electrode Potential Measurements.

The methods of measuring electrode potentials in the absence of an externally applied current have been given above. In general, these comments are applicable to polarization experiments, as well. The major difference between "equilibrium" and polarization measurements is that, in the latter case, an ohmic voltage drop is present between the test and reference electrodes due to the flow of current through the resistive electrolyte (between the test and auxiliary - see below- electrodes). In order to minimize this effect (it introduces an error in the measurements which virtually precludes the correct application of, for example, Equation 58), one uses a Luggin capillary (shown schematically in Figure 13). Since no current flows in the voltage measuring circuit (between the test and reference electrodes), the potential of the solution at the tip of the capillary is equal to the solution potential at the reference electrode. Therefore, if the capillary tip is located close to the test electrode, the actual interfacial potential difference can be measured. Barnartt (19) has given a detailed analysis of the effects of such capillaries.

Electrochemical Polarization Systems.

Figure 13 is a schematic representation of the three electrode system normally used in electrochemical polarization studies. This system includes two separate electrical circuits. One of these, between the test and reference electrodes, is a voltage measuring

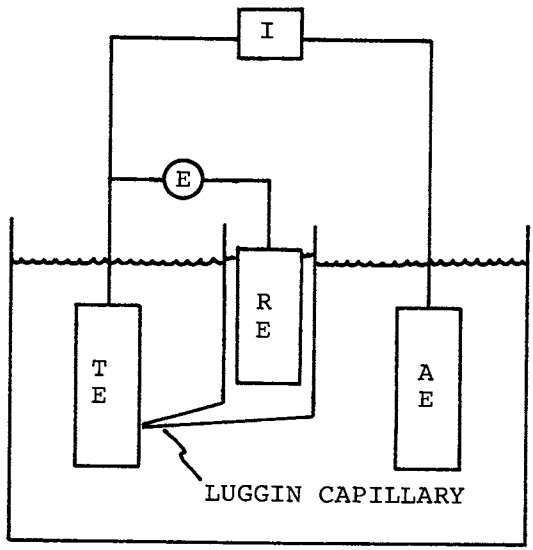

Figure 13. Schematic of electrochemical polarization system

circuit and has been discussed above. The other circuit passes current between the test electrode and an auxiliary electrode (AE). Since the product(s) formed at the auxiliary electrode are electrochemically active and could be transported to the test electrode, the test and auxiliary electrodes are usually maintained in separate compartments with a porous fritted glass disk or ion exchange membrane used to maintain electrolytic transport between the compartments. Normally, the auxiliary electrode is electrochemically inert, e.g., platinum, but, on occasion, the auxiliary electrode is the same material as the test electrode. The container used for these studies should be inert, e.g., glass, teflon, etc. Since the designs for such containers are as diverse as the number of researchers, no recommendations with respect to design will be given here.

Two methods are available to provide current flow between the test and auxiliary electrodes. These are the constant current (galvanostatic) and constant electrode potential (potentiostatic) methods. The former utilizes a constant voltage source with a variable resistance and ammeter in series between the test and auxiliary electrodes. This type of arrangement is simple and can be used for most electrochemical studies. The potentiostatic method is more complex, but is essential for studies where mass transport effects or passivity phenomena are to be studied. Potentiostats (available commercially) operate by comparing the actual potential difference between the test and reference electrodes with a "desired" potential difference and by passing a current between the test and auxiliary electrodes which makes the "difference" zero. Large impedances, particularly in the voltage measuring circuit, should be avoided in systems using potentiostats.

As noted above, potentiostats are particularly suited to the study of mass transport processes and passivity phenomena. In the case of transport processes, the instantaneous flux (current density) of the process can be measured easily in the region of mass transport control while, with galvanostatic experiments, the electrode potential at the limiting current density is unstable and either drifts slowly or oscillates. The utility of potentiostats in passivity studies is demonstrated in Figure 14. The solid curve represents typical data obtained at passivating metals using a potentiostat while the dashed line represents the data in the passive region which one obtains using a galvanostat. It is evident that it

In Corrosion Chemistry; Brubaker, G., et al.;
ACS Symposium Series; American Chemical Society: Washington, DC, 1979.

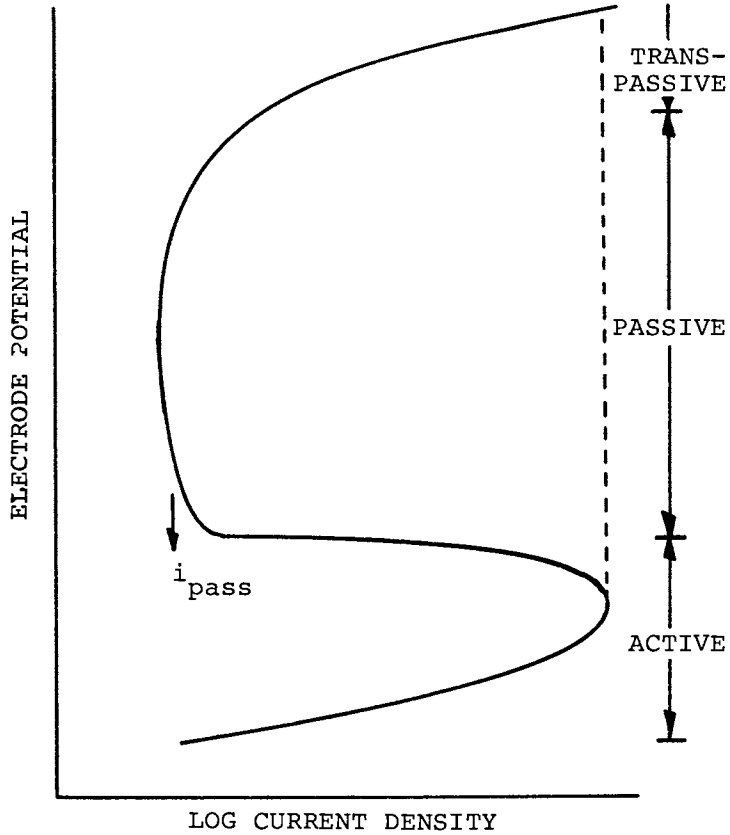

Figure 14. Comparison of potentiostatic (——) and galvanostatic (– – –) data in the passive region for metals capable of passivating during anodic polarization

In Corrosion Chemistry; Brubaker, G., et al.;
ACS Symposium Series; American Chemical Society: Washington, DC, 1979.

is only with a potentiostat that one can measure the passive current density, i_{pass}, (which provides a basis for determining whether anodic protection of a structure is advisable).

Symbols/Nomenclature

Symbol	Significance	Units
A	Surface area	cm^2
a	Activity	-
b	Tafel slope (base "10"	V
Cat	Catalyst in reaction	-
e^-	Electron	-
F	Faraday constant	
	Thermodynamic calculations (=2.31X10^4)	cal/V-equiv
	Kinetic/Transport calculations (=9.65X10^4)	A-sec/equiv
G	Free Enthalpy	cal/mole
H	Enthalpy	cal/mole
I	Current	A
i	Current density	A/cm^2
k	Specific rate constant	(variable)
k_c	Mass transfer coefficient	cm/sec
ℓn	Natural logarithm	-
M	Metal	-
N	Flux	$mole/cm^2sec$
n	Number of electrons in reaction	equiv
Ox	Oxidized form of chemical species	-
R	Gas constant (=1.99)	cal/mole-°K
Red	Reduced form of chemical species	-
T	Temperature	°K
z	Number of electrons in metal oxidation reaction	-
[ ]	Concentration	$mole/cm^3$
β	Tafel slope (base "e")	V
γ	Reaction order of Cat	-
ε	Polarization	V
ϕ	Electrode potential	V
η	Overpotential	V
μ	Chemical potential	cal/mole
ν	Stoichiometric coefficient	mole
ρ	Reaction order of Red	-
ω	Reaction order of Ox	-

In Corrosion Chemistry; Brubaker, G., et al.;
ACS Symposium Series; American Chemical Society: Washington, DC, 1979.

Symbol	Significance	Units
Superscripts.		
°	Standard property	-
z+	Ionic charge on metallion	-
Subscripts.		
a	Property of anode or anodic reaction	-
b	Property of bulk solution	-
c	Property of cathode or cathodic reaction	-
corr	Property at free corrosion	-
e	Property of electron	
env	Property of environment	-
J	Property of reactant species	-
j	Property of "jth" partial process	-
K	Property of product species	-
ℓ	Limiting (maximum) property	-
o	Equilibrium property	-
satn	Property at saturation	-
Y	Property of any chemical species	-
298	Property at 298°K	

Literature Cited

1. Pourbaix, M. "Atlas of Electrochemical Equilibria", Pergamon, Oxford, 1966.
2. - "JANAF Thermochemical Tables", U. S. Department of Commerce, Washington, 1965.
3. Lewis, G. N., Randall, M., Pitzer, K. and Brewer, L. "Thermodynamics", 2nd Edition, pp. 669-686, McGraw-Hill, New York, 1961.
4. de Bethune, A. J., Licht, T. S. and Swendeman, N., J. Electrochem. Soc., (1959), 106, 616.
5. Louthan, M. R. "Process Industries Corrosion", pp. 126-134, NACE, Houston, 1975.
6. Uhlig, H. H. "Corrosion and Corrosion Control", 2nd Edition, pp. 60-91, Wiley, New York, 1971.
7. Vetter, K. J. "Electrochemical Kinetics", Academic, New York, 1967.
8. Welty, J. R., Wicks, C. E. and Wilson, R. E. "Fundamentals of Momentum, Heat and Mass Transfer", pp. 578-589, Wiley, New York, 1969.

In Corrosion Chemistry; Brubaker, G., et al.;
ACS Symposium Series; American Chemical Society: Washington, DC, 1979.

9. Donahue, F. M. "Fundamentals of Electrochemical Engineering", Chapter IX, Engineering Summer Conferences, University of Michigan, Ann Arbor, 1978.
10. Donahue, F. M. "Physicochemical Processes for Water Quality Control", W. J. Weber, Editor, pp. 467-468, Wile-Interscience, New York, 1972.
11. Wagner, C. and Traud, W., Z. Elektrochem., (1938), 44, 391.
12. Stern, M. and Geary, A. L., J. Electrochem. Soc., (1957), 104, 56.
13. Stern, M. J. Electrochem. Soc., (1957), 104, 645.
14. Donahue, F. M., J. Electrochem. Soc., (1972), 119, 72.
15. Donahue, F. M. "Fundamentals of Electrochemical Engineering", Chapter X, Engineering Summer Conferences, University of Michigan, Ann Arbor, 1978.
16. Makrides, A. C., J. Electrochem. Soc., (1960), 107, 869.
17. Donahue, F. M. and Nobe, K. "Second International Congress on Metallic Corrosion", pp. 916-924, NACE, Houston, 1966.
18. Gatos, H., Corrosion, (1956), 12, 322t.
19. Barnartt, S., J. Electrochem. Soc., (1961), 108, 102.

RECEIVED September 1, 1978.

3

High-Temperature Corrosion

J. BRUCE WAGNER, JR.

Center for Solid State Science, Arizona State University, Tempe, AZ 85281

The purpose of this review paper is to survey the principles of high temperature oxidation or high temperature corrosion. A typical situation is that of a metal exposed to a hot gas which can act as an oxidant. In many cases the oxidation product forms a layer which separates the reactants, the metal and the gas atmosphere. Under special conditions, the kinetics are diffusion controlled, i.e., the rate of the reaction (the rate of oxide thickness growth) depends on the diffusion of species, ions and electrons, through the layer (sometimes called a tarnish layer). Actually when a metal or alloy is exposed to a corrosive gas, the reaction kinetics may be controlled by one or more of the following steps:

1. Transport of reactant gases to the surface.
2. Transport of reactants (or products) through a boundary layer adjacent to the surface.
3. A surface controlled reaction (phase boundary reaction) at the gas-metal interface.
4. Transport of reactants through a corrosion product layer either by bulk diffusion or by migration through cracks and pores.

In the present paper, attention will be focused on the fourth step involving bulk diffusion. This is a classical electrochemical situation involving an anode (the metal) where oxidation occurs and a cathode (the oxide at the oxide-gas interface) where reduction of oxygen occurs. The oxide layer acts as the solvent for point defects which diffuse through it as will be discussed below. Consider the diagram shown in Figure 1. The oxide layer thickens with time and so the rate of oxidation (governed by diffusion through the oxide layer) decreases with time, t. This special situation yields the parabolic rate law first reported by Tamman (1) and by Pilling and Bedworth (2). Tamman's rate equation was stated in terms of tarnish layer thickness, ΔX,

0-8412-0471-3/79/47-089-076$05.00/0

and is

$$\frac{d\Delta X}{dt} = k_T/\Delta X \qquad (1)$$

whence

$$(\Delta X)^2 = 2k_T t \qquad (2)$$

where k_T is the Tamman rate constant with dimensions of cm^2/sec. The Pilling-Bedworth rate equation was expressed in terms of weight change per unit area, $\Delta m/A$. It is

$$\left(\frac{\Delta m}{A}\right)^2 = k_P t \qquad (3)$$

where k_P is the Pilling-Bedworth rate constant with dimensions of gm^2/cm^4 sec.* These equations describe a parabolic law as is shown schematically in Figure 2.

Originally it was thought that oxidation proceeded by the migration of oxygen molecules through the product layer to the metal. A classic experiment known as marker movement was performed by Pfeil (3) in 1929 which in principle can distinguish whether the migrating species occurs from the gas atmosphere inward or from the metal outward through the oxide. (Fig. 3) Pfeil placed some inert oxide particles (markers) on the metal surface (iron) prior to oxidation. After oxidation had proceeded for some time, he examined the cross sections of the samples and determined the location of the inert oxide particles, the markers. It was found on iron that the particles remained at the metal-oxide interface indicating that the migrating species were the iron atoms diffusing from the metal-oxide interface to the oxide-gas interface. If the markers remained at the oxide-gas interface, then the inference would be that oxygen would have migrated inward towards the metal. These limiting cases can be visualized by imagining the moving atomic species as imparting momentum to the marker as they move past them. It

---

* The two rate constants are related by

$$k_T = \tfrac{1}{2}\left[\frac{|z_O|v}{A_O}\right]^2 k_P$$

where z_O denotes the valence of the oxidant (oxygen in the example), v the equivalent volume of the oxide, and A_O the atomic weight of the oxidant.

In Corrosion Chemistry; Brubaker, G., et al.;
ACS Symposium Series; American Chemical Society: Washington, DC, 1979.

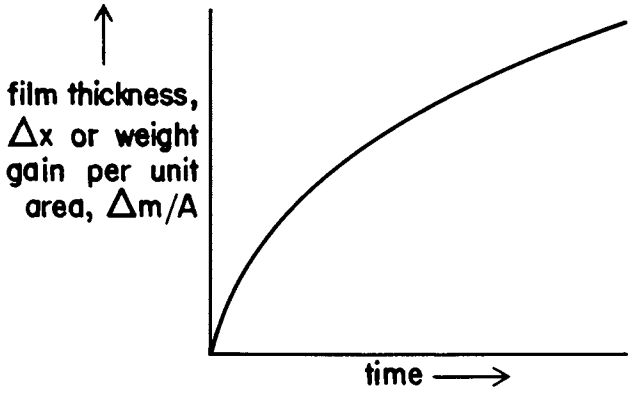

Figure 1. Schematic of film thickness or gain in weight per unit area vs. time for oxidation of a pure metal where diffusion is rate controlling. The kinetics are denoted as parabolic oxidation kinetics.

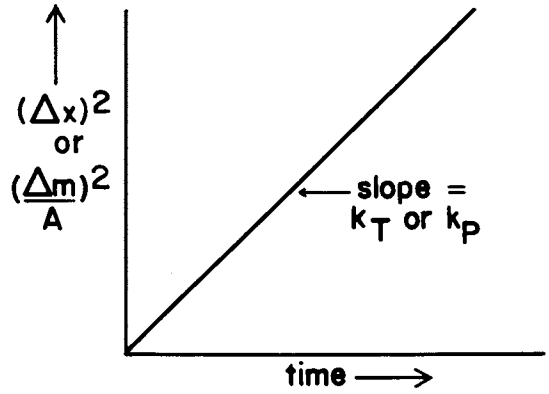

Figure 2. Schematic of parabolic oxidation kinetics replotted from data of Figure 1

In Corrosion Chemistry; Brubaker, G., et al.;
ACS Symposium Series; American Chemical Society: Washington, DC, 1979.

remained for Carl Wagner (4) to perform the classic experiment to distinguish the mobile species in a corrosion experiment. His experimental set-up is shown in Figure 4. The overall reaction he studied was

$$2Ag(s) + S(l) = Ag_2S(s).$$

His set-up provided an artificial reaction product layer of two preweighed silver sulfide pellets separating the reactants, liquid sulfur and the silver pellet which was also preweighed. After one hour all the pellets were reweighed. The pellet adjacent to the liquid sulfur had gained 124 mg while the pellet adjacent to the silver had not changed weight but the silver pellet had lost exactly one milliequivalent of weight (108 mg). Thus for this system, silver migrates from the silver pellet through both silver sulfide pellets and the reaction occurs primarily at the silver sulfide-sulfur interface.

The mechanism of diffusion through the corrosion product was still to be decided. C. Wagner proposed (4) that the migrating particles involved ions and electrons, the ions migrating via defects. These lattice defects may be missing cations or anions (vacancies) or cations or anions located in interstitial positions. The state of stoichiometry, i.e., strict adherence to Dalton's law is not usual in most inorganic compounds and the attainment of this state occurs only at well-defined temperatures and chemical potentials of the constituents. Kröger and Vink (5) developed a notation for point defects whereby all the ions of usual charge on usual lattice sites are denoted without charges while the defects, vacancies or interstitials, exhibit a charge relative to these ions on usual sites. Superior primes denote negative charges and superior heavy dots denote positive charges. Consider an oxide, MO, wherein both ions are normally divalent. The disorder in stoichiometric crystals may be classified in the following limiting cases and an equilibrium constant (a function of temperature only) relates the concentrations of each as follows:

1. Schottky Disorder: Equal concentrations of cation vacancies and anion vacancies

$$K_S = [V''_M][V^{\cdot\cdot}_O] \quad (4)$$

2. Frenkel Disorder: Equal concentrations of cation vacancies and interstitial cations

$$K_F = [V''_M][M^{\cdot\cdot}_i] \quad (5)$$

3. Anti-Schottky Disorder: Equal concentrations of cation

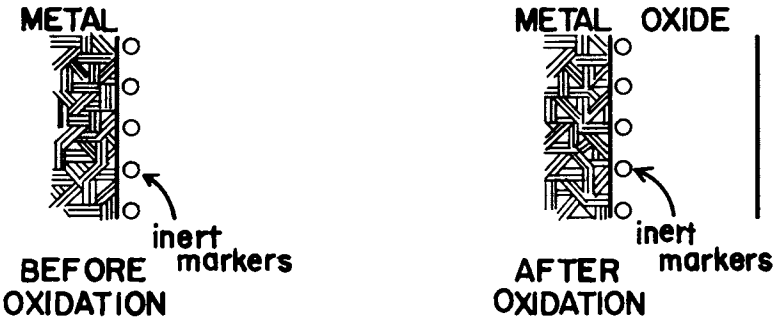

Figure 3. Schematic location of inert markers before oxidation (on the surface of the pure metal) and after oxidation (at the metal–metal oxide interface). From this limiting case one may infer that the mobile species diffuses from the metal–metal oxide interface outward through the scale or tarnish layer. If the marker were found at the oxide–gas interface, the inference would be that the mobile species diffused from the oxide–gas interface to the metal–oxide interface.

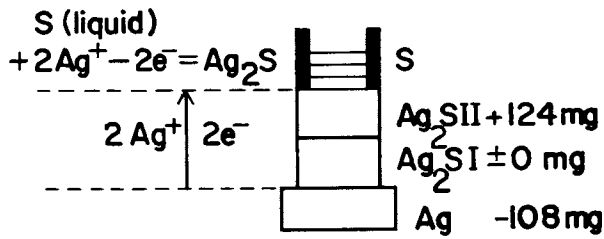

Figure 4. Schematic of the experimental setup used by C. Wagner (4) to determine the location of the reaction $2Ag + S = Ag_2S$ and the migrating species (silver) through the artificially prepared tarnish layer of Ag_2S separating the reactants, silver and liquid sulfur

In Corrosion Chemistry; Brubaker, G., et al.;
ACS Symposium Series; American Chemical Society: Washington, DC, 1979.

and anion interstitials

$$K_{A\text{-}S} = [O_i''][M_i^{\cdot\cdot}] \tag{6}$$

4. Anti-Frenkel Disorder: Equal concentrations of anion vacancies and anion interstitials

$$K_{A\text{-}F} = [O_V^{\cdot\cdot}][O_i''] \tag{7}$$

5. Anti-Structural Disorder: Cations located on anion sites and anions on cation sites

$$K_{\text{Anti-Str.}} = [M_O^{\cdot\cdot}][O_M''] \tag{8}$$

The above considerations apply to stoichiometry. For non-stoichiometric compounds, the excess or deficit of a component may also be expressed by equilibrium constants and chemical equations.

In view of the limitations of space, consider a few selected examples. The oxidation of cobalt is one of the better studied systems. Cobaltous oxide is a metal deficit compound. The ratio of Co to O is less than one. At a given temperature the equation for this situation may be written as

$$\tfrac{1}{2}\,O_2(g) = O_O + V'_{Co} + h^{\cdot} \tag{9}$$

where the notation of Kröger and Vink is again used.

Superior primes and heavy dots denote effective negative and positive charges, respectively. Ions on normal lattice sites are designated with no effective charge while defects are designated with effective charges relative to the normal ions. Thus a nickelous ion on a normal site in nickel oxide is denoted as Ni_{Ni} and a nickelic ion in NiO would be denoted as $Ni^{\cdot}_{Ni}$. The "extra" oxygen is accomodated on a normal lattice site and a cobalt ion vacancy (with a single effective negative charge) plus one compensating electron hole is formed. An alternative description of the electron hole is a cobaltic ion (Co^{+++} or $Co^{\cdot}$) situated in a sublattice of normally cobaltous ions. The equilibrium constant for Eq. (9) is written as

$$K_{10} = [V'_{Co}][h^{\cdot}] / p_{O_2}^{\frac{1}{2}} \tag{10}$$

$$K_{10} = \exp(-\Delta\bar{G}^{M}_{\frac{1}{2}O_2}/RT)$$

$$= \exp[(-\Delta\bar{H}^{M}_{\frac{1}{2}O_2} + T\Delta\bar{S}^{M}_{\frac{1}{2}O_2})/RT] \tag{11}$$

where $\Delta\bar{G}^{M}_{\frac{1}{2}O_2}$, $\Delta\bar{H}^{M}_{\frac{1}{2}O_2}$ and $\Delta\bar{S}^{M}_{\frac{1}{2}O_2}$ denote the partial molar free energy, enthalpy and entropy of dissolution of one-half mole oxygen into cobaltous oxide. In view of the requirement of electrical neutrality in the oxide $[V'_{Co}] = [h^{\bullet}]$. Consequently,

$$K_{10} = [V'_{Co}]^2 / p_{O_2}^{\frac{1}{2}} = [h^{\bullet}]^2 / p_{O_2}^{\frac{1}{2}}. \qquad (12)$$

Thus if one solves explicitly for the cation vacancy concentration or the electron hole concentration,

$$[h^{\bullet}] = [V'_{Co}] = \sqrt[3]{K_{10}}\, p_{O_2}^{\frac{1}{4}}$$

$$= p_{O_2}^{\frac{1}{4}} \exp\left(-\frac{\Delta\bar{H}^{M}_{\frac{1}{2}O_2}}{2RT} + \frac{T\Delta\bar{S}^{M}_{\frac{1}{2}O_2}}{2RT}\right). \qquad (13)$$

Because $D_{Co} \propto [V'_{Co}]$ then if one measured the radio tracer diffusion of cobalt in CoO, the isothermal oxygen pressure dependence should exhibit a one-quarter dependence. This is exactly what Carter and Richardson (6) did. Their results are shown in Figure 5. The electronic conductivity, σ, is

$$\sigma = [h^{\bullet}]\, u_h\, q \qquad (14)$$

where the symbol u_h denotes the mobility of an electron hole and is here assumed not to be dependent on composition. Because $[h^{\bullet}] \propto p_{O_2}^{\frac{1}{4}}$ then the isothermal electronic conductivity should also be dependent upon the one-quarter power of the oxygen pressure. This behavior was reported by Eror and Wagner (7) (see Figure 6). The diffusivity of oxygen is negligible compared to cobalt according to marker studies (8,9) and to stable oxygen isotope diffusion studies (10,11). Thus when cobalt is oxidized, the migrating species should be cobalt via cation vacancies and electrons (as electron holes).

For an oxide growing on a metal by a bulk diffusion controlled process, C. Wagner (4) derived an expression for the flux as

$$\frac{\dot{n}}{A}\ \frac{eq}{cm^2\,sec} = \frac{RT}{\Delta X\, F^2\, 2} \int_{p'_{O_2}}^{p''_{O_2}} \frac{(t_1 + t_2)\, t_3\, \sigma}{|z_2|}\, \frac{dp_{O_2}}{p_{O_2}} \qquad (15)$$

In Corrosion Chemistry; Brubaker, G., et al.;
ACS Symposium Series; American Chemical Society: Washington, DC, 1979.

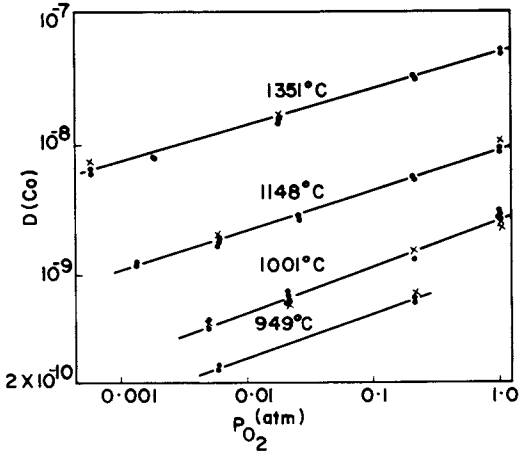

Journal of Metals

Figure 5. Tracer diffusion in cobaltous oxide as a function of oxygen pressure [and hence Co/O ratio given by Equations 9 and 13]. The symbols (×) denote data obtained by a sectioning technique while (●) denote data by the surface decrease method. The slopes of the lines are approximately one-fourth, indicating the existence of singly ionized cation vacancies (6).

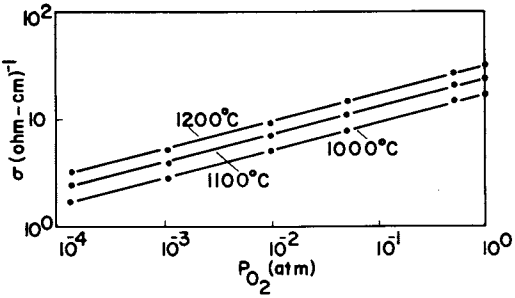

Journal of Physics and Chemistry of Solids

Figure 6. Electronic conductivity of cobaltous oxide single crystals as a function of oxygen pressure. The slopes of the lines are approximately one-quarter, indicating the eixstence of singly ionized cation vacancies and compensating electron holes (7).

where the flux $\dot{n}/A$ is the rate of oxide formation per unit area, F is Faraday's constant, N_o is Avogadros number, q is the electronic charge, t denotes a transference number and the subscripts 1, 2 and 3 denote the metal ion, the oxygen ion and electron, respectively. The total electrical conductivity is σ. Local equilibrium is assumed to occur at the metal-oxide interface and also at the oxide-gas interface. Therefore, the chemical potential of oxygen is fixed at each interface. The oxygen pressure at the metal-oxide interface is fixed as the dissociation pressure of the oxide and denoted as p'_{O_2}. The oxygen partial pressure in the gas phase, p''_{O_2}, is at equilibrium at the oxide-gas interface. (See Figure 7) This equation may be written as

$$\frac{\dot{n}}{A} = \frac{k_r}{\Delta X} \tag{16}$$

where k_r is the rational rate constant* expressed as eq/cm -sec. In other words, the flux is inversely proportional the film thickness--just the requirement of the parabolic rate law. When $t_3 \gg t_1$ or t_2, (the oxide is primarily an electronic conductor) the equation may be rewritten using the Nernst-Einstein equation,

$$D_i^S = B_i\, kT = \frac{u_i}{|z_i| q}\, kT. \tag{17}$$

Here B_i is the absolute mobility of the ith species, u_i the drift mobility, D_i^S the self diffusion coefficient and the other terms have their usual significance. It follows that

$$\frac{\dot{n}}{A} = \frac{C_{eq}}{2\ \Delta X} \int_{p'_{O_2}}^{p''_{O_2}} \left[\frac{z_1}{|z_2|}\ D_1^S + D_2^S\right] \frac{dp_{O_2}}{p_{O_2}} = \frac{k_r}{\Delta X} \tag{18}$$

where C_{eq} denotes the number of equivalents of oxide per cc. Particular note is made of the fact that the transport numbers and the diffusion coefficients are behind the integral because the parameters depend decisively on the metal-to-oxygen ratio and hence on the effective value of the oxygen potential. The valence of the cation and anion, z_1 and z_2 are behind the integral.

---

* The rational rate constant, k_r, is related to the Tamman rate constant,

$$k_r = k_T/v.$$ (See footnote on Page 2)

In Corrosion Chemistry; Brubaker, G., et al.;
ACS Symposium Series; American Chemical Society: Washington, DC, 1979.

Frequently, the values of D_1^s and D_2^s are very dissimilar and one term in brackets Eq. (18) may be neglected. For example, in the case of the oxidation of cobalt, it was noted earlier that $D_{Co}^s \gg D_O^s$ in CoO. Consequently, the second term in brackets may be neglected and

$$k_r \cong \underline{\text{constants}} \int_{p'_{O_2}}^{p''_{O_2}} \left|\frac{z_1}{z_2}\right| D_1^s \, d \ln p_{O_2}. \qquad (19)$$

Often authors plot the logarithm of the parabolic rate constant (usually k_P or k_T) versus log p''_{O_2} and infer from the oxygen pressure dependence ($\pm 1/n$) a mechanism. If one mechanism dominates across the oxide layer, that is, one mechanism is predominate between p'_{O_2} and the upper limit for p''_{O_2}, then

$$k_r \propto [p_{O_2}''^{\pm\frac{1}{n}} - p_{O_2}'^{\pm\frac{1}{n}}] \qquad (20)$$

where the value of n and its sign will depend on the type of defects in the oxide. For p-type oxides such as cobaltous oxide, $1/n = +1/4$, for cuprous oxide $1/n = +1/8$, etc. For an n-type oxide such as ZnO, $p_{O_2} = -1/4$. Details of the defect structure of many compounds may be found, for example, in the book by Kröger (12).

Note that an increase in oxygen pressure (p''_{O_2}) results in an increase in oxidation rate. However the sign of the exponent on the oxygen pressure in Eq. (20) exerts a large effect. For cobaltous oxide, $1/n = +1/4$. An increase in oxygen results in an increase in the concentration of cation vacancies and a consequent increase in oxidation rate. But for some metals, the change in oxidation rate with oxygen pressure is small. For example, zinc oxide growing on zinc metal. The dominant defects in zinc oxide are singly ionized zinc interstitials and compensating electrons (i.e., Zn/O > 1). The equation may be written as

$$ZnO = Zn_i^{\bullet} + e' + 1/2\ O_2. \qquad (21)$$

The corresponding equilibrium constant is

$$K_{22} = [Zn_i^{\bullet}][e'] \cdot p_{O_2}^{\frac{1}{2}} \qquad (22)$$

and electroneutrality condition is

$$[Zn_i^{\bullet}] = [e'] \qquad (23)$$

In Corrosion Chemistry; Brubaker, G., et al.;
ACS Symposium Series; American Chemical Society: Washington, DC, 1979.

so that

$$[Zn_i^{\bullet}] = \sqrt{K_{22}} p_{O_2}^{-\frac{1}{4}}. \quad (24)$$

Hence, increasing the oxygen pressure over zinc oxide growing on zinc metal affects the oxidation rate very little because diffusion through zinc oxide is via interstitial zinc ions. These limiting cases are shown schematically in Figure 8 (13).

The temperature dependence of the kinetics at constant oxygen pressure is often plotted as log k_P or log k_T versus 1/T. In addition to the migration enthalpy of the mobile species, the slope of such an Arrhenius plot may reflect an enthalpy for the change in composition of the oxide with temperature.

The oxidation rate of a pure metal may be calculated from self diffusion data. Conversely, oxidation kinetics may be used to calculate self diffusion data. Eq. (18) may be rearranged and the rate constant differentiated with respect to log oxygen pressure to yield

$$\left\{\frac{z_1}{|z_2|} D_1^S + D_2^S\right\} = \frac{\text{const.}}{C_{eq}} \frac{d k_r}{d \ln p_{O_2}} \quad (25)$$

When $D_1^S \gg D_2^S$ and $z_1 = z_2$, the equation may be simplified. Moreover the practical scaling constants may be introduced into Eq. (25) to yield

$$D_1^S = \text{constant} \frac{d k_P}{d \log p_{O_2}}. \quad (26)$$

Thus if one measures k_P (or k_T) as a function of oxygen pressure and plots the data as k_P (or k_T) versus log p_{O_2}'', the tangent to the curve generated yields a value of D_1^S at any fixed p_{O_2}''. Such procedures have been used by F. S. Pettit [FeO (14)], K. Fueki and J. B. Wagner [NiO (15), MnO (16)] and by S. Mrowec and coworkers [CoO (17, 18), Cu_2O (19)]. The agreement between self diffusion data calculated from direct radiotracer diffusion data and those calculated from oxidation kinetics is remarkably good indicating the validity of C. Wagner's theory.

Some metal-oxygen systems exist with more than one stable oxide compound. Examples are CoO and Co_3O_4; FeO, Fe_3O_4 and Fe_2O_3; and Cu_2O and CuO. When oxygen pressures high enough to nucleate a second phase are encountered, the rate of oxidation may be altered dramatically. As an example,

In Corrosion Chemistry; Brubaker, G., et al.;
ACS Symposium Series; American Chemical Society: Washington, DC, 1979.

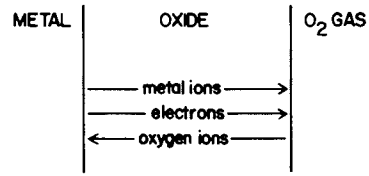

Figure 7. Schematic of transport processes through an oxide layer growing on a metal. Two limiting cases may be distinguished. First, metal ions and electrons may migrate from the metal toward the oxide–gas interface and second, oxygen ions may migrate toward the metal–oxide interface with electrons migrating in the opposite direction. In any volume element of the oxide, electrical neutrality is required. The chemical potential of oxygen is fixed at both the metal–oxide and the oxide–gas interface. The former is fixed by the dissociation pressure of the oxide, p_{O_2}', and the latter by the ambient oxygen partial presure, p_{O_2}''.

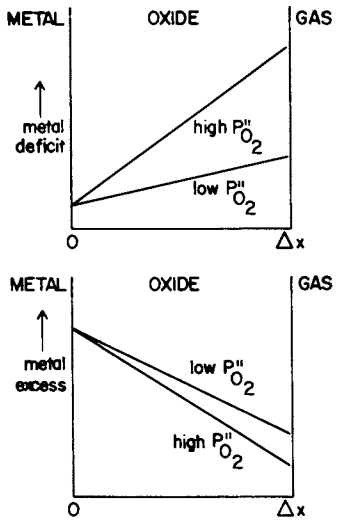

Figure 8. Schematic of the effect of oxygen partial pressure on the concentration of defects in a oxide growing via parabolic oxidation on a metal.

The upper figure shows the effect of increasing oxygen pressure on a metal deficit oxide, e.g., cobaltous oxide. See *Equations 9, 10, 11, 12, and 13. The lattice defects in CoO are* V_{Co}'. *Parabolic oxidation proceeds via diffusion of cobalt ions migrating by means of* V_{Vo}'. *Thus increasing* p_{O_2}'' *exerts a large influence on the oxidation rate of cobalt. The lower figure shows the effect of oxygen partial pressure on a metal excess oxide growing on a metal, e.g., zinc oxide. The lattice predominant defects in ZnO are* Zn_i'. See *Equations 21, 22, 23, and 24. Hence increasing the oxygen pressure does not appreciably affect the oxidation rate* (13).

In Corrosion Chemistry; Brubaker, G., et al.;
ACS Symposium Series; American Chemical Society: Washington, DC, 1979.

consider the oxidation of pure copper to cuprous oxide. The rate of oxidation increases with increasing oxygen pressure until the cupric oxide phase is formed on top of the growing cuprous oxide. In this example oxidation proceeds via diffusion of copper (via singly ionized copper ion vacancies) through the inner oxide. When p_{O_2}'' attains the value for the coexistence of Cu_2O and CuO, the gradient in oxygen activity and cation vacancy concentration is fixed (p_{O_2}' equals the dissociation pressure for Cu_2O or the coexistence oxygen pressure for Cu and Cu_2O). The value of the oxygen pressure at the Cu_2O-CuO boundary is fixed and because diffusion of copper through the Cu_2O is rate limiting, the kinetics become independent of oxygen pressure at this point. This situation is shown schematically in Figure 9.

Oxidation of alloys introduces a higher degree of complexity. When two components are present, each is competing for the oxygen in accord with the free energy of formation of the oxide per gram atom of oxygen. For illustrative purposes, consider again limiting cases. The first is a binary alloy, AB, which is very dilute in one component, e.g., 99.5 at % A and 0.5 at % B. Furthermore, assume the respective oxides, AO_ν and BO_ν form solid solutions. Such alloys of nickel have been extensively studied. When nickel containing small amounts of chromium is oxidized, the oxidation kinetics are more rapid than for pure nickel. The reason is that the small amount of chromium enters the nickel oxide creating a greater concentration of nickel ion vacancies which in turn increases the diffusion of nickel and hence the parabolic oxidation kinetics (20). The relevant equations are as follows. For pure nickel oxide the deviation from stoichiometry is similar to that for cobaltous oxide except that doubly ionized cation vacancies form in pure NiO at elevated temperatures.

$$\tfrac{1}{2}O_2 = O_O + V_{Ni}'' + 2h^\bullet . \qquad (27)$$

$$K_{28} = [V_{Ni}''][h^\bullet]^2 / p_{O_2}^{\frac{1}{2}} . \qquad (28)$$

The electroneutrality condition is

$$[V_{Ni}''] = \tfrac{1}{2}[h^\bullet] \qquad (29)$$

so that

$$[V_{Ni}''] = \sqrt[3]{4k_{28}} \cdot p_{O_2}^{\frac{1}{6}} . \qquad (30)$$

In Corrosion Chemistry; Brubaker, G., et al.;
ACS Symposium Series; American Chemical Society: Washington, DC, 1979.

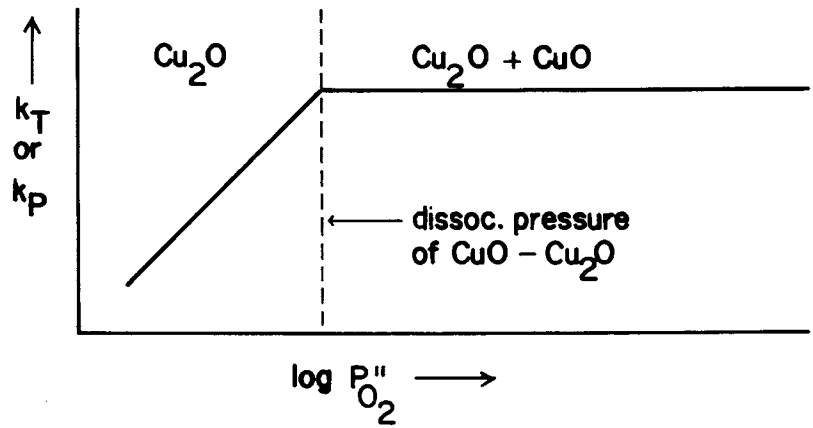

Figure 9. Schematic of the behavior of the parabolic rate constant as a function of oxygen pressure for the oxidation of copper. The rate increases [$1/n = 1/8$, see Equation 20] until the formation of CuO occurs. At that point the chemical potentials of oxygen are fixed both at the Cu–Cu_2O and at the Cu_2O–CuO interface, and the kinetics become independent of external oxygen pressure (13).

For a fixed oxygen pressure, adding a donor ($Cr^{\bullet}_{Ni}$) increases the concentration of cation vacancies according to

$$Cr_2O_3 = 2Cr^{\bullet}_{Ni} + 3O_O + V''_{Ni} \qquad (31)$$

accordingly the oxidation rate increases (20). Conversely, adding an acceptor (Li'_{Ni}) decreases the concentration of cation vacancies and the rate decreases* (20). Such modification of oxidation kinetics has been termed the doping effect by aliovalent additions. The defect chemistry (number and types of lattice and electronic defects) has been tested using chiefly electrical conductivity but also thermogravimetry and diffusion studies on doped crystals. The technique has been used extensively and quantitative predictions can be readily made provided the defect structure of the host lattice is known. For example, in the case of nickel containing small additions of chromium (21)

$$\left[\frac{k_P(\text{Ni-Cr alloy})}{k_P(\text{pure Ni})}\right]_{p_{O_2}''} = \text{const.}$$

$$\cong \frac{\text{mole fraction } Cr^{\bullet}_{Ni} \text{ in doped NiO}}{\text{mole fraction } h^{\bullet} \text{ in pure NiO}} . \qquad (32)$$

This holds for dilute alloys and dilute solid solution of oxides. If higher concentrations of chromium are used, a second phase of Cr_2O_3 may form on the outer surface. Consequently, a situation similar to that discussed above for the formation of CuO on Cu_2O obtains. However, transport through Cr_2O_3 is very slow and that step becomes rate limiting with a concurrent dramatic decrease in oxidation rate of the alloy.

Another limiting case is that of an alloy, AB, which oxidizes to form only one oxide, AO. An example is the nickel-platinum alloy. Platinum doesn't oxidize and only NiO is formed. When a given alloy is oxidized at high temperatures, the formation of NiO uses up the nickel in the surface of the alloy. More nickel must diffuse to the surface from the bulk of the alloy in order to form more NiO. Simultaneously, platinum

---

*The preparation of a Li-Ni alloy is exceedingly difficult owing to vaporization problems. The theory has been tested by vaporizing Li_2O onto the growing NiO as Ni was oxidized. A decrease in oxidation rate was observed. (20)

In Corrosion Chemistry; Brubaker, G., et al.;
ACS Symposium Series; American Chemical Society: Washington, DC, 1979.

must diffuse away from the surface (see Figure 10). The chemical potential of oxygen at the alloy-oxide interface is not fixed but changes slowly with time as the composition of the alloy changes according to

$$\text{Ni (in alloy)} + \tfrac{1}{2}O_2 = \text{NiO} \qquad (33)$$

$$K_{34} = \frac{a_{NiO}}{a_{Ni}p_{O_2}^{\frac{1}{2}}}. \qquad (34)$$

The NiO is pure so its activity is set equal to unity in Eq. (34). However the activity of nickel, a_{Ni}, decreases with time (the alloy becomes more concentrated in Pt) so the oxygen partial pressure at the alloy-NiO interface increases with time (see Eq. (34)). This effect is small and more significant is any change in oxygen pressure at the oxide-gas interface ($p_{O_2}'' \gg p_{O_2}' \neq$ constant). Furthermore, different alloys will oxidize at different rates. For alloys rich in nickel, the kinetics will be almost those of pure nickel. But as the concentration of platinum increases beyond a certain critical value, diffusion of nickel to the metal-metal oxide surface will be rate-determining and a large decrease in oxidation rate will occur, i.e., the rate limiting step will be diffusion in the alloy and not diffusion through the oxide scale.

Another limiting case is an alloy, AB, neither component of which initially reacts to form an external scale and in which component A has a much greater affinity for oxygen than B. A classical example is the silver-indium alloy system. Silver doesn't form an oxide at elevated temperatures, but it does dissolve oxygen. Small amounts of indium will therefore form an oxide within the alloy metal, a so-called subscale or internal oxide. The process is diffusion controlled and the diffusion of oxygen in the alloy is rate limiting. Such systems have been studied extensively by R. A. Rapp, especially the transition from only internal oxidation to the formation of an external scale (22).

When both components of a homogeneous, one phase alloy react with oxygen, there is a competition for the oxygen in terms of the affinity for oxygen as mentioned above. If the oxides so formed are immiscible, the nucleation and growth of each oxide phase as well as displacement reactions must be considered. As an example, consider 85-15 brass (85 wt % copper = 15 wt % zinc) oxidized at 700°C. For the first hour the kinetics are nearly parabolic, i.e., diffusion controlled.

In Corrosion Chemistry; Brubaker, G., et al.;
ACS Symposium Series; American Chemical Society: Washington, DC, 1979.

The free energy of formation for zinc oxide is much more negative than that for cuprous oxide. But transport of ions through Cu_2O is much greater than transport through ZnO. Consequently, cuprous oxide and some zinc oxide forms on this brass and as time proceeds, a displacement reaction occurs (23),

Zn (alloy) + Cu_2O (oxide layer) = ZnO (oxide layer) + 2 Cu (free). This is indicated by the appearance of free copper (pink color) in the cross sections of the samples and a decrease in rate as more ZnO forms with time. Furthermore, if the oxygen is pumped out of the reaction chamber and the sample given an anneal in an inert gas, the subsequent oxidation kinetics in oxygen are drastically reduced (see Figure 11). This large reduction in oxidation kinetics is due to the large proportion of ZnO formed during the anneal in an inert gas and the fact that diffusion through ZnO is slow. The importance of displacement reaction is that an oxide not in contact with the external gas atmosphere can grow by means of a displacement reaction.

As more and more demands are placed on materials for energy production, the diversity of corrosive atmospheres complicates and accentuates the corrosion problems. For example in coal gasification plants and in certain airplane turbine engine applications, mixtures of oxygen and sulfur bearing gases are encountered. Consider a pure metal exposed to a mixed oxidant, e.g., nickel exposed to oxygen and sulfur dioxide. The sulfur dioxide increases the rate of parabolic corrosion. One limiting case has been discussed by Alcock, Hockings and Steele (24). They suggested that sulfur entered NiO and created additional cation vacancies which increased the oxidation rate of nickel. J. B. Wagner (25) suggested the following equation,

$$SO_2(g) = S_O^{\bullet}(\text{in NiO}) + O_2 + e' \qquad (35)$$

and that if sulfur acts as a donor, it affects NiO in the same way as chromium doping, i.e., creates cation vacancies. However, the solubility of sulfur is very small [about 10^{18}/cc (26)] and some reported increases in rates were far in excess of that which Eq. (35) could account for. Worrell (27) made a very important suggestion. In SO_2-O_2 gas mixtures, it sometimes happens that two phase (duplex) scales are formed. These scales consist of thin channels or stringers of sulfide embedded in a matrix of oxide. Because diffusion in the sulfides is so much faster than diffusion in oxides, the rate is determined by diffusion through the channels. This type of

In Corrosion Chemistry; Brubaker, G., et al.;
ACS Symposium Series; American Chemical Society: Washington, DC, 1979.

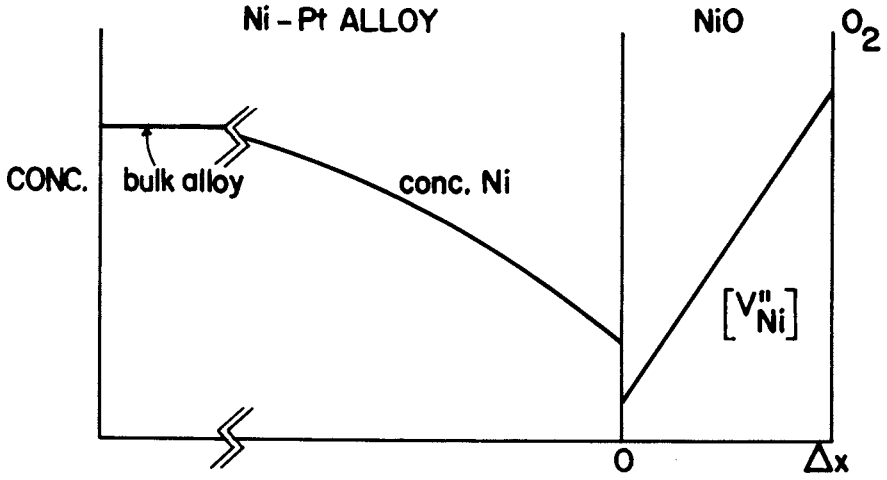

Figure 10. Schematic of the concentration profile of nickel in a Ni–Pt alloy being oxidized to form NiO as a growing oxide scale. The concentration profile of nickel ion vacancies in NiO is also shown. In the example discussed, the rate determining step is the diffusion of nickel from the bulk alloy to the surface (and of platinum in the opposite direction) rather than diffusion of nickel via vacancies in NiO (13).

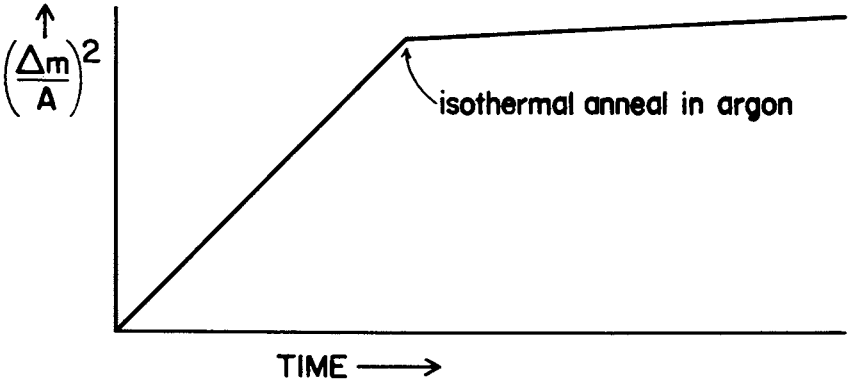

Journal of the Electrochemical Society

Figure 11. Schematic of the oxidation of 85 wt % Cu–15 wt % Zn at 700°C. Initially the kinetics are almost parabolic, and diffusion through a two-phase scale (Cu_2O and ZnO) is rate determining. The displacement reaction, Zn (alloy) + Cu_2O (oxide layer) = 2Cu (free) + ZnO (oxide layer), proceeds continuously. An interrupted anneal in argon allows the displacement reaction to proceed without the uptake of further oxygen from the ambient. Subsequent oxidation proceeds very slowly (23).

parallel diffusion path will be very important in corrosion of multiphase alloys that form multiphase scales.

In the foregoing, limiting cases of various high temperature, isothermal corrosion situations have been briefly discussed. Actually in most engineering uses, the corrosion is not isothermal but involves cyclic thermal treatment (e.g., in a turbine engine). In addition to seeking an oxide scale that will exhibit slow diffusion of the reactants, it is necessary that the oxide resist thermal shock. Most of the protective oxides involve Al_2O_3, Cr_2O_3 or SiO_2. Efforts to increase the adherence of the oxide on the metal have been directed to additions of certain rare earth metal oxides to the metal or alloy. These oxides are usually insoluble in both the metal and the oxide scale. Surprisingly, the small particles of these added oxides often segregate to the metal-oxide boundary where they appear to project up from the metal into the scale with a dramatic increase in resistance to spalling during thermal shock. One suggestion is that the oxide particles act as "pegs" to pin the oxide scale. Other explanations involve changes in the interface chemistry and concurrent adhesion between metal and scale or a change in plasticity of the oxide scale. In any case the effect is important and the most appropriate explanation awaits some challenging surface chemistry and microanalysis.

The foregoing survey was focused on situations where bulk diffusion processes were rate determining. Such systems are amenable to analysis using an electrochemical approach. Other factors such as transport down pores or cracks, volatilization or melting of the oxide scale may occur and require different analyses but diffusion controlled processes may be mathematically modeled and correlated with the defect chemistry of the corrosion product. These limiting cases provide a guide to understanding the more complex phenomena frequently encountered.

Literature Cited

1. Tamman, G., Z. anong. und allgem. Chemie, (1920) 111, 78.
2. Pilling, N. B. and Bedworth, R. E., J. Inst. Metals, (1923) 29, 529.
3. Pfeil, L. B., J. Iron and Steel Inst., (1929) 119, 501.
4. Wagner, C., Z. physik. Chemie, (1933) B21, 25.
5. Kröger, F. A. and Vink, H. J., in "Solid State Physics" (F. Seitz and D. Turnbull, eds) Academic Press, N. Y. 1956.

In Corrosion Chemistry; Brubaker, G., et al.;
ACS Symposium Series; American Chemical Society: Washington, DC, 1979.

6. Carter, R. E. and Richardson, F. D., J. Metals (1954) 6, 1244.
7. Eror, N. G. and Wagner, J. B., Jr., J. Phys. Chem. Solids (1968), 29, 1597.
8. Carter, R. E. and Richardson, F. D., J. Metals (1955) 7, 336.
9. Pettit, F. S. and Wagner, J. B., Jr., Acta Metall. (1964) 12, 415.
10. Chen, W. K. and Jackson, R. A., J. Phys. Chem. Solids (1969), 30, 1309.
11. Holt, J. B., Proc. Brit. Ceram. Soc., (1967), 9, 157.
12. Kröger, F. A., "The Chemistry of Imperfect Crystals," North Holland Publishing Co., Amsterdam, 1964.
13. Wagner, C., mimeographed course notes, course 3.63, Department of Metallurgy, MIT, Spring 1955.
14. Pettit, F. S., J. Electrochem. Soc. (1966), 113, 1249.
15. Fueki, K. and Wagner, J. B., Jr., J. Electrochem. Soc. (1965), 112, 284.
16. Fueki, K. and Wagner, J. B., Jr., J. Electrochem. Soc. (1965), 112, 970.
17. Mrowec, S., Bull. Acad. Polon. Sci., Ser, Sci. Chim. (1967), XV, 373.
18. Mrowec, S., T. Walec and T. Werber, Corrosion Sci. (1966), 6, 287.
19. Mrowec, S. and Stokłosa, Bull. Acad. Polon. Sci., Ser. Sci. Chim. (1970), XVIII, 523; Oxidation of Metals, (1971) 3, 291.
20. Pfeiffer, H. and Hauffe, K., Z. Metallk. (1952), 43, 364.
21. Hauffe, K., "Oxidation of Metals," English Translation by K. Vorres, Plenum Press, N. Y., 1965.
22. Rapp, R. A., Corrosion, NACE (1965), 21, 382.
23. Levin, R. L. and Wagner, J. B., Jr., J. Electrochem. Soc. (1961), 108, 954.
24. Alcock, C. B., Hocking, M. G. and Zador, S., Corrosion Sci. (1969), 9, 111.
25. Wagner, J. B., Jr., in "Defects and Transport in Oxides," (Seltzer, M. S. and Jaffee, R. I., eds.) p. 283, Plenum Press, N. Y., 1974.
26. Chang, D. R., Ph. D. Thesis, Northwestern Univ. 1973.
27. Worrell, W. L., lecture "The SO_2-O_2 oxidation of metals," presented at the U.S. Joint Seminar, "Defects and Diffusion in Solids," October 4-6, 1976, Tokyo, Japan, to be published.

RECEIVED July 6, 1978.

4

Ionic and Electronic Conduction in Nonmetallic Phases

JOHN W. PATTERSON

Engineering Research Institute and Department of Materials Science and Engineering, Iowa State University, Ames, IA 50011

PART I Open Circuit Theory and Parabolic Tarnishing Kinetics

Historical Background

About the turn of the century and shortly thereafter, certain developments in mathematical physics and in physical chemistry were realized which were to prove important in the theory of mass and charge transport in solids, later. Einstein[1] and Smoluchowski[2] initiated the modern theory of Brownian motion by idealizing it as a problem in random flights. Then some seventeen years or so later, Joffee[3] proposed that interstitial defects could form inside the lattice of ionic crystals and play a role in electrical conductivity. The first tenable model for ionic conductivity was proposed by Frenkel[4], who recognized that vacancies and interstitials could form internally to account for ion movement.

Figure 1 is a schematic representation of Frenkel's notion: an atom or ion can get dislodged from its normal site to form an interstitial-vacancy pair. He further proposed that they do not always recombine but instead may dissociate and thus contribute to diffusional transport and electrical conduction. They were free to wander about in a "random walk" manner essentially equivalent to that of Brownian motion . . . this meant they should exhibit a net drift in an applied field.

In the fluids considered by Einstein and Smoluchowski, all species large and small are capable of substantial migration at all times. In solid crystals, however, only the interstitial atoms and those next to vacant sites can enjoy any significant amount of motion. Thus, it was realized that the concentrations of mobile defects are the important things, at least in connection with the ionic conductivity of crystals. An elaborate analysis of thermodynamic equilibria of point defects was then developed by Wagner and Schottky[5-8] in which the laws relating defect concentrations to impurities, ambient partial pressures and temperature were worked out in detail.

Wagner followed this in 1933 by combining virtually all the foregoing concepts to explain the phenomenon of parabolic tarnishing of metal in aggressive environments[9]. He assumed that transport of neutral species was negligible compared to that of ions and

0-8412-0471-3/79/47-089-096$07.50/0

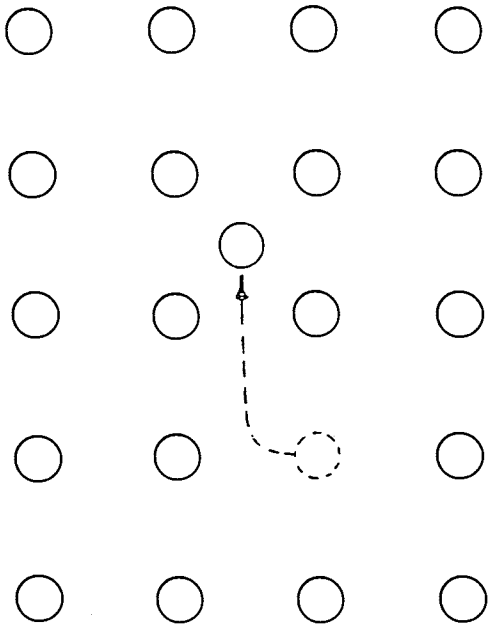

Figure 1. Frenkel defect in a crystal lattice

In Corrosion Chemistry; Brubaker, G., et al.;
ACS Symposium Series; American Chemical Society: Washington, DC, 1979.

electronic carriers, which no doubt must have seemed a rather bold assumption to many others at that time. But beyond that he also assumed that all the charged carriers migrated with Einstein-type mobilities under the combined influences of free energy (i.e., chemical potential) gradients and electric fields. In this way, he was able to transform the problem of parabolic scaling of metals to one of diffusional transport in a electrochemical medium.

The implication of Wagner's theory was that the parabolic scaling rate constants, many of which were known for certain gas-metal combinations, should be quantitatively related to two basic types of information.

A) Thermodynamic information, such as the formation free energy for the scale and partial pressure or activity data for the environment... and

B) Electrical property information for the scaling compound, such as electrical conductivity, ionic and electronic transference numbers or the open circuit emf established over the growing scale.

In addition, the theory predicted that a measurable emf would be established over the tarnishing layer, and moreover, that this voltage could be used to infer the average ionic and electronic transference numbers of the scale. Prior to Wagner's treatment, of course, there had been no reason whatever to think that the electrical properties of the scale compound should bear any relation to oxidation rates, nor was there any reason to think that voltages should appear over these coatings.

And so the metal scaling systems known to exhibit parabolic growth kinetics were soon selected for the critical testing of Wagner's theory. The conductivity-emf-transference number data required by the theory were measured and the scaling rate constant predicted. Then independent measurements of the same scaling constant were obtained, as for example from weight gain measurements and the results compared.(10-12). Astounding agreement was found and much excitement began to spread in corrosion engineering circles because Wagner's theory suggested many ways to possibly control or stop scaling. But this optimism was somewhat overdone because so few practical situations conform to the parabolic scaling prerequisites. Nevertheless, Wagner's theory has been applied and reviewed extensively and this continues up to the present time(13-19)

Presently, the major interest in Wagner's theory derives mainly from the open circuit emf relationships rather than the scaling rate predictions. Only a limited number of the metal scaling systems important to modern technology strictly conform to the conditions required by Wagner's theory, because of various complicating factors (abrasion, thermal gradients, contaminations, and so on). However, a variety of new solid electrolyte materials has been developed for remote sensor applications(20), fuel cell-battery applications(20), and for laboratory investigations of thermodynamic data(21-23). In all of these applications the solid electrolyte element can be expected to perform according to

In Corrosion Chemistry; Brubaker, G., et al.;
ACS Symposium Series; American Chemical Society: Washington, DC, 1979.

Wagner's tarnishing theory but significant modifications are required for the non-open circuit cases[19, 24]. In short, we can say that the present understanding of solid-state electrochemistry is largely due to Wagner's electrochemical theory of tarnishing and moreover that the concepts as he initially elucidated them have remained in tact to the present time. In part II of this paper, less simple mixed conducting phases and non open circuit conditions will be considered

Physical Processes Occurring During Parabolic Scaling

Patterson [19] has given a detailed discussion of Wagner's theory complete with flow-diagram summaries for the derivations of the quantitative formulas. But these derivations are much too elaborate to develop here. We will invoke a simplified model originally put forward by Hoar and Price[25], but this comes later. First let us outline the physical processes that can and do occur in parabolic scaling.

Figure 2 facilitates the physical description by showing the compound M_aX_b (oxide, fluoride, chloride, etc.) attached as a scaling layer to the substrate of metal M on the left. The layer is exposed to an atmosphere containing X_2 gas molecules (O_2, F_2, Cl_2, N_2, etc.) on the right where the X_2 molecules become adsorbed on the surface and eventually get incorporated as ions. Ultimately, however, the scaling rate--whether measured by weight gains or scale thicknesses -- is just the total assimilation rate of X atoms by the scale. This can happen in either of two ways: by combining with cations which emerge at L or by diffusing in as anions.

For simplicity, assume for the moment that only cations are mobile in the scale. Even though no X anions can move, adsorbed X atoms can still be assimilated because M cations can migrate from the other side to combine with the adsorbed gas atoms. Note however, that the scale would grow only at the gas side in this case. On the other hand, if anions are mobile, but cations are not, the adsorption-dissociation process $X_2(g) \rightarrow 2X$ (ads) on the right is followed by anion migration through the scale and growth occurs at the M, M_aX_b interface (left side). These two situations can be distinguished experimentally by identifying markers inside the scale. The apparent change of depth of the marker with time identifies the mobile ionic species.

If the scale is an ionic compound, X_2 molecules, which are neutral, can be incorporated only as anions, which are negatively charged X ions. Conversely, each incorporated M atom must become a positively charged cation. This has important electrochemical consequences because the region at L is forced to become increasingly electron-deficient or positively charged as the negative anions are "formed" and then wander off toward the metal-rich side. Similarly, the metal at the left accrues a surplus of negative charge due to the electrons liberated when M atoms enter the scale as cations.

In Corrosion Chemistry; Brubaker, G., et al.;
ACS Symposium Series; American Chemical Society: Washington, DC, 1979.

Eventually these oppositely charged outside layers cause a very strong coulombic field to build up, but it must be positive on the gas side and negative at the metal side. But of course this polarity necessarily opposes the migration of both anions and cations and increasingly so as the charging continues to build. That is, the incorporation of X atoms by the scale is self defeating if eletrochemical forces are at play. In fact, if there were no electronic leakage paths connecting the two surfaces, all cation and anion migration would soon grind to a halt. At this point, no further weight gain would be observed but an emf on the order of volts would be observed.

However, some degree of internal shorting within scales always occurs because scaling layers always exhibit at least a trace of internal conduction by electronic carriers. For this reason, it is best to think of scales as mixed (ionic and electronic) conductors. The effect of the internal short is to bleed off some of the charge on the surfaces and thus weaken the coulombic field accordingly. This would allow ionic migration to continue indefinitely but at an ever-decreasing rate as the thickness of the scale increases. In principle then, real scaling layers never achieve the completely arrested state alluded to above as a limiting case. Instead, they thicken indefinitely but according to the parabolic law. And since all the mobile species are presumed to be charged, applied electric fields or currents can be used to significantly alter the thickening kinetics and morphologies of mixed conducting scaling systems.

Now if the scale exhibits a large conductivity for electrons (large compared to the ionic conductivity), massive internal shorting occurs and no coulombic retardation of ion movement is possible. In this situation, scaling proceeds as fast as the unhindered ions can diffuse through the scale. And although the growth kinetics will still be parabolic, no perceptible open circuit emf will be found over the scaling layer. This is the limiting case in which electronic conduction dominates in the scale. This limiting case is at the opposite extreme to that in which ionic conduction dominates, as discussed first.

Equivalent Circuit Description of Mixed Conduction in Solids

In essence chemical free energy differences cause the ions to migrate during scaling. This is similar to the way batteries induce current flow in resistors. In parabolic scaling the cations migrate outward to the gas surface while the anions move inwards toward the metal. The molar free energy μ (often called the chemical potential) for the metal is highest at the metal side but very low at the gas surface, and vice versa for the non metal species X or X_2. Thus, every time a mole of metal migrates out from the inside, the total free energy of the entire system drops by the amount

$$\mu_M'' - \mu_M' = \Delta\mu_M \qquad 1$$

In Corrosion Chemistry; Brubaker, G., et al.;
ACS Symposium Series; American Chemical Society: Washington, DC, 1979.

Here as elsewhere below, a double prime indicates the gas side at L whereas a single prime quantity refers to the metal side at zero. Thus, the free energy change of equation 1 is a drop because μ_m'' is very low compared to μ_m' which prevails at the metal interface. By the same token every mole of X passing in the opposite direction changes the free energy inventory by

$$\tfrac{1}{2}\,\mu_{X_2}' - \tfrac{1}{2}\,\mu_{X_2}'' = -\tfrac{1}{2}\,\Delta\mu_{X_2} \qquad 2$$

and is also a decrease as μ_{X_2}'' refers to the gas side.

These free energy drops act as the chemical driving forces which cause the ionic migrations to take place in the first place. They continue to persist but become less and less effective as the coulombic fields build up at the opposite sides of the scale. In any case, we begin to see how an electrical formulation of the chemical process of scaling might become possible. The actual ionic migrations amount to internal electrical currents which are being driven at the expense of the chemical free energy inventory, just as occurs when batteries discharge through a circuit of resistors.

A successful equivalent circuit approach to Wagner's theory was worked out by Hoar and Price[25]. They developed a simple voltage divider circuit which gives quantitative formulas for emf and scaling rate that are very similar to those derived more rigorously by Wagner. A linear lumped version of their proposed circuit is shown in Fig. 3. The subscripts 1, 2 and 3 refer to M cations, X anions and electrons respectively.

The voltages V_1 and V_2 are given by the expressions

$$V_1 = -\,\Delta\mu_M/Z_1F \qquad 3$$

and

$$V_2 = -\,\tfrac{1}{2}\,\Delta\mu_{X_2}/Z_2F \qquad 4$$

Since the valences Z of the cations and anions are always opposite in sign and the two chemical potential differences are always opposed in scaling, it follows that both voltages will have the same sign. As a matter of fact, it can be shown that they are also of precisely the same value for two component scales. This equality, which derives from the so called Gibbs-Duhem relation between μ_1 and μ_2, merely means that the two batteries V_1 and V_2 are equivalent to, and hence may be replaced by, the single one shown dotted-in on the figure.

If voltages V_1 and V_2 simulate the chemical driving forces acting on the ions during scaling, the resistors R_1 and R_2 simulate the scale's resistance to cation and anion migration. Its impedance to electron flow is represented by the single resistor R_3 which is shown connected all the way across the scale thickness. The resistor R_3 simulates the electronic leakage path which weakens the coulombic fields and allows ion migration to continue indefinitely rather than halting. The usual definitional formulas hold

In Corrosion Chemistry; Brubaker, G., et al.;
ACS Symposium Series; American Chemical Society: Washington, DC, 1979.

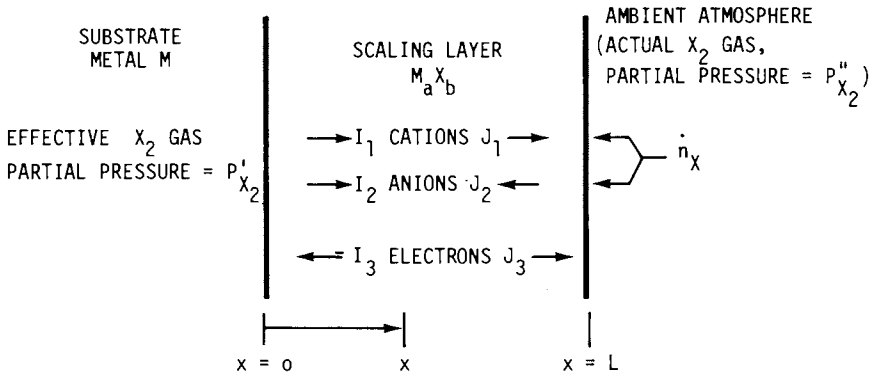

Industrial and Engineering Chemistry,
Product Research and Development

Figure 2. Physical arrangement of a metal (M) undergoing scaling (39)

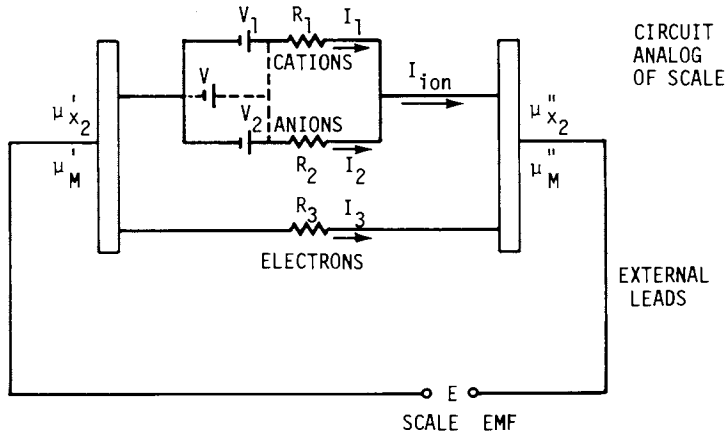

Industrial and Engineering Chemistry,
Product Research and Development

Figure 3. DC circuit analog to simulate scaling according to electrochemical theory (39)

for these resistors

$$R_i = 1/G_i = \frac{1}{\sigma_i}\frac{L}{A} \quad ; \; i = 1,2,3 \qquad 5$$

Here R is in ohms, the conductance G; is in reciprocal ohms. L and A are the scale's thickness (cm) and area (cm^2), respectively, and σ_i is the so called specific partial conductivity for species i in the scale.

Keep in mind that we have not really justified the analog circuit as a valid way to describe the scaling process. As a matter of fact a rigorous justification would probably be a very difficult task involving some very knotty, philosophical, questions. What one can do, however, is to proceed with the model on the tentative assumption that it may work and thus derive as many useful formulas as possible to see how they square with Wagner's more rigorous ones and with experimental results. This is more or less what Hoar and Price did and indeed we can gain a great deal of insight with relatively little effort by using their idea. We will exploit their approach here rather than trying to go through Wagner's more rigorous development, but it is worth mentioning that Wagner himself expressed reservations about the Hoar-Price paper. This appears in the discussion section that followed their presentation before the Faraday Society[25].

Let us consider the open circuit emf E that occurs in scaling. A fairly straightforward dc circuit analysis of Figure 3 leads to the following formula

$$E = [t_1 + t_2]V \qquad 6$$

Here V is the so called thermodynamic voltage and from Equation 4 is found to be

$$V = -\frac{RT}{2Z_2F} \ln \left| P''_{X_2} / P'_{X_2} \right| \qquad 7$$

P''_{X_2} is that of the gas atmosphere while P'_{X_2}, which prevails at the M, M_aX_b interface, is determined by the standard formation free energy ΔG^o_f for M_aX_b. The formula is

$$P'_{X_2} = \exp\left(2\Delta G^o_f / bRT\right) \qquad 8$$

which comes from thermodynamics. The t's are fractional conductances and are called transference numbers. When the common L/A factors are cancelled, they take the form

$$t_i = \sigma_i / \sum_1^3 \sigma_j = \sigma_i / \sigma_T \qquad 9$$

The demoninator here is simply the total electrical conductivity σ_T of the scale. It follows from the way they are defined that the transference numbers summed over all the species must always add up to unity. Accordingly the so called ionic transference

In Corrosion Chemistry; Brubaker, G., et al.;
ACS Symposium Series; American Chemical Society: Washington, DC, 1979.

number is related to the electronic one t_3 in the following way

$$t_{ion} = t_1 + t_2 = 1 - t_3 \qquad 10$$

Now Wagner's expression for the open circuit emf is

$$E = -\int_{'}^{''} [t_1 + t_2]\, d\mu_{x_2}/2Z_2F \qquad 11$$

This appears to be rather different from the Hoar-Price formula given in Equation 6 above, but actually they are almost the same thing. To see the very close similarity we must first realize that we applied the dc circuit analog to the whole scale. But point to point variations in the conductivities and hence transference numbers are possible. Hence, we must apply the analog to each differential thickness and add the results because they are all joined together in series to make up the total scale thickness. With this in mind the emf for each differential element is first obtained, i.e.,

$$dE = [t_1 + t_2]dV \qquad 12$$

where the t values apply only to the element in question. To obtain the overall emf we simply add the contributions from every location in the scale. But note that Equation 4 implies

$$dV = -\tfrac{1}{2}\, d\mu_{x_2}/Z_2F \qquad 13$$

and that the summing of differential increments amounts to nothing more than integrating. Hence, the Hoar-Price equivalent circuit expression for E should really have been written

$$E = \int_o^L [t_1 + t_2]dV \qquad 14$$

But this is virtually identical to Wagner's formula when Equation 13 for dV is considered. In this situation however, the differential resistors which enter into t_1 and t_2 are conceived to vary in value according to the local "voltage", which is unlikely for resistors of any sort. However, we can imagine ways in which the values could depend on the local μ_{x_2} value in a crystal and this is what is really to be done when applying the Hoar-Price approach.

The scaling rate at a given instant can be readily calculated from the sum of the two ionic currents as follows. Assimilation due to the arrival of cations at L would be I_1/Z_1F multiplied by b/a. This must be added to the moles of X that permeate through the scale and this would be $-I_2/Z_2F$. Adding these together and noting the virtual stoichiometry constraint that $Z_1a+Z_2b = 0$, we arrive at

$$\dot{n}_x = [I_1 + I_2]/Z_2F \qquad 15$$

In Corrosion Chemistry; Brubaker, G., et al.;
ACS Symposium Series; American Chemical Society: Washington, DC, 1979.

Here, $\dot{n}_X$ is the total molar acquisition rate of X atoms from the gas atmosphere. But from an analysis of the circuit in Figure 3, the following can be shown

$$-[I_1 + I_2] = I_3 = E/R_3 = \frac{A}{L}\ \sigma_3 E \qquad 16$$

where E is the open circuit emf discussed earlier. But here again the circuit analysis should be applied to each differential element because of point-to-point variations through the scale. When this is done, the E and L in Equation (16) become dE and dl, respectively, so that Equation (15) can now be written as

$$\dot{n}_x = A\ \sigma_3\ \frac{dE}{dx}\ /Z_2F \qquad 17$$

Separating variables, integrating and solving for $\dot{n}_x$ then gives

$$\dot{n}_x = \frac{A}{L}\int_o^L \sigma_3[t_1 + t_2]dV/Z_2F \qquad 18$$

This is to be compared with Wagner's expression for the same quantity which for this case would be

$$\dot{n}_x = \frac{A}{L}\int_{"} \sigma_T\ t_3[t_1 + t_2]\,d\mu_{x_2}/2Z_2^2F^2 \qquad 19$$

where σ_T is the total conductivity of the scale. But these two formulas are again virtually identical because $\sigma_3 = \sigma_T\ t_3$ by definition and because of Equation 13 for dV.

Summarizing the situation concerning equivalent circuit modelling, we cay say that this is a very useful approach and it leads to accurate results and insights if the proper precautions are taken. I think the day will come soon when the theory of mixed conduction will have to be considered in great detail all over again. For example, if solid electrolyte fuel cells and hydrolysis systems are built, their performance characteristics will to a large extent be dictated by mixed conduction processes that take place inside them during operation. It is my view that the equivalent circuit modelling approach-with proper precautions taken will prove to be the most expedient way to extend Wagner's to such closed circuit applications. Keep in mind that the entire development given above applies only to open circuit conditons.

Temperature and Partial Pressure Dependences of Partial Conductivities

In the previous section we saw the key roles played by the various partial conductivities--or equivalently the transference numbers--in mixed conduction theory. They appear prominently in the integrands of the formulas for open circuit emf and scaling rate. Thus, if they exhibit any dependences on partial pressure P_{x_2} which is equivalent to μ_{x_2}, these dependences will have very

In Corrosion Chemistry; Brubaker, G., et al.;
ACS Symposium Series; American Chemical Society: Washington, DC, 1979.

direct effects on the scaling rate and emf values predicted by the theory. In this section a useful scheme for visualizing these dependences is provided.

To begin with we note that the crucial thing here is the dependences of the various partial conductivities on temperature and μ_{X2}. If these could be determined reliably from direct experimental measurements, all the important predictions could be made by merely using those dependences in the integral formulas derived previously. In this sense the defect theory and mass action laws which are used to rationalize the dependences would be of only secondary importance.

However, it is not expedient to rely on measurements only in cases like this because too many would be required. Thus, the theory of defects provides a number of rather general laws concerning the dependences of interest so that far fewer measurements are necessary for us to arrive at many meaningful predictions and useful extrapolations.

Very briefly the conductivities of species in mixed conducting compounds can be written as

$$\sigma_i = c_i \nu_i \ell^2 q_i^2 / kT \qquad 20$$

where c_i is concentration, ν_i is jump frequency, T is temperature and everything else is constant (jump distance l, Boltzmann's k and charge q_i). Thus, the temperature and P_{X2} dependences of the conductivities are due to those of c_i and ν_i. In general ν_i will always exhibit an Arrhenius dependence on temperature because hopping is a thermally activated process. This means ν_i will always go as exp $(-Q/RT)$ where Q is a constant called the activation energy. No dependence of ν_i on partial pressure is expected theoretically and none are found experimentally.

The concentration term has a bit more flexibility for different behaviors: two kinds of temperature dependences (constant or exponential) and two kinds of partial pressure dependences (constant or exponential). Beginning with the temperature dependence, c_i will either be independent of temperature or it will also exhibit an Arrhenius dependence, albeit with a different activation energy than that exhibited by ν_i. If the carrier concentration is fixed by extrinsic contaminations, deliberate or not, it will remain independent of P_{X2}. In some cases however, the concentration may be small enough that incorporation of X atoms from the ambient P_{X2} will cause changes. On the basis of the law of mass-action arguments, etc., these c_i generally vary as P_{X2}^n. Here, n is a constant, usually a ratio of small integers, which ratio is characteristic of the defect reaction whose equilibrium is involved.

The result of all of this is that when individual conductivities are plotted on a log scale versus log P_{X2} and reciprocal absolute temperature 1/T, planar sheets generally always result. This means that only a few measurements (3 minimum) are needed to

In Corrosion Chemistry; Brubaker, G., et al.;
ACS Symposium Series; American Chemical Society: Washington, DC, 1979.

estimate values at other conditions. Figure 4 shows an example of the kinds of dependences that can occur. Note that the various conductivities plot as planar sheets though they are tipped at various angles. Actually, the dependences portrayed in Figure 4 are typical of those found in solid electrolyte materials. The log σ_n and log σ_p sheets are seen to rise up from far beneath the P_{x_2} independent ionic conductivity sheet. Thus, they dominate the total conductivity in the very high and very low P_{x_2} regimes. This means that $t_{ion} = [\sigma_1+\sigma_2]/\sigma_T$ must fall off to zero in these extreme conditions. By considering any particular isotherm of such a three-dimensional plot, we can generate any plot of $[t_1+t_2]/2Z_2F$ vs μ_{x_2} that he may need: as for example to evaluate an open circuit emf in accordance with Equation 11 above. Alternately, he could generate a plot of $\sigma_3[t_1+t_2]/2Z_2{}^2F^2$ vs μ_{x_2} if a prediction of scaling rate from Equation 19 was desired. A more expedient approach would be to simply write the dependences into computer programs which can then carry out the desired integration by standard methods.

Capstone Comments on the Open Circuit Theory of Parabolic Oxidation

We have looked at many aspects of the traditional theory of mixed conduction, but many stones have been left unturned. There are implications for the morphology of scaling layers, why they are so uniform in thickness and why one cannot retain that morphology if he tries to buck the scale emf in an attempt to make it grow thinner. There are many interesting predictions that can be made and tested concerning the morphology of the reaction interface formed when a metallic oxygen "getter" is put in contact with (and hence reduces) the oxide of a more noble metal. Sometimes the interface morphology is planar, sometimes not; however, the criteria for determining this stem mainly from Wagner's theory.

There are the many open circuit emf studies that have been carried out to search for new solid electrolyte materials. The specimen is placed in contact with electrodes which establish different but known partial pressures P_{x_2}'', P_{x_2}' and the emf is measured. The ratio of the measured emf E to the thermodynamic voltage calculated from Equation 7 gives a quick estimate of the materials ionic transference number, as implied by Equation 6 above. This is an estimate to be sure, because the ratio actually averages the value of t_{ion} over the scale. But the method very quickly reveals which materials might best be ruled out for further studies. Indeed, those which persist in registering a zero measured emf are predominantly electronic conductors and probably not much can be done (e.g., by way of doping etc.) to make them into ionic conductors, i.e., solid electrolytes.

There is also the matter of predicting the high temperature gas permeability of ceramic tubes. When an M_aX_b compound is properly affixed to its metal M as a scale, the calculation on $\dot{n}_x$ from Equation 19 can be translated into weight gain-or scale thick-

In Corrosion Chemistry; Brubaker, G., et al.;
ACS Symposium Series; American Chemical Society: Washington, DC, 1979.

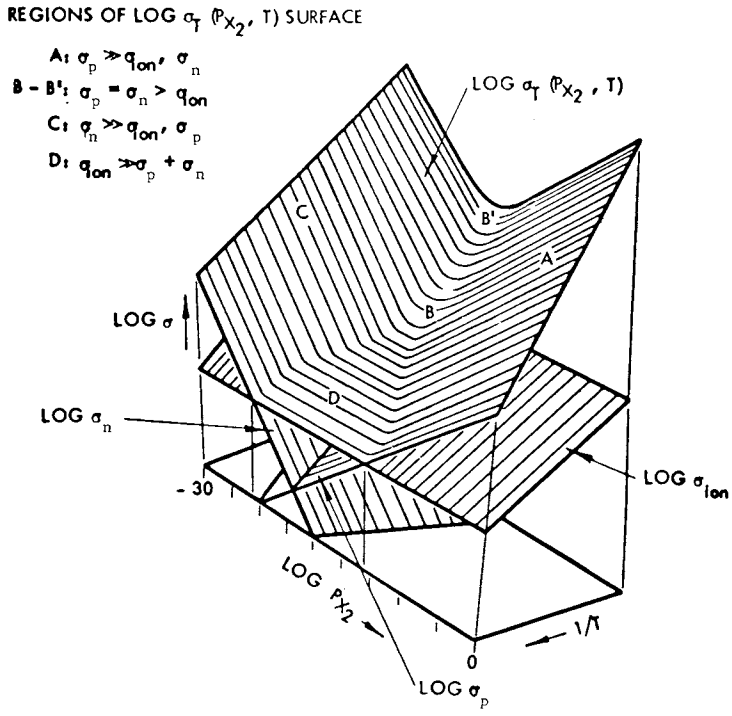

Journal of the Electrochemical Society

Figure 4. Schematic of the P_{x2}, T dependence of partial and total conductivities (40)

ening kinetics. But, if it is not in contact with its own metal, it cannot thicken and then n_X is simply its permeability to X_2 gas. For example, a sintered, crack-free oxide tube will leak oxygen from an oxide if it is evacuated at high temperature at a rate governed by the assimilation rate into the outside surface of the tube and subsequent oxide ion migration through this wall. Thus, Wagner's theory can be used to predict how much oxygen will permeate the tube in any given time. If the tube material is predominantly an electronic conductor, this permeability becomes a measure of the chemical diffusivity for oxygen in the compound. However, if it is a solid electrolyte material, e.g., doped zirconia or thoria, the permeability is limited by electronic conduction. Thus, some of the best estimates of positive hole conductivity in the oxide solid electrolytes have come from "gas permeability" studies made on tubes of these materials.

Actually, the list of interesting implications goes on and on and certainly many have been elucidated elsewhere. Here, I only wanted to provide a brief introduction to Wagner's ideas and perhaps some appreciation of the underlying fundamentals.

We will now be turning to the second part of this paper in which Wagner's ideas will be extended to non-open circuit conditions and somewhat more general kinds of mixed conductors. Before doing that, however, let us close off Part I here by drawing attention to the spectacular agreement between measured and calculated sealing rate constants that stirred up so much in the first place. Thus, we close Part I with the summary Table I which is adapted from one given by Kubaschowski and Hopkins (26). The close agreement shown in the two right-most columns seems all the more outstanding when the absolute magnitudes are considered.

Table I. Calculated and Measured Rate Constants for the Formation of Metal - Non Metal Compounds (ref. 26, p 77)

METAL	NON-METAL	COMPOUND	T°C	RATIONAL RATE CONSTANT EQUIVALENT x cm^{-1} sec^{-1}	
				Calculated	Observed
Ag	S (liq.)	Ag_2S	220	2.4×10^{-6}	1.6×10^{-6}
Cu	I_2 (gas)	CuI	195	3.8×10^{-10}	3.4×10^{-10}
Ag	Br_2 (gas)	AgBr	200	2.7×10^{-11}	3.8×10^{-11}
Cu	O_2; p = 8.3×10^{-2} atm.	Cu_2O	1000	6.6×10^{-9}	6.2×10^{-9}
Cu	O_2; p = 1.6×10^{-2} atm.	Cu_2O	1000	4.8×10^{-9}	4.5×10^{-9}
Cu	O_2; p = 2.3×10^{-3} atm.	Cu_2O	1000	3.4×10^{-9}	3.1×10^{-9}
Cu	O_2; p = 3.0×10^{-4} atm.	Cu_2O	1000	2.1×10^{-9}	2.2×10^{-9}

In Corrosion Chemistry; Brubaker, G., et al.;
ACS Symposium Series; American Chemical Society: Washington, DC, 1979.

Part II Multicomponent Mixed Conductors Under Closed Circuit Conditions

Motivating Factors

In part I above, C. Wagner's theory of mixed conduction was reviewed in terms of an equivalent circuit approach. The implications of mixed conduction theory for parabolic scaling of metals in high temperature atmospheres were also detailed. It was pointed out, however, that current interest in mixed conduction theory is no longer motivated by corrosion considerations; because far too few systems of practical interest conform to the conditions required for parabolic oxidation.

Instead modern interest in mixed conduction theory is expected to derive from high temperature solid electrolyte applications. These solid electrolytes do conform to the conditions laid out in Wagner's theory and many important applications can be foreseen which would require devices based on such solid electrolytes. Some of these applications are of the open circuit variety such as solid electrolyte emf sensors for high temperature environments where contamination of the electrolyte may be a problem. But many other applications will be of the closed circuit variety and to a large extent this aspect has not been negotiated very rigorously in the traditional theory. Significant extensions of the traditional theory will have to be made before the performance characteristics of fuel cells and high temperature steam hydrolyzers can be successfully analyzed via the theory of mixed conduction in solids.

Moreover, hydrogen will likely be present in many of these applications and it is known that hydrogen dissolves into oxide solid electrolytes and becomes a mobile charge carrier. Thus, in addition to extending the theory to close circuit or load conditions, it is also desirable to extend it so that the effects of mobile foreign ions such as hydrogen can be treated (27-29).

Here in Part II, I will conjecture about how to extend Wagner's theory in these important ways. Thus, we shall examine a situation in which an understanding of electrochemical corrosion is being used to launch into other areas of interest which at first blush might seem totally unrelated.

What is clearly needed is a working model for multicomponent, mixed-conducting electrolytes, one which would be applicable to closed as well as open circuit conditons and yet would be relatively

In Corrosion Chemistry; Brubaker, G., et al.;
ACS Symposium Series; American Chemical Society: Washington, DC, 1979.

easy to understand intuitively. Thus, an improved dc circuit analog seems to be called for and one is developed below which serves the purpose. It is an extension of the one described by Choudhury and Patterson(19,24) which in turn, is very similar to that suggested long ago by Hoar and Price(25) in their "electrochemical interpretation" of Wagner's theory of parabolic scaling (9) and to that of Miley(30) who interpreted other scaling rate laws from the equivalent circuit viewpoint. More recent discussions of these kinds of circuit analogs can also be found (31,32).

The present paper furthers the discussion of these kinds of circuit models in two major respects. The first has to do with the point-to-point variations which may be expected to occur. This has been discussed to some extent by Choudhury and Patterson (19, 24). They provide a very useful parametric method which automatically adjusts the local resistances but it was not presented in a form that is easy to visualize. Hence, a reformulation of their approach will be outlined here which ties it in more closely with the more traditionally accepted "fixed resistor" analogs. The second major point has to do with extending the equivalent circuit models in such a way as to allow for additional mobile ionic species in the electrolyte.

The mixed conducting medium considered here is generalized in the sense that the number of mobile ionic species is left open; but the treatment is specialized in that steady state conditons are presumed. A more rigorous treatment of a still more generalized medium has been given by Wagner (33), but it seems to be restricted to open circuit cells only.

In the present treatment, both charging and discharging modes are considered in addition to open circuit operation; however, only diffusive transport is permitted in the electrolyte--convection is not. Consequently, the results are most directly applicable to solid electrolyte media; however, liquid media (acqueous, molten salt, etc.) in a previous matrix should also conform to such assumptions.

By and large, phenomena extraneous to the electrolyte, such as electrode exchange kinetics and the like, have been deliberately separated out of the present treatment by assuming that all pertinent chemical potentials are given at the electrode boundaries. Concentration polarization effects at the electrode surfaces could be accommodated here by invoking models which simulate the electrode kinetic phenomena. These would relate the chemical potentials out in the electrode to the ones just inside the electrolyte (which are presumed here to be given). Interfacial differences in chemical potential would thus be brought into the present analysis in much the same way that voltage drops at contacts are brought in as I R drops in regular circuit theory. However, since electrode models are not within the intended scope here, the endpoint or interfacial drops will not be given explicit consideration below.

In Corrosion Chemistry; Brubaker, G., et al.;
ACS Symposium Series; American Chemical Society: Washington, DC, 1979.

Transport in a mixed conducting medium is treated here, but only in terms of ion and electron migration. This avoids unnecessary confusions in connection with defect theory and emphasizes the fact that important results can be arrived at quite independently of specific assumptions about the defects involved (19). Any further breakdown of the ions and electrons into defect species is neither necessary nor desirable for most purposes. This is accepted for liquid electrolytes (33), but it may seem surprising that the use of ionic and electronic imperfections (34) can be avoided when treating solid media; indeed, defects are undoubtedly responsible for transport in solid electrolytes. By resisting this temptation, however, (as Wagner did originally) we actually arrive at formulas of a more general nature which can be specialized later in accordance with whatever defect structure may seem most appropriate.

Fundamental Considerations and the Local Equilibrium Approach

Consider a generalized, mixed-conducting electrolyte interposed between two electrodes as shown in the cell configuration of Figure 5. The term "mixed conductor" is used here to indicate that electron transport is not ruled out.

The electrochemical potentials of the k different ionic species are represented as η_i, i = 1,2,3,...k, while the chemical potentials of the corresponding neutral species are denoted by μ_i, or perhaps $(1/2)\mu_{i2}$, i = 1,2,...k. For example, if species 1 were zirconium, η_1 might refer to Zr^{+4} cations, whereas μ_1 would be the molar Gibbs free energy of uncharged or neutral Zr metal. However, if one of the other species, say species 2, were oxygen, then the electrochemical potential symbol η_2 would be replaced by $\eta_{O^{-2}}$ to denote the molar Gibbs energy of the oxide ions O^{-2}. But in this case $1/2\ \mu_{O_2}$ would be used for the neutral species because neutral oxygen ordinarily exists in the form of dimeric gas molecules. A similar approach would be used for N_2, Cl_2, Br_2, F_2, etc. The electrochemical potential for electrons--which have no neutral counterpart--is denoted by η_e.

Since the species in an electrolyte are charged, electrochemical potentials η_i and partial conductivities σ_i (which reflect the species mobility) are both used in Figure 5. Conditions at the left electrode surface x = 0 are indicated by a single prime while double primes signify those at the other end, x = L.

Traditionally, the chemical potential μ_i characterizes only the chemical energy interactions between a species i and its surroundings. If a charged species is involved, interactions of an electrostatic nature must also be considered. Accordingly, the so called electrochemical potential η_i is conceived in such a way as to include both types of energy as follows

$$\eta_i = \mu_i^{z_i} + z_i F\phi \qquad 21$$

In Corrosion Chemistry; Brubaker, G., et al.;
ACS Symposium Series; American Chemical Society: Washington, DC, 1979.

Here μ_i^z represents all the chemical interactions between the ion of type i its surroundings and $Z_iF\phi$ represents the electrostatic part of the electrochemical potential. Thus, Z_i is the valence of the ion, F is the Faraday, and ϕ is the local electrostatic potential. Actually, the separation of chemical and electrostatic components in this way is based more on conceptual preference than on operational meaningfulness (35, 36), but the separation has a great deal of historical precedence and is mentioned here for that reason. But the approach used here does not make use of such distinctions and in this sense at least would be in accordance with the recommendations elaborated by Guggenheim (35). It may be called the local equilibrium approach and may be summarized as follows.

The electrochemical condition at each point in the medium--i.e., the concentrations and mobilities of its constituent ions and electrons--is determined by the prevailing chemical potentials or activities of the constituent "atoms", which are neutral. Accordingly, point-to-point variations in the medium are most meaningfully characterized either in terms of voltage profiles or in terms of chemical potential (activity) profiles of the appropriate neutral species or in terms of both. That is, only voltages (electric potential differences operating on ions and electrons) and chemical potential differences for neutral species (not those for the ions) are amenable to direct measurement and control (19,35,36). Thus, even though the electrochemical potential profiles and gradients for ions and electrons arise quite naturally from the basic flux equations given later, they are to be eliminated in favor of their more measurable counterparts. This elimination process is effected by assuming local equilibrium for internal dissocation reactions and proceeds along the following lines.

If Z_i is the valence of ionic species i in the medium, the i-type ions and electrons may be related to the appropriate neutral species, but equilibrium of the following dissociation reaction must be presumed

$$i \text{ (or } \tfrac{1}{2} i_2) \longrightarrow i^{z_i} + Z_i e \qquad 22$$

Formally, this prototype reaction serves for cations as well as anions. Cations by definition always have positive Z values and derive from metal atoms. As an example of this, the following reaction, which would apply to the zirconium constituent in the well known solid electrolyte calcia-stabilized zirconia (CSZ), may be cited

$$Zr \longrightarrow Zr^{+4} + 4e \qquad 23$$

Anions, on the other hand, always have negative Z values; hence Equation 22 applied to the oxygen ion constituent of CSZ yields $(1/2)O_2 \rightarrow O^{-2} - 2e$. However, transposing the -2e yields the more

familiar form

$$\tfrac{1}{2} O_2 + 2e \rightarrow O^{-2} \qquad 24$$

By assuming local equilibrium of the dissociation reactions, a zero free energy condition results which relates the local chemical potential of the neutral species to the charged species actually present. Thus, local equilibrium of reaction(22) implies the following generalized free energy equality

$$\mu_i = \eta_i + Z_i \eta_e \qquad 25$$

Note that Equation 25 embraces as special cases the zirconium and oxygen examples mentioned earlier. In particular we have

$$\mu_{Zr} = \eta_{Zr^{+4}} + 4\eta_e \qquad 26$$

and

$$\tfrac{1}{2}\mu_{O_2} + 2\eta_e = \eta_{O^{-2}} \qquad 27$$

Thus the single relation, Equation 25, can indeed be used to eliminate electrochemical potential differences for both cations and anions. One is then left with chemical potential differences for neutral species (which are measurable) and electrochemical potential differences for electrons which are directly related to measurable voltages V_L as follows (19,24,37,38)

$$\eta_e'' - \eta_e' = Z_e F V_L = -F V_L \qquad 28$$

where Z_e is -1 and, again, F is the Faraday. Certain precautions are necessary, however, because the leads to the measuring device must be good electronic conductors and must be identical in chemical composition (35,37,38). Identical composition is also required to avoid the thermocouple emfs that can arise when the cell and measuring instruments are at different temperatures.

By combining Equations 25 and 28, the electrochemical potential $\eta_i'' - \eta_i'$ for i-type ions may be written in the following abbreviated form

$$\eta_i'' - \eta_i' = -Z_i F[V_i - V_L] \qquad 29$$

where for convenience, the abbreviated symbol V_i has been substituted to save writing out the chemical potential differences for the corresponding neutral atoms. For monoatomic species, the substitutional relation employed is

$$V_i = -[\mu_i'' - \mu_i'] / Z_i F \qquad 30$$

In Corrosion Chemistry; Brubaker, G., et al.;
ACS Symposium Series; American Chemical Society: Washington, DC, 1979.

but again if the neutral species is ordinarily a dimer gas such as O_2, Cl_2...etc., then V_i is given by

$$V_i = -\tfrac{1}{2}\left[\mu''_{i_2} - \mu'_{i_2}\right]/Z_iF = -\tfrac{1}{2}\frac{RT}{Z_iF}\ln\left[P''_{i_2}/P'_{i_2}\right] \qquad 31$$

The quantity V_i is of fundamental importance and will be referred to hereafter as the thermodynamic voltage for species i--it represents the chemical driving force or affinity which acts to drive the i-type ions through the medium. Like V_L, V_i has units of volts.

It is worth digressing here to point out some important points. First of all it should be noted that differences or gradients in η_i are a measure of the overall or combined "driving force" for migration of the i type particles. However, in view of Equation 29, we see that this overall "force" has two parts: A chemical gradient part arising from the V_i term and an electric field component arising from differences or gradients in V_L. In almost all cases of practical interest these two parts oppose each other and the direction of net migration is determined by whichever is the stronger force. In electrolysis (charging mode) the V_L gradient is stronger whereas in the discharge mode the chemical driving forces prevail. And for multicomponent electrolytes it is most important to realize that some species may be undergoing electrolysis while others are simultaneously discharging in the same cell! This possibility has profound implications for the performance characteristics and efficiencies of practical electrochemical devices of all types.

If the cell electrodes have a virtually infinite capacity, the endpoint values of μ_{i_2} will not drift towards each other to any significant extent even under constant load when ionic permeation is taking place through the electrolyte. To simulate this condition V_i is thought of as a fixed quantity as if it were a battery voltage. For example, coexistence metal, metal oxide electrodes in an oxide solid electroltye cell, would function in this way. However, if the electrode chambers are of very limited capacity, the endpoint chemical potentials will vary as ions pass through the electrolyte. The "thermodynamic voltage" V_i changes accordingly and in this sense V_i acts more like a capacitor than a battery. In such cases, we might wish to show a capacitor in the equivalent circuit to emphasize the variable nature of V_i. When V_L overpowers V_i, i ions are forced backwards; that is, from the low to the high chemical potential sides and V_i builds up in value much as if it were a real capacitor being charged by a battery. And of course when V_i overpowers V_L, ions flow from the high chemical potential side to the low and V_i drops as the electrode inventories approach each other.

In contrast to the ionic species, the thermodynamic voltage for electrons always remains at zero. Their state of charge is

In Corrosion Chemistry; Brubaker, G., et al.;
ACS Symposium Series; American Chemical Society: Washington, DC, 1979.

not altered by merely passing through an electrolyte/electrode interface and also unlike the ions, there is no neutral counterpart to an electron. This is taken into account by always setting V_e to zero in any electronic branch of an equivalent circuit.

Steady State Migration Fluxes in Multicomponent Electrolytes and the Central Problem with Closed Circuit Theory

The flux of charged species i past any point x in an electrolytic medium is taken to be proportional to the magnitude of the prevailing electrochemical potential gradient $\nabla\eta_i$, with flow directed down that gradient. However, it is more useful in the present approach to work with the electrical current due to species i. This current I_i is internal to the electrolyte and thus can not be measured separately; but the following formula for I_i can be inferred from the diffusion flux

$$I_i = -A \frac{\sigma_i}{Z_i F} \nabla\eta_i = -A \frac{\sigma_i}{Z_i F} [\nabla V_i - \nabla V_L] \qquad 32$$

Here, A is the cross-sectional area perpendicular to the flow direction, F is the Faraday, and σ_i is the specific electrical conductivity (in the appropriate units) for the charged species in question. Writing the constant of proportionality in terms of σ_i is somewhat arbitrary, but it is certainly not without precedent (19,24). Nevertheless, it is worth noting that the absolute mobility, the electric mobility, the diffusivity or the transference number-total conductivity product may replace σ_i as the transport parameter of central interest, and such alternatives are sometimes used.

After steady state sets in, Equation 32 becomes constant because I_i--the current carried by each species i--must be invariant from point to point along the direction of flow. Then the following operations are carried out to get the important result of Equation 33 below: Equation 32 is first solved for $\nabla\eta_i$, then it is integrated from O to L to get $\eta_i'' - \eta_i'$ in terms of I_i. Next Equation 29 is used to eliminate $\eta_i'' - \eta_i'$ and the result is solved for the constant I_i. The final result of all this is

$$I_i = G_i [V_i - V_L] \qquad 33$$

where G_i here is simply the reciprocal of R_i which in turn is the total series resistance presented by the cell to species i. Thus G_i is the macroscopic conductance for species i according to the formula

$$G_i = \left[\int_O^L \frac{dx}{\sigma_i(x)\ A(x)} \right]^{-1} = \frac{1}{R_i} \qquad 34$$

In Corrosion Chemistry; Brubaker, G., et al.;
ACS Symposium Series; American Chemical Society: Washington, DC, 1979.

Since planar geometry is assumed here, A(x) may be replaced by a constant; however, other geometries could be considered by merely employing the appropriate A(x) dependence.

Of course the dependence of σ_i on x is also required if the integral in Equation 34 is to be evaluated. But determining that dependence is such a complicated matter that no solution can be given here at least for the most general case. For this reason, this matter of evaluating the conductance term G_i defined in Equation 34 is the single most difficult problem here and it always arises when one tries to extend the theory of mixed conduction to non-open circuit conditions. In particular we must not only know how σ_i depends on the chemical potential of i or partial pressure or activity but in addition he must also determine the chemical potential profile. But even worse than that, this profile will in general vary depending on the load conditions. This introduces a troblesome non-linearity into the theory, because we cannot rule out the possibility that the conductances G_i are voltage or current dependent. The problem of evaluating G_i can be solved only in special situations where the conductivity properties of the solid electrolyte are presumed to be known functions of temperature and partial pressure P_{x2}.

It may be helpful at this point to explain why the formidable "central problem" discussed above doesn't show up in the traditional theory of mixed conduction as developed by Wagner. He only treats two situations: ion blocking electrode conditons and open circuit conditions. When the electrodes are ion blocking, I_i vanishes in Equation 32 (for each ionic species) in which case Equation 32 is easy to integrate.

In open circuit situations, the sum of all the I_i's vanishes and, though the integration is not quite as simple as for the ion blocking case, still a closed form integral relation can be derived which holds for a wide variety of solid mixed conductors. In fact the formula that results in this way is Wagner's well known open circuit emf formula (Equation 31 in part one) and applies to any binary (two component) mixed conducting compound.

Returning to the main thread here, we note that Equations 33 and 34 apply to each mobile species individually; however, in all cases of practical interest simultaneous migration of more than one species must be considered. This is especially true in the case of multicomponent electrolytes in which many kinds of ions may be mobile. But if several species are in motion they merely make simultaneous contributions to the current exchanged with the external circuit. The relative contribution of each will depend on the ease of transport in the elctrolyte, i.e., on G_i and on the chemical and electrical potential gradients which act on it. But these matters are better discussed in terms of the extended equivalent circuit approach which will now be developed.

In Corrosion Chemistry; Brubaker, G., et al.;
ACS Symposium Series; American Chemical Society: Washington, DC, 1979.

Equivalent Circuit Relations

It is fruitful to reconsider all the foregoing notions in conjunction with the simple dc circuit analog shown in Figure 6. The k parallel branches in the circuit model automatically account for the simulataneous contributions made by all the ion species to the external (load) current I_L. To minimize confusion, all currents (including I_L) are considered positive if they are directed to the right in the cell, and V_L as well as any thermodynamic voltage is positive if its positive terminal is to the right (toward x = L) in Figure 6. Confusion about the direction of species migration in relation to the sign of its charge can be greatly reduced by focusing only on the currents (rather than the diffusion fluxes) because the signs and directions of currents and voltages are easier to think out. Some would say the conventions make it all automatic.

According to Kirchhoff's law, the load current in Figure 6 is obtained by summing over all the parallel branches

$$I_L = I_1 + I_2 + \ldots I_k + I_e = \sum_{k,e} I_i \qquad 35$$

where $\sum_{k,e}$ indicates that the summation on i goes from 1 through k (all ion species) with a final term for the electron contribution as well. This symbol is used below as well.

If we insert Equation 33 for each I_i in Equation 35, collects terms, and then notes that the same load voltage V_L--whatever that turns out to be--is necessarily impressed on each of the parallel branches, we can produce the following sequence

$$I_L = \sum_{k,e} G_i[V_i - V_L] = \sum_{k,e} G_i V_i - V_L \sum_{k,e} G_i$$

$$= G_T \left[\sum_{k,e} t_i V_i - V_L\right] \qquad 36$$

where the k,e notation means the same as it did above. Also, to simplify notation here, the total conductance G_T and the transference numbers t_i have been introduced. They are defined as follows:

$$G_T = \sum_{k,e} G_i \qquad 37$$

and

$$t_i = G_i / G_T. \qquad 38$$

however the G_i values in 37 and 38 derive from the troublesome Equation 34. The transference number t_i may be regarded as a kind of normalized conductance or conductivity. These definitions together with Equation 36 yield

$$I_L = G_T [\bar{V} - V_L] \qquad 39$$

In Corrosion Chemistry; Brubaker, G., et al.;
ACS Symposium Series; American Chemical Society: Washington, DC, 1979.

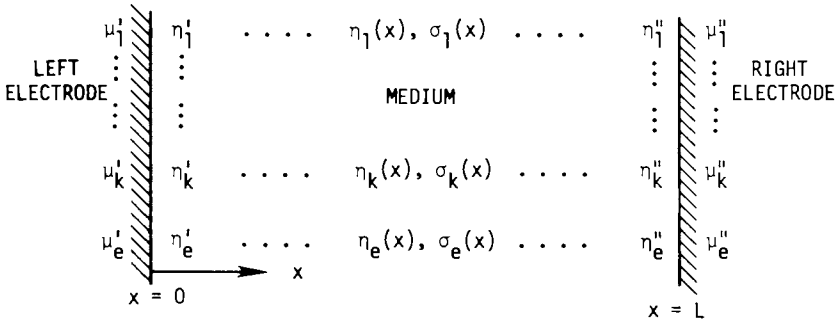

Figure 5. Schematic of a generalized electrochemical cell

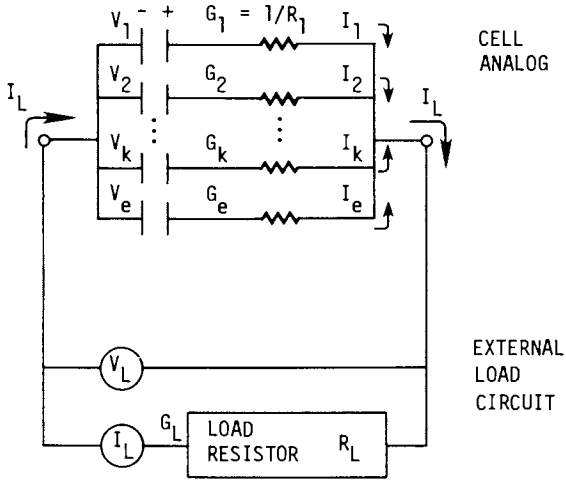

Figure 6. Direct current (dc) analog for a multicomponent mixed conducting electrolytic cell

where $\bar{V}$ is also a shorthand symbol. It stands for the summation

$$\bar{V} = \sum_{i}^{k} t_i V_i. \qquad 40$$

and is a quantity of considerable significance. Equation 40 should also include a term $t_e V_e$ but this has been deleted here because V_e is always zero.

$\bar{V}$ represents the overall thermodynamic driving force for the cell and is seen to be a weighted average of all the individual thermodynamic voltages V_i. The weight factors are the transference numbers t_i which means that each V_i has been weighted in proportion to the conductance G_i with the result normalized to the total conductance of the electrolyte. To evaluate $\bar{V}$, the V_i's are first calculated from Equation 30 or 31 and then each is multiplied by the corresponding transference number in order to form the normalized weighted average of Equation 40. A graphical interpretation for $\bar{V}$ which may prove helpful, especially to those familiar with ternary phase diagrams, is presented in Figure 7.

With Equations 34 and 37-40, virtually all the essential properties of the electrolyte have been brought into the analysis. However, the external circuit--the agent for exchanging charge and energy with the cell--must also be brought in if meaningful, performance analyses are to result.

In order to examine the performance characteristics of a cell under load, we let the external circuit consist of a variable ohmic resistor R_L whose value may range anywhere from zero to infinity. In this sense, the load conductance G_L may be regarded as a convenient control parameter which permits various current-voltage load conditons to be placed on the cell at will. Ohms law for the external element yields

$$I_L = G_L V_L \qquad 41$$

which together with Equations 39 and 40 completes the basic system of equations needed for the present analysis.

For most performance analyses, however, it is better if explicit formulas for V_L, I_L, and the power $W_L = I_L V_L$ are available. That is readily accomplished as follows: first one solves Equations 39 and 41 simultaneously for V_L and I_L and then multiplies the two to give W_L. This results in the following three equations which are parametric in G_L:

$$V_L = \frac{G_T}{G_L + G_T} \cdot \bar{V} \qquad 42$$

$$I_L = \frac{G_L G_T}{G_L + G_T} \cdot \bar{V} \qquad 43$$

In Corrosion Chemistry; Brubaker, G., et al.;
ACS Symposium Series; American Chemical Society: Washington, DC, 1979.

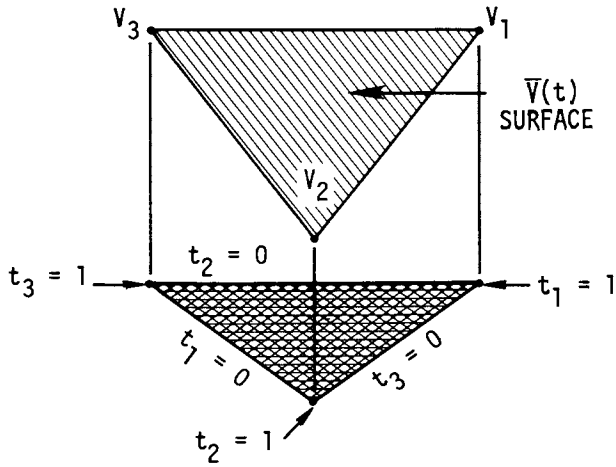

Figure 7. Ternary schematic of the overall thermodynamic voltage of an electrochemical cell

In Corrosion Chemistry; Brubaker, G., et al.;
ACS Symposium Series; American Chemical Society: Washington, DC, 1979.

$$W_L = \frac{G_L G_T^2}{[G_L + G_T]^2} \cdot \bar{V}^2 \qquad 44$$

Equations 37-44 with Equations 30 and 31 serve as a system of basic relationships that are quite useful for analyzing the performance of a generalized electrochemical cell under various modes of operation.

It is worth re-emphasizing, however, that the mathematical simplicity of the equations in this system may be simplicity in appearance only. Again, the G_i quantities in G_T and in the various t_i values which enter into $\bar{V}$ are not necessarily constant in general: rather, they are apt to vary somewhat with loading conditons as was pointed out in the discussion subsequent to Equation 34 above.

Capstone Comments

This is one of those tasks that one never really finishes. Rather one pauses from time to time to sum up, hoping either to continue again later or perhaps to abandon the effort for good. In this case I hope to continue, at least for a while, and in summing up here, let me explain why I will only use one example to do this but many others exist as well.

There have been cases wherein a fluoride ion solid electrolyte, in particular CaF_2, has been placed between two different metal oxide electrodes and behaved as if it were an oxide solid electrolyte. That is, the emf was found to be equal to that measured previous with calcia- or yttria-stabilized zirconia! No very suitable explanation has been offered yet, but I think that these findings have been published or soon will be. But if my conjectures above are correct, the following explanation could be offered.

The CaF_2 electrolyte is capable of incorporating oxide ions and transporting them simultaneously with, but perhaps to a much lesser extent than, fluoride ions. Then CaF_2 could be thought of as a two-anion electrolyte. Since the electrodes are reversible and highly "buffered",as it were, with respect to oxygen, the thermodynamic voltage V_O for oxygen acts like a stable battery in the equivalent circuit. There is of course a fluoride ion branch as well, but its thermodynamic voltage V_F behaves not like a stable battery but rather like a capacitor. This is due to the fact that fluorine inventories are not fixed by the oxide electrodes and so the trace amounts that do reside therein can change drastically as the fluoride "counter-ions" get pushed in the direction opposite to the flow of oxide ions through the CaF_2". In short, the battery-like voltage V_O in the oxide-ion branch of the

In Corrosion Chemistry; Brubaker, G., et al.;
ACS Symposium Series; American Chemical Society: Washington, DC, 1979.

circuit charges up the capacitor-like thermodynamic voltage in the fluoride branch until they become equal. At this time, the load on V_O drops off considerably since it then has only to "back-pump" the trace amounts of electrons that leak through the CaF_2 (the e branch). If electronic conduction is small, as in the case here, the steady state cell emf will virtually equal V_O --as observed!

As I said this is only one example though many others could have been given. I am presently trying to outline similar explanations for other confusing drift effects in solid and molten electrolyte devices. It simply is not appropriate here to list the possibilities; however, I will say that some of the most fascinating and important (but alas! most complicated and difficult) applications may be found in the area of fuel cells and batteries. And many of these devices are based on multi-component electrolytes.

I only hope that more progress can be realized, especially in solving the central problem in all this which was mentioned above, namely, that of evaluating the individual ionic conductances and chemical potential profile in an operating cell. And of course I hope I can be a partial contributer to such future progress. Or better yet, that somebody in the audience will be led to contemplate the issues I have discussed here and perhaps find a better way to analyze mixed conduction in multicomponent electrolytes.

Acknowlegement

Preparation of this manuscript spanned many months but it had to be put into final form during off hours while I was on a summer leave of absence from ISU. I was working in Dr. Hugh Isaacs group at Brookhaven National Laboratory at the time and I am indebted to many of the BNL people for very helpful discussions.

Of utmost importance at that time was the willingness of Ms. Yvonne Oden to sacrifice many of her off work hours, thus making it possible to complete the manuscript just before the deadline. I shall be forever in her debt for that.

I also wish to acknowledge the Iowa State University, Engineering Research Institute for continued financial support of research in high temperature electrochemistry and for help during the initial stages of manuscript preparation.

Finally, I wish to thank the Chicago Chapter of the Electrochemical Society and my host, Prof. Bruce Wagner for their kind invitation and cordial hospitality.

Literature Cited

1. A. Einstein, Ann d. Phys. 17, 349 (1905); ibid 19 371 (1906)
2. M. Von Smoluchowski, Ann d. Phys. 21, 756 (1906)
3. A. Joffe, Ann d. Phys. 72, 461 (1923)
4. J. Frenkel, Z. f Phys. 35, 652 (1926)
5. C. Wagner and W. Schottky, Z. Phys. Chem. B 11, 163 (1930)
6. C. Wagner, ibid., Bodenstein Festband 177 (1931)
7. C. Wagner, Phys. Z. 36, 721 (1935)
8. W. Schottky, Z. Phys. Chem. B 29, 335 (1935)
9. C. Wagner, Z. Phys. Chem. B 21, 25 (1933)
10. K. Nagel and C. Wagner, Z. Phys. Chem. B 25, 71 (1934)
11. C. Wagner, Z. Phys. Chem. B 32, 447 (1936)
12. C. Wagner and K. Grunewald, Z. Phys. 40, 455 (1938)
13. C. Wagner in "Diffusion" (Proceedings ASM Seminar) Amer. Soc. Metals, Cleveland (1950)
14. W. Jost Diffusion (in Solids, Liquids and Gases) Academic Press, N.Y. (1962)
15. O. Kubascheivski and B.E. Hopkins, Oxidation of Metals and Alloys, Butterworths London (1962)
16. F.A. Kroger, "The Chemistry of Imperfect Crystals" North Holland Amsterdam (1964)
17. K. Hauffe , "Oxidation of Metals" Plenum Press, N.Y. (1965)
18. P. Kofstat, "High Temperature Oxidation of Metals" Wiley, N.Y. (1966)
19. J.W. Patterson, Chapter 9 in N.M. Tallan (editor) "Electrical Conductivity in Ceramics and Glass, Marcel Dekker, N.Y. (1974)
20. M. Voinov in "Electrode Processes in Solid State Ionics" M. Kleitz and J. Dupuy editors, NATO Advanced Study Institute Series, D. Reidel Publ., Boston (1976)
21. K. Kiukkola and C. Wagner, J. Electrochem. Soc., 104, 376 (1957)

In Corrosion Chemistry; Brubaker, G., et al.;
ACS Symposium Series; American Chemical Society: Washington, DC, 1979.

22. R.A. Rapp and D.A. Shores in Part 2 of "Physicochemical Measurements in Metals Research" R.A. Rapp editor, Vol. IV of the Series, "Techniques of Metals Research", R.F. Bunshah editor, Interscience Publ. (Wiley) N.Y. (1970)

23. T.H. Etsell and S.N. Flengas, "Chem. Rev." 70, 339 (1970)

24. N. S. Choudhury and J.W. Patterson, J. Electrochem. Soc. 118, 1389 (1971)

25. T.P. Hoar and L.E. Price Trans. Faraday Soc. 34, 867 (1938)

26. O. Kubaschewski and B.E. Hopkins, Oxidation of Metals and Alloys, Butterworth (1962)

27. S. Stotz and C. Wagner Berichte der Bunsenges, 70, 781 (1966)

28. C. Wagner Berichte der Bunsenges, 72 778 (1968)

29. D. A. Shores and R. A. Rapp, J. Electrochem. Soc., 114, 300 (1972)

30. H.A. Miley, Trans. Electrochem Soc., 81, 381 (1942)

31. T. Takahashi, "Physics of Electrolytes", Vol. 2, p. 989, J. Hladik (editor), Academic Press, New York (1972)

32. J.W. Patterson, "Extended Abstracts, ERDA Workshop on High Temperature Solid Oxide Fuel Cells", H. Isaacs (editor), Brookhaven National Laboratory, (May 1977)

33. C. Wagner, "Advances in Electrochemistry and Electrochemical Engineering", Vol. IV, p. 1, P. Delahay (editor), Interscience, New York (1966)

34. F.A. Kroger, "The Chemistry of Imperfect Crystals", North Holland Publishing Co., Amsterdam (1964)

35. E.A. Guggenheim, J. Phys. Chem., 33, 842 (1929); 34, 1540 (1930)

36. John Newman, "Advances in Electrochemistry and Electrochemical Engineering", Bol. V, pp. 129-131, C.W. Tobias (editor), Interscience, New York (1967)

37. E.A. Guggenheim, "Thermodynamics", p. 372ff, North Holland Publishing Co., Amsterdam (1957)

38. K. Denbigh, Principles of Chemical Equilibrium, Cambridge Univ. Press, Cambridge, U.K. (1968), section 2.9

39. J.W. Patterson, Ind. Eng. Prod. Res. Dev. 17(1), 19(1978).

40. J.W. Patterson, J. Electrochem. Soc. 118(7), 1036 (1971).

RECEIVED September 1, 1978.

5

Dissolution of Iron

MORRIS COHEN

National Research Council of Canada, Division of Chemistry, Ottawa, Canada

In this lecture I will deal with the mechanisms involved in first, the dissolution or corrosion of iron and second, in the inhibition of corrosion by the formation of various types of oxide films. A few definitions will help to focus attention on the specific nature of my subject.

Mechanism

1. A sequence of steps in a chemical reaction.
2. The fundamental physical processes involved in or responsible for a reaction.

Dissolution

The act or process of dissolving or breaking up.

Corrosion

Destruction of a metal by chemical or electrochemical reaction with its environment.

Inhibitor

A chemical substance which, when added to the environment, usually in small concentrations effectively decreases corrosion, after concentrations.

Passivity

A metal is passive if it substantially resists corrosion in an environment where thermodynamically there is a large free energy decrease associated with its passage from the metallic state to appropriate corrosion products.

Corrosion and its inhibition or passivity both involve reactions between the metal surface and the solution. In the case

0-8412-0471-3/79/47-089-126$06.75/0

of corrosion the reaction products are either soluble or form solids which are either loose or porous and do not protect the metal. In the first part of this presentation I will deal with conditions in which corrosion of iron continues while in the last part I will outline some of the mechanisms for the formation of solid protective films which can lead to both anodic passivity and inhibition.

Surface of Metal

Metals normally exist as polycrystalline solids in which the atoms are arranged in a manner characteristic of the metal. The atoms in iron are arranged in a cubic array, (i.e.) the metal is composed of groups of cubic cells in which there are iron atoms at each corner of the cube and one in the middle. Large groups of these form crystals which join with some misfit at grain boundaries to make up the body of the metal. Aside from these grain boundaries other imperfections in the solid can be subgrain boundaries, dislocations, vacancies and either segregated or soluble impurities. Of course, all of these imperfections show up at the surface and affect the manner in which the iron will react. Some of these imperfections are shown in Figure 1. In this figure one can see ledges, impurity atoms, vacancies where an atom is missing and a kink step which results from the emergence at the surface of a dislocation. These imperfections will all have different reactivities and at near equilibrium conditions, will react at quite different rates. Under conditions far from equilibrium, such as in electropolishing the imperfections will have very little influence on dissolution rate and smoothing takes place. Under etching conditions both the effects of imperfections and crystal structure can be observed. This is shown in Figure 2 for iron electrolytically dissolved in perchloric-acetic acid in the etching region. On different grains one can observe either triangular or tetragonal pits, depending on the orientation of the grain.

Aside from basic structural imperfections the dissolution rate and mechanism can be markedly affected by both bulk and surface impurities. Some surface impurities may act as preferred sites for hydrogen atom recombination and hydrogen evolution and hence increase the rate of dissolution. Others may act to poison the hydrogen re-combination reaction and lead to hydrogen dissolution followed by embrittlement and cracking. Some bulk impurities act as nucleating points for hydrogen atom recombination and lead to blistering. Carbon in iron is a hardener and makes iron more susceptible to stress-corrosion cracking. These effects make it necessary to study both the surface and bulk composition of the iron in order to predict its corrosion behavior.

In Corrosion Chemistry; Brubaker, G., et al.;
ACS Symposium Series; American Chemical Society: Washington, DC, 1979.

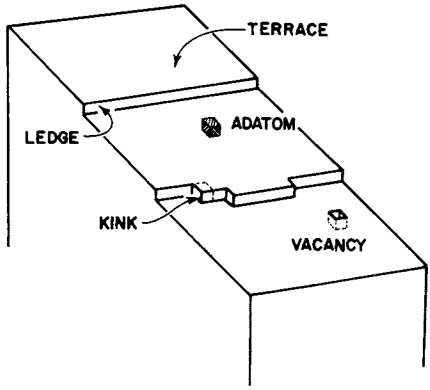

Figure 1. Imperfections on solid surfaces

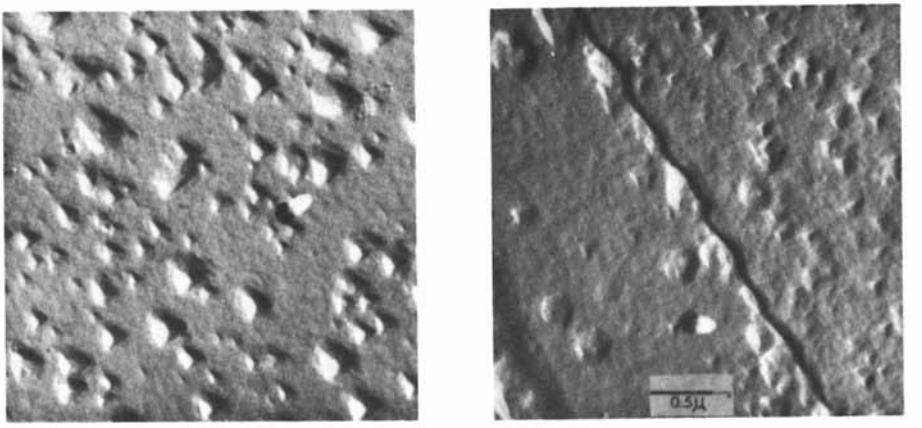

Figure 2. Geometric pitting and grain boundary etching in anodic dissolution, original mag. × 30,000

In Corrosion Chemistry; Brubaker, G., et al.;
ACS Symposium Series; American Chemical Society: Washington, DC, 1979.

Solution Composition

The second reactant in the dissolution or corrosion system is the solution. In most cases this is basically water containing dissolved substances which ionize more or less to cations and anions. The solution may also contain dissolved gases such as O_2, H_2, or CO_2. These constituents of the aqueous system can affect the corrosion rate in a variety of ways. O_2 in small amounts may act to increase the rate of corrosion and in sufficiently high concentrations to inhibit it. In the presence of chloride ions, pits tend to go acid with a consequent increased rate of dissolution of the iron. Some metal ions such as copper, plate out on the iron surface by an exchange reaction and increase the corrosion rate by acting as hydrogen depolarizers. Complexing agents increase the reaction by lowering the effective concentration of the dissolved ferrous ions. Other constituents, such as organic amines may adsorb on the surface and slow down the rate of solution. Others, oxidizing agents, such as chromate or molybdate, help to form protective oxide films and inhibit the dissolution reaction. Hence a knowledge of the effects of various possible constituents of solutions is necessary before predicting the corrosion behavior of iron.

Application of Thermodynamics

With sufficient thermodynamic and equilibrium data it is possible to predict whether or not a dissolution reaction will take place. Also with a knowledge of the free energy change for a reaction one can calculate the potential E at which the reaction will occur from the relationships

$$\Delta G = nFE_o$$

$$\text{and } E = E_o + \frac{nF}{RT} \log \text{Concentration}$$

where ΔG is the free energy change for the reaction, n is the number of electrons involved, F is the Faraday and E_o is the Standard Potential.

Using these considerations, M. Pourbaix and co-workers at CEBELCOR constructed "equilibrium" potential-pH diagrams showing some of the stable phases for iron in aqueous solutions.(1) By further assuming that the formation of a stable solid oxide would lead to stifling of corrosion (passivity), he simplified the diagram for iron to that shown in Fig. 3. In this diagram areas of pH and potential are designated by the terms Immunity, Corrosion and Passivation. In the area labeled Immunity any ferrous ions in solution would be plated back on the metal (i.e.) iron is thermodynamically stable in water in this region. In the area labelled corrosion the corrosion product is either ferrous or ferric ion in solution. In the area labelled passivation the iron

In Corrosion Chemistry; Brubaker, G., et al.;
ACS Symposium Series; American Chemical Society: Washington, DC, 1979.

is supposed to be covered by a solid film of Fe_2O_3 or Fe_3O_4 which stops corrosion completely. Dashed line (b) is the equilibrium potential for O_2 and (d) for H_2.

The Pourbaix diagram, within its assumptions gives a good general picture of iron corrosion behavior. However it cannot be applied to specific situations for a number of reasons. Iron can form a large number of solid corrosion products with water including hydrated and anhydrous oxides as well as ill-defined gels and amorphous products. Some of these may form protective coatings while others will not. The solid products formed may be porous and lead to pitting, cracking, etc. We must always remember that in all regions other than that labelled immunity the iron is thermodynamically unstable and in the long run nature will have its way and the metal will corrode.

The addition of other ions to the solution, while probably having a small effect on the overall thermodynamics of the situation can have a very large effect on the kinetics and hence on the kinetics of dissolution or corrosion. They may, as in the case of chlorides, lead to localized attack by breakdown of protective films. In this way although the most of the metal surface follows the behavior predicted by the Pourbaix diagram, dissolution at confined areas leads to failure by pitting or cracking.

The Pourbaix diagrams also tell one very little about mechanism of reaction, kinetics of reaction or inhibition of reaction. These aspects will be dealt with in the rest of this chapter.

Electrochemistry and Corrosion

Materials can dissolve by direct dissolution or by separate steps. An example of the former is the dissolution of sugar in water and of the latter the corrosion of iron in aqueous solutions. Direct dissolution or iron may occur in some organic solvents and in the presence of some constituents in aqueous solutions. In most aqueous corrosion systems iron (and most other metals) goes into solution via an electrochemical process in which there are separate anodes and cathodes. In a de-aerated solution the separate reactions are

$$Fe \longrightarrow Fe^{2+} + 2e \qquad \text{(anode)}$$
$$2H + 2e \longrightarrow H_2 \qquad \text{(cathode)}$$

In the presence of oxygen the overall cathodic reaction is

$$O_2 + 2H_2O + 4e \longrightarrow 4OH^- \qquad \text{(cathode)}$$

If we measure the potential of the dissolving iron, we will not obtain an equilibrium potential (as in the Pourbaix diagram) but a value somewhere between the anodic and cathodic potentials. This number will depend on such factors as how the potentials

In Corrosion Chemistry; Brubaker, G., et al.;
ACS Symposium Series; American Chemical Society: Washington, DC, 1979.

change with current, (i.e) the slopes of the polarization curves, the various resistances in the system, and diffusion of reactants and reaction products. With iron the slope of the anodic polarization curve is considered to be much less than that of the cathodic curves. With these considerations in mind U.R. Evans suggested what are now known as the Evans' diagrams to describe the electrochemical mechanism of corrosion. Typical curves for iron are shown in Figure 4, (2).

In Figure 4 the top curves with the downward slopes are for cathodic reactions. In 4(a) are shown curves for anodic and cathodic reaction which are only controlled by activation polarization. A typical example is a well stirred acid solution. The top cathodic curve is for oxygen and the lower one for hydrogen. Obviously the possible corrosion rate in the presence of oxygen is higher than that in the presence of hydrogen only. Because of this oxygen is sometimes called a good cathodic depolarizer. In 4(b) and 4(c) are shown the effects of polarization due to diffusion control. In (b) excess cathodic polarization may be caused by a low concentration of oxygen from the bulk of the solution. In (c) high anodic polarization may be caused by slow diffusion of ferrous ions away from the anode. With both (b) and (c), the polarization curves and hence the dissolution rate will be highly dependent on concentration and stirring. With (c) iron ion complexing agent will also markedly affect the rate of dissolution by increasing the diffusion rate by increasing the concentration gradient.

The polarization curves shown in 4(d) are typical of systems in which anodes and cathodes are separated by corrosion products and/or solutions of some resistance. The corrosion rate (current density) depends on the average resistance between the anodes and cathodes and the potential which is measured depends on the position of the probe electrode in relation to the resistance separating the anode and cathode. In a corroding system of this type there is a current flowing through the solution which can be calculated by measuring the potential differences between two spaced electrodes in the solution and the resistance of the solution. Evans and his co-workers did this with iron in bicarbonate solutions and showed that all the corrosion could be accounted for by the currents flowing between anodes and cathodes, (3). This confirmed the electrochemical mechanism of corrosion.

Mechanisms of Reactions

Although the overall anodic and cathodic reactions are those given in Equations 1-3, it is usually considered that the reactions take place in a series of steps, one of which is the Rate Determining Step. The most widely accepted anodic scheme is that proposed by Kelly (4) and is particularly applicable in acid solutions. The reaction steps are as follows.

In Corrosion Chemistry; Brubaker, G., et al.;
ACS Symposium Series; American Chemical Society: Washington, DC, 1979.

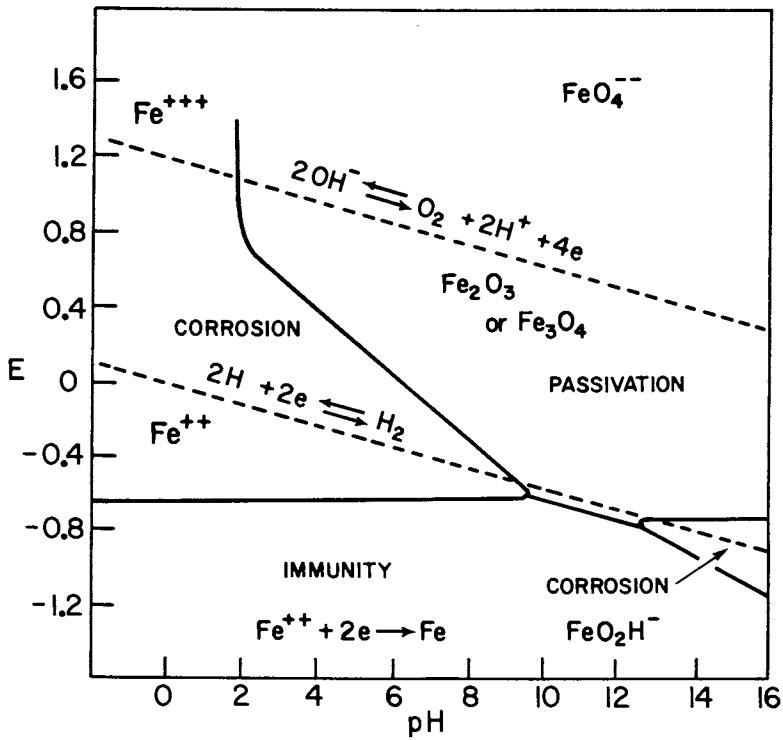

Figure 3. Pourbaix diagram for iron in water

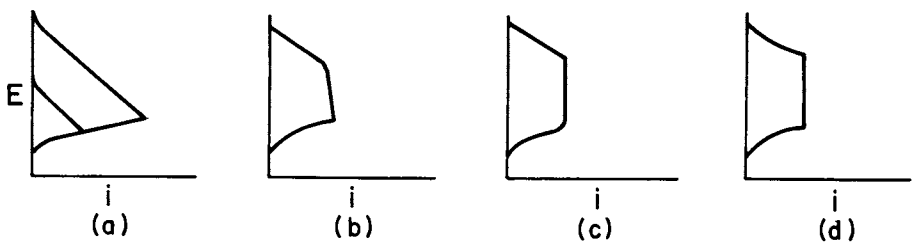

Figure 4. Evans-type polarization curves: (a) anodic curve intersecting two possible cathode reactions; (b) diffusion control of cathodic reaction; (c) diffusion control of anodic reaction; and (d) resistance polarization, measure E will depend on where probe is in relation to anode and cathode

In Corrosion Chemistry; Brubaker, G., et al.;
ACS Symposium Series; American Chemical Society: Washington, DC, 1979.

$$Fe + H_2O \rightleftharpoons Fe(H_2O)\ \text{adsorbed}$$
$$Fe(H_2O)ads \rightleftharpoons Fe(OH^-)ads + H^+$$
$$Fe(OH^-)ads \rightleftharpoons (FeOH)ads + e$$
$$Fe(OH)ads \longrightarrow (FeOH)^+ + e \qquad \text{RDS}$$
$$(FeOH)^+ + H^+ \rightleftharpoons Fe^{++} + H_2O$$

This mechanism postulates that the electron transfer step takes place in two stages with the oxidation of (FeOH)ads being the rate determining step(RDS).

In the presence of halides there is a change in mechanism and Lorenz (5) has suggested the following steps.

$$Fe + H_2O \rightleftharpoons Fe(H_2O)ads$$
$$Fe(H_2O)ads + X^- \rightleftharpoons FeX^-_{ads} + H_2O$$
$$FeX^-_{ads} + OH^- \longrightarrow FeOH^+ + X^- + 2e \qquad \text{RDS}$$
$$FeOH^+ + H^+ \rightleftharpoons Fe^{++} + H_2O.$$

Here the oxidation involves an adsorbed halide iron-surface metal atom complex. In both cases oxidation is to ferrous ion in solution. The final concentration of $FeOH^+$ and Fe^{++} is strongly pH dependent. The two ions will only be stable in acid or oxygen-free systems. In the presence of oxidants the Fe^{++} will be oxidized to various insoluble ferric compounds such as Fe_3O_4. Fe_2O_3 and the hydrated oxides, α, β and γ FeO(OH).

The two main cathodic reactions involved in dissolution (and corrosion) reactions are the reduction of H^+ to H_2 and the reduction of dissolved O_2 to OH^-. The following reaction schemes are the ones which have been postulated.

H^+ Reduction

$$H^+_{aq} + e \rightleftharpoons H_{ads} \qquad (1)$$
$$\text{or } H_2O + e \rightleftharpoons H_{ads} + OH^-_{aq} \qquad 1(a)$$
$$H + H \rightleftharpoons H_2 \qquad 2$$
$$H^+_{aq} + H\ ads + e \rightleftharpoons H_2 \qquad 3$$
$$H_2O + H_{ads} + e \rightleftharpoons H_2 + OH^-_{aq}. \qquad 3(a)$$

(1) and (3) will predominate over 1(a) and 3(a) at low ph's. The rate determining step depends in part on the catalytic properties of the surface. This is particularly true for the recombination reactions (2) and 3 or 3(a). In some cases the recombination reaction is more difficult than dissolution of atomic hydrogen into the metal and an alternative reaction

In Corrosion Chemistry; Brubaker, G., et al.;
ACS Symposium Series; American Chemical Society: Washington, DC, 1979.

$$H_{ads} \longrightarrow H_{metal} \qquad (4)$$

becomes a predominant reaction. If catalytic sites for hydrogen atom recombination exist within the metal, such as inclusions, then hydrogen gas is formed in the metal and blistering and rupture can occur.

O_2 Reduction

$$O_2 + e^- \rightleftharpoons O_2^- \text{ ads.}$$
$$O_2 + H^+ \rightleftharpoons HO_2 \text{ ads.} \qquad O_2 + 2H^+ + 2e$$
$$HO_2 + e^- \rightleftharpoons HO_2^-$$
$$HO_2^- + H^+ \rightleftharpoons H_2O_2 \text{ aq} \qquad \rightarrow H_2O_2.$$

$$H_2O_{2ads} + e^- \longrightarrow OH + H^- \qquad H_2O_2 + 2H^+ + 2e$$
$$OH + e \longrightarrow OH^-$$
$$OH^- + 4H^+ + 4e \longrightarrow 2H_2O. \qquad \longrightarrow 2H_2O.$$

$$O_2 + 4H^+ + 4e \longrightarrow 2H_2O.$$

H_2O_2 has been identified as a transient species. These reactions are all quite rapid in comparison to the hydrogen evolution reaction and hence the oxygen is a better cathodic depolarizer than H^+ ion.

Kinetics of Dissolution

The rates of both chemical and electrochemical reactions are affected by the availability of the reactants and products, and hence their concentrations and rates of diffusion, and by a term known as the activation energy for the reaction. The rate of an electrochemical reaction can also be affected by the various resistances in the system.

If we can set up a system in which the reaction is not controlled by either diffusion or resistance, the rate of the reaction will be determined by the activation over-potential. This follows from the Arrhenius equation which states that

$$k = A \exp(-\Delta G^*/RT)$$

where k is the reaction rate, A is a constant, ΔG^* is the activation energy, R the gas constant and T the absolute temperature. As pointed out earlier ΔG^* can be related to potential by the relation

$$\Delta G^* = nF\Delta E^*$$

In Corrosion Chemistry; Brubaker, G., et al.;
ACS Symposium Series; American Chemical Society: Washington, DC, 1979.

where ΔE^* is the Activation overpotential. The application of a potential to the electrode will therefore increase the rate of either the forward or reverse reaction.

A schematic activation energy diagram for a reaction is shown in Fig. 5. The dotted line represents the equilibrium state and the solid line a polarized state due to an applied potential. In the equilibrium state

$$i_a = A_a e^{-\frac{\Delta G^*_a}{RT}}$$

$$i_c = A_c e^{-\frac{\Delta G^*_c}{RT}}$$

where subscripts a and c are anodic and cathodic and $i_a = i_c = i_o$ - where i_o is the exchange current. When a potential E is applied in an anodic direction then

$$\text{then } \Delta i_a = + A_a e^{\left(\frac{-(\Delta G^*_a - nFE)}{RT}\right)}$$

$$\text{and } \Delta i_c = A_c e^{\left(\frac{-(\Delta G^*_c + (1-\alpha)nFE)}{RT}\right)}$$

where α is the proportion of the applied potential which is effective at the anode. As a rule $\alpha = 0.5$. The effect of the applied anodic potential is to increase i_a and decrease i_c. For the total current we must add i_o. However at sufficiently high overpotentials both i_c and i_o become small in relation to i_a and

$$E = a + b \log i. \quad \text{(Tafel equation)}.$$

Some of these relationships are illustrated graphically in Figure 6. E_o is the equilibrium potential. At sufficiently high overpotentials a straight line Tafel region is observed. At higher applied potentials current may become independent of potential because of diffusion control or may fall off the straight line due to resistance polarization. In the anodic reaction this is usually due to the formation of films on the surface of the metal.

These concepts can be applied quite directly to the corrosion behavior of iron. The effect of diffusion control on the corrosion rate was shown in the Evans Diagrams (b) and (c) of Figure 4. In the cathodic case the current becomes constant over a wide range of potentials because of control by the rate of diffusion of the reactant oxygen gas to the cathode. The anodic reaction can be dependent on the rate of diffusion of Fe^{++} from the anode. The rates in both cases can be increased by stirring. The rate of Fe^{++} ion removal from the anode can also be increased by the presence of complexing agents in the solution. This effect will be illustrated later on with inhibitors.

In Corrosion Chemistry; Brubaker, G., et al.;
ACS Symposium Series; American Chemical Society: Washington, DC, 1979.

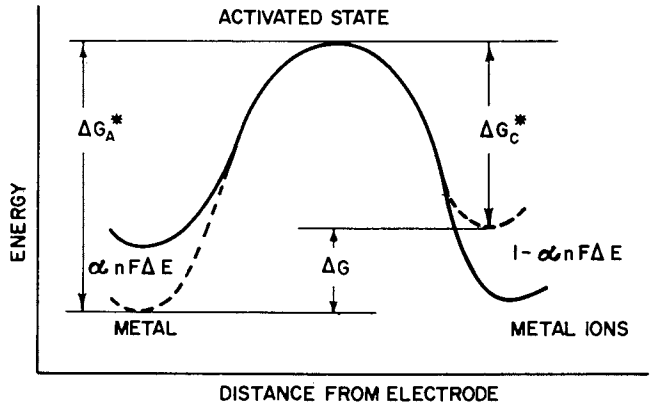

Figure 5. Activation energy diagrams for metal dissolution reaction. Equilibrium state (– – –); shift attributable to application of potential E (——).

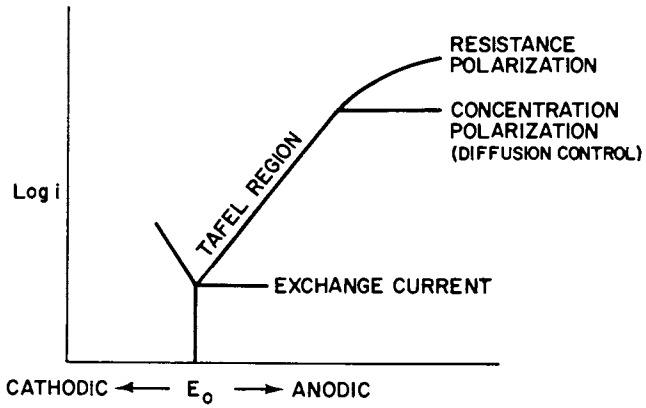

Figure 6. Polarization curves for anodic reactions

In Corrosion Chemistry; Brubaker, G., et al.;
ACS Symposium Series; American Chemical Society: Washington, DC, 1979.

The effect of the formation of films under some anodic conditions has been known and studied for many years. Müller (6) observed that at high applied potentials salt films could form at the anode which would reduce the current density. When these films diffused away, the current rose again. This is a case of intermittent resistance polarization. In some solutions it is possible to stop iron from dissolving under some conditions. Two of these sets of conditions are illustrated in Fig. 7. In Fig. 7(a) the current density is raised in steps. The potential current relationship starts out in the normal way but at a sufficiently high current density a sudden discontinuity occurs in the log i-E curve with a sharp rise of potential. At the same time the metal stops dissolving and a second anodic reaction such as oxygen evolution takes over. This type of behavior was first shown by Edeleanu (7) who also suggested the use of anodic protection to prevent corrosion. In Fig. 7(b) the potential is raised in steps. Again, at some potential the current drops sharply and iron stops dissolving and remains "passive" over quite a wide range of potential. This type of behavior is characteristic of iron over a wide range of pH conditions and has been studied extensively. It is of interest not only for anodic protection but also for understanding the action of anodic inhibitors. This passive condition is not something that would be predicted from kinetic considerations and is probably due to the formation of a solid protective phase over the iron which slows down the reaction.

Passivation of Iron

(a) Electropolishing. The deviation from the theoretical anodic dissolution behavior can be used to advantage in several ways. One of these is for the electropolishing of iron. An anodic polarization curve for iron in a perchloric-acetic acid solution is shown in the Fig. 8. It can be seen that there are three regions of the curve. In the first region, A, the log i-E curve is the expected one and the iron dissolved in a general way with macro etching. In Region B the current changes very little with potential and the specimen smooths. This is probably due to the formation of film which is resistant to cation movement from the metal. At higher potentials, Region C, this film breaks down locally and the specimen dissolves by a combination of smoothing and pitting. Region B can be considered as a region of passivation in that the dissolution is less than would be expected from the overpotential. Under some conditions this anodic dissolution can be made very small and the specimen is considered to be anodically passivated.

(b) Anodic Passivation. Anodic passivation can be obtained over a wide range of pH's and in a variety of electrolytes. In this section, however, I shall deal mainly with neutral solutions

In Corrosion Chemistry; Brubaker, G., et al.;
ACS Symposium Series; American Chemical Society: Washington, DC, 1979.

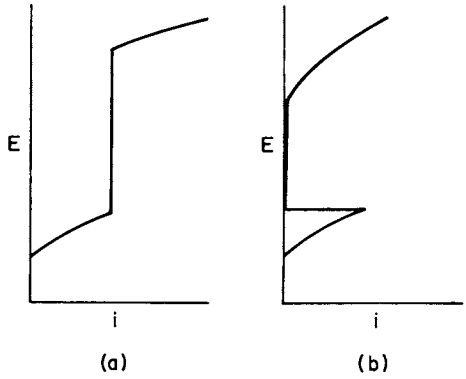

Figure 7. Anodic passivation curves

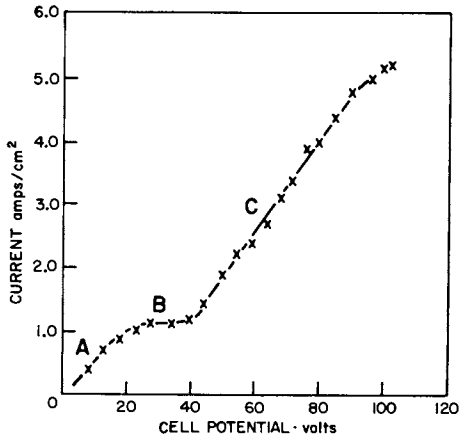

Figure 8. Anodic dissolution in perchloric–acetic acid

In Corrosion Chemistry; Brubaker, G., et al.;
ACS Symposium Series; American Chemical Society: Washington, DC, 1979.

because, first, it is the medium in which I have done most of my own work and second, because results in this range are most applicable to later considerations of passivity in inorganic inhibitor systems.

In Fig. 9 three polarization curves for iron in buffered sodium borate solutions are shown. In A the solution was sodium borate-boric acid at a pH of 8.4 (8). The curve was obtained by polarizing iron at a constant potential and measuring the current after 20 minutes. Starting with an oxide-free specimen the current first increases as the potential is increased, reaches a maximum and then decreases again. There is a region of over a volt in which iron does not dissolve, or is passive, and then the current rises again, due mainly to oxygen evolution. In the passive region the iron is covered by a thin film of cubic oxide of the γ-Fe_2O_3-Fe_3O_4 type which is probably formed by a reaction such as

$$2Fe + 3H_2O \rightarrow Fe_2O_3 + 6H^+ + 6e.$$

This is the same type of film as is formed by the reaction of clean iron with dry air or oxygen.

For Curve B the solution was sodium chloride-boric acid buffered to pH 7.8. The polarization conditions were the same. However in the presence of the chloride the maximum current before the onset of passivity was increased and the potential range for passivity was decreased. The high currents observed in the "passive region" were mainly due to localized attack which leads to pitting. The major part of the surface is still covered by the same type of iron oxide film as that found with the pure borate buffer.

A third type of anodic polarization curve, C, is obtained if the borate buffer solution contains Fe^{++} ion in solution. This may be present as an added Fe^{++} salt or due to some dissolution of the specimen during passivation. In this case the passive current is again higher than in the borate buffer itself. This is due to the anodic oxidation of the dissolved Fe^{++} at the electrode and the consequent deposition of γFeOOH on the iron surface. The anodic reaction is

$$Fe(OH)^+ + H_2O \rightarrow FeO(OH) + 2H^+ + e.$$

This deposit is formed over the oxide film as well as at pores within the oxide film.

The dissolution of iron by corrosion processes almost always takes place because of film breakdown and the rate of corrosion depends not only on the thermodynamic and kinetic considerations mentioned in the first part of this chapter but also on the factors leading to film breakdown and repair. This is the subject of the last part of this chapter.

In Corrosion Chemistry; Brubaker, G., et al.;
ACS Symposium Series; American Chemical Society: Washington, DC, 1979.

Film Breakdown and Repair

When film free iron is exposed to dry air or oxygen at room temperature, it will form a protective film of a cubic oxide of the Fe_3O_4-γFe_2O_3 type which grows logarithmically to about 15-20 A° thick. This is the same type of film as is formed by anodic passivation and by the action of certain oxidants in solution. Under other conditions the overall composition of this cubic film can be altered by the addition of hydrated oxides or other insoluble oxides, such as Cr_2O_3, which can change the thickness, topography and stability of the overall film. In some cases these impurities are present as separate inclusions within the film leading to weakened areas at which localized breakdown may occur or they may be on top of the cubic oxide film, such as a deposited γ-FeOOH and enhance the protectiveness of the film. These various cases are discussed in this section.

Structure of the Oxide Film

The major portion of the protective oxide film on iron is structurally the same whether it is grown by exposure to air, inhibitor solutions or formed by anodic oxidation (9,10). It is cubic in nature and grows in an epitaxial manner with the underlying metal. Although the oxide formed on single crystals is highly oriented, there is some mismatch between individual crystallites and the particle size is 15-30A°. The thickness of the air-formed film at room temperature is 15-20 A°. The films formed anodically in neutral solution can be up to 40 A° in thickness, the thickness increasing with higher polarization potentials. An electron diffraction pattern of the oxide on single crystals of iron is shown in Fig. 10. This shows the very ordered structure as well as the broadened spots due to small particle size. The pattern is characteristic of the cubic Fe_3O_4-γFe_2O_3 system. This system has a constant face-centered cubic lattice of oxygen with varying amounts of iron in both octahedral and tetrahedral positions. The oxide probably varies in composition from the metal-oxide interface to the oxide-gas or solution interface with the γFe_2O_3 at the outside.

Under some conditions the film will contain inclusions of other iron compounds, such as hydroxides or phosphates, and as mentioned earlier may also have an overlay of precipitated or deposited compounds.

Breakdown of Films

In general, oxide films can be removed as protective layers by chemical dissolution, undermining, or cathodic reduction.

Anhydrous oxide films are usually quite difficult to dissolve. The rate of solution increases with lower pH and higher temperature. In neutral solution the rate of dissolution of the

In Corrosion Chemistry; Brubaker, G., et al.;
ACS Symposium Series; American Chemical Society: Washington, DC, 1979.

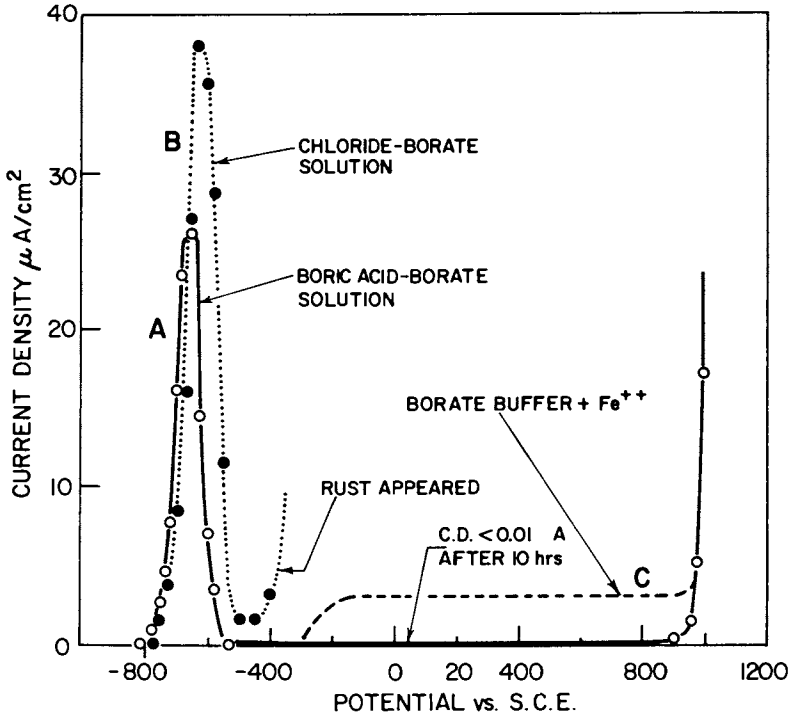

Figure 9. Anodic polarization curves in borate buffer solutions

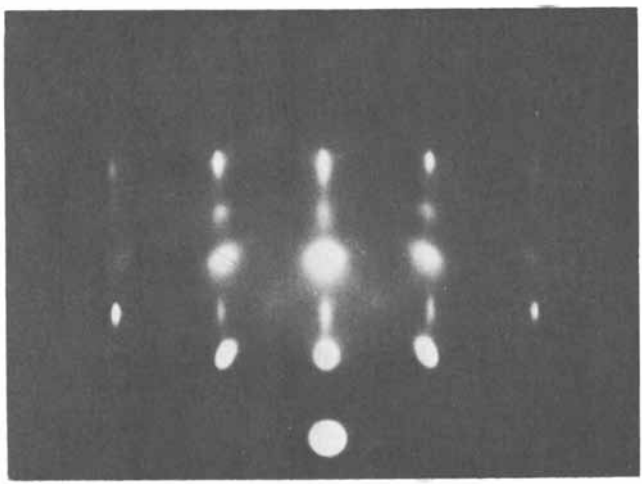

Figure 10. Electron diffraction pattern of thin cubic oxide film on iron

passive film is so slow that it is probably not a factor in the breakdown of oxide films on iron. The hydrated oxides are more easily dissolved, especially in slightly acid solutions and their removable by dissolution could be a definite factor in film breakdown. If the film has pores in it which expose the metal to the corrosive solution, the metal can dissolve both at the bottom of the pore and between the film and the metal. This latter effect loosens the oxide by undermining and eventually leads to its removal. U.R. Evans took advantage of this phenomenon to strip oxides from iron for chemical and physical examination (11). To prevent cathodic reduction of the oxide he made the system anodic.

The major cause of removal of oxide films on iron is the reductive dissolution of the oxides. The anodic current for the process may be supplied by an outside source or by areas of the metal at which iron is dissolved. In both cases the ferric oxide is reduced to Fe^{++}. The solubility of $Fe(OH)_2$ is much higher than either Fe_2O_3, Fe_3O_4 or the FeOOH's and it dissolves. The magnetite component of the oxide is reduced in part to Fe^{++} and in part to Fe metal.

The cathodic reduction of an anodically formed oxide film is shown in Figure 11. The film was formed by anodic oxidation in a neutral sodium borate solution. It was cathodically reduced in the same solution, in the absence of oxygen, at $10\mu A/cm^2$. Two major waves are observed. First the Fe_2O_3 is reduced with almost 100% current efficiency to form dissolved Fe^{++} ion. The second wave corresponds to an inefficient reduction of Fe_3O_4 to form both soluble Fe^{++} ion and metallic iron. The equations for these processes are

$$\text{1st Arrest } \gamma Fe_2O_3 + 3H_2O + 2e \longrightarrow 2Fe^{++} + 6OH^- \qquad (A)$$

$$\text{2nd Arrest } Fe_3O_4 + 4H_2O + 8e \longrightarrow Fe + 8OH^- \qquad (B)$$

$$Fe_3O_4 + 4H_2O + 2e \longrightarrow 3Fe^{++} + 8OH^- \qquad (C)$$

During the second arrest there is also considerable hydrogen evolution form the alternate cathodic reaction

$$2H^+ + 2e \longrightarrow H_2.$$

If the reduction process is carried on for a long time, there is also some electrodeposition of iron from Fe^{++} in the solution.

The major source of electrons for the cathodic reduction process on open circuit is the corrosion of the iron itself. These are supplied by the reaction

$$Fe \longrightarrow Fe^{++} + 2e$$

The potential for this reaction is more negative than that for reaction (A) and hence the electrons are available for the reductive dissolution of γFe_2O_3. On open circuit the oxide can be removed

In Corrosion Chemistry; Brubaker, G., et al.;
ACS Symposium Series; American Chemical Society: Washington, DC, 1979.

by a combination of reductive dissolution to open up pores and undermining to remove the remaining Fe_3O_4 and unreduced film.

The rates of dissolution of Fe_3O_4 and the hydrated oxides both increase quite quickly with decrease in pH. Hence breakdown of films is more rapid in acid solutions. It is also more rapid in solutions containing ions which lead to acid formation in the anodic pores. Chloride ion is the most damaging of this type of ion although sulphates are also destructive. The iron chloride salts which form during corrosion in the pores hydrolyse to give precipitated iron salts and acid. Chloride may also act somewhat like a complexing agent to increase the corrosion rate. The effect of various ions on film breakdown was recently discussed at a symposium on passivity (12).

Inhibition of Corrosion

Inhibitors can slow down the corrosion rate by interfering with either the anodic or cathodic reactions. The cathodic inhibitors can be effective by either poisoning the surface for hydrogen evolution and/or oxygen reduction or by increasing electronic resistance. Some examples are zinc salts which form precipitates, adsorbing organic substances and possibly the polyphosphates under some conditions. The discussion in this lecture will deal mainly with anodic inhibitors. These act by interfering with the anodic dissolution-process by assisting in the formation and preservation of an oxide film, similar to that produced during anodic oxidation of iron.

Anodic Inhibitors

The anodic inhibitors are usually inorganic salts which, above a minimum concentration decrease corrosion to a negligible amount. A typical concentration versus weight-loss curve is shown for sodium nitrite in Figure 12. In the absence of inhibitor or very low concentrations the corrosion is localized and takes the form of pitting. At sufficiently high concentration the iron is completely protected. This phenomenon of pitting at concentrations just below that required for inhibition is important and must be taken into account when anodic inhibitors are used. The concentration of inhibitor required to stop corrosion is dependent on the composition of the solution and is usually decreased by the presence of oxygen and increased by additions of chloride or complexing agents. The effect of a strong complexing agent, versene, is shown in Figure 13. The time required to achieve inhibition, as measured by the attainment of a passive potential is increased as the concentration of complexing agent is increased. The complexing agent keeps the iron in solution and prevents the repair of pores by deposition of ferric salts.

The close connection between potential and corrosion is shown by the two sets of graphs in Figure 14. Here one can see, that for iron in phosphate solution in the presence of oxygen, the time

In Corrosion Chemistry; Brubaker, G., et al.;
ACS Symposium Series; American Chemical Society: Washington, DC, 1979.

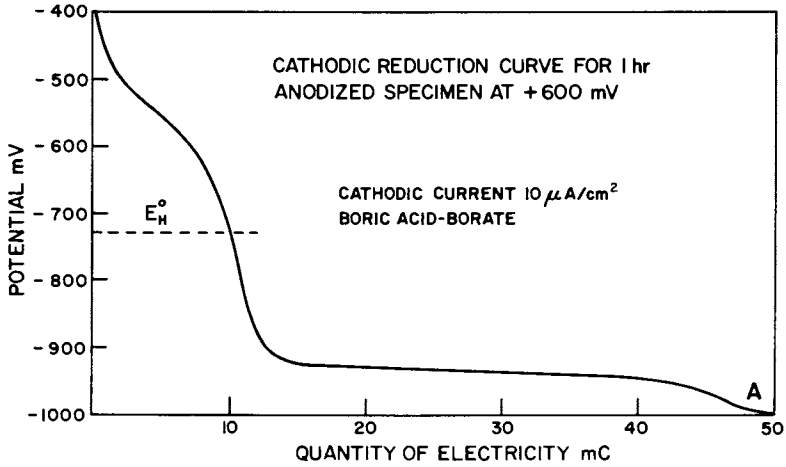

Figure 11. Cathodic reduction of anodically formed oxide film on iron

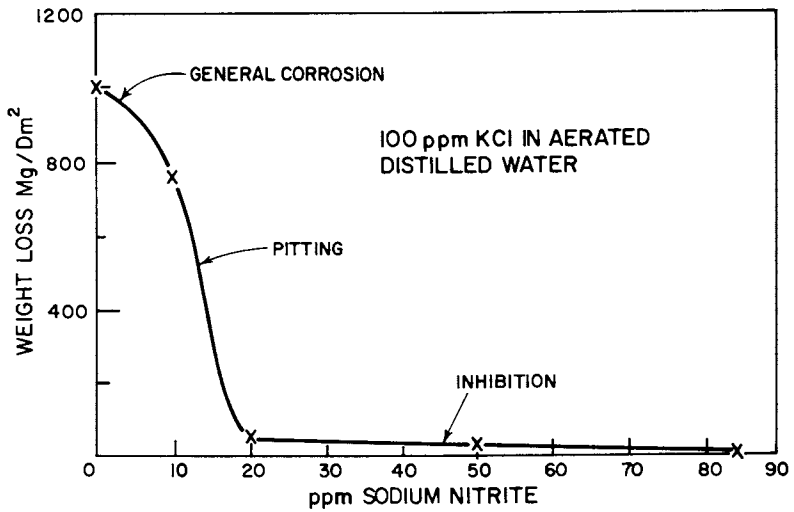

Figure 12. Inhibition of corrosion by sodium nitrite

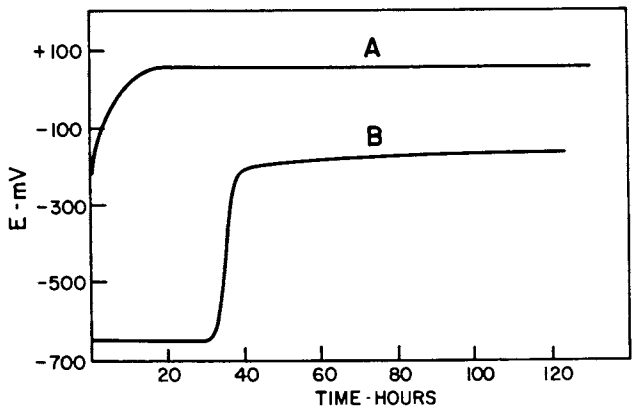

Figure 13. Effect of complexing agent, versene, on passivation by sodium nitrite: (A) etched iron in $NaNO_2$ solution; (B) same as in A plus versene

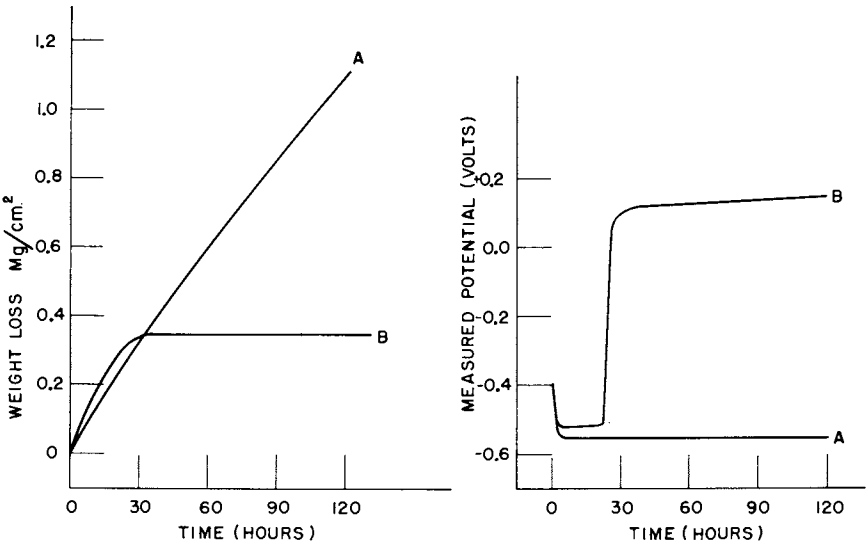

Journal of the Electrochemical Society

Figure 14. Relationship between corrosion and potential in neutral phosphate solutions: (A) deaerated solution; (B) air saturated (10)

at which the potential rises to the passive region is also the time at which corrosion ceases. In the absence of oxygen corrosion continues and the potential remains in the active region.

The necessity for the presence of oxygen for inhibition is common to a large number of inorganic substances. In general these are non-oxidizing salts which have some buffering capacity in the neutral region. There is also a group of anodic inhibitors which are oxidizing agents and inhibit in both the presence and absence of oxygen. The oxidizing agents inhibit at a much lower concentration than the non-oxidizing agents in the presence of oxygen (13). This is shown in Figure 15. Potential time curves for the same series of inhibitors are shown in this Figure. The potentials for the non-oxidizing inhibitors in the absence of oxygen reach a steady value for iron in a saturated solution of Fe^{++} at a concentration characteristic of the pH of the salt solution. The potential of the oxidizing inhibitors is somewhat higher and with sufficient time goes into the passive region-characteristic of oxide-covered metal. Sodium chromate is not shown in this Figure, but the potential of iron in de-aerated solution goes into the passive region very rapidly. Until recently chromate was the preferred inhibitor for many applications. However chromate is undesirable from an environmental standpoint and there is renewed research and development in the use of nitrite, molybdate and small concentrations of phosphate.

There is another group of inhibitors which act by adsorption onto either the metal or the oxide. These are usually organic materials and the most effective are either alcohols or amines. They are mainly used in specialized applications such as inhibition of acid corrosion during pickling or in mitigation of corrosion in acid oil wells. The exact action of these inhibitors is beyond the scope of this chapter but they are discussed by Hackerman and others (14). Some buffering inhibitors, such as sodium benzoate may also act by adsorption on the surface.

Localized Corrosion

In the discussion to this point we have noted three cases where the corrosion occurred in a localized manner via pitting. These were in an electropolishing solution at a current density (and potential) higher than in the polishing region, in a borate buffer solution containing chloride at a potential a few hundred millivolts higher than the passivation potential, and in inhibitor solutions at just below the concentration of inhibitor required to prevent corrosion. In all of these examples the major portion of the specimen is covered with the usual Fe_3O_4 - γFe_2O_3 type of protective film and corrosion is concentrated at pores within this film. The corrosion at the anodic pores is accelerated by the large area covered by protective film acting as a cathode. This breakdown of the protective film at isolated areas is an important factor in two of the most damaging types of corrosion failure,

In Corrosion Chemistry; Brubaker, G., et al.;
ACS Symposium Series; American Chemical Society: Washington, DC, 1979.

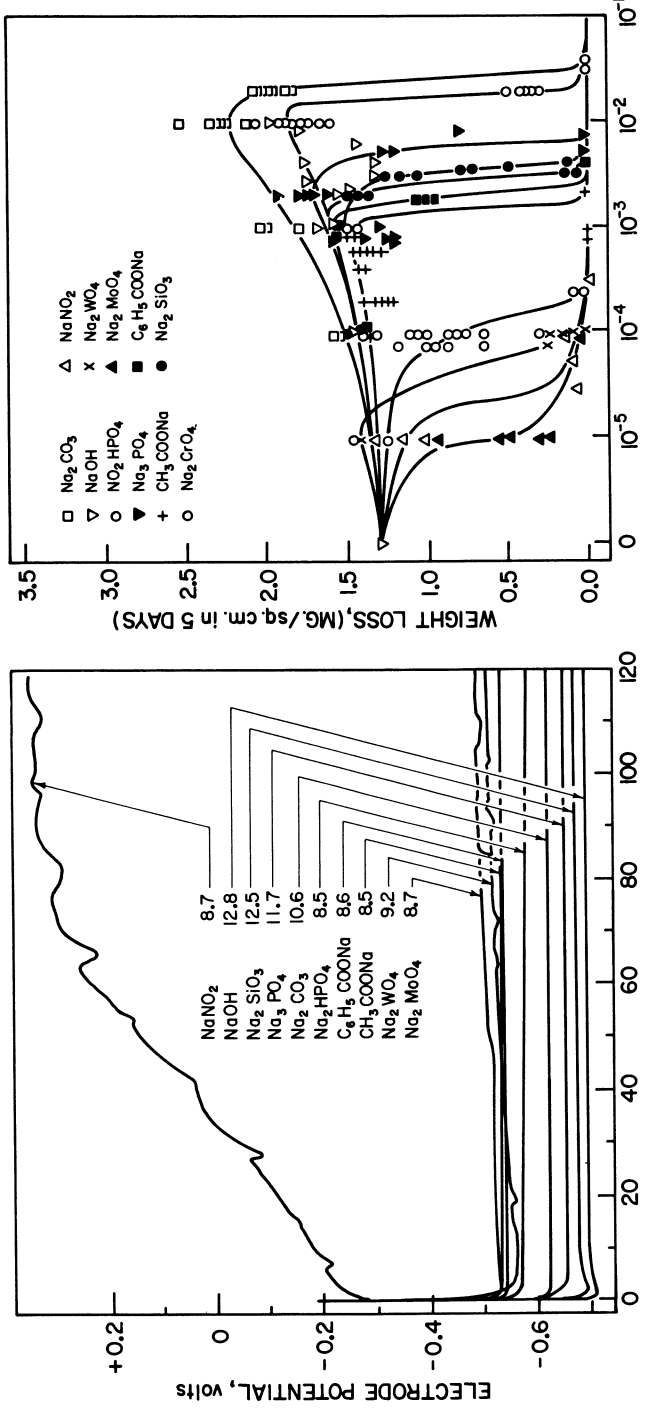

Journal of the Electrochemical Society

Figure 15. Inhibition in both oxidizing and nonoxidizing inhibitors. Weight-loss data in aerated solutions. Electrode potential curves in absence of oxygen (13).

namely the perforation of metal by pitting and stress corrosion cracking.

Examples of pitting in phosphate solutions with different chloride contents are shown in Figure 16. Two things are evident. First, the larger the chloride concentration the larger the pits. Second, the number of pits is dependent on the grain structure. This latter fact would indicate that the perfection of the oxide is partially dependent on the metal orientation. The dependence of pit behavior on stirring of the solution is shown in Figure 17. Here one can see that stirring causes an increase in the potential of iron in nitrite solutions. This is probably due to the lowering of cathodic polarization by increasing the rate of oxygen and nitrite arrival at the cathode. This increase in cathodic curent appears to aid the repair of the pore. In contrast to this behavior, stirring decreases the potential of the pitted specimen in phosphate solution. This indicates that stirring leads to depolarization of the anodic areas, possibly by removing corrosion products at the pits. Recovery with phosphate is slow. In general, the potentials with phosphate are lower than with nitrite, indicating a large proportion of active areas and hence a mixed potential which is closer to that of the anode.

Stress corrosion cracking also involves localized breakdown of the protective film. The corrosion is narrowly confined within the metal due to stress factors which may arise from either residual internal stress or applied external stress. In some cases the stress failure can be accelerated by chemical factors, such as surface adsorption or hydrogen dissolution from cathodic hydrogen leading to embrittlement.

Localized film breakdown can result from a number of causes. Chemical and physical inhomogeneities within the film are the usual reasons although breakdown can also occur by stresses set up within the film either by poor epitaxial fit of the oxide to the metal, or as Sato (15) has suggested by equivalent condenser pressure during anodic growth of the film. Vermilyea (16) has shown current increases due to the cracking and repair of films during stretching of passivated iron wires. The role of stress is still a subject of active research.

Some of the reactions which can take place at imperfections in films and which can lead to either dissolution or film repair are shown in the final figure, Figure 18. Here a specimen covered with an oxide film with pores or imperfections is shown. A number of different reactions can take place both at the pores and on the oxide surface. In general the reactions at the pores represent either anodic or dissolution processes, while those on the oxide surface are cathodic in nature. Reaction 1 coupled with reactions (6) or (7) represents the standard dissolution process. This can be accelerated by a number of factors such as lowered pH, presence of chloride and complexing agents. Reaction (1) coupled with reaction (8) gives both dissolution and removal of the protective film, which will then lead to accelerated dis-

In Corrosion Chemistry; Brubaker, G., et al.;
ACS Symposium Series; American Chemical Society: Washington, DC, 1979.

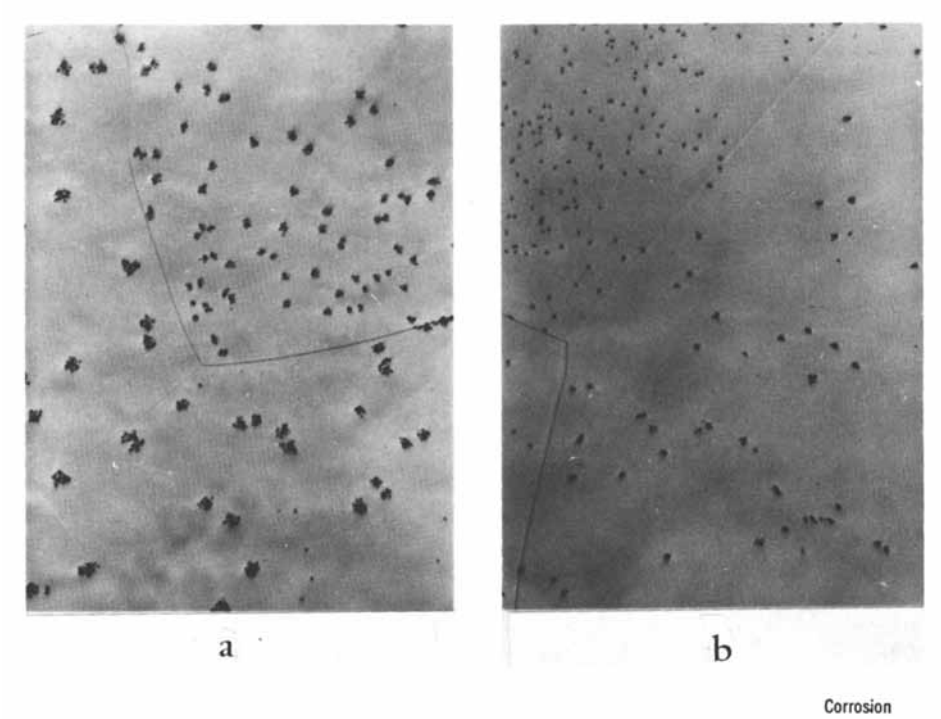

Figure 16. Pitting in phosphate–chloride solutions, 1000 ppm Na_2HPO_4; (a) 100 ppm Cl^-, (b) 10 ppm Cl^- (17)

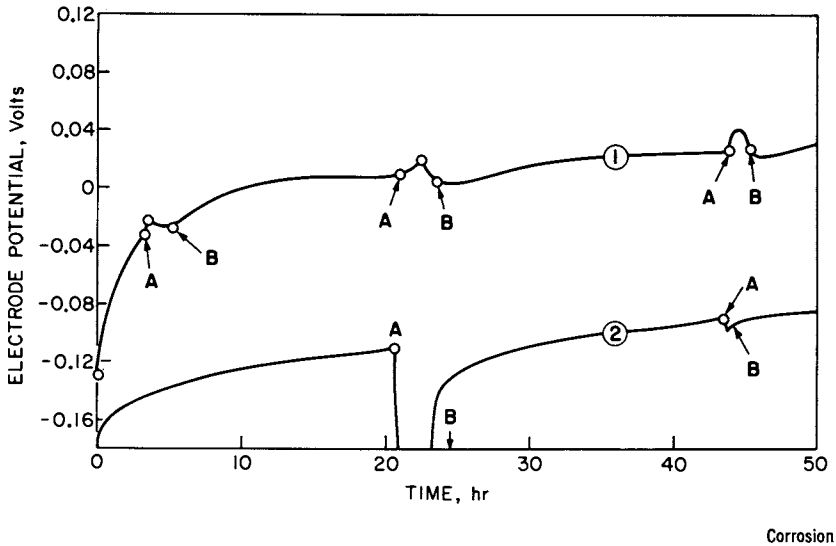

Figure 17. Effect of stirring on potential of iron in chloride and inhibitor solution: (A) started bubbling; (B) stopped bubbling; ① 1000 ppm $NaNO_2$ + 100 ppm NaCl; ② 1000 ppm Na_2HPO_4 + 25 ppm NaCl) (17)

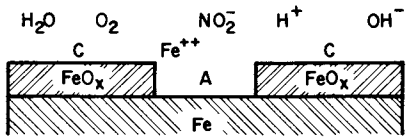

AT A

$$Fe \longrightarrow Fe^{++} + 2e \quad (1)$$

$$2Fe + 3H_2O \longrightarrow Fe_2O_3 + 6H^+ + 6e \quad (2)$$

$$Fe^{++} + 2H_2O \longrightarrow FeOOH + 3H^+ + e \quad (3)$$

$$4Fe + 3O_2 \longrightarrow 2Fe_2O_3 \quad (4)$$

$$4Fe + NO_2^- + 3H^+ \longrightarrow 2Fe_2O_3 + NH_3 + N_2 \quad (5)$$

AT C

$$2H^+ + 2e \longrightarrow H_2 \quad (6)$$

$$O_2 + 2H_2O + 4e \longrightarrow 4OH^- \quad (7)$$

$$NO_2 + H_2O + e \longrightarrow NH_3 \text{ (etc)} \quad (8)$$

$$Fe_2O_3 + 2e + 3H_2O \longrightarrow 2Fe^{++} + 6OH \quad (9)$$

Figure 18. Reaction on film with pore

solution. The pores can be repaired either electrochemically, by anodic oxidation as in (2) and by anodic deposition as in (3). It is also possible for the film to be repaired chemically by the action of inhibitors as depicted in reactions (4) and (5). This type of approach lends itself to a systematic treatment of the problems of dissolution and its inhibition.

Literature Cited

1. Pourbaix, M. "Atlas of Electrochemical Equilibrium in Aqueous Solutions", Pergamon Press, 1966.
2. Evans, U.R. "An Introduction to Metallic Corrosion", Edmund Arnold Co. London 1948, Pages 71-3.
3. Thornhill, R.S. and Evans, U.R. J. Chem. Soc. (1938) 614.
4. Kelly, E.J. J. Electrochem. Soc. (1965) 112, 124.
5. Lorenz, W.J. Corrosion Science, (1965) 5, 121.
6. Muller, W.J. Trans. Faraday Soc. (1931), 27, 737.
7. Edeleanu, C. and Gibson, G. Chem. Ind. (1961), 301.
8. Nagayama, M. and Cohen, M. J. Electrochem. Soc. (1962), 109, 781.
9. Nagayama, M. and Cohen M. J. Electrochem. Soc. (1963), 110, 670.
10. Cohen, M. J. Electrochem. Soc. (1974), 121, 191C.
11. Evans, U.R. and Stockdale, J. J. Chem. Soc. (1929), 2651.
12. Staehle, R.W. and Okode, H. Editors. Passivity and Its Breakdown on Iron and non-Base Alloys, U.S.A.-Japan Seminar. NACE, Houston, Texas. 1976.
13. Pryor, M.J. and Cohen, M. J. Electrochem. Soc. (1953), 100, 203.
14. Hackerman, N. and Cook, E.I. J. Phys. Chem. (1952), 56, 524.
15. Sato, N. Electrochimica Acta. (1971), 16, 1683.
16. Bubor, S.F. and Vermilyea, D.A. J. Electrochem. Soc. (1966), 112, 882.
17. Cohen, M., Corrosion (1976) 32, 461.

RECEIVED September 1, 1978.

Ferrous Passivation

V. BRUSIC

Manufacturing Research Laboratory, Systems Products Division,
IBM T. J. Watson Research Center, Yorktown Heights, NY 10598

The progress of civilization has been marked by an increasing use of tools and machines. Contemporary man is bound to lean increasingly on sophisticated computerized mechanisms to do his work for him with tighter requirements to function without decay over years in terrestrial atmosphere. Materials, mainly metals, used in this fabrication must be stable.

A piece of metal indeed remains stable for an almost indefinite period of time provided it is stored in vacuum. In normal terrestrial environments metals become unstable in various ways: they develop cracks and break upon strain, suffer fatigue when subjected to periodic stress, undergo a process of embrittlement, as well as react with the surroundings. With the exception of the expensive noble metals, metallic surfaces are transformed into oxides and salts which can peel off or just dissolve away. Yet technology predominantly depends on these thermodynamically unstable, corrosive, non-noble metals, the most widely used being aluminum, copper, nickel and, of course, iron. They owe much of their usefulness to the existence of the passive state. The passivation phenomenon was first observed and described by the action of nitric acid on iron centuries ago. (1-3) From then to the present the complexity of the problem and the practical importance of its application has earned the attention of many scientists.

The present discussion draws particularly on studies that have been published recently and are concerned with iron electrodes under conditions producing passivity which are the ones that best clarify the passivation process.

Passivation Phenomena

A) Description, Terminology and Some Practical Aspects of Anodic Protection. Passivation can be defined as a constant

0-8412-0471-3/79/47-089-153$08.00/0

slowing down of any action, process, or reaction. More specifically the term is applied to the sometimes observed transformation of a corroding and unstable surface to a passive and stable surface by superimposing a double-layer field which should accelerate the metal-dissolution reaction rather than hinder it, i.e., by a shift of the electrode potential in the positive direction. This phenomenon of enforced passivation(4) seems unnatural or at least unexpected. Its study is facilitated by the use of a potentiostat.

If iron is made a part of the electrochemical cell, a test electrode, and placed in a potentiostatic circuit, Figure 1, the experimental current-potential plots show an interesting pattern, Figure 2: with an increase of potential, starting from the corrosion potential, the dissolution current increases, just as expected. Metal ions go into the solution

$$M \rightarrow M^{2+} + 2e^{-} \qquad (1)$$

undergoing hydration. At still higher potentials, however, the curve deviates from simple logarithmic dependence (Tafel law, metal dissolution). Apparently metal dissolution is hindered by another process, that is, the formation of a protective film,(4) through a reaction of the type

$$M + H_2O \rightarrow M - O + 2H^{+} + 2e^{-} \qquad (2)$$

At the passivation potential V_p a limiting passivation current i_p is reached and the acceleration of metal dissolution is equal to the retardation of the process. Above V_p the current-potential curve changes direction, metal dissolution is increasingly hindered by a process which evidently terminates at V_{pp}, a potential of "complete passivity." Thereafter the dissolution rate, i_c, sometimes orders of magnitude smaller than the passivation current, is independent of potential. The increase in current at some higher potential is determined by the overpotential of oxygen discharge, or the presence of some oxidation - reduction system. The region is termed "transpassive."

The term "Flade potential," V_F, has a variety of connotations. Many investigators, following Flade's original definition, assign this name to the potential at which an already passivated metal begins to lose passivity.(5-7) Some prefer to assign this term to the passivation potential V_p (8) or to V_{pp}.(9) According to Tomashov and Charnova(4) V_F is the thermodynamic potential at which the formation of a metal oxide becomes possible and it is lower than V_p, Figure 2. As much as possible the discussion in this paper will refer to

In Corrosion Chemistry; Brubaker, G., et al.;
ACS Symposium Series; American Chemical Society: Washington, DC, 1979.

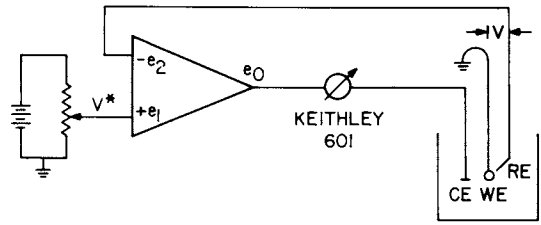

Figure 1. A potentiostatic circuit: an imposed potential difference (V) drives the current (I) from an auxiliary electrode to the test electrode until the potential difference (V) becomes equal to V**

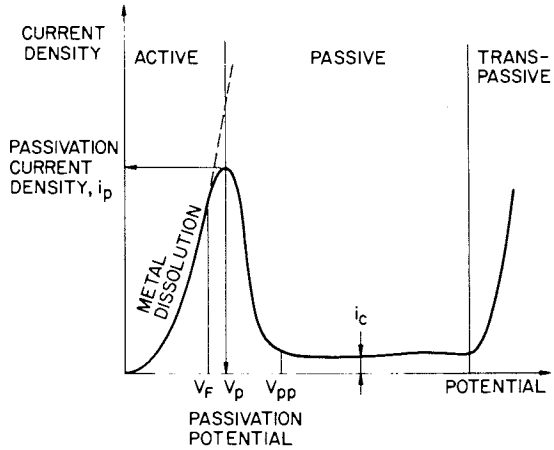

Figure 2. A typical i–V curve on iron or steel

the terminology given in this figure.

The definitions of the passive state are based on the observation: a metal is passive when the amount of metal consumed by a chemical or electrochemical reaction at a given time is significantly less under conditions corresponding to a higher affinity of the reaction than under the conditions corresponding to a lower affinity (Wagner (10)), or, a metal is in a state of improved corrosion resistance (under conditions where, from a thermodynamical point of view, the metal is reactive) accounted for by inhibition of the anodic process (Tomashov (5)). Such a definition enables us, without hypothesizing about the nature of the oxidized state, to distinguish between "the passivity" on one hand and "the inhibition" (and diminuation of the corrosion rate by paints or galvanoplastic deposits) on the other. In the latter the adsorption of the active species from the solution influences the reaction kinetics at the metal-solution interface without appreciably influencing the potential difference. Also this definition differentiates clearly passivity or anodic protection from the cathodic protection of a metal at low potentials where metal is said to be "immune." As seen from Figure 3 the metal dissolution current in the passive region, i_c, to be supplied for anodic protection is usually much smaller than the cathodic protective current. Also the potential region is such that there can be no hydrogen evolution (and metal embrittlement). Figure 3 is a more detailed version of Figure 2, indicating the location of the corrosion potential and showing that i_{app} (or $i_{measured}$) is always the difference between i_{ox} and i_{red}.

Similar curves can be given to illustrate some practical aspects of iron passivation:

- iron can be passivated by concentrated but not dilute nitric acid (Figure 4), i.e., iron can spontaneously passivate.
- if corroding in an electrolyte under complete diffusion control an increase of the electrolyte velocity may passivate the iron. The smaller the pasivation current, the easier the passivation (Figure 5).
- coupling with Pt may involve passivity on Ti (Figure 6) but not on iron (Figure 7) as long as its active-passive transition range lies above the reversible hydrogen potential.

Both theoretically and practically, however, the most interesting aspect of the passivation phenomenon is seeking the mechanism underlying the enforced passivation, the search for the "cause" of passivation and fuller understanding of the surface changes resulting in active-passive transition.

In Corrosion Chemistry; Brubaker, G., et al.;
ACS Symposium Series; American Chemical Society: Washington, DC, 1979.

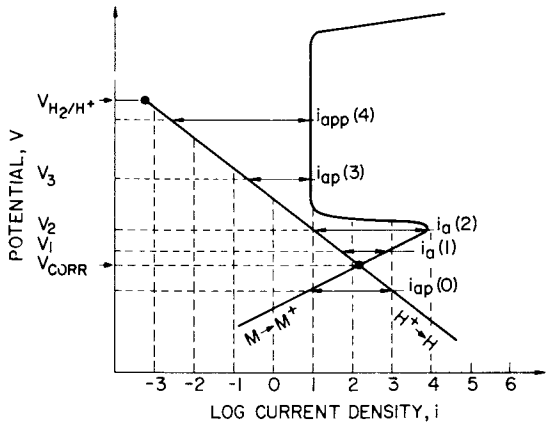

Figure 3. Effect of applied anodic and cathodic currents on the behavior of an active–passive system

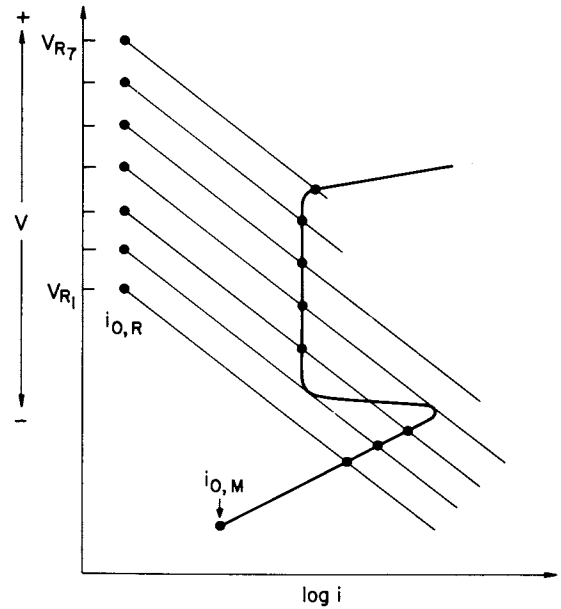

Figure 4. Effect of oxidizer concentration on the electrochemical behavior of an active–passive metal

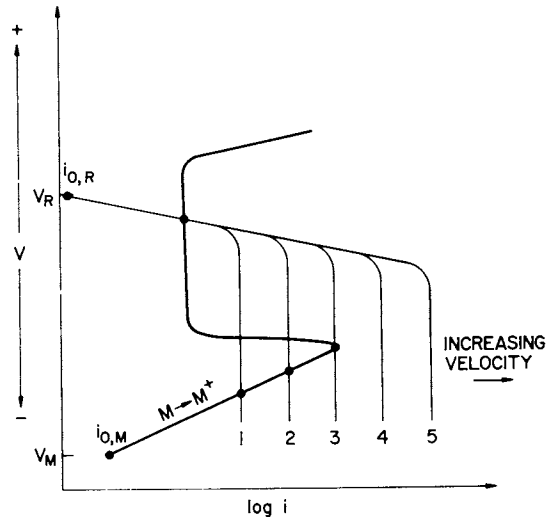

Figure 5. Effect of velocity on the electrochemical behavior of an active–passive metal under diffusion control

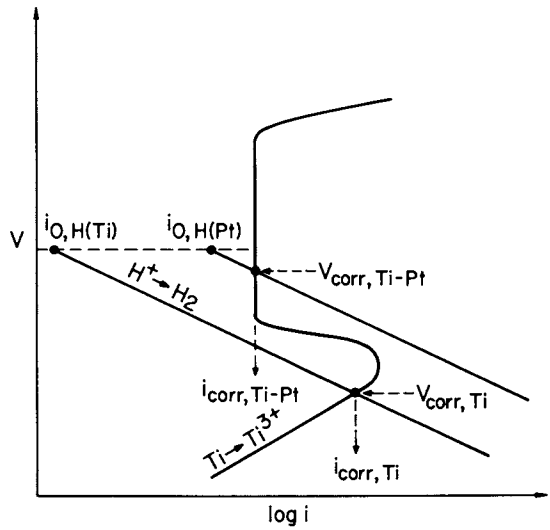

Figure 6. Spontaneous passivation of titanium by galvanically coupling to platinum

In Corrosion Chemistry; Brubaker, G., et al.;
ACS Symposium Series; American Chemical Society: Washington, DC, 1979.

B. Passivation Theories, Iron et al. The first theory of passivity was suggested over a century ago when Faraday (3) stated "my strong impression is that the surface is oxidized ....." However, the investigation of the nature of the "passivating material" introduced the traditional polemics between those supporting the adsorption theory and those supporting the oxide-film theory of passivity.

The controversy is at least partly due to semantic ambiguities in the description of passivating films. The terms most often used are the following: adsorbed (chemisorbed) oxygen and oxygen-containing species, (12) monomolecular oxide, (13) monolayer (or less) of oxide, (14-20) ordered, monomolecular, two-dimensional film of a definite chemical phase, (21) three-dimensional film, (22,23) oxide not related to any known oxide, (24) nonstoichiometric oxide, (25) and duplex oxide. (26-29) It is not always clear what is meant by "surface oxides" or "surface adsorption," especially when coverage with oxygen is less than a monolayer. In the opinion of this author the term "adsorbed layer" should be reserved for the situation shown in Figure 8a, characterized by the formation of preferentially unidirectional bonding between adsorbate (oxygen) and substrate (metal) without metal ions leaving their lattice site.

In contrast, it is suggested that in the monomolecular (or less) oxide layer, metal atoms have left their regular position in the lattice (at kink sites and any other sites) to enter together with oxygen atoms into a new, alternating arrangement of oxygen and metal, which, even if two-dimensional, resembles the arrangement in the formation of the nuclei of the respective oxides (i.e., lateral bonds are formed, Figure 8b. (30)

In the three-dimensional oxide there is a repeated distance and symmetry relationship in a vertical dimension also, with either a more or less continuous relationship with the substrate (as in epitaxial film) or with a complete misorientation, as in nonepitaxial, deposited film.

There are also scientific difficulties in approaching the problem of the entities formed in passivation. This is particularly so in the region of low electrode coverage, where there is no possibility of clearly distinguishing between the adsorbed or (monomolecular or less) oxide layer without an experimental method that is sufficiently sensitive and applicable in situ. Experimental approach to the problem was for a long time connected with the measurement of electrochemical parameters, which usually measured an average current density and thus gave little information about the local current distribution, the nature and thickness of the passive film, and the film distribution over the surface. An

In Corrosion Chemistry; Brubaker, G., et al.;
ACS Symposium Series; American Chemical Society: Washington, DC, 1979.

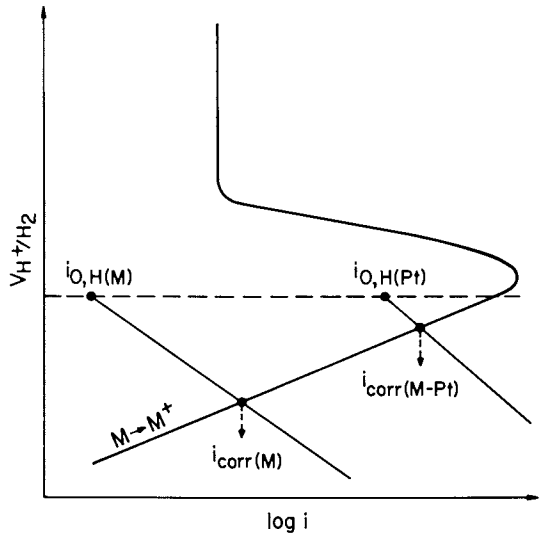

Figure 7. Increased corrosion rate of iron galvanically coupled with platinum in air-free acid solution

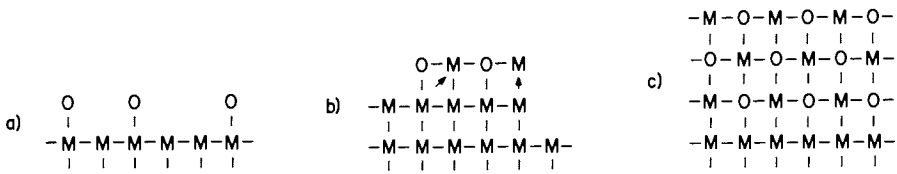

Figure 8. Characterization of passivating films; (a) adsorbed layer, (b) monomolecular (or less) oxide, and (c) three-dimensional oxide

application of non-electrochemical methods on the other hand may either disturb the system under test (el. diffraction, microscopy, Mossbauer) or be complicated in interpretation (ellipsometry). Some other difficulties involved in this type of experiment include a poor characterization of the surface, its pretreatment, crystallographic orientation and topography ... and the fact that in the region of interest more than one reaction occurs simultaneously and the kinetics parameters of individual reactions are difficult to follow. All these factors contributed somewhat to interpreting the passivation of metals in terms of a variety of theoretical models.

1. The Adsorption Theory. The adsorption theory has been developed by Uhlig, Frumkin, Kabanov and Kolotyrkin. According to Kolotyrkin, (31) passivity is described as a specific case of the widespread phenomenon of the change in the kinetics of an electrodic reaction due to the activated adsorption of the oxygen of water; the dissolution rate is generally represented by

$$i = k_1 c' \exp\left(\frac{\alpha_1 F}{RT}\right) V , \qquad (3)$$

where α is the transfer coefficient equal to βz; when the valency of the dissolving ion, z, is unity, α is equal to the symmetry factor β, or to the fraction of the potential available to lower the energy barrier for dissolution. The quantity c' is the number of atoms per square centimeter, and if with the superimposition of adsorption, c' changes with potential in such a way that

$$c' = c'_0 \exp\left(-\frac{\alpha_2 F}{RT}\right) V \qquad (4)$$

the total current becomes

$$i = k_1 c'_0 \exp\left[\frac{(\alpha_1 - \alpha_2)F}{RT}\right] V . \qquad (5)$$

Providing that in the first stage of the passivation process (at $V_p < V < V_{pp}$) $\alpha_2 >> \alpha_1$ and in the second stage (at $V > V_{pp}$) $\alpha_2 = \alpha_1$, this equation can explain the experimentally observed drop of the current with potential and its independence of potential in the passive region. The basic anodic processes, even in the passive potential region, are direct dissolution of the metal as one and the competitive adsorption of anions

In Corrosion Chemistry; Brubaker, G., et al.;
ACS Symposium Series; American Chemical Society: Washington, DC, 1979.

as another.

In Uhlig's earlier view, one of the factors determining passivation (and chemisorption) is the ratio of the work function to the enthalpy of sublimation ΔH_s. If this ratio is less than unity, conditions are favorable to passivation because the electron would escape more readily than the atom, favoring the chemisorption of substances like oxygen. A passive film is composed, then, from chemisorbed atomic and molecular oxygen (supplemented perhaps by OH and H_2O). The formation of chemical bonds satisfies the surface affinities of the metal without metal atoms leaving their lattice site.

It is argued (12) that on typical transition metals (Ni, W, Cr, Ti, Ta) the formation of such a layer (i.e., $M\text{-}O\text{-}O_2$) proceeds with more favorable free energy of formation than the oxide formation, as they have unfilled d electron energy levels leading to the formation of strong chemical bonds between oxygen and the metal. These are the metals that typically exhibit passivity. For nontransition metals with filled d levels, such as copper or zinc, the heats of oxygen adsorption are expected to be lower, and the formation of oxides is less favorable. Such metals do not exhibit thin-film passivity.

Correlation of the observed onset of Wagner's passivity on alloys like Ni-Cu, Ni-Zn-Cu, and Cu-Ni-Al to the occupancy of the d levels of the alloys is given in support of the theory. According to the theory, the same type of passive film (i.e., $M\text{-}O\text{-}O_2$) is formed in solutions, interposing a stable barrier between metal and electrolyte, displacing adsorbed H_2O and increasing the activation energy for the hydration and dissolution of the metal lattice. Such films are assumed to decrease the exchange-current density i_0 and thus to increase the polarization of the metal in the noble direction, where more oxygen can be adsorbed, which in turn forms nucleation of metal oxides. Thus in the passive state a thicker oxide film may be detected.

Briefly, the theory explains the onset of passivity by the formation of a thin adsorbed layer that either shifts the electrode potential in the double layer or influences the kinetics of the anodic process; that is, the important happenings occur in the small interface region between the metal and the solution. Kolotyrkin's theory, however, does not define a physical reason for the change of α's with potential. On the other hand, a chemisorbed film of $M\text{-}O\text{-}O_2$ composition in the electrolyte is not very likely for the following reason: Most metals (Cr, (32) Ti, (32) Fe, (28,33) Ni, (34)) can be passivated in a solution saturated with deoxygenated argon - that is, with water oxygen - as long as some water is present in the solution; (34) in such solutions,

In Corrosion Chemistry; Brubaker, G., et al.;
ACS Symposium Series; American Chemical Society: Washington, DC, 1979.

the formation of molecular oxygen at low cathodic potentials is impossible, and without its presence the total number of millicoulombs determined in the film (0.01 C/cm^2 according to Uhlig, or 1 to 2 mC/cm^2 according to Nagayama and Cohen(28) and Brusic(33) at V_{pp}) and recalculated into film thickness would exceed reasonable limits for the adsorbed monolayer of oxygen ions. In the usual correlation between the number of millicoulombs and film thickness it is assumed that 0.5 mC/cm^2 corresponds to the monolayer of O^{2-} ions if each metal ion adsorbs one oxygen ion. If the adsorbed layer has a structure that contains both metal and oxygen ions (as suggested more recently by Uhlig(12) and by Garner and MacRae(35) for oxygen adsorption and equally for the formation of the initial film formed with the adsorption of water,(36) the resulting passivating film is several layers thick - that is, a thin oxide is more likely than an adsorbed multilayer of O^{2-}. Finally, factors that favor adsorption may also favor the formation of oxides.

2. The Oxide-Film Theory. The oxide-film theory describes the state of improved corrosion resistance through the formation of a protective film on the metal substrate; this consists of the reaction products of the metal with its environment. Such a film is a new phase, even if it is as thin as a single monolayer.(21) Electron diffraction (21) and ellipsometric(33) studies give the experimental evidence for the theory. In this case the physicochemical properties of the metal relative to a corrosive medium depend to a large degree on the properties of the protective film. The properties of the film, however, are not uniquely determined.

Adherents to this theory have different opinions on the potential at which the film forms, its thickness, the mechanism of formation, and, most important, the "cause" of passivity. In the earlier theories it was postulated that the passivation follows the formation of a "primary layer" of small conductivity, with porous character, which is sometimes due to precipitation of metal salt on and near the electrode.(32) In the pores the current increases, and by polarization at an "Umschlagspotential" ($V_F = V_p$, Figure 1) an actual passive layer is formed. Thus the essential concept of the passivation process is connected with the change of the properties (chemical or physical) of the primary film at a certain potential. The passive film is free from pores and presents a barrier between the metal and the environment. It is electronically conductive and slowly corrodes in solution.(6,8,24,37)

These general ideas were further developed in detail by Sato and Okamoto,(38,39) and Bockris, Reddy, and Rao.(40) Sato

In Corrosion Chemistry; Brubaker, G., et al.;
ACS Symposium Series; American Chemical Society: Washington, DC, 1979.

and Okamoto have studied the i-V curve for nickel in acid solution and have calculated the passivation potential as a potential for NiO/Ni_3O_4 transition. This was in fair agreement with the experimentally observed value. The higher valence oxide was thought to have a self-repairing ability; that is, a higher valence oxide theory of passivity was suggested. In contrast to this higher valence oxide film, a surface oxide film NiO has the same valency as the ions of active dissolution; thus it has no self-repairing ability and cannot passivate the metal. Because anodic dissolutions at active potentials proceed at a high rate, Sato and Okamoto have suggested that the primary film forms by a dissolution-precipitation mechanism, although no direct experimental evidence was offered. Bockris, Reddy, and Rao(40) have studied the passivation of nickel in acid solution by a combination of electrochemical methods and *in situ* ellipsometry. In their view the primary oxide is relatively thick (60 Å), is formed by the precipitation, is poorly conducting, and is transformed into well-conducting, nonstoichiometric NiO. This transformation is thought to be the essential step in the passivation process.

This theory, however, is not generally accepted. To start with there is experimental evidence indicating a loss of conductivity and the appearance of the more ordered structure in the passivating nickel oxide.(41) Also, as pointed out by Hoar,(14) some of the best passivating films, as those on aluminum or tantalum, are poor electron conductors, whereas many poorly passivating films, such as CuO or PbO_2, are excellent electron conductors. Also, it may very well be that the experimental results, in particular the ellipsometric data of Bockris, et al., are in error due to the possible influence of the continuous electrode roughening in the active potential region (see, for example, Refs. 33 and 42). Such an error may be the reason that the reported refraction index for the first passivating film is unusually high (about 4.0), that the changes of ellipsometric and coulometric data in the passive potential region are not consistent, and that the main indicator of the prepassive-film transition into electronically conducting film is not trustworthy. The latter was derived from the variation of the ellipsometrically determined change of the extinction coefficient with potential.

De Gromoboy and Shreir(43) argued in their experimental study of nickel in sulfuric acid that higher oxides may form directly from the metal and at the metal surface; the observed "passivation potentials" (determined from anodic charging curves) were found to correspond closely with the potentials calculated for $Ni \rightarrow NiO$, $Ni \rightarrow Ni_3O_4$, $Ni \rightarrow Ni_2O_3$, and

In Corrosion Chemistry; Brubaker, G., et al.;
ACS Symposium Series; American Chemical Society: Washington, DC, 1979.

$Ni \rightarrow NiO_2$, the phenomenon being sharply dependent on the presence or absence of small concentrations of thiourea. Similarly Arnold and Vetter(15) suggest the direct formation of NiO at the electrode. From the anodic charging curves these authors have concluded that the film reaches a monomolecular dimension at the potential of complete passivity.

This and many other similar hypotheses can be said to form the monolayer-oxide theories. Here the onset of passivity is due to the formation of a single phase, an oxide, which is very thin in this potential region (at V_p, $\theta < 1$) and grows to a monolayer at V_{pp}.(13-18,44,45) Its formation is a potential-dependent reaction involving the direct oxidation of the metal by the discharge of water, which, once thermodynamically possible, is suggested to be kinetically easier in its crucial primary stage than is metal dissolution. However, metal or oxide dissolution can still be simultaneous electrode processes. The decrease in the anodic current is described as a result of a decrease in film-free area or blocking of the most active, kink, sites(44) caused by film formation and its influence on the kinetics of the anodic reaction.

In this respect and regarding the discussion on the initial passivations, as pointed out by an increasing number of writers, the oxide-film and adsorption theories do not contradict but rather supplement one another. In looking at the primary act of passivation as the formation of a tightly held monolayer containing oxide or hydroxide anions and metal cations, Hoar(14) concurs with "adsorptionist" Uhlig and Frankenthal as well as "filmists" Schwabe and Arnold, Vetter and Evans. In the formation of such a film, adsorption may, however, play an important role.(46) Adsorption is the first stage of the process; in an oxygen atmosphere molecular oxygen is adsorbed, dissociated, and chemisorbed, whereas in an aqueous solution water molecules or OH^- will be adsorbed and chemisorbed (see Figure 8a). The second stage is the intrusion of metal ions from the lattice into the adsorbed layer (see Figure 8b), which in the third stage may grow in the third dimension. With time and potential (at $V > V_{pp}$) oxide growth is a function of the film's ionic and electronic conductivity. The thickness of the film will then be further responsible for the retardation of the anodic processes, both growth of the oxide and anodic dissolution, since the ions have to pass through the protective film. Thus one may speak of a combined oxide-film- adsorption theory of passivity.(5)

In Corrosion Chemistry; Brubaker, G., et al.;
ACS Symposium Series; American Chemical Society: Washington, DC, 1979.

Characterization of Active and Passive State

A) Thermodynamics of the Active-Passive Transition

If faced with the task of deciding whether a particular metal would be suitable as a fabrication material in a given environment, one likes to know a) what kinds of spontaneously occurring reactions are expected and b) what is the magnitude of the rate of metal dissolution. The latter is the real criterion in making the decision and is usually evaluated through experimentation. The former provides a yes or no answer regarding the stability of the metal and falls within the scope of equilibrium thermodynamics.

The factors that determine whether an anode in aqueous solution is active, passive, or brightening are (a) the metal-solution potential difference and pH and (b) the anion/water ratio.

1. The Metal-Solution Potential Difference. The metal-solution potential difference, combined with the influence of pH, determines whether the formation of aquocations or oxide formation is the thermodynamically prevailing possibility. Such thermodynamic data, even if unsupplemented by information of a kinetic nature, are usefully expressed in the graphical form devised by Pourbaix.(11) The Pourbaix diagram for iron is shown in Figure 9. Here, for example, one can make use of the relation between free-energy change and equilibrium potential to obtain free energy changes for possible corrosion, i.e., iron dissolution caused by the hydrogen evolution reaction: as the sum of the two free energy changes yields the total free energy change for the corrosion process

$$G = -nFV \qquad (6)$$

a diagram indicates that iron in deaerated aqueous solutions will have a tendency to dissolve as long as the pH is less than about 8.5. In order that oxide formation may proceed, the anode potential must be at least as high as that for oxide or hydroxide formation from the metal and water in the particular solution.

If the oxide forms as a "monolayer," there is a question as to whether or not one can apply with some assurance these thermodynamic data, obtained on the bulk oxides. Some experimental evidence does indicate that for many metal-oxide systems the free energy of formation of the first monolayer is indeed close to that observed for the bulk phase,(47) and hence no appreciable difference in the reversible potential should be expected. On the other hand, Vermilyea(48) has shown that, if the first monolayer forms by two-dimensional nucleation, the potential of the two-dimensional-film formation may be lower than that expected from the

In Corrosion Chemistry; Brubaker, G., et al.;
ACS Symposium Series; American Chemical Society: Washington, DC, 1979.

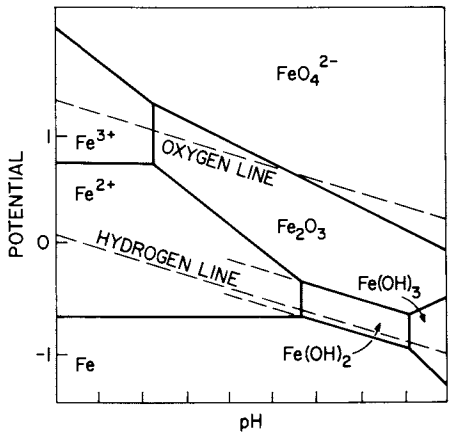

Figure 9. Pourbaix diagram for the system Fe–H_2O at 25°C, taking into consideration passivation by $Fe(OH)_2$ and Fe_2O_3 only and assuming a total ionic concentration of 10^{-6} M/L

In Corrosion Chemistry; Brubaker, G., et al.;
ACS Symposium Series; American Chemical Society: Washington, DC, 1979.

thermodynamics, the actual potential being dependent on the relative values for the interfacial energies between metal-film, film-solution, and metal-solution.

2. The Anion/Water Ratio. The second factor is Hoar's(14) extension of the Pourbaix diagram, shown schematically in Figure 10. It illustrates the joint influence of the measurable anode potential and the anion/water ratio, when the anions, such as halides, interact with oxide causing its breakdown. At a low c_{X^-}/c_{H_2O} ratio the electrode may behave according to the appropriate Pourbaix diagram, showing regions of active, passive (sometimes having more than one oxide with passivating properties), and transpassive behavior. At higher c_{X^-}/c_{H_2O} ratios the electrode brightens (process 7), this becoming more likely at higher potentials (process 6). Since thermodynamic data on ion adsorption on metals and oxides are very scarce, the diagram should be taken only as a qualitative display of experimental results.

Thermodynamic data can, of course, give only information on what is possible, without telling us which oxide or hydroxide is in fact most readily formed from a number of possible candidates that may be thermodynamically stable under a particular set of conditions, and without telling us whether any particular oxide is protective.

B) Experimental Approaches of Interest.

1) Electrochemical. Both galvanostatic and potentiostatic measurements have been very useful in characterizing passivation processes, in spite of the earlier mentioned weaknesses in their application, especially since they have been supplemented by other techniques, such as potentiodynamic analysis, coulometry and ac-impedance(49-52) investigation on either stationary or rotating electrodes. They can indicate if a metal undergoes an active-passive transition under the given conditions, provide the rates and mechanisms of relevant reactions, give corrosion rates, determine the presence of reaction intermediates (impedance(49)), evaluate electrode capacity, speculate on oxide composition, (28,29,44,45,53) and detect its first appearance(21) and thickness.(28,44)

2) Optical. At least two methods should be mentioned: ellipsometry and photopotential measurement. Both can be applied in situ while the metal is a part of the electrochemical cell and under an electrochemical investigation. Ellipsometry is based on the sensitivity with

In Corrosion Chemistry; Brubaker, G., et al.;
ACS Symposium Series; American Chemical Society: Washington, DC, 1979.

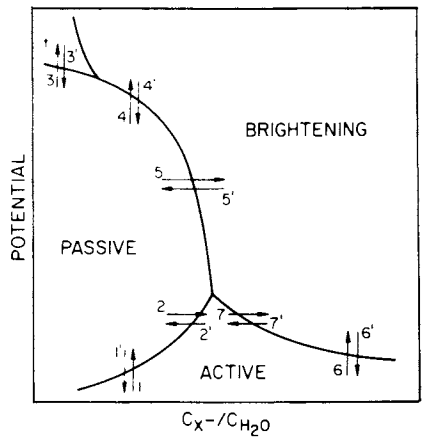

Corrosion Science

Figure 10. Scheme showing anode behavior at various potentials in solutions of various anion/water concentration ratios c_{X^-}/c_{H_2O}. The processes are as follows: (1) anodic passivation; (1′) activation—the Flade relation; (2) activation by adding "corrosive" anions; (3) transpassivation by raising the anode potential; (3′) repassivation by lowering the anode potential; (4) breakdown via pitting, leading to anodic brightening by raising the anode potential; (4′) repassivation by lowering the anode potential; (5) breakdown via pitting, leading to anodic brightening by adding "corrosive" anions; (5′) repassivation by removing "corrosive" anions; (6) anodic brightening by raising the anode potential in concentrated solution; (6′) anodic etching of brightening metal by lowering potential in concentrated solution; (7) anodic brightening from etching by increasing the anion concentration; (7′) anodic etching from brightening by decreasing the anion concentration (14).

In Corrosion Chemistry; Brubaker, G., et al.;
ACS Symposium Series; American Chemical Society: Washington, DC, 1979.

which polarized light follows the variation of surface states of a metal. Figure 11 gives a schematic representation of the instrument. Changes introduced by the passivation process are measured as changes in the readings of the polarizer and analyzer, and compared with the values for a bare substrate; these in turn are used to calculate the thickness and the refractive index (composition ?) of the newly formed film. Relative changes of less than 1 Å are detectable. The evaluation of the absolute values, however, may not be straightforward if the film is absorbing and its refractive index unknown.

The photopotential data are measured by a pulse technique, the duration of the light pulse being $0.2 - 1 \times 10^{-3}$ sec and the ratio of light to dark time $1 - 2.5 \times 10^{-2}$. The oscillographic recording of the photopotentials allows the determination of p or n-type semiconducting properties of the surface layers. The correlation between the oxide film characteristics and the photopotential sign for given experimental conditions is formulated by Rosenfeld et al.(41,54) as

$$\Delta V_{(h\nu)} = \frac{kT}{2e} \ln \frac{[O^{2-}]}{[M^{n+}]} - C \qquad (7)$$

where k is Boltzmann's constant, T temperature, and in square brackets are the concentrations, exceeding the stoichiometry, of the respective ions. Positive photopotential indicates hole conductivity. Furthermore, the specimen may be tested with light of different wavelengths: thus it is possible to speculate on the kind of surface product through the approximate value of its photoelectric gap.(55)

3) Other Non-Electrochemical Methods. B. Cahan(56) is examining the passivation of iron and ferrous alloys by a combination of electromodulation, ellipsometry, ESCA, LEED and Auger spectroscopy coupled with electrochemical methods. The novelty of the technique is a cell with a thin layer of electrolyte (10^{-3} cm) which will be frozen during sample transportation from the electrochemical set-up into the Auger, for example, and then sublimed under a very high vacuo. In this way, the errors due to air exposure will be, hopefully, avoided. Results are not yet available.

C) Kinetics and Mechanism of Relevant Reactions - Quantitative Evaluation of the i-V Curve. Iron passivation has been widely studied, especially in neutral solutions both experimentally and theoretically.

In Corrosion Chemistry; Brubaker, G., et al.;
ACS Symposium Series; American Chemical Society: Washington, DC, 1979.

(28,42,45,50,57-59) Seeking to understand qualitatively and quantitatively the processes responsible for a typical i-V curve, two viewpoints will be brought into focus: 1) the work of Brusic(33) and Bockris et al., (60) which gives the first direct evaluation of the growth mechanism of the film on iron in the active potential region and 2) the work of Ebersbach, Schwabe and Ritter(18,19) containing the first theory that succeeded in calculating an i-V curve (for nickel) in good agreement with the experimental results.

1) The Model of Brusic, Bockris et al. This model assumes, as does that of others,(18,45) that in the active region both film formation and dissolution reactions proceed as simultaneous processes. The advantage held here is that many of the unknown parameters concerning the mechanism of the film-forming reaction have been experimentally determined for iron in borate buffer. Kinetic parameters were evaluated by a combination of electrochemical and ellipsometric measurement in a purified, deaerated solution, with and without stirring. The ellipsometer was used as a quasi-automatic instrument, recording changes with time as short as 0.01 sec. The essential results are

- Film growth commences less than 0.01 sec after switching on the current or potential. The growth rate is not affected by stirring. After the first several seconds at any one time the growth rate is independent of the potential. Ellipsometric changes obtained in oxidation and subsequent reduction are reversible (Figure 12).
- Change of ellipsometric parameters with potential show two inflection points, one associated with V_{pp} and the other with a higher, passive potential, Figure 13.
- The number of millicoulombs obtained in film reduction is always lower than the number spent in oxidation (iron dissolution, hydrogen oxidation). For evaluation of the film thickness the reduction charge was used, correcting for hydrogen evolution (Figure 14).
- The evaluated thickness at constant, active, potential is linearly proportional to time up to about one-third of a monolayer (up to $\sim$ 0.1 sec); thereafter it is proportional to log t (Figure 15).
- The most likely oxide composition and thickness evaluated from both ellipsometric and coulometric results are given in Figure 16 as $Fe(OH)_2$ below V_{pp} and Fe_2O_3 above it.

The suggested mechanism, which yields good agreement (qualitative and quantitative) with the observed results, is as follows:

1. Discrete centers grow, initially two-dimensionally, up to 30% coverage.

In Corrosion Chemistry; Brubaker, G., et al.;
ACS Symposium Series; American Chemical Society: Washington, DC, 1979.

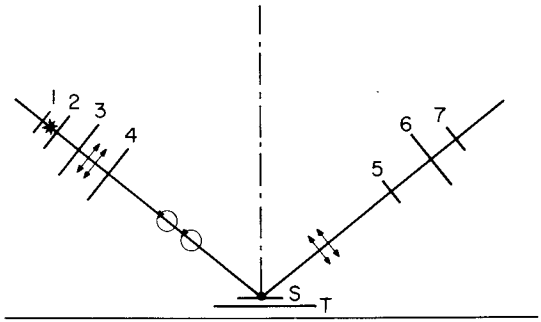

Figure 11. Schematic of ellipsometer: (1) source of light; (2) collimator; (3) polarizer; (4) compensator; specimen (S) on table (T); (5) filter; (6) analyzer; (7) light detector

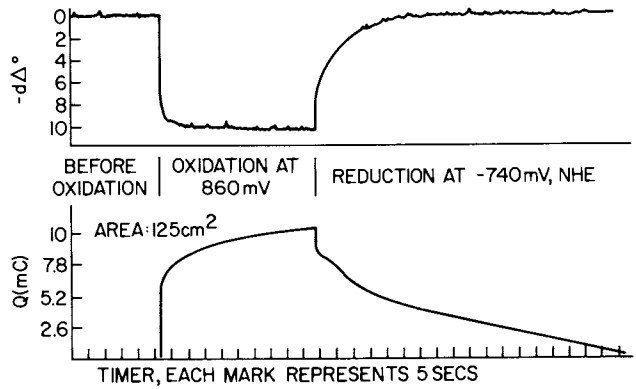

Figure 12. Laboratory record of potentiostatic oxidation at +860 mV (she) and reduction with simultaneous recording of ellipsometric intensity (i.e., Δ) and charge. Stirred solution.

In Corrosion Chemistry; Brubaker, G., et al.;
ACS Symposium Series; American Chemical Society: Washington, DC, 1979.

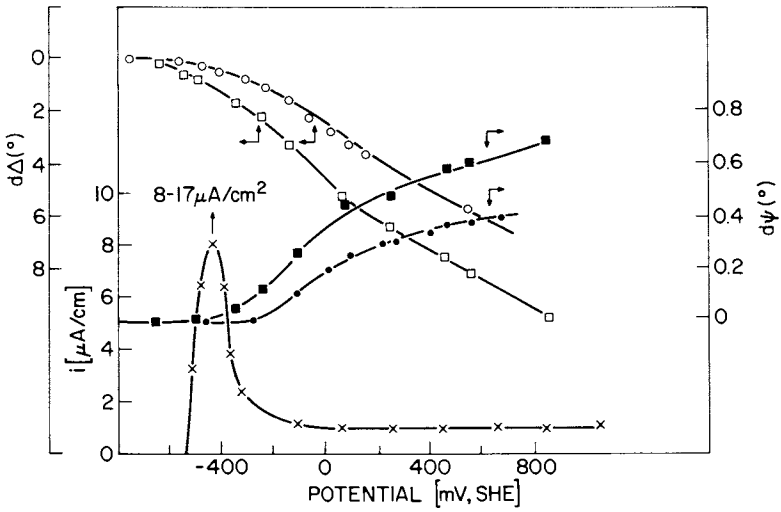

Figure 13. Variation of Δ and Ψ with potential in steady state and transient (x, 0.8; 0, 0.32; Δ, 0.08 mA cm⁻²) oxidation; and i–V relation in steady state oxidation. (●,○)Galvanostatic oxidation transients; (■,□) potentiostatic (steady state) oxidation.

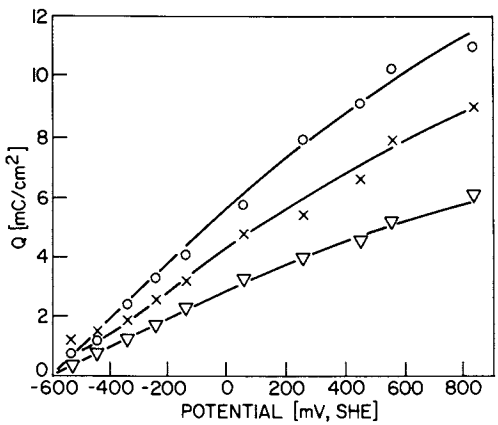

Figure 14. Charge (Q) as a function of oxidation potential obtained during the oxidation (○), reduction (×), and reduction corrected for hydrogen (△)

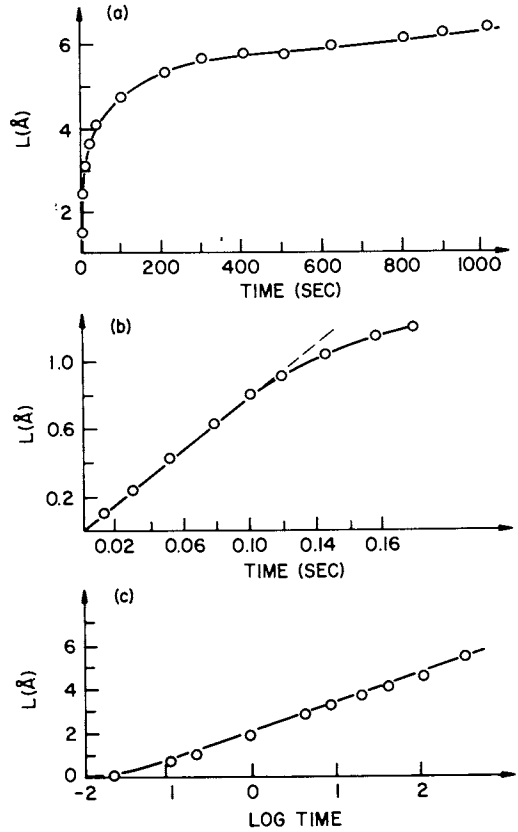

Figure 15. (a) Increase of film thickness with time; (b) during the initial state; and (c) with log (t) at −490 mV (she)

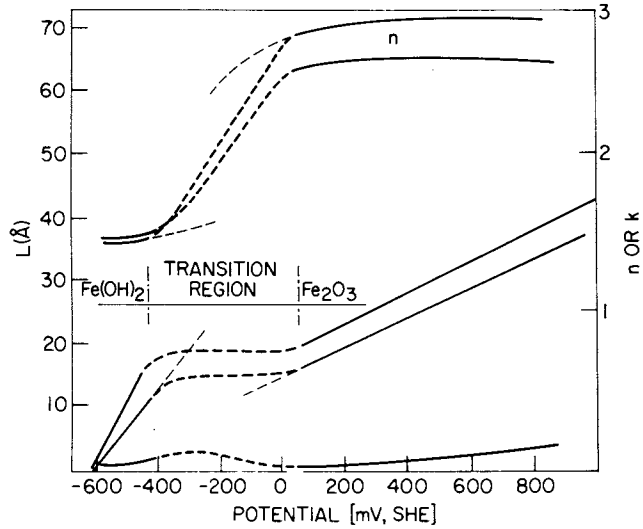

Figure 16. The solution of the ellipsometric results using coulometry

2. At higher coverages the growth involves a rapid place-exchange step with a rate-determining Temkin discharge of OH^- into sites where the metal is already attached to an OH group. This initial OH group is displaced into the first layer of metal atoms beneath the surface, forming a two-dimensional oxide lattice. Thus the processes that determine the i-V curve are

$$\begin{array}{ccc} & \text{Fe} + \text{OH}^- \rightleftarrows \text{FeOH} + e^- & \\ & \swarrow \qquad\qquad \searrow & \\ \text{dissolution} & & \text{film formation} \end{array} \qquad (8)$$

$$\text{FeOH} \rightarrow \text{FeOH}^+ + e^- \qquad (9)$$

$$\text{FeOH} \rightleftarrows \text{HOFe} \qquad (10)$$

$$\text{FeOH}^+ \rightleftarrows \text{Fe}^{2+} + \text{OH}^- \qquad (11)$$

$$\text{HOFe} + \text{HO}^- \rightarrow \text{Fe(OH)}_2 + e^- \qquad (12)$$

where Eq. (9) gives i_{diss} and Eq. (12) i_{ff}. At any time $i_T = i_{diss} + i_{ff}$. The dissolution mechanism is basically that of Bockris et al.,(61) recently confirmed by Epelboin.(52)

Since, according to the determined mechanism of film growth $i_{ff} \neq f(V,L)$ at t = const and $i_{ff} \rightarrow 0$ at t large, the experimental i-V curve is largely determined by i_{diss}. The latter is calculated as a function of increasing $Fe(OH)_2$ coverage from 0 to about 0.8 at potentials in the prepeak region and in the regions of final covering of the electrode by the formation of Fe_2O_3 at potentials between V_p and V_{pp}. The final rates are as follows:
at $V < V_p$:

$$i_{diss} = k_1 c_{OH^-} \exp (VF/RT) \qquad (13)$$

$$i_{ff} = k_2 \theta_{FeOH} \exp (FV/RT) \exp (-f(\theta_T)/RT)_{OH^-} \qquad (14)$$

where θ is the electrode coverage with

$$\theta_T = \theta_{OH,ads} + \theta_{Fe(OH)_2} \qquad \text{and}$$

$$f(\theta)_T \approx \beta(\text{const} + FV)$$

In Corrosion Chemistry; Brubaker, G., et al.;
ACS Symposium Series; American Chemical Society: Washington, DC, 1979.

at $V_p < V < V_{pp}$: $\theta_T \rightarrow 1$

$$i_{diss} = k_1 K(1 - \theta_T) \exp (3FV/2RT) \quad (15)$$

and

$$i_{ff} = k_2 K(1 - \theta_T) \exp (3FV/2RT) \quad (16)$$

with

$$(1 - \theta_T)_t = A \exp [-k_2 K e^{3FV_t/RT} t] \quad (17)$$

The theory was found to be in fair agreement with the observed kinetics parameters such as the Tafel slope of free dissolution of 150 mV, $di_{ff}/dV = 0$, and the observed i-V curve.

Place exchange, in the formation of the first or second layer of the film, may be relatively rapid, helped by existing defects at the surface or by the influence of metal image forces on the activation energy for the step. At higher film thicknesses (thus at higher potentials) place exchange may become a rate-determining step, or, in general, the mechanism suggested for the prepassive potential region ceases to be valid.

If compared with other models of iron passivation the present model, showing clearly that an ellipsometrically detectable phase is formed negative to the peak potential with an effective thickness of one, perhaps two, monolayers at V_{pp} is not in agreement with models favoring the adsorption of O^{2-}, OH^-, etc. It is in agreement with a more general picture of monomolecular oxide formation, in parallel to iron dissolution(44) directly at the electrode surface,(14) possibly favored by the d-character of the substrate (raction 8).(12)

It also agrees with theories proposing the appearance of a higher valent oxide at $V > V_p$.(58) As for the film composition in general, the transition $Fe_3O_4 \rightarrow Fe_2O_3$ seems to have more supporters than the suggested $Fe(OH)_2 \rightarrow Fe_2O_3$ process. It remains to be determined by more direct experimental approaches(56) which of the two is more likely.

2) The Model of Ebersbach, Schwabe and Ritter (18,19). It was assumed that the metal-dissolution reaction (rate i_1) and the film-forming reaction (i_2) at an initially bare

electrode can proceed simultaneously with a possibility of the film's being dissolved by the action of the electrolyte, especially if some adsorbable anions are present. Thus

$$i = (i_1 + i_2)\ (1 - \theta) \tag{18}$$

where θ, the electrode coverage, varies with time according to

$$\frac{d\theta}{dt} = Ci_2(1 - \theta) - K\theta - B\theta\ , \tag{19}$$

V, a_{A^-}, a_{H^+}

where B, the rate of oxide film degradation, is a function of c_{H+} according to

$$MO + 2H^+ \rightleftarrows M^{2+} + H_2O \tag{20}$$

and K, the rate of oxide-film degradation, is a function of c_{A-} according to

$$MO + 2A^- + H_2O \rightleftarrows MA_2 + 2OH^- \tag{21}$$

Then

$$i = (i_1 + i_2)\left(1 - \left(1 + \frac{K + B}{Ci_2}\right)^{-1} \{1 - \exp[-(Ci_2 + K + B)t]\}\right) \tag{22}$$

where

$$i_1 = i_1^0 \exp\left[\frac{\alpha_1 F}{RT}\ (V - V_1)\right]\ ,\ i_1^0 = fc_{H^+}\ , \tag{23}$$

$$i_2 = i_2^0 \exp\left[\frac{\alpha_2 F}{RT}\ (V - V_2)\right]\ ,\ i_2^0 = fc_{H^+}\ , \tag{24}$$

In Corrosion Chemistry; Brubaker, G., et al.;
ACS Symposium Series; American Chemical Society: Washington, DC, 1979.

with V_1 and V_2 being the equilibrium potentials for active dissolution and film formation.

The dissolution rate i_1 may be determined by the reaction sequence given by Eqs. 8, 9, and 11 (Bockris' dissolution mechanism). The mechanism of film formation, resulting in i_2, is assumed to be as follows:

$$M + H_2O \rightleftarrows MOH + H^+ + e^- \quad , \tag{25}$$

$$MOH + H_2O \rightarrow M(OH)_2 + H^+ + e^- \quad , \tag{26}$$

$$M(OH)_2 \rightleftarrows MO + H_2O \quad , \tag{27}$$

with the second electron transfer being rate determining. The mechanism involves the direct formation of the passivating film at the electrode surface, experimentally supported by work on a rotating nickel disk electrode,(62) which indicates that the rate of the passivation process is independent of stirring and of the solubility of the nickel salt.

For the steady state, $t \rightarrow \infty$,

$$i = \frac{i_1^0 \exp[(\alpha_1 F/RT)(V - V_1)] + i_2^0 \exp[(\alpha_2 F/RT)(V - V_2)]}{1 + (\{Ci_2^0 \exp[(\alpha_2 F/RT)(V - V_2)]\}/(K + B))} \tag{28}$$

and if no oxide-film degradation occurs,

$$i = \frac{i_1 + i_2}{\exp(i_2 Ct)} \tag{29}$$

According to Eq. (19), the constant C is the covered area per coulomb and was estimated on the basis of the area required for oxygen atoms as 10^4 cm^2/A-sec. The rate constants K and B at constant pH and

anion concentration were given as first-order rate constants with estimated values of $10^{4} > (K + B) > 10^{-8}$ sec^{-1}. These limits were chosen arbitrarily, assuming that film degradation is slower than film formation. Current-potential curves were calculated for a large variation of parameters and did indeed show a resemblance to the experimental results (carried out for nickel in acid).

Examples are shown in Figures 17 and 18 for $\gamma = \beta_2 Z_2/\beta_1 Z_1 = 2$ (or 1), $i_1^0 = 10^{-7}$ A/cm^2 (chosen arbitrarily from the region of values reported to be between 10^{-7} and 10^{-10} A/cm^2), $i_2^0 = 10^{-10}$ (again arbitrarily assumed to vary between 10^{-7} and 10^{-10} A/cm^2, that is, in the same region of values as the dissolution current i_{diss}). These figures show the variation in peak current or peak potential with both time (Figure 17) and the velocity of the oxide-film degradation reactions (Figure 18). Thus, according to this model, the total current will be zero when $\theta = 1$ at V_{pp}. Furthermore, according to Eq. (29), in the stationary state (when $t \to \infty$) a finite current can flow only when $i_2 \to 0$. It is argued that, in reality, a measurable current will always flow after passivation even if $i_2 \to 0$ because the surface film is not perfect nor is the surface perfectly covered, and that the passive surface film is not absolutely impermeable. Thus, as polarization increases (at $V > V_{pp}$), ions increasingly penetrate into the film, increasing its thickness.

Also, the theory gives an acceptable model of a variety of passivating behaviors observed on different metals:

1) metals with $V_2 - V_1 << 0$: the passivation reaction occurs fast and metal in aqueous solution always forms an oxide, as in the case of Al, Ti, Zr, Ta, and W.

2) $V_2 - V_1 \approx 0$: in that case the metal is initially active; the more negative $(V_2 - V_1)$ and the smaller the ratio i_1^0/i_2^0, the faster the passivation a) $i_1^0/i_2^0 > 1$: this is the case for Fe, Co and Ni in solution without halides. Passivation is possible only at higher anodic potentials. b) $i_1^0/i_2^0 << 1$ passivation occurs easily, the case of Cr.

3) $V_2 - V_1 >> 0$: a) $i_1^0/i_2^0 >> 1$, the case of Ag; the passivation potential is not easily reachable even at high anodic current densities. Passivation may set in after a salt formation, e.g. Ag_2SO_4 in whose pores Ag_2O_2 can be formed. b) $i_1^0/i_2^0 << 1$ - metals of the Pt group with slow dissolution and easier passivation.

Thus this theory satisfactorily describes the i-V curve in the active potential region, with a qualitative description of possibilities in the passive potential region and a semi-quantitative explanation of the passivation behavior of a variety of metals.

In Corrosion Chemistry; Brubaker, G., et al.;
ACS Symposium Series; American Chemical Society: Washington, DC, 1979.

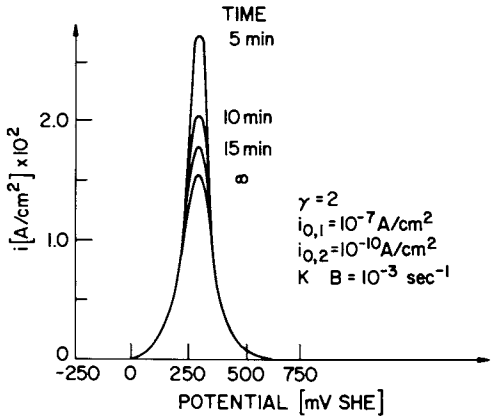

Electrochimica Acta

Figure 17. Effect of time on the current density–potential curves by potentiostatic measurements (calculated for $K + B = 10^{-3}$ sec^{-1} (18))

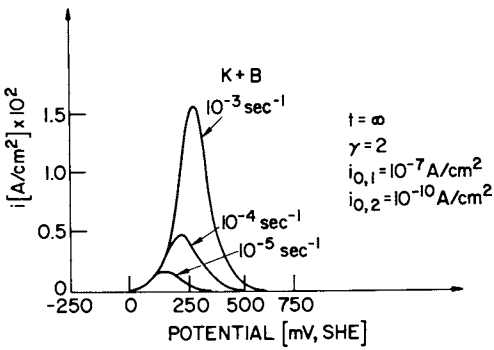

Electrochimica Acta

Figure 18. Current density–potential curves calculated for $t = \infty$ showing dependence on the sum of the constants K *and* B (18)

Final Remarks

Modern passivation theory views the primary passivation act as a formation of a tightly held layer of monomolecular dimensions, containing oxide or hydroxide anions and metal cations; the process involves the formation of a new phase, an oxide, in steps that include the adsorption as an important intermediate stage. Thus the long-time controversial aspects of the adsorption and oxide theories are, in one sense, combined.

The observed current-potential behavior is a function of the simultaneous processes of film formation, its dissolution, and metal dissolution. The latter seems to be mostly responsible for the magnitude of the current at all potentials. In the active potential region dissolution is hindered by a decrease in the free electrode area, and in the passive region dissolution depends entirely on the properties of the passivating film.

LITERATURE CITED

(1) Lomonosov, M. V., Collection: Vol. 1, Moscow, Izd. Akad. Nauk SSSR (1950).
(2) Keir, J., Phil. Trans. Roy. Soc., London No:359 (1890).
(3) Faraday, M., Phil. Mag. 9:57, 122, 153 (1836).
(4) Tomoshov, D. and Chernova, G. P., "Passivity and Protection of Metals Against Corrosion,"Plenum Press, New York, 1967.
(5) Uhlig, H. H. and King, P. F., J. Electrochem. Soc.,106, 1 (1959).
(6) Weil, K. G., Z. Elektrochem., 59, 711 (1955).
(7) Franck, U. F., Z. Naturforsch., 4A, 378 (1949).
(8) Vetter, K. J., Electrochemical Kinetics Theoretical and Experimental Aspects (trans. by Scripta Technica), Academic Press, New York, 1967.
(9) West, J. M., Electrodeposition and Corrosion Processes, Van Nostrand, New York, 1965.
(10) Wagner, C., Corrosion Sci., 5, 751 (1965).
(11) Pourbaix, M., "Atlas of Electrochemical Equilibria in Aqueous Solutions," Pergamon Press, New York, 1966.
(12) Uhlig, H. H., Electrochem. Acta., 16, 1939 (1971).
(13) Davies, D. E. and Barker, W., Corrosion 20, 47 t (1964).
(14) Hoar, T. P., Corrosion Sci., 7, 341 (1967).
(15) Arnold, K. and Vetter, K. J., Z. Elektrochem., 64, 407 (1960).
(16) Popova, T. J., Bogotsky, U. S. and Kabanov, B. N., Zh. Fiz. Khim., 36, 1432 (1962).
(17) Schwabe, K., Electrochim. Acta 3, 186 (1960).

In Corrosion Chemistry; Brubaker, G., et al.;
ACS Symposium Series; American Chemical Society: Washington, DC, 1979.

(18) Ebersbach, U., Schwabe, K. and Ritter, K., Electrochim. Acta, 12, 927 (1967).
(19) Schwabe, K., Zushke, H. D. and Time, M., Zash. Met. 10, 491 (1974).
(20) Devanathan, M. A. V. and Lakshmanan, S., Electrochim. Acta, 13, 667 (1968).
(21) Fleischmann, M. and Thirsk, H. R., J. Electrochem. Soc., 110, 688 (1963).
(22) Evans, U. R., Z. Elektrochem., 62, 619 (1958).
(23) Evans, U. R., Electrochim. Acta, 16, 1825 (1971).
(24) Bonhoeffer, K. F. and Franck, U. F., Z. Elektrochem., 55, 180 (1951).
(25) Pryor, M. J., J. Electrochem. Soc., 106, 557 (1959).
(26) Weil, K. G., Z. Elektrochem. 59, 711 (1955).
(27) Vetter, K. J., J. Electrochem. Soc., 110, 597 (1963).
(28) Nagayama, N. and Cohen, M., J. Electrochem. Soc., 110, 670 (1963).
(29) Sato, N. and Cohen, M., J. Electrochem. Soc., 111, 519 (1964).
(30) Damjanovic, A. in "Modern Aspects of Electrochemistry (J. O'M. Bockris, ed.) Vol. 5, Plenum Press, New York, 1969.
(31) Novakovskii, V. M. and Kolotyrkin, Y. M., Zash. Met., 8, 283 (1972).
(32) Tomashov, N. D. and Vershinina, Z. P., Electrochim. Acta, 15, 501 (1970).
(33) Brusic, V., Ph.D. Thesis, Univ. of Pennsylvania, 1971.
(34) Schwabe, K. and Schmidt, W., Corros. Sci., 10, 143 (1970).
(35) Germer, L. and MacRae, A., J. Appl. Phys., 33, 2923 (1962).
(36) Germer, L. and MacRae, A., Proc. National Acad. Sci., U.S., 48, 997 (1962).
(37) Muller, W. J., Z. Elektrochem., 33, 401 (1927).
(38) Sato, N. and Okamoto, M., J. Electrochem. Soc., 110, 605 (1963).
(39) Sato, N. and Okamoto, M., J. Electrochem. Soc. 111, 197 (1964).
(40) Bockris, J. O'M., Reddy, A. K. N. and Rao, B., J. Electrochem. Soc., 113, 1133 (1966).
(41) Oshe, A. I., Oshe, E. K. and Rozenfeld, I. L., Elektrokhimiya, 7, 1419 (1971).
(42) Kruger, J. and Calvert, J. P., J. Electrochem. Soc., 114, 43 (1967).
(43) deGromoboy, T. S. and Shreir, L. L., Electrochim. Acta, 11, 895 (1966).
(44) Frakenthal, R. P., J. Electrochem. Soc. 116, 580 (1969).
(45) Frakenthal, R. P., Electrochim. Acta 16, 1845 (1971).
(46) Hoar, T. P., J. Electrochem. Soc., 117, 17C (1970).

In Corrosion Chemistry; Brubaker, G., et al.;
ACS Symposium Series; American Chemical Society: Washington, DC, 1979.

(47) Brennan, D., Hayward, D. O. and Trapnell, B. M. W., Proc. Royal Soc. (London), A256, 81 (1960).
(48) Vermilyea, D. A., in Advances in Electrochemistry and Electrochemical Engineering (P. Delahay, ed.) Vol. 3, Interscience, New York, 1963.
(49) Epelboin, I. and Keddam, M., J. Electrochem. Soc., 117, 1052 (1970).
(50) Epelboin, I., Gabrielli, C., Keddam, M., Lestrade, J. C. and Takenouti, H., J. Electrochem. Soc. 119, 1632 (1972).
(51) Epelboin, I., Keddam, M. and Takenouti, H., J. Appl. Electrochem., 2, 71 (1972).
(52) Epelboin, I. and Keddam, M., Electrochem. Acta, 17, 177 (1972).
(53) Pigeand, A., J. Electrochem. Soc., 122, 80 (1975).
(54) Oshe, E. K. and Rozenfeld, I. L., Zash. Met., 5, 524 (1969).
(55) Trabaneli, G., Zucchi, F. and Brunoro, G., Thin Solid Films, 13, 131 (1972).
(56) Cahan, B., Case Western Univ., Cleveland, Ohio, private communication.
(57) Novoselskii, I. M., Andreev, I. N. and Khakimov, M. G., Elektrokhimiya, 7, 421 (1970).
(58) Miligy, A. A., Geana, D. and Lorenz, W. J., Electrochem. Acta 20, 273 (1975).
(59) Sato, N., Noda, T. and Kudo, K., Electrochim. Acta 19 471 (1974).
(60) Bockris, J. O'M., Genshaw, M. A., Brusic, V. and Wroblow, H., Electrochim. Acta 16, 1859 (1971).
(61) Bockris, J. O'M., Drazic, D. and Despric, A. R., Electrochim. Acta 4, 325 (1961).
(62) Ebersbach, U., Schwabe, K. and Konig, P., Electrochim. Acta, 14, 773 (1969).

RECEIVED September 1, 1978.

Corrosion of Valve Metals

J. E. DRALEY

Argonne National Laboratory, Argonne, IL 60439

I had a little problem deciding what kind of talk to give you. I concluded that it should not be a general survey of everything I can find that is related to corrosion of valve metals or film-forming metals; that it should not contain just one or two topics within that subject--about which I could talk enough to give you some depth--but a compromise between these two. Secondly, I had to decide whether to talk theoretically or mathematically, on the one hand, or phenomenologically on the other, and I have chosen the latter approach. My intent is to give you some perspective about the way these materials corrode. I have selected some examples that I think are sufficiently general and illustrate the principles well enough to do this. Many of the slides are taken from our own work of some years ago. It must be acknowledged that the unique corrosion characteristics of a number of the valve metals are not identified, and behavior in a number of common environments is not addressed.

First of all, I have found the title valve metals to be confusing for a number of people; for example, someone asked if they are the metals of which valves are made. Let me give you a few guidelines. First, the valve metals form relatively perfect oxide films. That means they are relatively perfect with respect to protection against corrosion, which we shall amplify a little. Secondly, they are relatively perfect insofar as there is not much local breakdown or leakage when they are anodized. Partly related to that there are high fields in these oxides during the period of growth--fields greater than about 10^6 volts/cm.

In the first figure, we see illustrated a relationship often drawn between the energy of the bond between oxygen and the metal and the field required to produce an anodic film. In this instance, the field is that

0-8412-0471-3/79/47-089-185$12.50/0

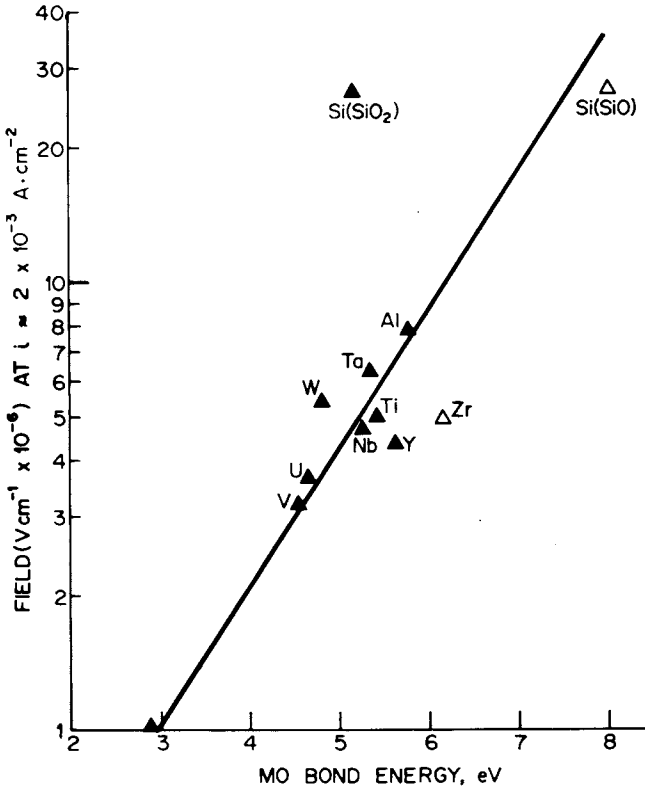

Journal of the Electrochemical Society

Figure 1. Field required to sustain an ionic current density of 2×10^{-3} A · cm^{-2} for anodic oxides as function of metal–oxide bond energy (1)

which corresponds to a given small current in anodizing, or production of the oxide film. The factors responsible for sound and protective films are not well known. It is still a bit of a mystery why some systems form better films than others. A number of individual principles have been brought up. Pilling and Bedworth years ago wrote that if the volume of the oxide produced on a metal surface is less than the volume of metal from which it is produced, there is little chance that the oxide film will be protective. As stated, that is a good guiding principle, but of all the systems for which there is expansion in the formation of oxide, the rule doesn't predict reliably which oxides will be protective and which will not.

Strong bonding between the oxide and the metal substrate seems to be essential to the formation of highly protective films. That's one principle I think you can hold on to. The others don't work very well. There are a lot of peculiarities; for example, in some cases the oxygen dissolves significantly in the surface layers of the metal. This doubtless reduces the effective size of the surface metal atoms and allows adjustment of the positions of the surface atoms of the substrate so they will nearly match the positions of the contiguous cations in the oxides.

Figure 2 shows that which metals form good films depends not only on the bond energy but also on the solution in which the films are formed. These curves are for anodizing aluminum in a series of solutions. The top 5 curves are for a family of solutions in which the films remain resistant to greater thicknesses than for the two less ideal solutions. In other solutions, one can't get anodized films at all. The resistivity on the ordinate is for the film itself. I think it is important to note that many metals form hydrated oxides, in which hydroxide ions are constituents. As a general rule, highly protective films are anhydrous; it is often speculated that the high field present during the formation of the film (vide supra) contributes to the formation of anhydrous rather than the hydrated oxide. It is easy to see that a high field operates when one anodizes by the application of a potential; it is less obvious, but evidently equally true during unassisted thin-film oxidation. Local fields from multiply-charged cations might contribute to the formation of compact, anhydrous oxides; the best films usually contain cations with a charge of 3 or more. One more thing about films: they often are not very stable in water or in aqueous solutions. This tends to cause confusion about the protectiveness of

In Corrosion Chemistry; Brubaker, G., et al.;
ACS Symposium Series; American Chemical Society: Washington, DC, 1979.

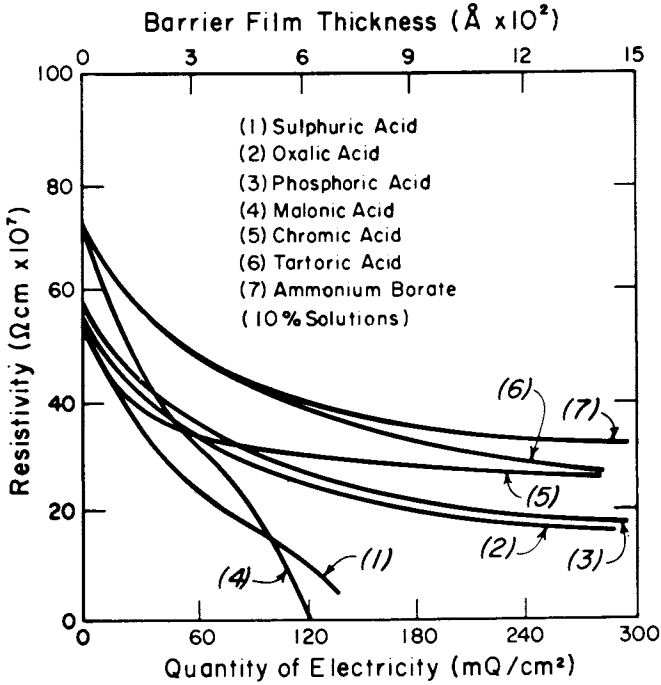

Figure 2. Differential specific resistance for growing barrier films on aluminum (2)

oxide films. The film itself may be a very good one, but it may deteriorate, sometimes slowly, sometimes rapidly; sometimes rather generally and sometimes locally. Its protectiveness thus may be temporary or imperfect as a function of time. One of the conundrums about such protective films has always been how to rationalize the demonstrated requirement to adsorb species on some metal surfaces or on some metal oxide surfaces to provide protection. It appears to me that the function of the adsorbate is to protect the oxide film against the hydrating or solvating effect of the water. The film itself is good enough, then, to provide protection.

In Figure 3 we see the relationship between metal-oxide bond energy and the Tafel slope--the relationship between potential and log current during oxide film formation. It says, in effect that when the bond energy is higher, it takes more voltage increase for a given increase in current, which is to say that when the bond energy is higher it is more difficult to pass extra current through a more protective film.

Corrosion and oxidation of valve metals generally consist both of the growth and degradation of oxide films. I'd like to begin discussion of the growth of oxide films with Figure 4, taken from Hauffe(3). In this case iron is oxidized directly to ferric oxide in a nitric-nitrous acid solution. The author has suggested the existence of concentration gradients for cation lattice defects, oxygen vacancies, and electrons. During the growth of the film, it is proposed that electrons, cations, and anions migrate. A large space charge variation is proposed within the oxide film--a case which was ignored for years by people who studied oxidation. The resultant combination of fields from surface charges and from the space charge leads to no electrical field at the interface between Zones I and II at which location new oxide is proposed to form. Other more complicated models have been developed; I have chosen to show this because of its generally applicable principles.

In Figure 5 we see that sometimes seemingly perfect thin films are far from perfect. This is for an aluminum alloy that, from some techniques, would appear to carry a perfect film. We see some of a series of platelets growing out in this transmission electron micrograph taken across an edge. Figure 6 shows a case in which oxide nuclei grow on a metal surface. This one is for iron in low pressure oxygen; similar results have been observed for other metals. If we look at this surface during oxidation, we see only a very thin

In Corrosion Chemistry; Brubaker, G., et al.;
ACS Symposium Series; American Chemical Society: Washington, DC, 1979.

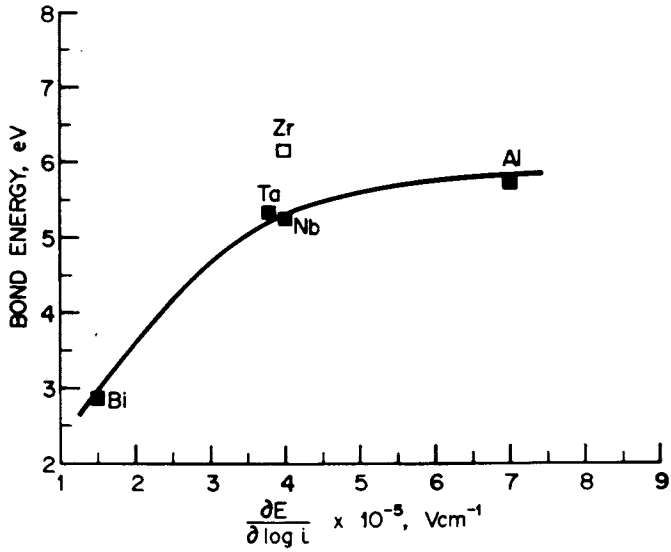

Journal of the Electrochemical Society

Figure 3. Relationship between metal–oxygen bond energy and Tafel slope for film growth (1)

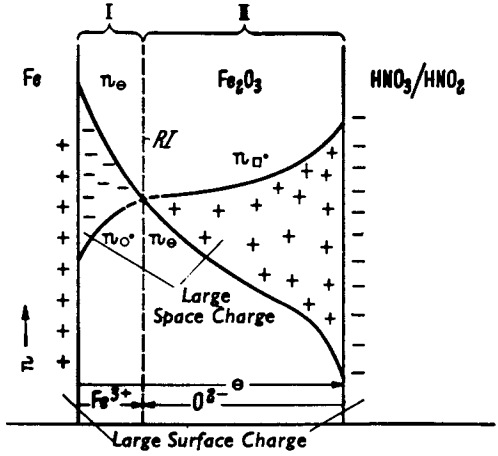

Plenum Press

Figure 4. Schematic of the concentration of the free electrons and ion–defect positions in the homogeneously structured passive layer Fe_2O_3 with space-charge inversion (3)

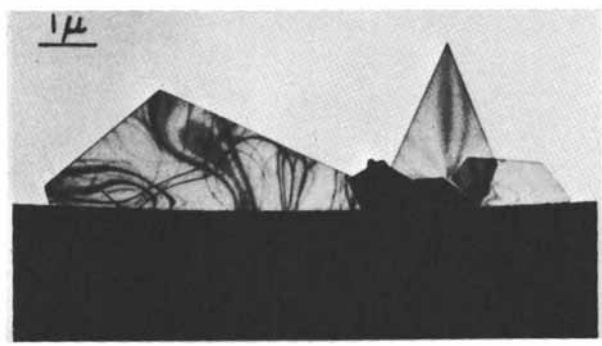

Academic Press

Figure 5. Oxide platelets viewed by electron silhouette on aluminum after corrosion for 30 hours in steam at 540°C (4)

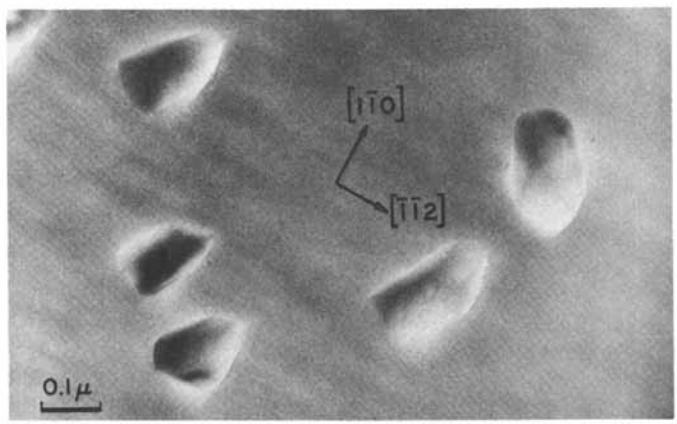

Maruzen Co., Ltd.

Figure 6. Oxide nuclei on (111) iron foil after oxidation at 540°C and 1.1 × 10^{-5} Torr for 55 minutes (5)

In Corrosion Chemistry; Brubaker, G., et al.;
ACS Symposium Series; American Chemical Society: Washington, DC, 1979.

film until nuclei show up at the same time at many places over the surface. These crystals then grow at measurable rates. Their orientation can be determined and related to the orientation of the metal substrate.

I'd now like to show you some unpublished color photographs of a series of iron samples which were oxidized for three days in water at elevated temperatures. We've changed the potential for oxidation by using different concentrations of oxygen in water. With 290 ppm oxygen concentration at 260°C, a highly perfect ferric oxide film formed showing a little tint of interference color--that is often valuable for giving some clues. The color indicates that the thickness is uniform over a big enough area to develop the interference color; in a few minutes, we'll see that thicknesses sometimes vary from grain to grain. At 35 ppm oxygen areas of breakdown are observed. The next slide shows some photographs of samples at 150°C, but otherwise at the same conditions. You'll see that for the same oxygen concentrations in the water the protection is not as good. A greater oxidizing potential (oxygen concentration) is required for a highly protective film as the temperature is lowered; the trend continues to at least as low as 100°C (third slide) at which temperature 540 ppm O_2 provided an excellent film(6). To the best of my knowledge, nobody has used this system to maintain the potentially excellent aqueous corrosion resistance of iron. The next slide shows a range of interference colors for contiguous grains on a specimen of iron, under conditions identical to those shown earlier. If there is a deficiency of oxygen--insufficient oxygen to provide good protection--sizeable pits are formed in pure water. A lesson from this is that pitting doesn't occur only in strong electrolytes or selected electrolyte solutions.

If the composition of the alloy is changed the composition of the oxide changes, and it is possible to make the oxide considerably more protective on a metal like iron. The next slide shows the effect of a little bit of chromium. Croloy-5 contains 5% chromium and some molybdenum; you can see that at 260°C with 35 ppm O_2 corrosion resistance is substantially better than that of iron. As shown in Figure 7 the corrosion behavior of such alloys also seems favorably influenced by high oxygen concentration in water. In Figure 8 it is seen that there is considerable chromium enrichment in the oxide films on oxidized iron-chromium alloys; evidently the greater protectiveness of the films for the chromium-bearing alloys is related to this composition. Figure 9 shows that the ratio of oxygen to

In Corrosion Chemistry; Brubaker, G., et al.;
ACS Symposium Series; American Chemical Society: Washington, DC, 1979.

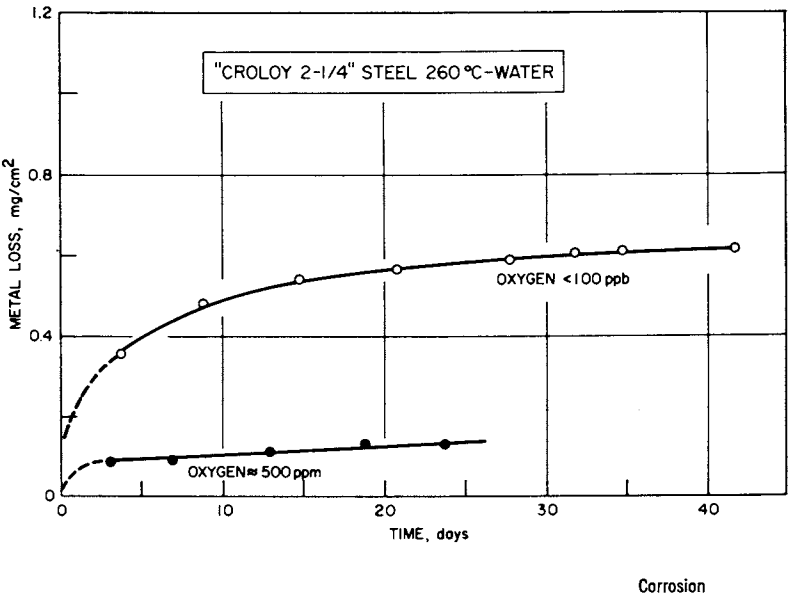

Figure 7. Corrosion of Croloy 2¼ steel in water at 260°C (6)

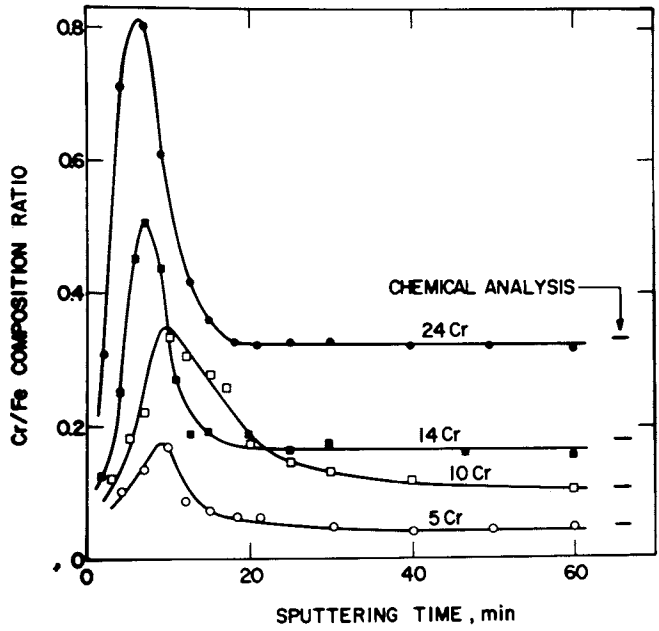

Journal of the Electrochemical Society

Figure 8. Cr/Fe ratio as a function of distance from surface for four oxidized iron–chromium alloys (7). Ratios for alloys on right.

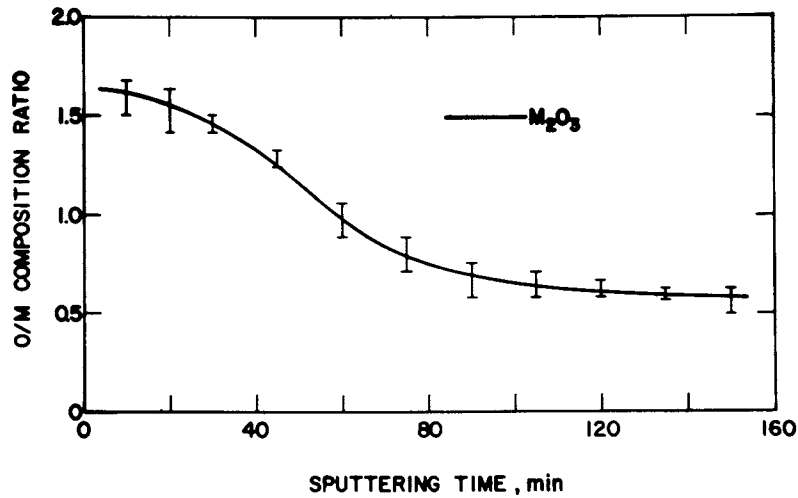

Journal of the Electrochemical Society

Figure 9. O/M ratio as a function of depth in oxide in iron and iron–chromium alloys (7)

metal also varies within the film. That corresponding to M_2O_3 is shown. As one gets closer to the metal, shown by surface analysis after sputtering some material off the surface, the oxide is seen to have less oxygen in it. It is another pecularity of some of these systems that in the thin film range, the stoichiometry of the oxide is not as expected.

As most of you know, if nickel is added to chromium alloys a series of stainless steels is produced with quite good corrosion resistance. These alloys have a widespread use; these days those with compositions close to 18 Cr-8 Ni are increasingly being used in many practical applications. I guess I should warn you that if you listened to Roger Staehle you heard that there are a number of instances when they also crack unexpectedly after a period of exposure. So they are by no means perfectly resistant to corrosion; nevertheless, they offer a very substantial improvement in the performance of low to moderate cost materials. Figure 10 is made up to show that if aluminum is added to 304 stainless steel--that is roughly the simple 18 and 8 stainless steel--the corrosion protection provided by the oxide to superheated steam is very markedly increased. This element also increases resistance to oxidation by gases--air, oxygen, and carbon dioxide. Aluminum is an effective alloying constituent for improving the corrosion-oxidation resistance of iron as well. The protective film is enriched in aluminum as compared to the metal composition. In both systems, the alloys containing aluminum tend to be brittle.

I have been talking to you about the formation of oxide films; for completeness it is appropriate to mention that films also grow or form by recrystallization of a substrate layer or by hydration of a material that was originally formed in an anhydrous form. As a general rule, those cases produce films that are not highly protective. There is a practical exception to that: if one anodizes aluminum in some environments, notably sulfuric acid, the coating is relatively porous, with the oxide only partially hydrated. By boiling in water, hydration is increased, the volume of the oxide is increased and the pores are sealed, and an effective protective layer is formed.

I'd like to switch now and talk to you about degradation of films. In order to talk about corrosion one has to consider both the growth of films and their degradation. As one studies them, one finds that the combination of the two is the key to getting a measure of understanding of the behavior of the system. Some of the results are a little unexpected at first glance.

In Corrosion Chemistry; Brubaker, G., et al.;
ACS Symposium Series; American Chemical Society: Washington, DC, 1979.

% Al	Metal Loss, mg/cm^2
0	18.0
1	17.0
2	8.8
4	0.06
5	0.03

Samples exposed in as cast condition, surfaces electropolished.

Corrosion

Figure 10. Corrosion of aluminum-modified Type 304 SS for 28 days in steam contg. 30 ppm O_2 at 650°C (8)

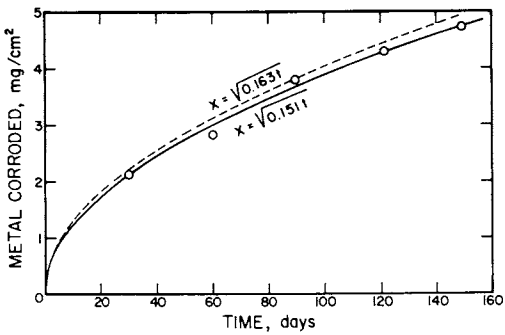

Figure 11. Parabolic corrosion of experimental aluminum alloy A288 (Al + 1% Ni, 0.5% Fe, 0.1% Ti) in stagnant water at 260°C (9)

It is well for us to be alert for such things. Let me make an obvious platitude for you about a film that degrades at a constant rate. It is obvious that the metal will corrode at a constant rate if degradation is uniform all over the surface, although it might take some time to reach that stage while it builds up a film. That is not a rare phenomenon. It is more common, I think for degradation not to be that uniform over the surface. We're going to talk about some of those cases.

First, let us consider a rather simple case: the film dissolves in water. When iron or steel corrodes in high temperature water without oxygen, the rate of corrosion is determined by the rate at which the film dissolves and is lost from the surface. This rate remains constant if there is some procedure that cleans up the water and keeps it from becoming saturated. One such procedure is passage through a loop containing a lower temperature septum in which some of the material precipitates. Another is passage through an ion exchange resin or some other device that will purify the water. Such loop systems often contain suspended solid corrosion product in the water. This material in nuclear reactor systems is called crud and it has been the source of a lot of irritation and money. These come about because the crud is radioactive and deposits in all parts of the system, complicating maintenance.

If one chooses the temperature and the alloy (e.g. A288 containing 1% Ni) aluminum forms in water a film such that the rate of formation is inversely proportional to the thickness. That gives what's called the parabolic growth law; data for such behavior are shown in Figure 11 (together with a dashed curve for another experiment). In the kind of system in which fresh water is continuously added and the excess allowed simply to leak out, at least a partially saturated solution is lost all of the time. The two specimens of Figure 12 have been fitted by curves that have the same growth rate constant as in Figure 11 and different dissolution rates. They were in the same autoclave at slightly different locations; probably the water contained a little more dissolved aluminum at one specimen than at the other. The expression for the paralinear behavior in its simple form is:

$$\frac{dL}{dt} = \frac{k_p}{L-(g+ft)} \quad ,$$

In Corrosion Chemistry; Brubaker, G., et al.;
ACS Symposium Series; American Chemical Society: Washington, DC, 1979.

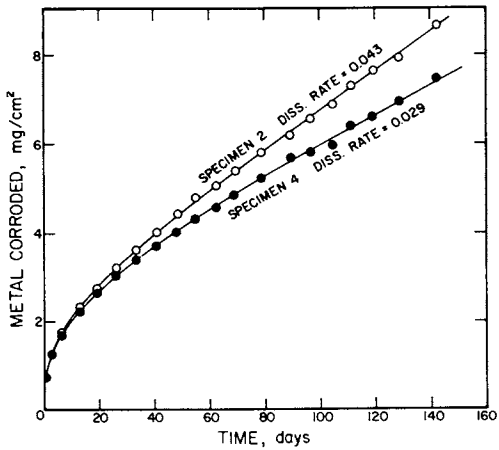

Figure 12. Paralinear corrosion of aluminum alloy A288 in refreshed water at 260°C (9)

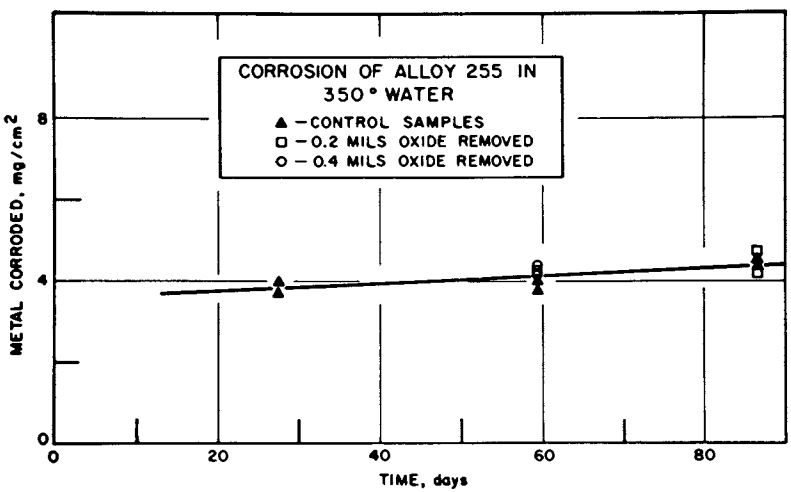

Journal of Nuclear Materials

Figure 13. Influence of corrosion-oxide removal on the corrosion of an Al-1Ni-0.1Ti alloy (10)

where L is the amount of metal loss (determined through the use of a special metal thickness gauge), k_p the parabolic growth constant, f the rate of dissolution for the specimen, and g the amount of dissolution that occurs early in the exposure. At long times the curve for L versus time resembles a straight line with slope f.

Paralinear corrosion (related to dissolution of corrosion product) does not occur for all aluminum alloys in water at all high temperatures. In Figure 13 are plotted data for an alloy (Al, 1% Ni, 0.1% Ti) corroded in water at 350°C (10). The corrosion rate was low and constant, as shown better in other figures in the same publication. For some specimens in the figure 1/3 or 2/3 of the corrosion product was removed mechanically after the first exposure period. There was no discernible effect on subsequent corrosion, indicating that control of corrosion probably resided close to the metal-oxide interface. Similar experiments for the alloys and temperatures where paralinear behavior occurs showed that removing some of the product caused an increase in subsequent corrosion rate.

The use of Figure 14 begins discussion about low temperature corrosion of aluminum in water. Again we'll see that the total film is not controlling. This is the kind of curve obtained in a couple of tests that ran for a long time in continuously refreshed systems. Note that the rate is decreasing continually with time for at least a few years--we'll analyze that curve shape starting with Figure 15. At the beginning of the tests (from 0.1 to nearly 10 hours) and subsequent to about 100 hours, the weight gain and the metal corroded (determined through the use of a sensitive metal thickness gauge) varied as the logarithm of time. The initial film is boehmite, the same partly hydrated oxide that forms at high temperatures. When this film breaks down, beginning in half a day at these conditions, we find that the total amount of corrosion and the total oxide present quickly increase severalfold. The new product is the completely hydrated oxide bayerite. If one runs the test a long time (Figure 16) one finds that the logarithmic rate law holds. The dashed lines indicate that the initial period is sensitive to the test procedure that is used. The height of the plateau varies inversely with how well refreshed the solution is. The requirement for measurement sensitivity in this test was substantial. As a matter of fact, the (eddy current) gauge limitation came not by its sensitivity (about ten Angstrom units in diameter for

In Corrosion Chemistry; Brubaker, G., et al.;
ACS Symposium Series; American Chemical Society: Washington, DC, 1979.

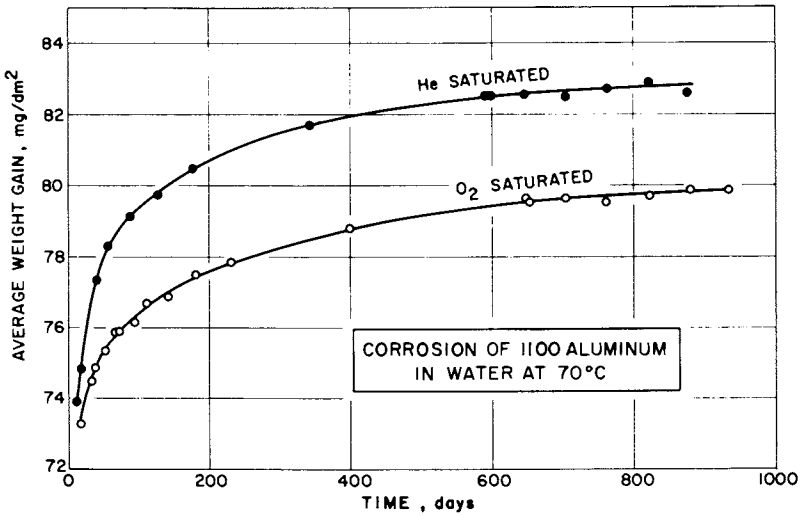

U.S. Atomic Energy Commission and
European Atomic Energy Society

Figure 14. Corrosion experiments in water at two oxygen concentrations (< 0.4 and 19 mg/L) (11)

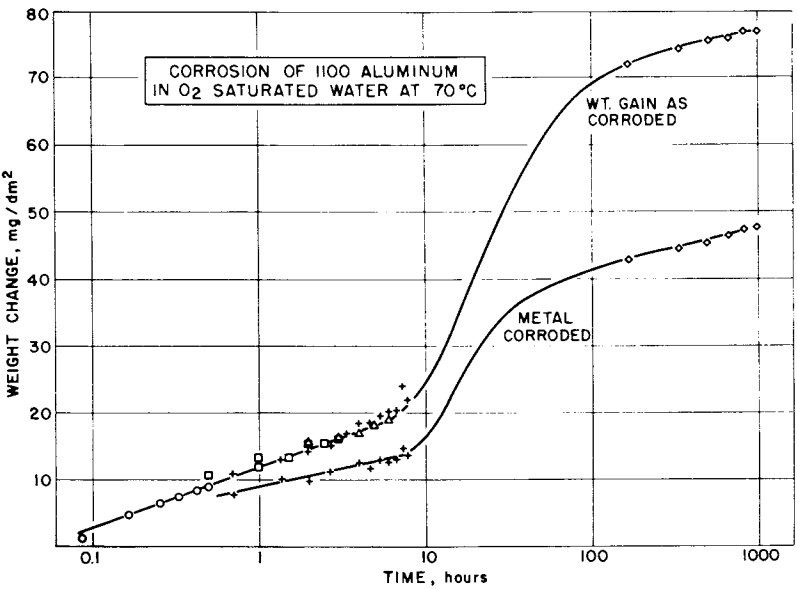

U.S. Atomic Energy Commission and
European Atomic Energy Society

Figure 15. Early stages in corrosion of aluminum (11)

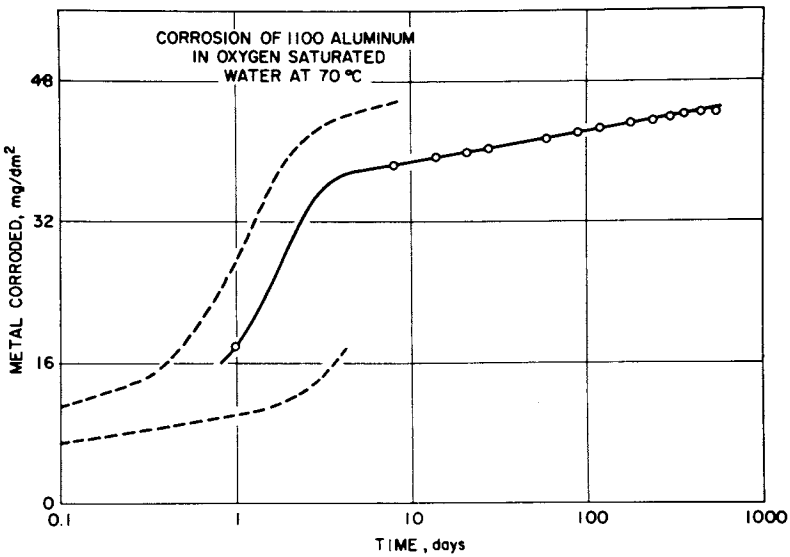

Figure 16. Long-time corrosion of aluminum (12)

a round specimen) but because of the metallurgical changes that occurred in the samples.

Now I'd like to analyze what happens to the oxide during the second logarithmic corrosion period. Figure 17 shows the amount of aluminum dissolved from a specimen (1100 aluminum) and carried away in the discharge water. This was determined by very carefully collecting the effluent solution, boiling off the water, collecting the aluminum, and analyzing the microgram quantities. Dissolution (amount = ξ) occurred at a constant rate during the second logarithmic period. Combining these data with weight gain (G) and metal lost from the single specimen (L), the amount of boehmite (a) and the amount of bayerite (b) shown in Figure 18 were calculated (13). The curve for boehmite layer growth close to the metal closely follows the curve for the amount of corrosion (both even showing an atypical increase in slope near the end), while the amount of bayerite slowly decreases (presumably by dissolution). The evidence is that in this system boehmite makes a protective (rate-controlling) layer while the bayerite dissolves and obscures the truth.

I would like to tell you about another kind of unusual kinetic behavior, that of zirconium. An alloy called Zircaloy 2 contains minor amounts of iron, chromium and nickel and a little tin. The alloy was invented by accidentally contaminating a zirconium-tin alloy with stainless steel. Since that time people have been making it on purpose. The weight-gain slopes on the log-log plot in Figure 19 are approximately 1/3 and the rate expression that is nearly followed is called cubic oxidation. It occurs initially in water; it is followed by film breakdown and an increase in oxidation rate with new kinetics (showing straight lines and slopes very close to 1 on this plot). A log-log straight line with a slope of one is unusual, since it requires the particular straight line on cartesian coordinates that passes through the origin. At the time of "breakaway" there is a recrystallization of the zirconium oxide to a less coherent film. That is an additional form of degradation.

Lest you believe things are too simple during "cubic" oxidation I've chosen to show this slide (Figure 20) based on data by Bob Shannon at Hanford, Washington, which shows that individual specimens corrode in series of waves. Paul Pemsler once christened those the Picturesque Hills of Shannon during a meeting. What this illustrates is that we're not

In Corrosion Chemistry; Brubaker, G., et al.;
ACS Symposium Series; American Chemical Society: Washington, DC, 1979.

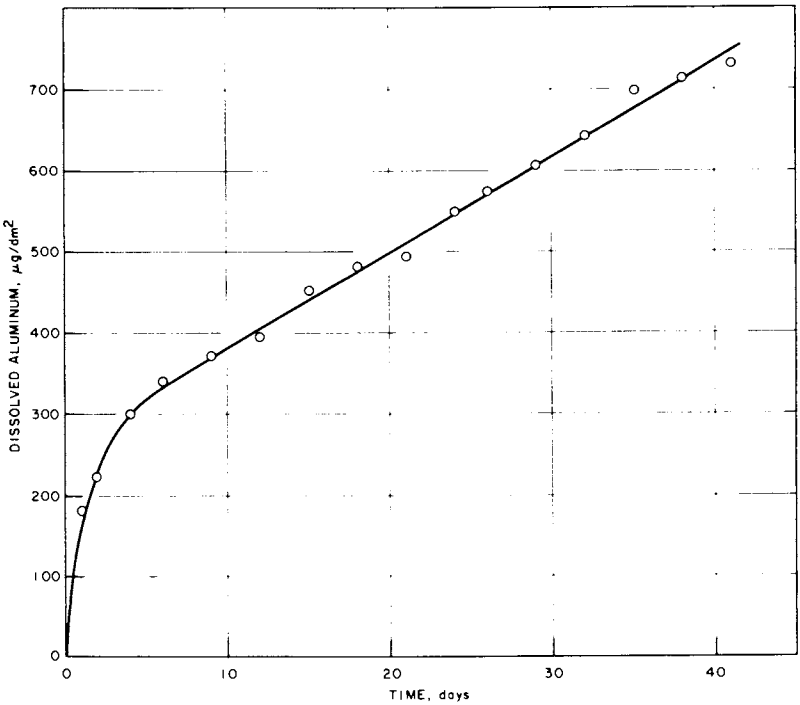

Figure 17. Corrosion product dissolved from specimen of Figure 18 (13)

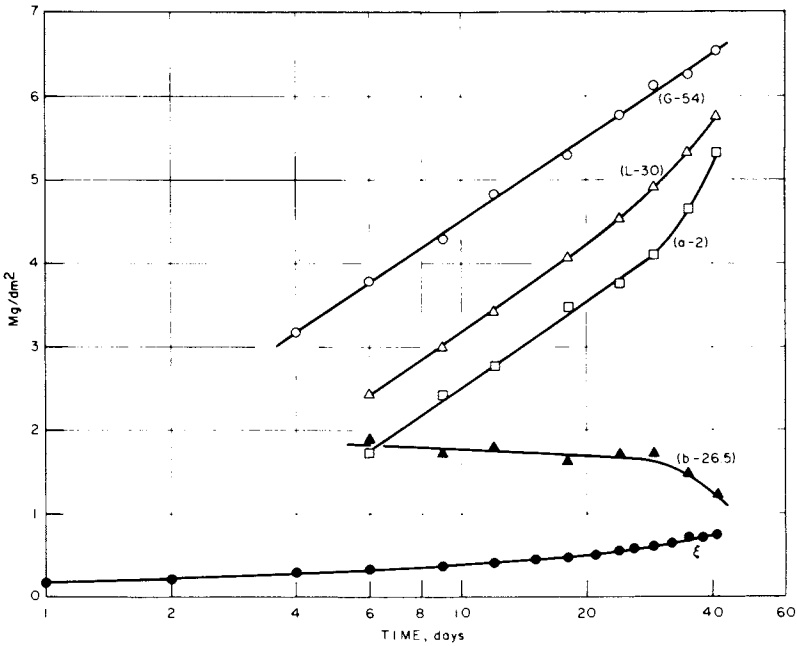

Journal of the Electrochemical Society

Figure 18. Summary of corrosion for one specimen of 1100 aluminum in oxygenated water at 700°C (13)

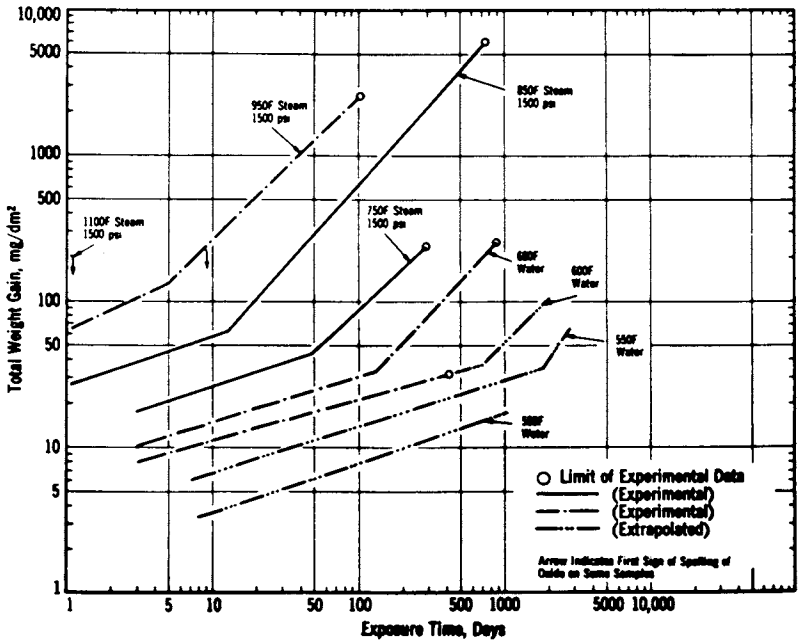

Figure 19. Corrosion of beta-quenched Zircaloy-2 in water and steam (14)

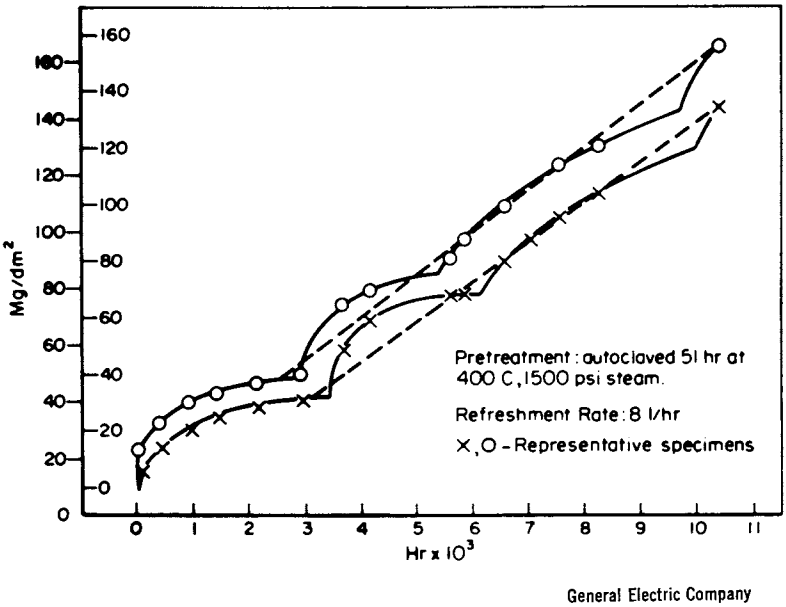

Figure 20. Corrosion weight gain of Zircaloy-2 in water at 360°C (15)

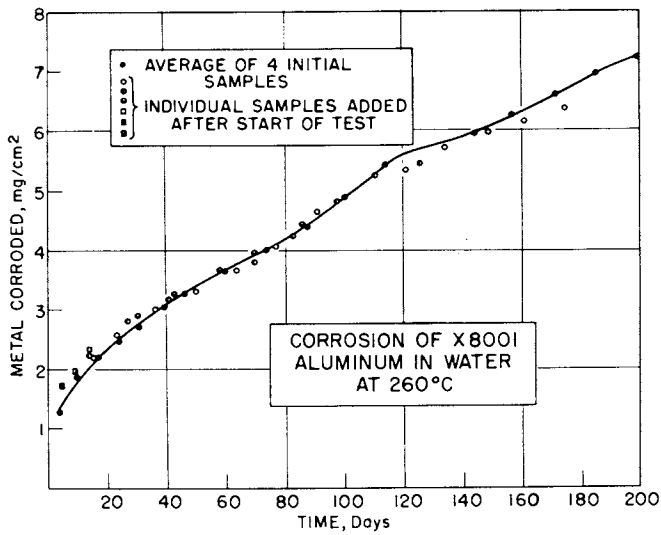

Figure 21. Corrosion of an aluminum alloy (1100 Al + 1% Ni) in high-temperature water (9)

dealing with continuous films continuously growing without breakdown. It happens that the breakdown on these specimens occurred over much of the surface at the same time so the phenomenon is visible. If it occurred locally and not at the same time at different places, you would not see the "hills", but odd kinetics such as roughly cubic. The phenomenon is by no means unique to zirconium. Figure 21 shows similar behavior by aluminum, also in high temperature water.

The oxidation of zirconium in oxygen at elevated temperatures follows near-cubic kinetics for awhile, then parabolic kinetics. A number of efforts have been made to explain the near-cubic behavior, with localized or line diffusion as that perhaps generally preferred. I'll describe for you my own thinking, put together and presented informally in 1967. It has not been published. At 700°C there is an initial layer of zirconium oxide that is relatively perfect, that forms interference colors on small areas; the rate of growth of film and the rate of diffusion of oxygen into the metal depend on the orientation of the metal crystal. Polycrystalline specimens prepared metallurgically in different ways, always pure and equally carefully treated, oxidize at quite different rates initially, but the rates become equal at long (parabolic) times. To fit these facts I developed the following model. The film that grows on the metal surface is proposed to be unique and different from the one that is stable on the outside and at long times. X-ray diffraction patterns taken in our laboratory during initial oxidation (special apparatus) suggest that this oxide is tetragonal rather than the commonly found monoclinic oxide. At any small area on the surface, for example for a single crystal surface, the initial film grows and oxygen diffuses into the metal at rates that are unique for that area until the film thickness reaches the value s (proposed to be the same for all areas). The initial film then transforms nearly instantaneously into final film, and the initial film then grows again in a second cycle, again to the limiting thickness s. The parabolic rate constant for the final film is c (value the same for all areas) and the rate of growth of initial film at a particular area is

$$\frac{dx_i}{dt} = \frac{b_i}{x_i + \frac{b_i}{c}(n-1)s} - \sqrt{\frac{k_i}{2t}} \quad ,$$

In Corrosion Chemistry; Brubaker, G., et al.;
ACS Symposium Series; American Chemical Society: Washington, DC, 1979.

where n is the number of the growth cycle at time t and k_i is the local diffusion constant for oxygen in metal.

An estimate of the type of oxidation curve to be expected from this model was developed from an initial case where two types of surfaces (A and B) were identified, and rate constants assigned that were not in conflict with any known data. Weight gains expected for the first thousand minutes are shown in Figure 22 for areas A and B and for a specimen consisting of 80% type A and 20% type B. The ends of the first growth cycle for each area can be identified. A number of weight-gain points for this hypothetical specimen are plotted in Figure 23 along with a reproduced weight gain recorder tracing (the solid line). A perfect cubic line is also shown for comparison (dashed line).

The fit is so good that it seems highly likely that the use of more types of areas to smooth out the average in the model would lead to excellent fitting of real-sample data. It isn't possible to say much more at this time; I do believe that the weight-gain curve for the single crystal wafer (more than 80% of area of one orientation) shown in Figure 24 displays breaks and slopes of the right order for the segments on a log-log plot. My personal conviction is that some kind of statistical models are going to be required to fit correctly much of the corrosion and oxidation data of the valve metals.

You've heard electrochemistry of corrosion as a lecture; I shouldn't spend much time on it but I'd like to describe some electrochemical effects for film formers. First the general principles. If you put a good electronic conductor (a metal) in an aqueous solution, you will typically find that an electrical potential is developed between the piece of conductor and the solution. When ions of the metal enter the solution and leave extra electrons behind a negative potential is developed. All oxidation reactions occurring on the surface are expected to produce this result. Similarly, reduction reactions that use electrons from the metal are expected to produce a more positive potential in the metal. The solution potential of the metal influences the rate of an electrochemical half-cell reaction in accordance with Le Chatelier's Principle, so it is possible to predict through the use of the Nernst Equation the potential that will exist when the only significantly rapid reactions are the oxidation and reduction parts of a reversible reaction. When more than one potentially reversible process occurs, the rate of oxidation will be expected to exceed the rate of reduction for at least one and the converse for at least one. At

In Corrosion Chemistry; Brubaker, G., et al.;
ACS Symposium Series; American Chemical Society: Washington, DC, 1979.

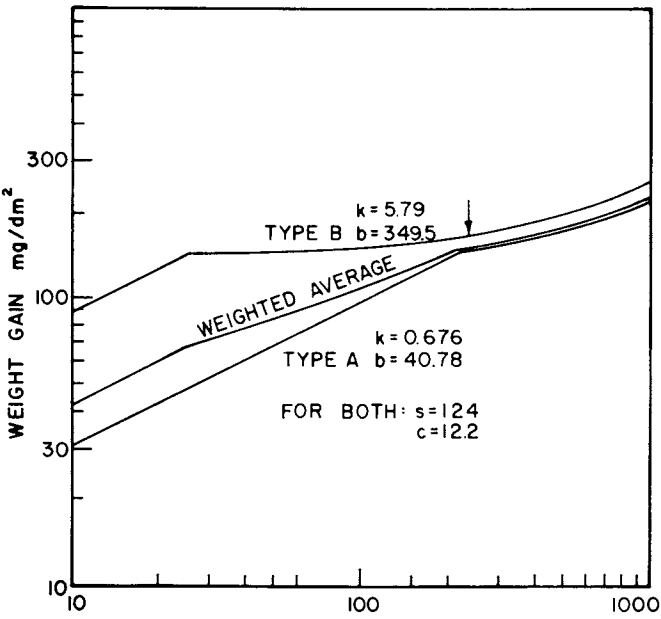

Figure 22. Calculated curves for oxidation of zirconium grains at 700°C (16)

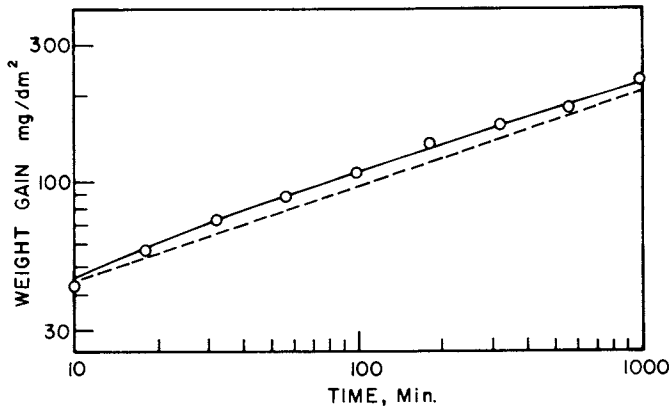

Figure 23. Oxidation of polycrystalline zirconium at 700°C, comparison of calculated and actual oxidation (16)

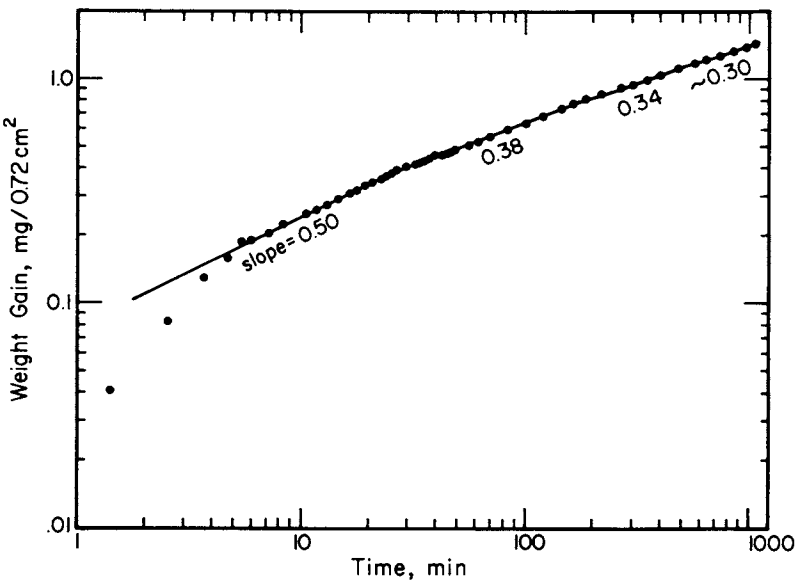

Figure 24. Observed oxidation of zirconium crystal at 700°C, 100 mm O_2 (16)

In Corrosion Chemistry; Brubaker, G., et al.;
ACS Symposium Series; American Chemical Society: Washington, DC, 1979.

a steady-state potential, the sum of the rates of all of the anodic reactions will equal the sum of the rates of all the cathodic reactions.

For film formers, a typical anodic reaction is

$$M + H_2O \rightarrow MOH + H^+ + e^- ,$$

so an oxide is formed and the solution becomes acid. The most common cathodic reactions are

$$H_2O + e^- \rightarrow 1/2\ H_2 + OH^- \quad \text{and}$$

$$1/2\ O_2 + 2H_2O + 2e^- \rightarrow 2OH^- ,$$

so cathodic reactions produce alkali. Directly related to the pH are the stabilities of the various species for the corroding metal. Thus for iron, the so-called Pourbaix Diagram for iron in Figure 25 shows potential-pH zones in which Fe_2O_3 or $Fe(OH)_2$ are stable and thus in which protective films of these substances might form at a total ionic concentration of 10^{-6} M.

When a film is present, the hydrogen produced from the second reaction above is not necessarily all liberated directly into the water or solution. Some of it may be liberated beneath the film as shown in Figure 26. The result may be local rupturing of the oxide film--a form of degradation--the formation of metal hydride, or the entry of hydrogen into the metal, depending on which are feasible or most favorable. I believe there are a number of cases where film rupture occurs, although they are often not easy to identify. We have declared the belief that it is important in the corrosion of aluminum alloys below the boiling point of water (19). To provide evidence of this, we ran a series of experiments to determine the logarithmic corrosion rate constant for 1100 aluminum at 70°C with potentials controlled by a special interrupting potentiostat (20). The results, in Figure 27, show that anodic polarization (diamond-shaped points) caused lower corrosion rates than the unpolarized runs (circular points). A reduction in cathodic damage to the film is suggested. The potential above which hydrogen should not be liberated cannot be identified because the local pH during anodic polarization could be considerably below the 6+ of the distilled water at 70°. We shall see something enlightening on this later. For pH 6 the potential for the reversible hydrogen liberation reaction is calculated to be about -0.4 volt.

Most notably at higher temperatures, aluminum also suffers from the entry of corrosion product into the

In Corrosion Chemistry; Brubaker, G., et al.;
ACS Symposium Series; American Chemical Society: Washington, DC, 1979.

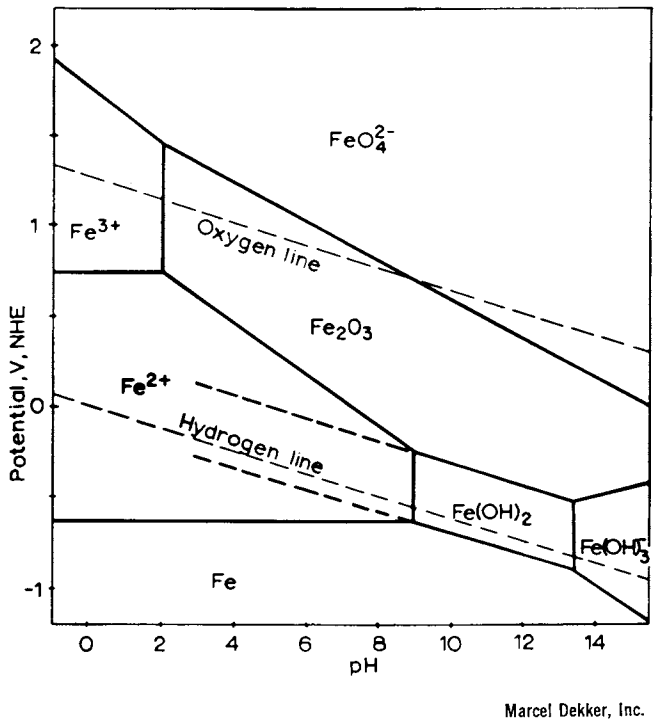

Figure 25. Pourbaix diagram for the system Fe–H_2O at 25°C (17)

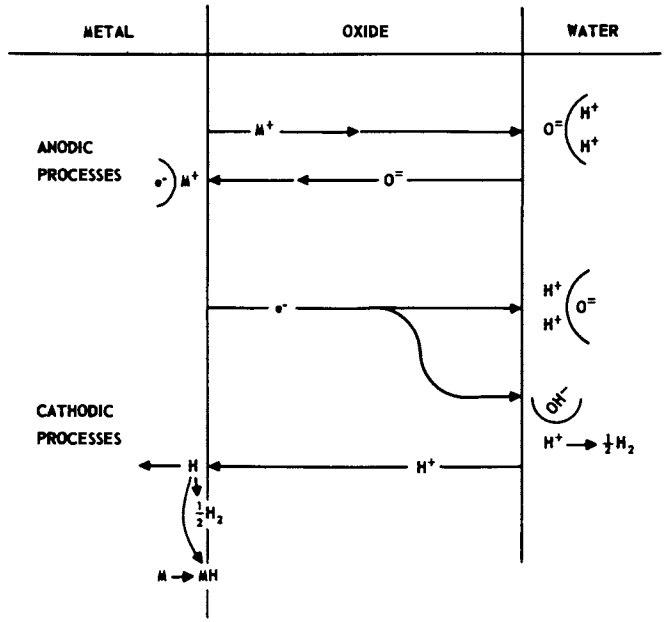

Journal of the Electrochemical Society

Figure 26. Schematic of corrosion processes (18)

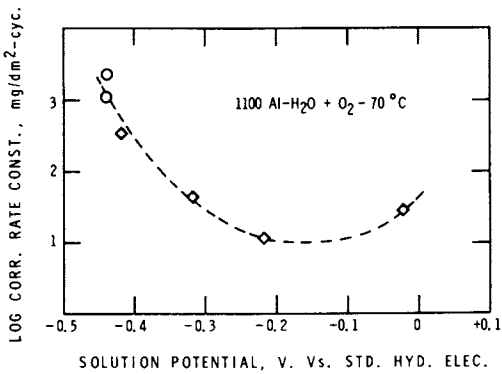

Figure 27. Effect of controlled-solution potential on logarithmic corrosion-rate constant for aluminum (12)

metal. In Figure 28 are shown specimens of commercially pure aluminum after two weeks exposure to water at 275°C. The blistering progresses with more severe exposure conditions, as shown in Figure 29 (66 hours, 300°C). Some of the blisters are hollow before the water gains access and before they become oxide-metal mixtures. Figure 30 shows what happens at a higher temperature; this exposure was four hours at 315°C. If varying amounts of material are etched from the surface of a series of samples corroded for a brief period, and each remaining sample is analyzed for hydrogen content, the hydrogen in the etched-off layers can be calculated. The results in Figure 31 show that the hydrogen content of the surface layers increased quite a bit, and demonstrate that the gas that formed the blisters was hydrogen. If the hydrogen is produced largely at a position remote from the metal surface, as in Figure 32, the severe damage is prevented. In this case, the aluminum is simply bolted to a piece of stainless steel. Exposure conditions were as in Figure 30. If to the water are added ions that are reducible to metal (largely at active cathode spots) metal dendrites are formed. The nickel dendrites in Figure 33 were formed in this way; no severe corrosion of 1100 aluminum was observed during corrosion exposure to stable nickel salt solutions at elevated temperatures. Figure 34 suggests that if deposits of something like the nickel-aluminum compound $NiAl_3$ were used they would act as very effective cathodes for hydrogen liberation. For this reason, we made aluminum-nickel alloys in which $NiAl_3$ precipated. As indicated in Figure 35, some 1% nickel alloys showed excellent corrosion resistance in high temperature water. I won't discuss details of composition and metallurgical preparation; they were found to be important.

Uranium corrodes in oxygen-free water at a constant rate to form UO_2 in the form of a relatively unprotective layer; Figure 36 shows such corrosion rates on an Arrhenius plot. When the rate gets very large at elevated temperatures, uranium hydride can be found mixed in with the oxide powder. If oxygen is present in the water, for a long period protective oxide films are formed; these eventually break down locally and spread. Figure 37 shows that the whole surface eventually becomes bad. We believe that some hydride was regularly formed beneath the oxide both in deaerated and aerated water, and that the hydride subsequently was converted to the more stable oxide. This is believed to be a case of film degradation by the formation of hydride beneath it. For selected uranium alloys, oxide films

In Corrosion Chemistry; Brubaker, G., et al.;
ACS Symposium Series; American Chemical Society: Washington, DC, 1979.

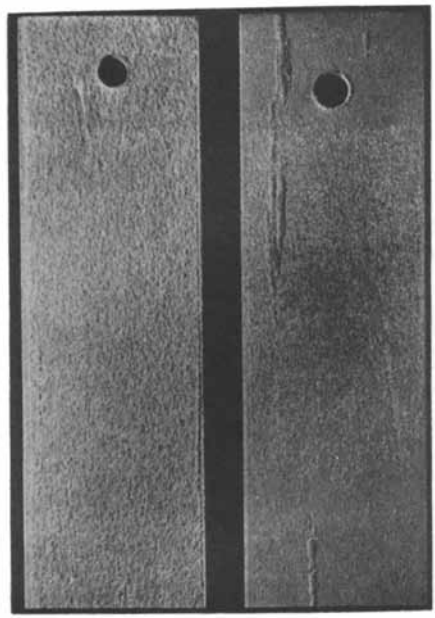

Journal of the Electrochemical Society

Figure 28. Typical appearance of 1100 aluminum after about two weeks in distilled water at 275°C (18)

Corrosion

Figure 29. Surface of "normal" 1100 aluminum sample after 66 hours in distilled water at 300°C, 20× (21)

Corrosion

Figure 30. 1100 aluminum after four hours in distilled water at 315°C (22)

TREATMENT	AVERAGE METAL ETCHED AWAY	HYDROGEN CONTENT (WHOLE SAMPLE)	ESTIMATE OF HYDROGEN IN INCREMENTS OF ETCHED METAL
AS CORRODED	-	12.1 ppm	-
AS STRIPPED	-	7.3	
ETCHED (DILUTE HNO_3-HF)	0.016 mm	3.0	280 ppm
ETCHED "	0.041	1.8	59
ETCHED "	0.071	1.1	24
ETCHED "	0.120	1.0	5
ETCHED "	0.22	0.8	3
BLANK (NO CORROSION)	-	0.6	-

Argonne National Laboratory

Figure 31. Hydrogen analyses of 1100 aluminum after two days corrosion in water at 290°C (23)

In Corrosion Chemistry; Brubaker, G., et al.;
ACS Symposium Series; American Chemical Society: Washington, DC, 1979.

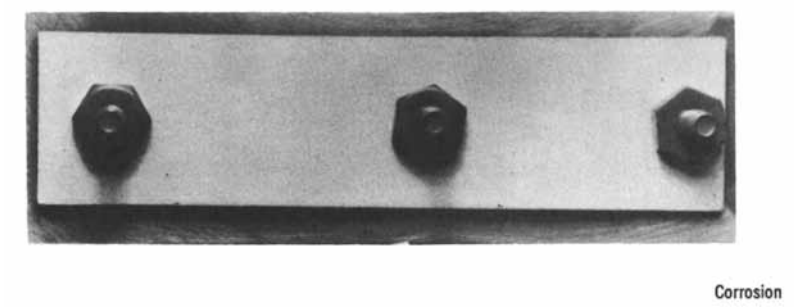

Corrosion

Figure 32. 1100 aluminum, coupled to 347 stainless steel, after four hours in distilled water at 315°C (22)

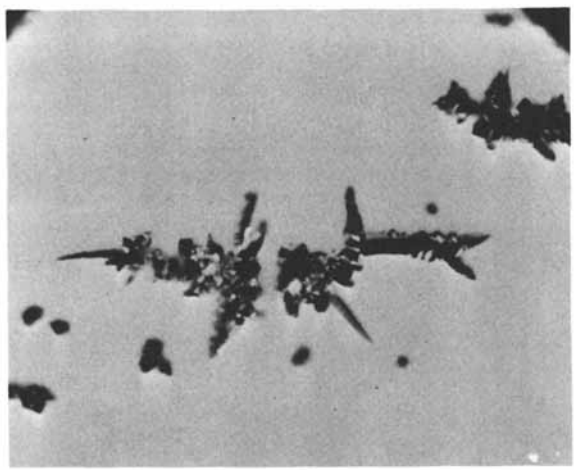

Corrosion

Figure 33. Dendritic nickel deposited on 1100 aluminum from $NiSO_4$ solution (50 ppm Ni^{++}) 250× (21)

In Corrosion Chemistry; Brubaker, G., et al.;
ACS Symposium Series; American Chemical Society: Washington, DC, 1979.

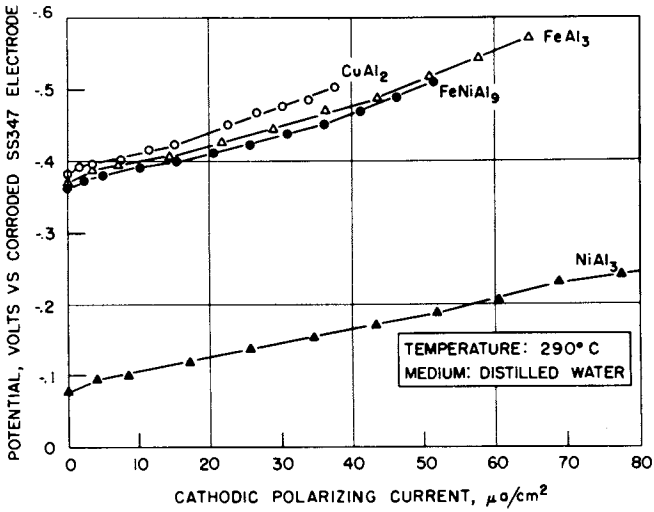

Figure 34. Cathodic polarization curves for some aluminum intermetallic compounds (9)

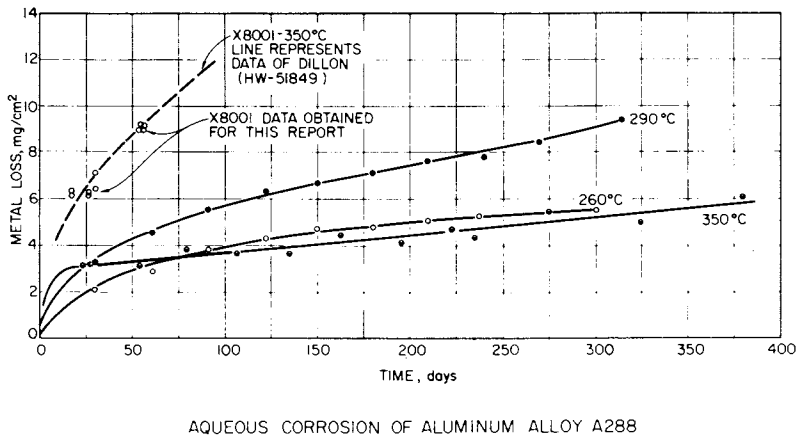

Figure 35. Aqueous corrosion of aluminum alloy A288 (Al + 1% Ni, 0.5% Fe, 0.1% Ti) (24)

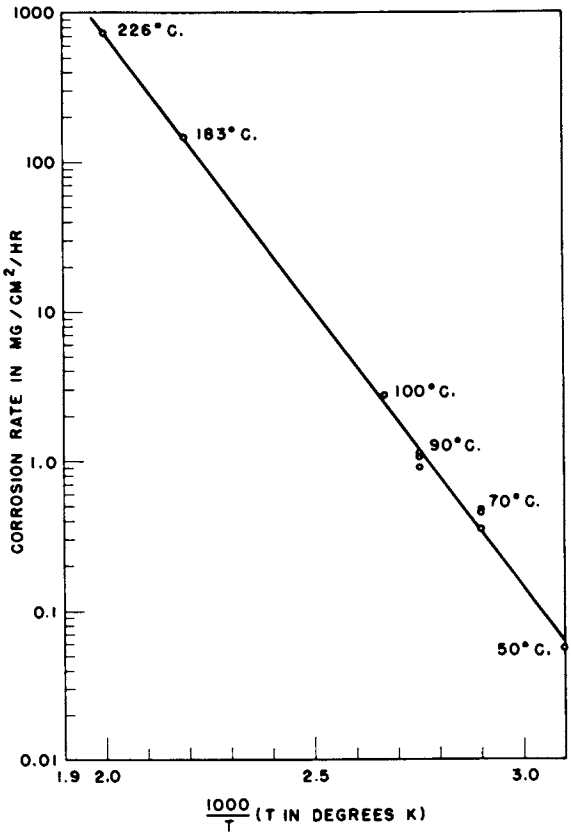

Figure 36. Corrosion rate of uranium in hydrogen-saturated water (25)

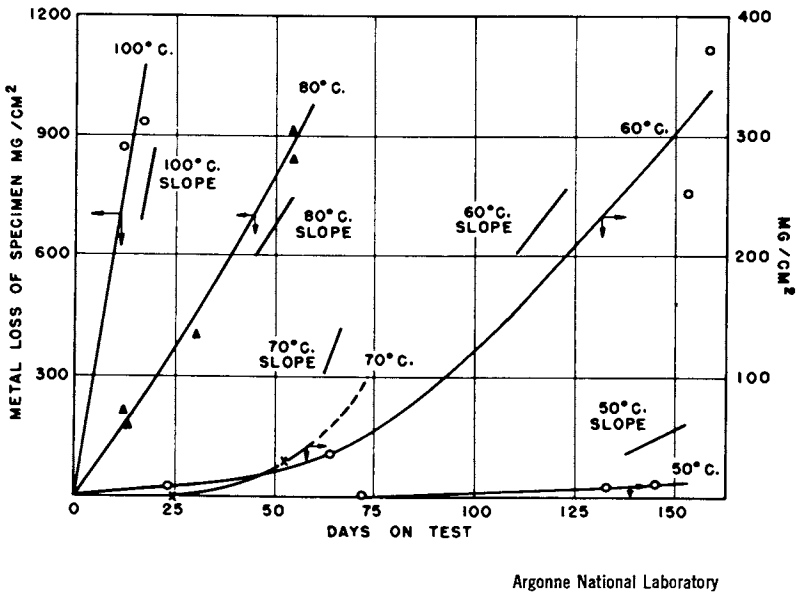

Figure 37. Corrosion of uranium in aerated distilled water (26)

are protective even in the absence of oxygen, and for very long periods. Figure 38 shows some corrosion rates which are respectably low. The maximum temperature shown is 400°C. These films also break down eventually, and this appears to involve the formation of some uranium hydride locally. The breakdown certainly involves the buildup of hydrogen in the metal. For the particular alloy and temperature in Figure 39 specimens lasted much longer before damage occurred when they were pretreated in a vacuum before corroding.

When zirconium is oxidized in water, a considerable fraction of the corrosion product hydrogen enters the metal. There is evidence that the oxide recrystallization and the transition in kinetics that were shown in Figure 19 are related to a buildup of hydrogen in the surface of the metal. It has been suggested that at that time some zirconium hydride forms beneath the film. The addition of alloying elements which form active cathodes for hydrogen liberation have reduced hydrogen uptake, have delayed transition, and have resulted in the formation of more coherent oxide after transition. There has been no clear resolution as to mechanisms (29).

It is possible to consider gaseous oxidation producing a stable oxide film as an electrochemical process in which oxidation occurs at the metal-oxide interface where metal ions leave the metal (see Figure 4) and reduction occurs at the outer surface of the oxide where electrons combine with oxygen. On the basis of this line of reasoning it is possible to predict (a) the formation of a potential difference between metal and oxide exterior for those systems in which the resistance or "retardance" to the passage of ions through the growing oxide is not much greater than the retardance to the passage of electrons, and (b) a change in oxidation rate from the application of an electrical potential between metal and oxide exterior. An illustration is the behavior of zirconium for which a potential in excess of one volt can be measured (Figure 40) and whose oxidation rate at points of electrical contact can be markedly influenced (Figure 41). The contact consisted of points at which the specimen rested upon conducting powder. Since the area of contact diminished under sharpening points of anodically stimulated growth and increased where growth was retarded cathodically, the rate of weight gain for the entire specimen in the figure was considerably more reduced by applied cathodic current than it was accelerated by applied anodic current.

In Corrosion Chemistry; Brubaker, G., et al.;
ACS Symposium Series; American Chemical Society: Washington, DC, 1979.

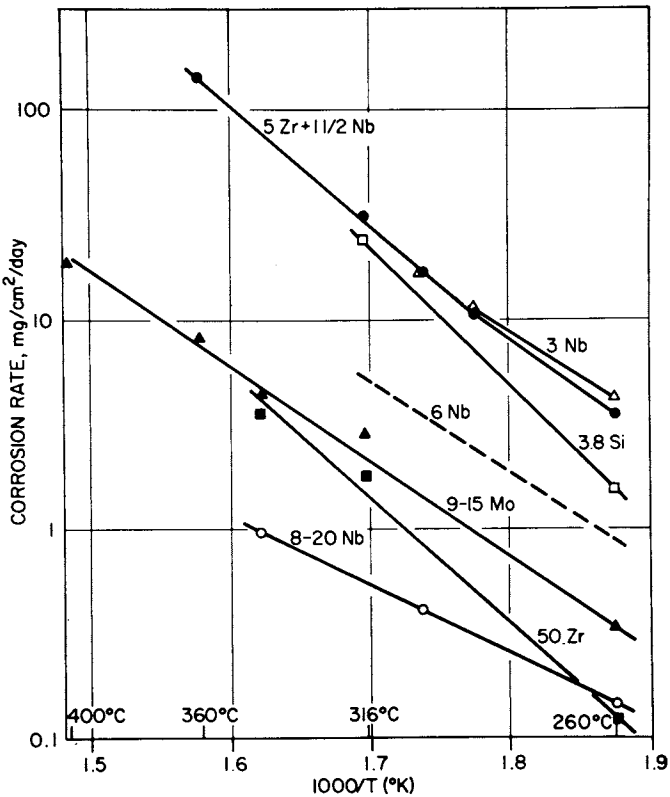

Figure 38. Corrosion of uranium alloys in water (27)

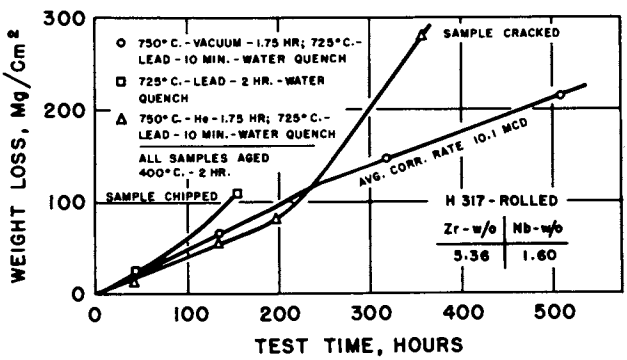

Journal of the Electrochemical Society

Figure 39. Effect of gas removal on corrosion in water at 290°C of U-5% Zr-1½ Nb alloy (28)

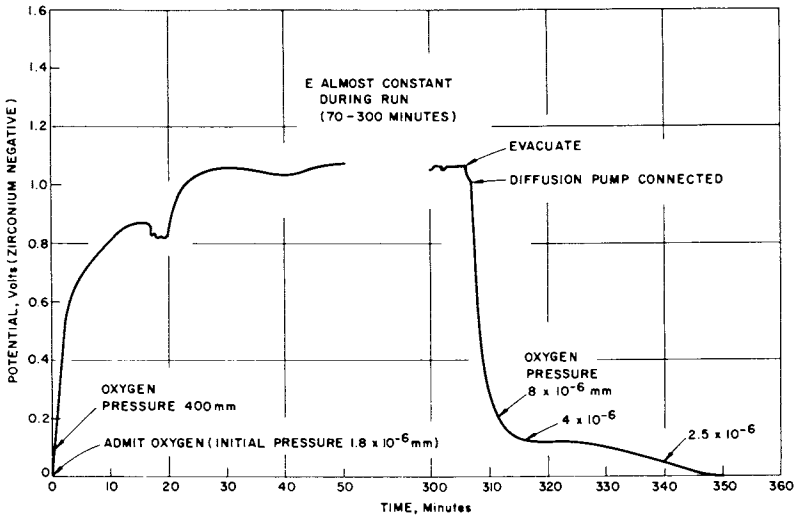

Journal of the Electrochemical Society

Figure 40. Potential developed during oxidation of zirconium at 700°C (30)

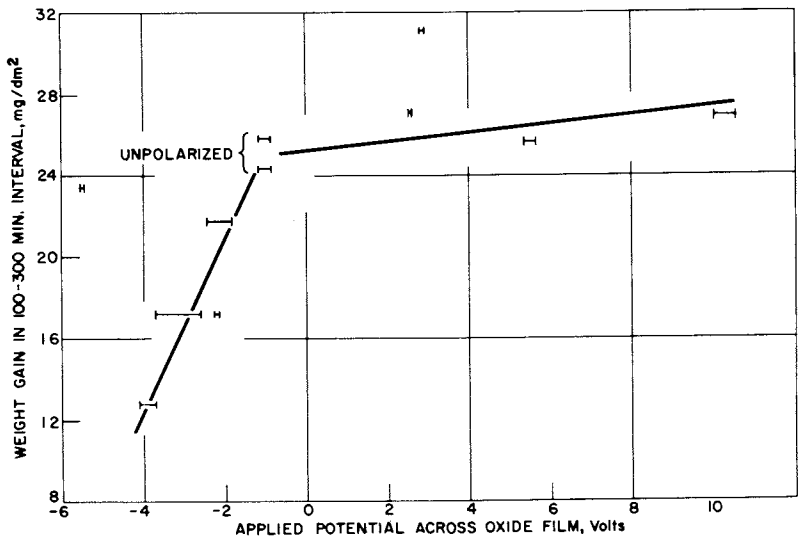

Journal of the Electrochemical Society

Figure 41. Variation in oxidation rate with applied potential: zirconium in oxygen at 700°C (30)

Before we finish, I'd like to spend a few minutes on pitting. As you know, there are local sites at which corrosive attack occurs for some systems preferentially. If this local attack continues, quite deep pits can form. This is one of the insidious kinds of corrosion attack for a material. Some of the film-forming metals tend to be quite susceptible to pitting attack under appropriate conditions. One of the characteristic requirements for it is the formation of low pH within a protected pit--protected in some way from the general environment. We think that commonly there are local cathodes at which hydrogen liberation is very great, at which film rupture occurs. This is made easier by the fact that the cathodes are often a second, cathodic phase so there is often an imperfection in the oxide at the point anyhow. At first there is a high anodic reaction rate next to the cathode because of the proximity. When the anodic reaction has undercut the cathodic particle destroying electrical contact, the two half-cell reactions will no longer be very close together and there will be pH changes so that the anode area will become acid. The result of this is that a protective film doesn't form as a primary product of the reaction; instead, metal ions are formed in solution. As these ions diffuse out to the surface of the oxide film, the environment becomes more nearly neutral and oxides precipitate. This leads to the characteristic barnacled appearance of a pit, with precipitated oxide over it. In this way the solution within the pit is isolated from the bulk solution, and the acidity can be great. If the barnacle becomes a sufficiently effective barrier to the flow of the ionic current which must pass through the solution from remote cathodes, the pit stops growing. Figure 42 shows the cleaned surface of a ground piece of 1100 aluminum after about 4 hours in oxygen-saturated distilled water. There are occasional small pits (black in the photograph). After nearly two years exposure (Figure 43), there are no large pits; the appearance is as if essentially all of the surface had in turn served as the location for micro pit formation. The low conductivity of the water might have contributed to early stifling of pit growth. At higher magnification the pits (Figure 44) are not unlike larger ones seen in other systems. Presumably another lecturer in this series will give or has given you some details of practical pitting problems and the most promising approaches to control them.

A number of investigators have made efforts to measure the pH in pits; values as low as 1.5 have

In Corrosion Chemistry; Brubaker, G., et al.;
ACS Symposium Series; American Chemical Society: Washington, DC, 1979.

U.S. Atomic Energy Commission
and European Atomic Energy Society

Figure 42. Cleaned 1100 aluminum surface after 4¼ hours in oxygen-saturated distilled water at 70°C, 25× (11)

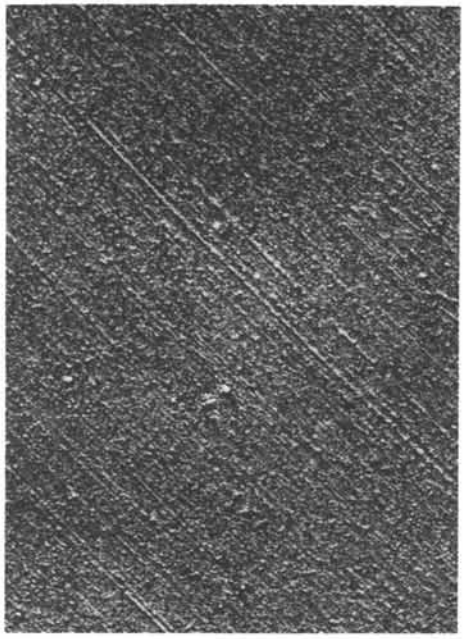

U.S. Atomic Energy Commission
and European Atomic Energy Society

Figure 43. Cleaned 1100 aluminum surface after 704 days corrosion in oxygen-saturated distilled water at 70°C, 25× (11)

In Corrosion Chemistry; Brubaker, G., et al.;
ACS Symposium Series; American Chemical Society: Washington, DC, 1979.

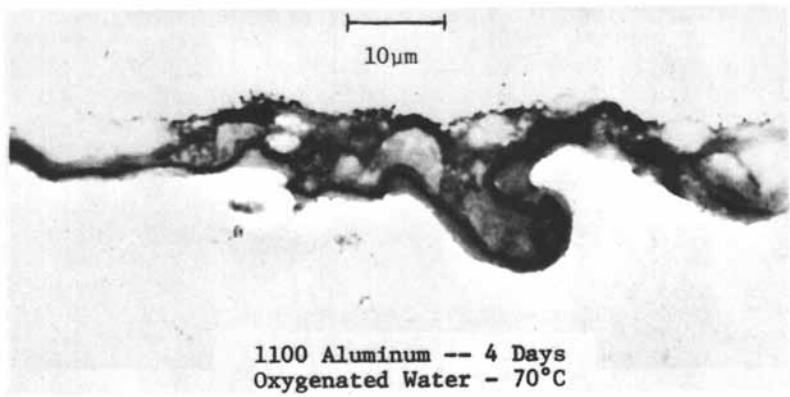

Figure 44. Electron micrograph of corroded surface of "commercially pure" aluminum (12)

been reported. Even exposed to the bulk water, we found, through the use of a special electrode a few tenths of a millimeter in tip diameter (Figure 45), that the pH near specimens of 1100 aluminum corroding in distilled water reached values below 3 (Figure 46).

Some years ago, Howard Francis, then of the Armour Research Foundation, made some time-lapse motion pictures of a potential map of the solution next to steel and aluminum alloys pitting in salt water. The presence of some active cathode points and growing pits was readily displayed. I suggested that he run the film backwards to see whether the active pits had been active cathodes just before their initiation. He later told me he had done so, and they had been with few or no exceptions.

At high temperatures film breakdown and pitting for aluminum alloys takes an unusual form especially when there is a high rate of flow of water past the metal surface. If there are a lot of specimens in the system, the corrosion rate is lower than if the area is small. The results of some exploratory experiments are shown in Figure 47. A large area (factor of 20) of aluminum alloy inhibited corrosion while a large area of stainless steel did not. The effect is certainly related to corrosion product in the system somehow. In Figure 48 one can see that the corrosion product lost from the specimen was substantially in excess of that which dissolved in the system. We thought that, at local pits and breaks the corrosion product, as it reached the oxide surface and was approximately neutralized, was swept away as particles of oxide. We thought that the addition of colloidal particles to the solution would tend to "plug" openings, reduce the loss of oxide, and lower the corrosion rate. Figure 49 shows that when a hydrated colloid was injected in to the system, a very low corrosion rate was obtained. In the same system the effects of polarizing current on corrosion rate (Figure 50) are similar to what I showed you at low temperature in Figure 27: anodic protection and cathodic stimulation.

The message I'd like to leave with you tonight is that some films are very good and very protective, some films have breaks in them, and they are moderately good, some become bad by some of the strangest mechanisms: an understanding or corrosion phenomena sometimes requires quite a bit of ingenuity.

In Corrosion Chemistry; Brubaker, G., et al.;
ACS Symposium Series; American Chemical Society: Washington, DC, 1979.

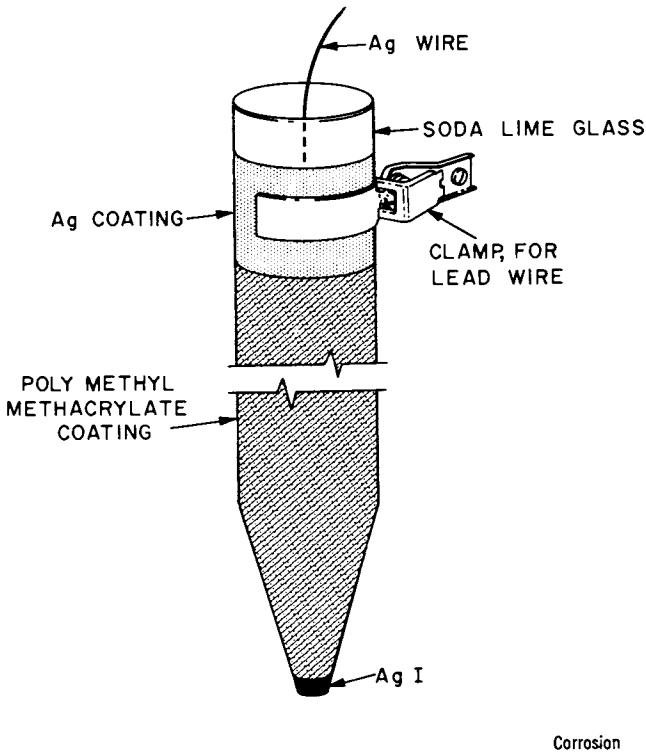

Figure 45. Glass, silver/silver iodide pH microelectrode (31)

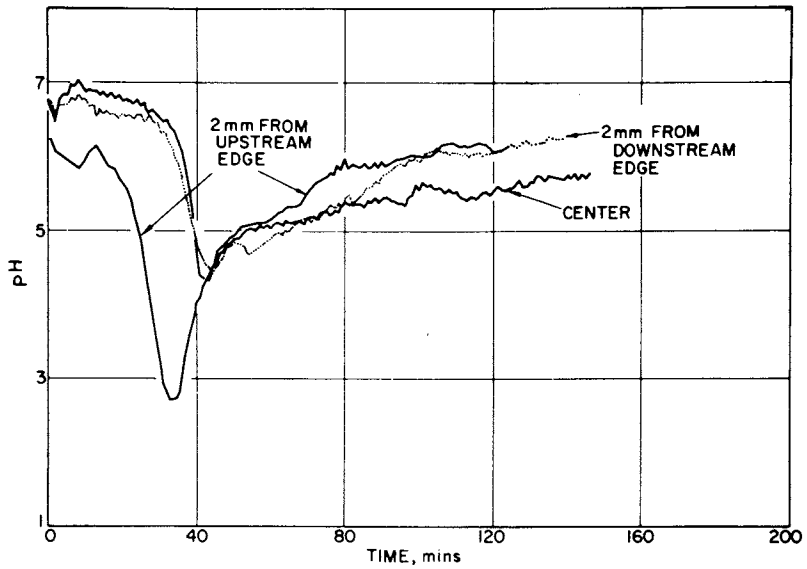

Corrosion

Figure 46. Effect of position on pH of 50°C oxygen-saturated water 0.1 mm from corroding 1100 aluminum (31)

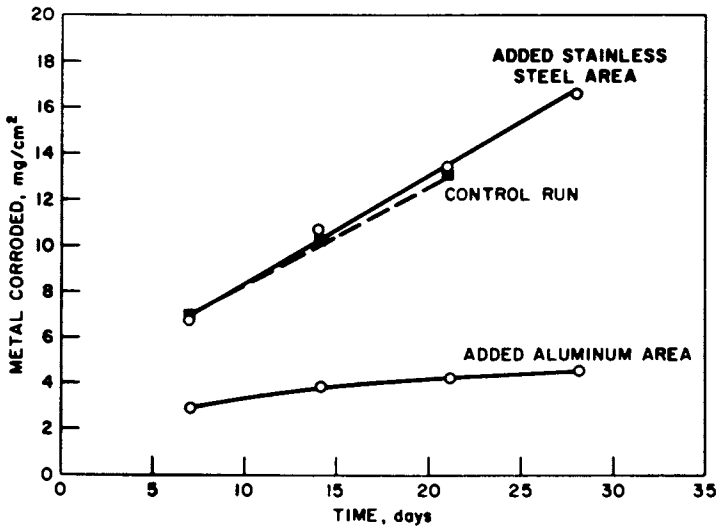

Argonne National Laboratory

Figure 47. Effect on aqueous corrosion of 8001 aluminum at 260°C, 7 m/sec velocity of added surface of aluminium or stainless steel (32)

	Normal (small) Area, 21-day Exposure	Large Area, 28-day Exposure
Average Metal Loss	13.1 mg/cm^2	4.60 mg/cm^2
Estimated $Al_2O_3 \cdot H_2O$ Produced (from metal loss)	29.1 mg/cm^2	10.2 mg/cm^2
Actual Average Product Remaining	11.6 mg/cm^2	7.9 mg/cm^2
Corrosion Product Lost	17.5 mg/cm^2	2.3 mg/cm^2
Corrosion Product Present at End of Test Compared with Total Produced	40%	78%
Aluminum Area	70 cm^2	1470 cm^2
Maximum Dissolved Corrosion Product, from Solubility Data (2×10^{-4} g of Al_2O_3 per liter at 1.5-liters/hr refreshment)	2.4 mg/cm^2	0.14 mg/cm^2
Ratio Dissolved to Actual Loss	0.14	0.06
Corrosion Rate in Last 7-day Period	40 mdd	5.8 mdd

Argonne National Laboratory

Figure 48. Comparison of two dynamic corrosion tests. Water at 260°C, 7 m/sec velocity (32).

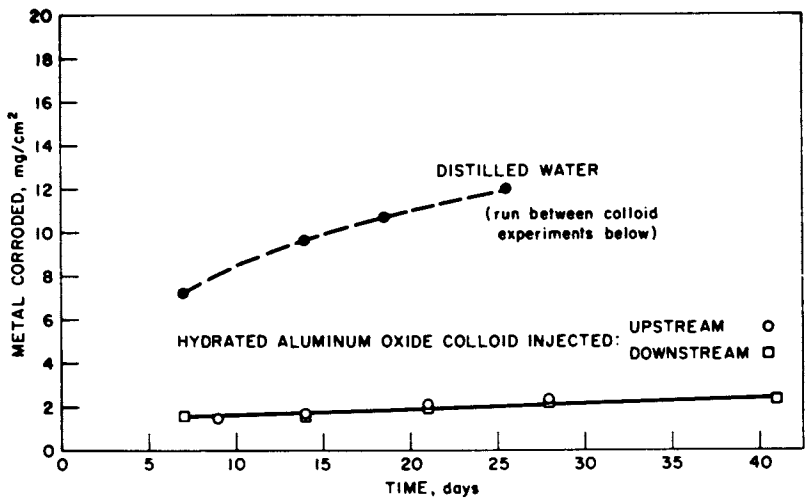

Argonne National Laboratory

Figure 49. Influence of 35-ppm colloid on the aqueous corrosion of 8001 aluminum at 260°C, 7 m/sec velocity (32)

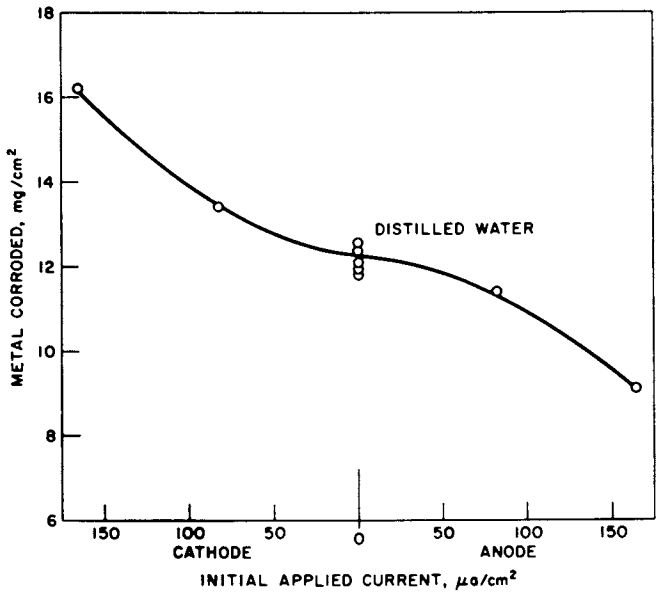

Figure 50. Effects of applied current on corrosion of 8001 aluminum at 260°C in flowing water, 5.6 m/sec (32)

Literature Cited

1. Vijh, A. K., J. Electrochem. Soc. (1972) 116, 972.
2. Tajima, S., Baba, N., and Shimura, F. M., Electrochimica Acta (1967) 12, 955.
3. Hauffe, Karl, "Oxidation of Metals," p. 419, Plenum Press, New York, New York, 1965.
4. Hart, R. K., "Morphology of Corundum Films on Aluminum," Fifth Int. Cong. for Electron Microscopy, Philadelphia, Pennsylvania, Aug. 29 - Sept. 5, 1962, Paper No. C-10, Academic Press, New York, New York, 1962.
5. Hart, R. K., and Maurin, J. K., "Growth of Oxide Nuclei on Iron," Sixth Int. Cong. for Electron Microscopy, Kyoto, Japan, Aug. 28 - Sept. 4, 1966, p. 539, Maruzen Co., Ltd., Tokyo, Japan, 1966.
6. Ruther, W. E., and Hart, R. K., Corrosion (1963) 19, 127t.
7. Frankenthal, R. P., and Malm, D. L., J. Electrochem. Soc. (1976) 123, 186.
8. Ruther, W. E., Schleuter, R. R., Lee, R. H., and Hart, R. K., Corrosion (1966) 22, 147.
9. Ruther, W. E., and Draley, J. E., unpublished work.
10. Draley, J. E., Ruther, W. E., and Greenberg, S., J. Nucl. Matl. (1962) 6, 157.
11. Draley, J. E., TID-7587, "Aqueous Corrosion of 1100 Aluminum and of Aluminum-Nickel Alloys," Int. Conf. on Aqueous Corrosion of Reactor Mat'ls., Brussels, Oct. 14-17, 1959, p. 165, U. S. Atomic Energy Commission and European Atomic Energy Society, July 1960.
12. Draley, J. E., Mori, S., and Loess, R., unpublished figure.
13. Mori, S., and Draley, J. E., J. Electrochem. Soc. (1967) 114, 352.
14. WAPD-MRP-107, "Pressurized Water Reactor (PWR) Project Technical Progress Report October 24, 1963-January 23, 1964," Westinghouse Atomic Power Div.
15. Griggs, B., Maffei, H. P., and Shannon, D. W., HW-67818, "Multiple Rate Transitions in the Aqueous Corrosion of Zircaloy," Hanford Laboratories, General Electric Company, December 20, 1960.
16. Draley, J. E., unpublished work.
17. Diggle, John W. (Ed.), "Oxides and Oxide Films," Vol. 1, p. 38, Marcel Dekker, Inc., New York, New York, 1972.
18. Draley, J. E., and Ruther, W. E., J. Electrochem. Soc. (1957) 104, 329.
19. Draley, J. E., and Mori, Shiro, and Loess, R. E., J. Electrochem. Soc. (1963) 110, 622.

In Corrosion Chemistry; Brubaker, G., et al.;
ACS Symposium Series; American Chemical Society: Washington, DC, 1979.

20. Youngdahl, C. A., and Loess, R. E., J. Electrochem. Soc. (1967) 114, 489.
21. Draley, J. E., and Ruther, W. E., Corrosion (1956) 12, 480t.
22. Draley, J. E., and Ruther, W. E., Corrosion (1956) 12, 441t.
23. Draley, J. E., and Ruther, W. E., ANL-5658 "Experiments in Corrosion Mechanism: Aluminum at High Temperatures," Argonne National Laboratory, April 1957.
24. Draley, J. E., and Ruther, W. E., "The Corrosion of Aluminum Alloys in High Temperature Water," IAEA Conf. Corrosion of Reactor Materials, Salzburg, June 1962, Vol. I, p. 477.
25. McWhirter, J. W., and Draley, J. E., ANL-4862 "Aqueous Corrosion of Uranium and Alloys: Survey of Project Literature," Argonne National Laboratory, May 14, 1952.
26. Mollison, W. A., English, G. C., and Nelson, F., CT-3055 "Corrosion of Tuballoy in Distilled Water," Argonne National Laboratory, June 23, 1945.
27. Greenberg, S., and Draley, J. E., unpublished figures.
28. Draley, J. E., Greenberg, S., and Ruther, W. E., J. Electrochem. Soc. (1960) 107, 732.
29. Parfenov, B. G., Gerasimov, V. V., and Venediktova, G. I., "Corrosion of Zirconium and Zirconium Alloys," Translated from Russian by Ch. Nisenbaum, Israel Program for Scientific Translations, Jerusalem, 1969.
30. Bradhurst, D. H., Draley, J. E., and Van Drunen, C. J., J. Electrochem. Soc. (1965) 112, 1171.
31. Mori, S. Loess, R. E., and Draley, J. E., Corrosion (1963) 19, 165t.
32. Draley, J. E., and Ruther, W. E., ANL-7227, "Corrosion of Aluminum Alloys by Flowing High Temperature Water," Argonne National Laboratory, January 1967.

Acknowledgement

This paper was prepared with the support of the U. S. Energy Research and Development Administration.

RECEIVED September 1, 1978.

The Role of Water in Atmospheric Corrosion

P. B. P. PHIPPS and D. W. RICE

IBM Corporation, San Jose, CA 95193

This paper is divided into three parts. The first part reviews several types of measurements which we have made on atmospheric corrosion. These are intended to provide a self-consistent set of data from which generalization can be made. Differences between atmospheric corrosion and dry oxidation become apparent. The dominant role played by relative humidity in aggravating atmospheric corrosion is remarkably widespread. This fact focuses our attention on the second part -- water adsorption. Experiments on water adsorption are described and, together with published data suggest important generalizations regarding the adsorbed aqueous medium. In the third part the data on atmospheric corrosion presented in part one is viewed from the perspective of the adsorbed aqueous phase of part two. Many observations received a direct explanation. The value and limitations of measurement techniques such as weight gain, ellipsometry, surface analysis, and bulk electrochemistry can be seen in perspective.

0-8412-0471-3/79/47-089-235$06.75/0

1.0 Observations on Atmospheric Corrosion

1.1 The Test Atmosphere. Measurements of the response of metals to the corrosive atmospheres which they must withstand in applications are of great practical value. In testing these responses we have two courses, field exposure and exposure to a synthetic test condition. Field exposure has several limitations. It is slow, the sample of the environment is very small and poorly defined. Laboratory testing solves these problems. It can be accelerated, and well defined. On the other hand it is not obvious that any single gas mixture can represent the response of many metals to varied field conditions. Certainly, the acceleration factors cannot be predicted without much prior knowledge of sensitivities to gas concentrations, and temperatures and the probability of finding these conditions. We have selected a test atmosphere by analyzing the statistics of those pollutants (1), which might cause corrosion. The test conditions, given in Table I, are characteristic of heavily polluted urban atmospheres. Attention has been given to measuring the corrosion by sensitive techniques rather than increasing the severity of the test to unreasonable extremes. We believe that the definition of this test is a prerequisite to rationalization of atmospheric corrosion responses.

1.2 Corrosion Response. The responses of metals to this test have been measured by several methods. A brief survey which follows forms a self-consistent basis of some generalizations on atmospheric corrosion. Unless stated otherwise, the examples will be of the corrosion of an alloy $Ni_{80}Fe_{20}$.

In some cases weight gain can be used to monitor attack. Figure 1 shows, for example, the rate of weight gain of a foil of $Ni_{80}Fe_{20}$ as a function of the sulfur dioxide level in our gas mixture with all other gases constant. This test was conducted at several relative humidities. It is striking that reducing the water vapor pressure by a factor of two reduces the rate of attack as much as reducing the sulfur dioxide pressure a factor of twenty. It is found that most of the effect of temperature on corrosion is described by the temperature dependence of water vapor pressure contained in the RH. This graph implies linear kinetics which are demonstrated in Figure 2. Here, the corrosion product thickness was measured by ellipsometry and weight change, and the composition was shown to be

In Corrosion Chemistry; Brubaker, G., et al.;
ACS Symposium Series; American Chemical Society: Washington, DC, 1979.

Table I Accelerated reference atmosphere test

T°C	25
H_2O	80% RH
NO_2	480 ppb
SO_2	310 ppb
O_3	170 ppb
H_2S	15 ppb
Cl_2	3 ppb

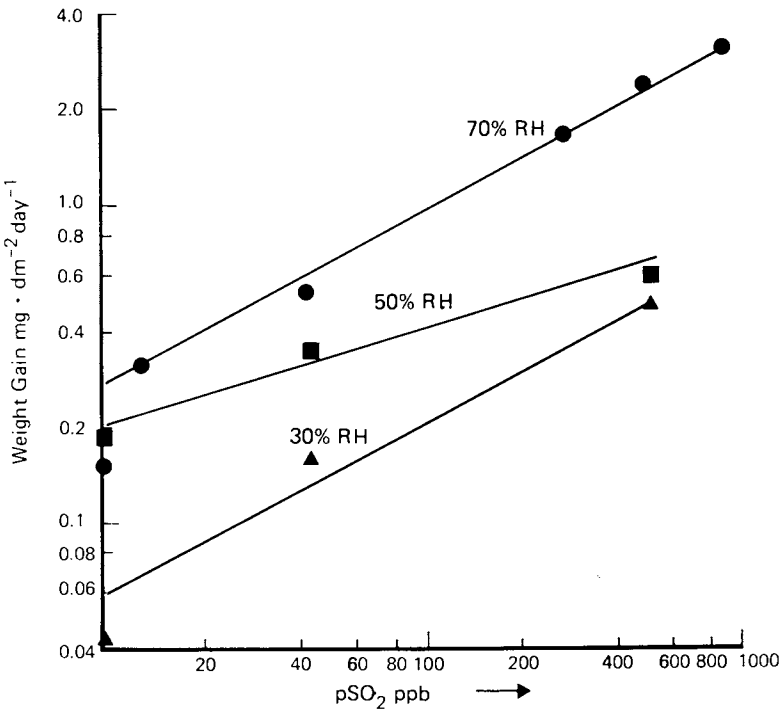

Figure 1. Weight gain of $Ni_{80}Fe_{20}$ foil as a function of pSO_2 and RH

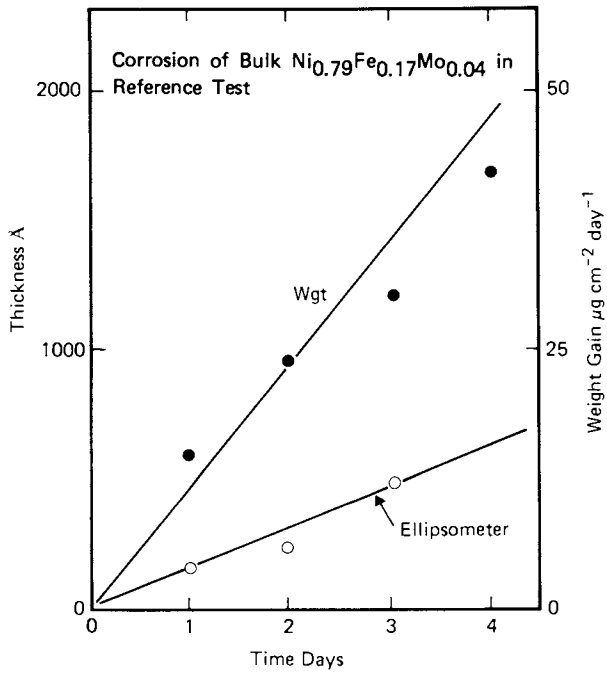

Figure 2. Kinetics of weight gain and corrosion-product thickness for $Ni_{80}Fe_{20}$

$(NiFe)SO_4 \cdot 6H_2O$ by xray diffraction. The two types of measurement can be compared by using published density and refractive index. We believe that the discrepancy between the two may be an error in the ellipsometry due to the serious roughening of the surface. In our experience atmospheric corrosion almost always leads to sufficient roughening to affect ellipsometric data. This roughening must be taken into account in any model of the corrosion process.

Direct measurement of roughening has proved to be a sensitive monitor of the corrosion of thin films. This is because the initial condition of vapor deposited or electroplated films can be very smooth. A semiquantitative measure of roughness is provided by the intensity of the light reflected by a sample examined under a microscope with dark field illumination. Data taken by this technique is shown in Figure 3. The pronounced dependence of attack on RH is very clear in this example. Roughening is much more severe at high RH than at low.

Chromium and aluminum are resistant to atmospheric corrosion individually but when porous chromium in intimate contact with aluminum is exposed to high humidities substantial corrosion occurs at the interface of the two materials. This is illustrated by the roughening data of Figure 4. Auger electron spectroscopy shows O, S, Cl -- all varying in quantity with RH (Figure 5). ESCA has shown SO_4^{2-}, SO_3^{2-}, and perhaps $S_2O_3^{2-}$. Infra red adsorption has enabled us to identify hydrated sulfate, nitrate, nitrite (Figure 6). Besides these reduced anions, highly oxidized species such as Co^{3+} have been detected.

1.3 Summary of Atmospheric Corrosion Data. From the raw data we can draw several salient points.

(i) Different measurements reveal different aspects of a complex phenomenon.

(ii) Several phases are often (3) present in real atmospheric corrosion products. A wide range of oxidation levels is present on samples at one time.

(iii) Structures containing dissimilar metals show galvanic interactions qualitatively like those seen in aqueous environments.

(iv) The rough morphology and the mixed products suggest that models of the rate-limiting steps will be more complex than those of, e.g., tarnishing. As is true of low temperature oxidation (2), kinetic studies of the rate of growth contain too few parameters to resolve these complexities. Mechanistic experiments must be designed.

In Corrosion Chemistry; Brubaker, G., et al.;
ACS Symposium Series; American Chemical Society: Washington, DC, 1979.

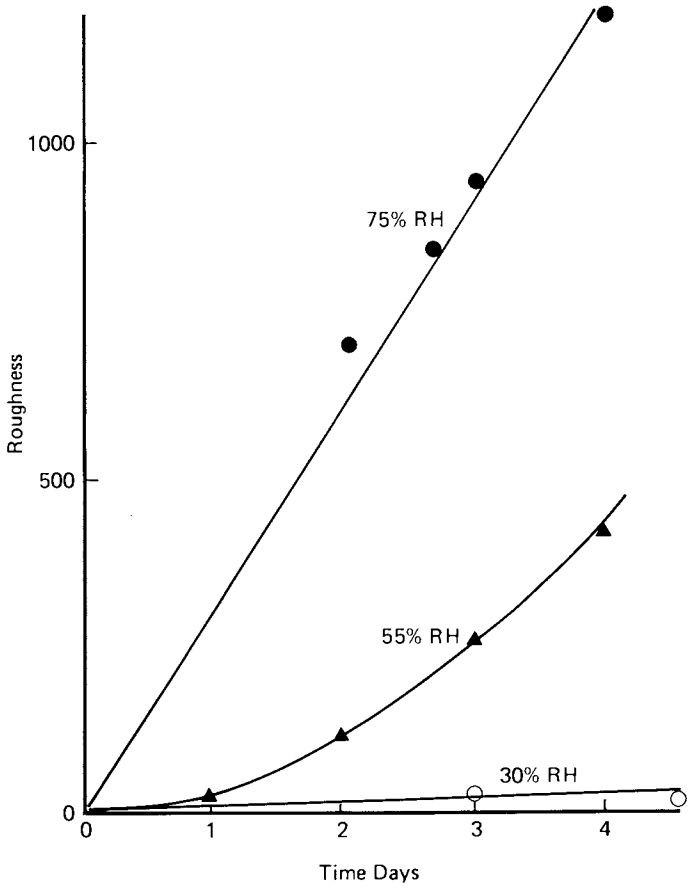

Figure 3. Roughening attributable to atmospheric corrosion measured by light scattering. Corrosion of plated NiFe films in reference test.

In Corrosion Chemistry; Brubaker, G., et al.;
ACS Symposium Series; American Chemical Society: Washington, DC, 1979.

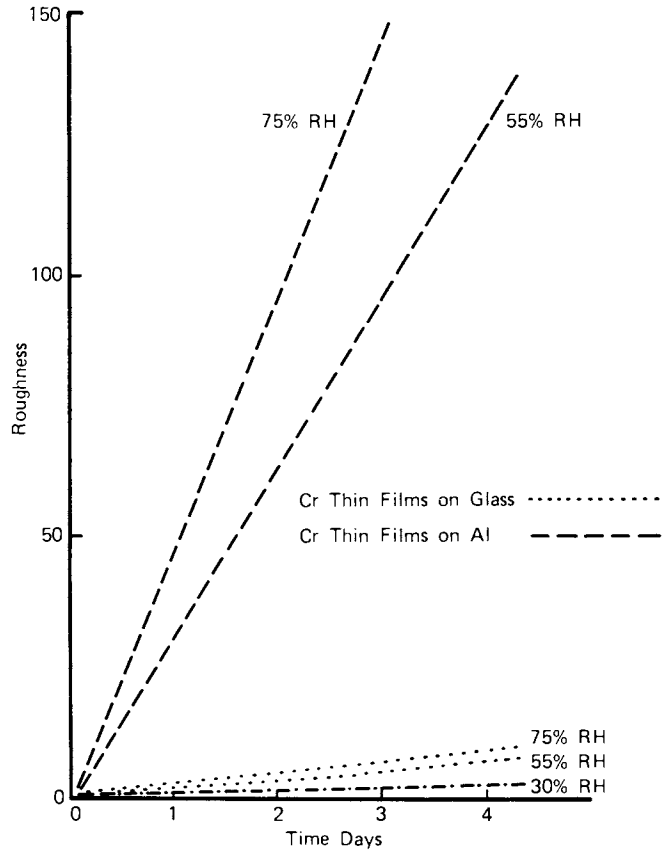

Figure 4. Galvanic corrosion of aluminum in contact with chromium

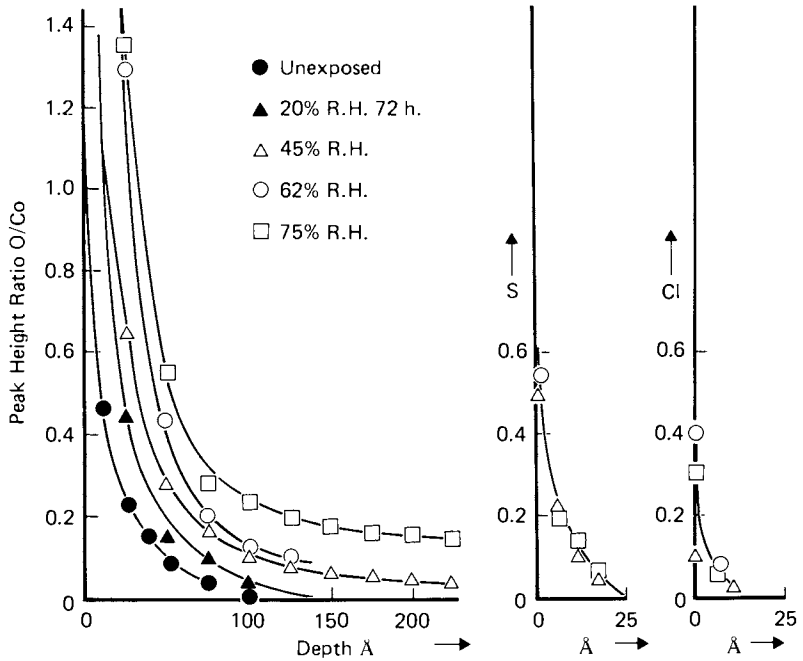

Figure 5. Auger electron spectroscopy of cobalt exposed to various atmospheres; cobalt corrosion

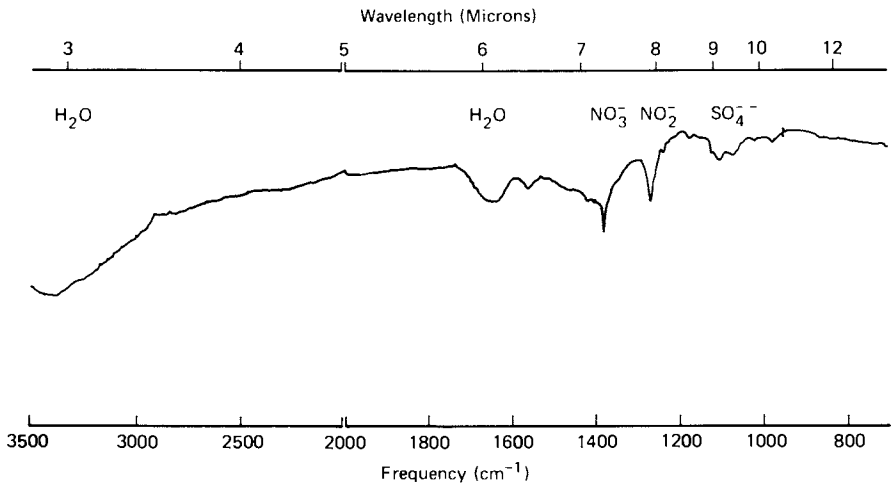

Figure 6. IR adsorption of corrosion products formed on NiFe in this "standard test atmosphere"

(v) RH is a dominant variable in many examples. Although the RH at which corrosion is negligible depends on the other gases present and the sensitivity of detection, different authors see the same trend. This is brought out by comparing some published "critical relative humidities" at which corrosion is minimal, see Table II. Several workers (4,5,6) have reported electrochemical currents between dissimilar metals, connected by adsorbed water. It is inferred that this current between particular metals at a single potential represents "the time of wetness", and this will be a measure of the amount of (galvanic) corrosion between heterogenities on a single metal or between any dissimilar metals exposed to the same atmosphere. This constitutes an extreme statement of the generality of RH as the controlling variable in many cases of atmospheric corrosion.

We might summarize that the RH is generally a dominant factor. For most metals, oxides are always present on the surface except at the bottom of growing pits, but no corrosion is detected below 15% RH and most metals do corrode above 75% RH regardless of the particular gas concentrations or species in the accelerated atmospheric test.

This focuses attention on the question of what is changing so dramatically when the RH changes a factor of five times. Clearly, the quantity of adsorbed water is increasing but, at 15% RH (3 mm at 25°C), a significant quantity of adsorbed water is present and at 75% RH, by definition, the equilibrium quantity cannot be so great that the water has bulk properties. (Bulk water would evaporate if the RH is less than 100%!) Water adsorption data on corroding metals surfaces is not available. Water adsorption comprises the subject of the second section of this paper.

2.0 Water Adsorption

Two types of water adsorption experiments are relevant to our analysis. As an example of one type, thin films of high purity aluminum, deposited at 10^{-9} torr, show changes in work function (7) and LEED pattern (8) and gain mass (9) due to exposure to 10^{-6} torr sec of H_2O. This data can be attributed to M-OH dipoles

In Corrosion Chemistry; Brubaker, G., et al.;
ACS Symposium Series; American Chemical Society: Washington, DC, 1979.

Table II Critical relative humidities

Metal	SO_2 ppm by Volume	Crit. RH %	Ref.
Fe	3000	75	1
	100	65	3
	200	85	5
	100	>90	5
	0.5	80	6
	0.1	80	7
Cu	3000	60	1
	100	63	2,3
	0.5	80	6
	0.1	90	7
	0.1	90	8
Ni	1000	70	2
Al	3000	82	1
	1000	52	4
	300	52	4
	0	85	4
	0.1	90	7

References

1. Sanyal, B. and Bhadwer, D., J. Sci. Ind. Res. India (1957) 18A, 69.
2. Vernon, W.H., Trans. Far. Soc. (1935) 31, 1668.
3. Vernon, W.H., J. Electrochem. Soc. (1933) 64, 31.
4. Aziz, P.M. and Godard, H.P., Corrosion (1959) 15, 39.
5. Skorchelletti, V.V. and Tukachinsky, S.E., J. App. Chem. USSR (1953) 26, 27, (1955) 28, 65.
6. Clarke, S.G. and Longhurst, E.E., J. Applied Chem. (1961) 11, 435.
7. Sydberger, T. and Vanneberg, N.G., Corr. Sci. (1972) 12, 775.
8. Duncan, J.R. and Spedding, D.J., Corr. Sci. (1973) 13, 993.

oriented on the surface. Similar results have been reported for cleaved Al (10), for Au (11), W (12), Pt (13), Fe (14). In a second type of experiment, powdered metal oxides with high catalytic activity and surface area are exposed to water and an adsorption isotherm is plotted. Infrared adsorption (15,16), NMR relaxation (17,18,19) or dielectric dispersion (20,21,22) may be measured on the substantial number of molecules adsorbed on the substantial area. Unfortunately, it is difficult to apply either of these fields of investigation to the elucidation of atmospheric corrosion.

The definition of the powder surfaces tends to be in terms of the process for making it (23). This limits interpretation of their properties and also limits generalization of properties to surfaces which have been generated by atmospheric corrosion. Conversely, the LEED, Auger electron spectroscopy, photo emission properties, etc., are measured on fresh surfaces in UHV, because interpretation is difficult for more complex configurations and because experience has shown that these properties are profoundly modified and confused by exposure to real atmospheres.

The experiment described below is an attempt to bridge this gap. Surfaces relevant to atmospheric corrosion were prepared from clean metal surfaces by reaction with water vapor under clean conditions. The properties measured -- water adsorption characteristics -- were selected because they were believed to have a major and direct application to atmospheric corrosion.

2.1 Water Adsorption Experiments. The objectives were to measure water adsorption isotherms on surfaces which were well defined in terms of their preparation and also relevant to atmospheric corrosion.

The quantity of water adsorbed on the appropriate metal surface was measured by means of a piezoelectric quartz microbalance (24). With suitably cut crystals and good temperature control, it was possible to measure adsorption corresponding to coverage by a fraction of a monolayer.

The sequence of operations leading to adsorption data described here can be followed by reference to Figure 7.

(i) A thermostated quartz crystal was coated with NiFe by electron beam evaporation in an oil-free system at a pressure of less than 10^{-8} torr, so that the rate of incidence of metal atoms was at least a thousand times that of other species.

In Corrosion Chemistry; Brubaker, G., et al.;
ACS Symposium Series; American Chemical Society: Washington, DC, 1979.

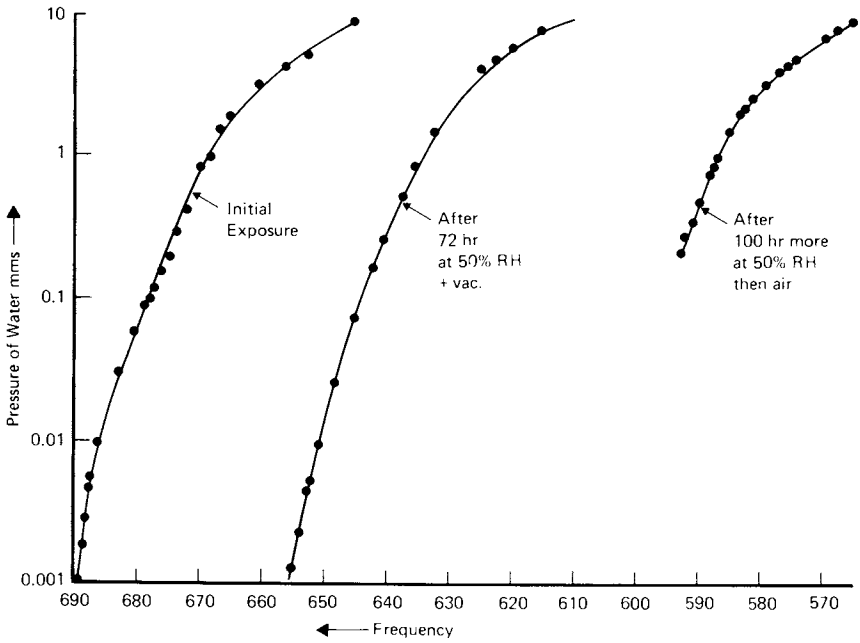

Figure 7. Mass changes as a function of water pressure; adsorption of water on $Ni_{80}Fe_{20}$ film at 25°C

(ii) The clean metal surface was now exposed to water vapor. This was obtained from water which had been repeatedly distilled in the UHV chamber. The pressure of water was determined by the temperature of this water. Total gas pressure in the vacuum system was monitored by an ion gauge, which was not operated continuously, and by a thermal conductivity gauge. After a brief transient the frequency of oscillations decreased to a steady value indicating that the mass of the quartz crystal surface had increased due to reaction with the water. An effect was observed for pressure as low as 10^{-6} torr.

(iii) The metal film was now exposed to a greater water vapor pressure and the adsorption was monitored until equilibrium was achieved. This procedure was repeated for progressively higher water vapor pressure up to ~ 10 torr.

(iv) The water vapor was pumped off to 10^{-7} torr, but the mass of the film did not revert to its original value, part of the adsorbed water could not be desorbed at this temperature and pressure.

(v) The water pressure was returned to 11 torr, and the film was left to equilibrate for 72 hours.

(vi) The water adsorption curve was now measured on the reacted surface. The irreversible adsorption which occurred during measurement was negligible compared with that which had taken place during this 72 hours of conditioning at the highest pressure. Reversible adsorption data was recorded. (It is interesting to note that a high pressure of hydrogen developed in the vacuum chamber -- as indicated by a gas with a very high thermal conductivity which could not be sorption pumped or cryopumped but could be removed by titanium sublimation. This was probably formed by reaction of the water vapor with the freshly deposited metal on the walls of the chamber.)

(vii) The film was now exposed to water vapor at 11 torr for a further 100 hours. The frequency decreased monotonically.

(viii) Dry air was introduced. The crystal showed that no mass change occurred. The adsorption curve was remeasured.

The equilibrium mass changes are plotted in Figure 8 on the basis of the BET model (25). From this model we derive the activation enthalpy for water adsorption and the area of the film. These

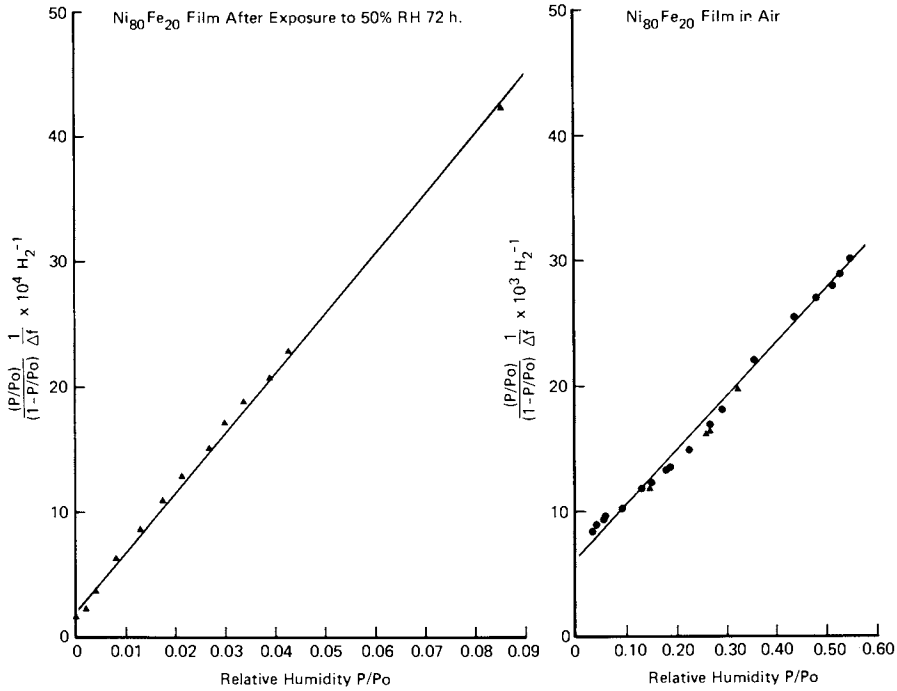

Figure 8. Adsorption isotherms plotted on the basis of the BET model

In Corrosion Chemistry; Brubaker, G., et al.;
ACS Symposium Series; American Chemical Society: Washington, DC, 1979.

parameters are shown in Table III as the ratio of the true area to the apparent area. The quantity of water adsorbed is plotted in units of layers of water on the basis of this analysis (Figure 9).

(ix) Finally, several metals were deposited on quartz crystals and the water adsorption was measured in laboratory air at controlled relative humidities.

These measurements were intended to represent a more practical degree of cleanliness than the surface prepared in UHV. Some data are shown in Figure 10 and 11, and results for a number of metals are shown in Table III which compares these measurements with published data.

2.2 Discussion. The clean film of metal reacts rapidly with water vapor at pressure above 10^{-6} torr to produce H_2 and in the order of a monolayer of metal hydroxide/oxide. (Evidence on the nature of this reaction product is reviewed below.) The reaction is effectively irreversible. The frequency transient observed when the metal was first exposed is probably due to a thermal gradient in the quartz associated with this rapid highly exothermic reaction. Subsequent water is adsorbed (reversibly) on top of this reaction product (~ 1 monolayer at 25% RH, ~ 2 at 50% RH). This adsorbed water reacts with the substrate metal much more slowly than the initial reaction. (One monolayer reacting in sixty hours at 10 torr H_2O.) Dramatic reductions in reaction rate after the formation of the first monolayer have been reported from observations in solution (26). It has been shown that water is necessary for this passivation of nickel (27). As the compound film grows thicker, the activation energy for water adsorption does not change but the area increases. This is consistent with the linear growth rate. Reaction rate is limited by the monolayer. This is constantly, but slowly, regenerated. The quantity of adsorbed water increases with time at constant RH because the area of porous hydroxide increases with time. The newly generated surface is a relatively clean (reproducible) adsorbent (perhaps this accounts for the similar adsorption on films exposed to laboratory air and those prepared in an ultraclean environment).

We turn now to discuss first the evidence on the nature of the adsorbing surface, then the properties of the adsorbed aqueous phase. This leads us to a model for atmospheric corrosion.

In Corrosion Chemistry; Brubaker, G., et al.;
ACS Symposium Series; American Chemical Society: Washington, DC, 1979.

Table III Water adsorption parameters

Heats of Adsorption of Water at High Coverage			
Adsorbent	Isosteric Heat kcals/mole	Roughness BET	Ref.
Au	11.84	2.5	1,2
	12	6	3
	11.5	10	4
Fe	11.72	3	2
	13.2	2	3
Co	11.7	2.9	2
Ni	11.76		2
Pt	10.1-12.4		6
	11.3 13.3		8
Sn	12.75		5
Ni Fe	12.44	3.5	1
	11.74	5.4	2
Fe Cr	11.73	4	2
Fe Ni Cr	13	2.2	5
Al O OH	12±0.5		7
Fe_2O_3	12.8		9
Ni O	11.6		10

References

1. This work, UHV.
2. This work, air exposed.
3. Bowder, F.P. and Throssel, W.R., Proc. Roy. Soc. (1951) A209, 297.
4. Thomas, J.H.,III and Sharma, S.P., J. Vac. Sci. Tech. (1976) 13, 549.
5. Armbruster, M.H., J. Am. Chem. Soc. (1966) 68, 1342.
6. Allen, K.W., J. Chem Soc. A (1971), 3028.
7. Garner, R.L., Thesis Texas Tech. Coll. (1965).
8. Cole, H.D.F., Thesis University of Texas (1964).
9. Zettlemoyer, A.C. and McCafferty, E., Z Phys. Chem. NF (1969) 64, 41.
10. Cronin, C.L., Thesis Lehigh University (1976).

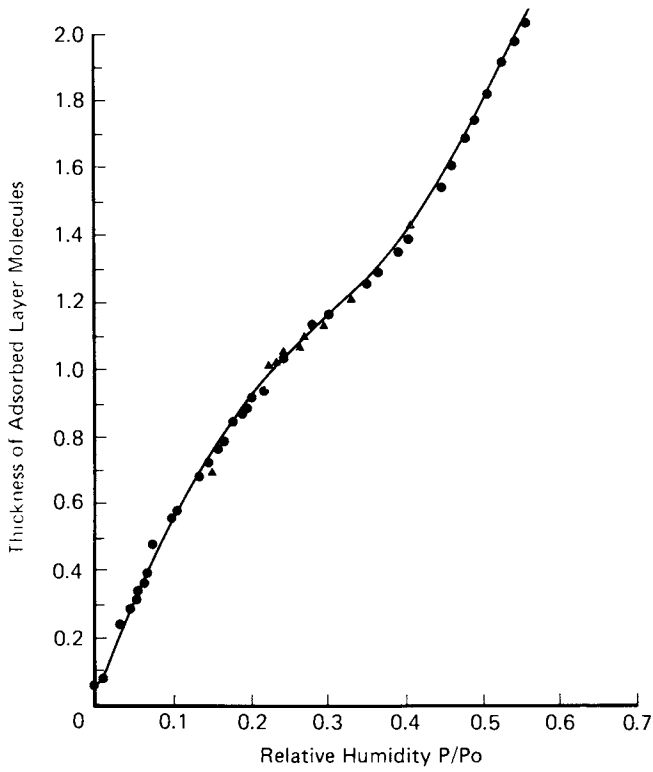

Figure 9. Water adsorption in monolayers on Permalloy in air

In Corrosion Chemistry; Brubaker, G., et al.;
ACS Symposium Series; American Chemical Society: Washington, DC, 1979.

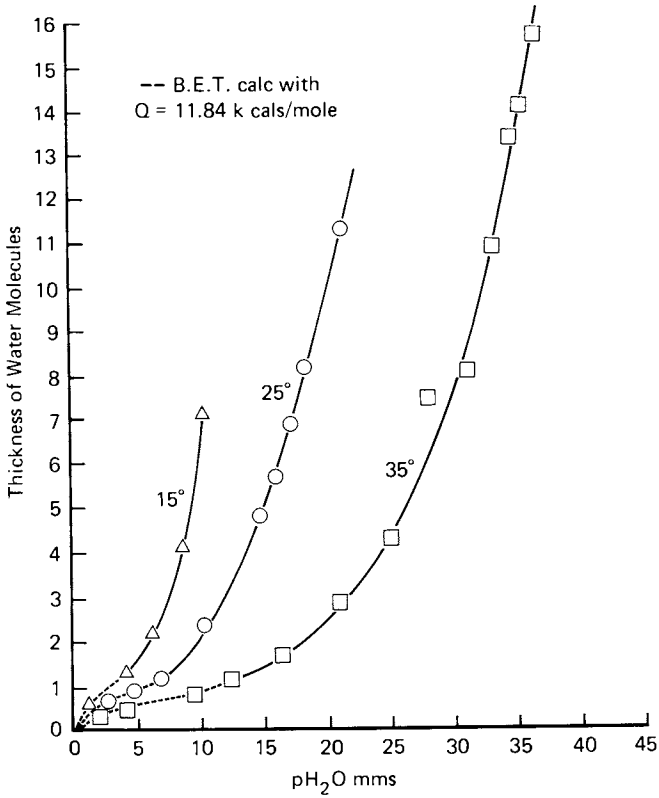

Figure 10. Water adsorption on gold film

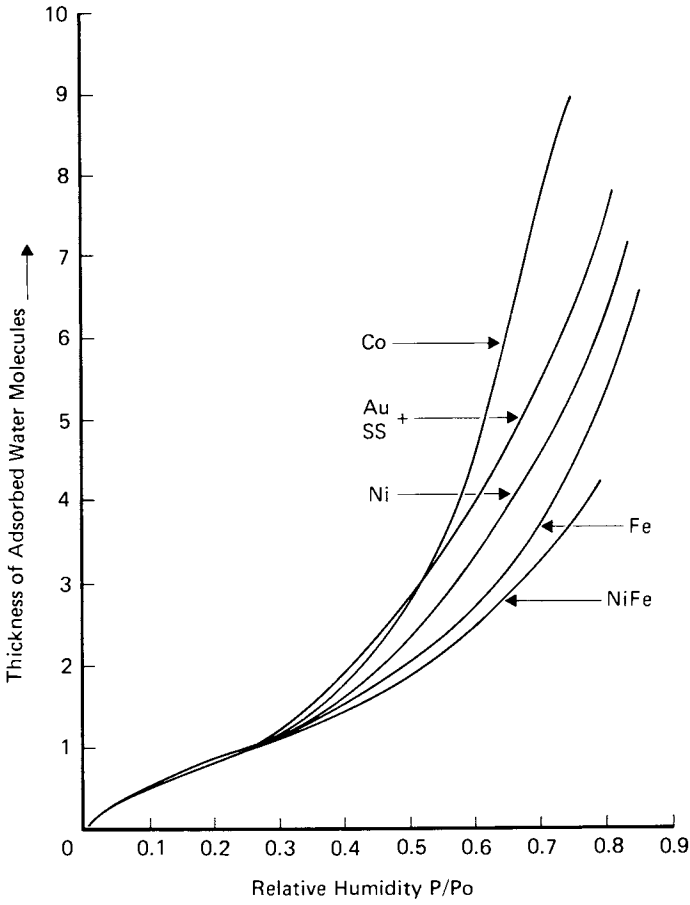

Figure 11. Water adsorption on several metals exposed to air

In Corrosion Chemistry; Brubaker, G., et al.;
ACS Symposium Series; American Chemical Society: Washington, DC, 1979.

2.3 The Solid Adsorbent. In characterizing the layer on which adsorption of water takes place reversibly, we make the following observations:

(i) The initial reaction of a clean metal surface with water vapor is effectively irreversible and involves dissociation. This is supported by the evolution of hydrogen, the rapid exothermic reaction, and published data for several metals (7,8,9,10,11).

(ii) The initial reaction product protects the metal from further attack. By the word "protect," we are contrasting the rate of formation of the initial irreversibly bound layer within ~ 10^{-4} torr seconds with the subsequent growth of an irreversibly bound monolayer in ~ 60 hours at 11 torr = 2.5 x 10^6 torr seconds. Auger electron spectroscopy (14 and 16) has shown that a layer which can be represented as Fe O OH protects iron from further attack. Direct evidence of hydrogen being present in the passive film formed in solution was provided by mass spectrometry (30). Electron diffraction (28,29) has shown that the protective surface layers which form on iron which has been air oxidized or passivated in solution are surprisingly similar. The structures are based on the cubic close packed oxygen lattice of γ Fe O OH, or Fe_3O_4.

The details of the processes by which particular monolayers limit the kinetics of metal oxidation and "oxide" dissolution have been the subject of much investigation. (See references on passivity, (26 and 28).) We do not attempt to review or develop these studies here, but to establish a connection between atmospheric corrosion and the relatively well studied disciplines of aqueous corrosion and dry oxidation.

(iii) The critical interaction which binds water when it is ostensibly adsorbed on a corroding metal is the interaction with an oxide or oxyhydroxide. The observation of similar adsorption characteristics on many metals (after the initial irreversible reaction) and on many oxides supports this (Table III). The generalization is reinforced by the observation that if exposure is prolonged the area of the adsorbent increases, but the other characteristics do not change. Apparently, the growing layer is relatively porous, and the protection is probably due to the layer adjacent to the metal. This follows from the increasing area and the constant rate of growth.

In Corrosion Chemistry; Brubaker, G., et al.;
ACS Symposium Series; American Chemical Society: Washington, DC, 1979.

This discussion of the solid phase on which the water is adsorbed has brought us to a conclusion which is important for our subsequent examination of the aqueous adsorbed phase. The water which is not (irreversibly) decomposed is adsorbed on an oxyhydroxide whose exact nature has only a minor effect on the adsorption phenomena. There is substantial literature on the properties of adsorbents on this type of surface. A review of this literature allows us to propose the following generalizations concerning the aqueous phase in atmospheric corrosion.

2.4 The Aqueous Adsorbate. The aqueous phase acts as (i) solvent, (ii) dielectric and (iii) transport vehicle and will be discussed under these three topics.

(i) The solvation of gas, metal ions, protons and hydroxide is of major importance in atmospheric corrosion but relevent data is scarce and theories which might support extrapolation from other measurements are difficult to apply to solutions in adsorbed water.

Consideration of the parameters of the gases given below

Gases	H_2O	NO_2	SO_2	HCl	O_2
B P °K	373	294	263	188	90
Heat of evap. H_v kcal/mole	10.5	5.1	6	3.8	3.2
Pressure in air atmospheres	10^{-2}	10^{-7}	10^{-7}	10^{-9}	10^{-1}

shows that, generally, water will be adsorbed multilayers and other gases, if there were no water, to fractions of monolayers. (In the BET model the heat of adsorption of layers after the first is equal to H_v.) Expressions have been developed to describe the adsorption of mixed gases on the basis of the BET or Langmuir models (31). If the gases interact little, the observations can be fitted to the theory, e.g., N_2, and O_2 on TiO_2 (32); but with greater interaction, e.g., C_2H_6 and CO_2 on Cr_2O_3 (33) agreement is poor. The layer

In Corrosion Chemistry; Brubaker, G., et al.;
ACS Symposium Series; American Chemical Society: Washington, DC, 1979.

dipoles, the ambidentate character of SO_3^{-2} and NO_3^-, and the strong interaction with bulk H_2O lead us to doubt the use of these adsorption models. Although detailed treatments of interactions and of aqueous solubility have been given, they require more knowledge of the solvent properties than is available for adsorbed water on oxide.

It is proposed that a qualitative account can be rationalized on the basis of the strength of the interactions between solvent, solute, and adsorbent. As an example of weak interactions, the coverage of nitrogen on argon on titanium dioxide is reduced by ~ 0.2 layers if one layer of water is adsorbed and a further 0.1 layer if four layers of water are adsorbed (34). The isotherm after four layers of water proves to be very similar to that of nitrogen on ice (35). This additive behavior resembles Raoult's law with positive deviations. The water-water and water-oxide interactions, being stronger than the argon-oxide or argon-argon or argon-water, the argon pressure is raised over that of an ideal solution, i.e., the quantity of argon adsorbed is reduced at a given pressure. The more polarizable xenon and krypton have been reported to form clathrates with adsorbed ice (36). An example of a strongly interactive system may be taken from the literature of catalysis. Water adsorbed on silica (or alumina) behaves as a Bronsted acid (37) and can be titrated with ammonia. The concentrations of adsorbed ammonia and ammonium can be measured spectroscopically (38).

(ii) Dielectric properties of adsorbed water - The solvation of gases, metal ions, protons and hydroxide ions is crucial in electrochemical corrosion. The details of the hydration sheath in these adsorbed layers cannot be given, but a microscopic parameter is provided by measurements of the dielectric constant of adsorbed layers. The dielectric constant dispersion of adsorbed water has been measured on several oxide powders (20,21,23). It appears that the first layer is relatively unpolarizable and the dielectric constant in the order of three but, with an average of only two layers, the dielectric constant was in the order of thirty for a frequency of 100 Hz. The characteristic frequency is ~ 1 kHz. Evidence indicates clusters of water being heterogeneously distributed. As the thickness increases beyond three layers, the characteristic frequency approaches that of ice, suggesting a development of hydrogen bonding between water molecules.

In Corrosion Chemistry; Brubaker, G., et al.;
ACS Symposium Series; American Chemical Society: Washington, DC, 1979.

Measurements of the DC conductivity have been interpreted to suggest that the dielectric constant increases with thickness and the dissociation energy falls from 0.6 eV towards that seen in the bulk 0.35 eV (39,40).

(iii) Mobility - The first layer of water is relatively immobile. The direct measurement of viscosity in thin layers has been the subject of some controversy, but rheological abnormalities (if any) do not extend beyond a few molecular diameters (41,42). NMR measurements have shown that monolayers of water are oriented on silicate and silica gel (17,18). Reduced diffusion in these layers is shown by pulsed spin echo NMR (19) and by neutron scattering (43).

Infrared adsorption frequencies and line broadening (15,16) have been interpreted to show that water is bound O downwards to the HO M. The lifetime, and population, of aggregates and hydration sheaths is strongly affected by the rotational freedom of the water molecules. In bulk water this is restricted by hydrogen bond breaking. In adsorbed layers the interaction with the adsorbate dominates reorientation for all molecules within six to ten molecular diameters.

2.5 Summary of Water Adsorption. The discussion of the adsorbed aqueous phase has been drawn from many fields and recapitulation may be helpful. Most metals adsorb a monolayer of water rapidly and "irreversibly."

This initial layer reacts slowly in many cases. Subsequent water adsorption is similar for many metals and oxides. At 20% RH there will be ~ one monolayer, and at 75% ~ five layers. Corrosive gases will not form multimolecular layers, but compete with water for the first "irreversible" layer. The "solution" of gas will be very dilute. There is ample evidence for strong interactions between adsorbed water and other adsorbed gases, but a quantitative model is not available. The solution and ionization within thin adsorbed layers will depart strongly from that in bulk water. This may be seen from the variation of dielectric constant with thickness of adsorbed water. A monolayer has a dielectric constant in the order of three, but at 50% RH we have two or three layers with a mean dielectric constant in the order of twenty five -- a medium like methanol. Ionic mobility will be possible in this layer, but mobilities may be an order of magnitude less than those in bulk solution.

In Corrosion Chemistry; Brubaker, G., et al.;
ACS Symposium Series; American Chemical Society: Washington, DC, 1979.

We now return to discuss the observations of atmospheric corrosion described in the first part of this paper in terms of the models of the adsorbed phase developed in the previous sections.

3.0 The Role of Water in Atmospheric Corrosion

3.1 General Observations. We saw that water vapor plays a dominant role in many atmospheric corrosion processes (Figures 1,3,5), and that there is an implicit observation that the temperature dependence of corrosion may be approximately represented by the vapor pressure of water (i.e., RH is the rational variable). These observations are consistent with the adsorption model with high rates of galvanic corrosion occuring in thick layers of water and only slower oxidation occuring in the regime of RH at which monolayer coverage occurs. The similar dependence on RH for several metals and for several reactants is also consistent with adsorption on similar oxyhydroxide layers even though the area tends to increase. The simultaneous presence of several oxidation products in porous layers (Figures 5 and 6) is consistent with the inhomogeneous galvanic reactions. The process is different from the gradation of stoichiometry necessarily present in adherent protective layers. Deliquescence of the products is expected to affect corrosion rates and their dependence on RH considerably (4,5,10,44), the water thickness being greatly increased.

3.2 Intermediate RH. At intermediate RH, ~ 40%, weight changes are minor but roughening is seen (Figure 3) and sensitive surface chemistry shows that thin layers of corrosion products can be detected (Figure 4 and 5). This roughening may be associated with the fact that adsorption shows clustering even on homogeneous surfaces, and practical surfaces are certainly inhomogeneous with respect to adsorption. The preferred sites for attack may be related to the specific adsorption sites described for SO_2 (45,46) and H_2S (47); they may be sites where the water adsorption is favored; or they may be sites at which the oxide is weak. Once corrosion is initiated, deliquescent corrosion products may aggravate local attack (see below).

3.3 Low RH. At those sites, and for those conditions, in which the average thickness is in the order of one molecule, the dielectric constant is low and hydration of ions H^+, OH^-, O_2^-, M^{n+}, SO_3^{2-}, etc., is

In Corrosion Chemistry; Brubaker, G., et al.;
ACS Symposium Series; American Chemical Society: Washington, DC, 1979.

energetically unfavorable. (Atmospheric corrosion monitors based on recording galvanic currents record a time of dryness, i.e., no corrosion for these times of localized attack.) Metals may be consumed also by mechanisms which resemble tarnishing (Figure 5)(48). It is proposed that reaction rates are not limited by diffusion across the monolayer since it is so thin, since it does not prevent rapid reaction when the adsorbed layer is thicker, and since similar viscinal layers do not prevent rapid reactions at electrode surfaces in bulk electrolytes.

3.4 High RH. At relative humidities for which the water is more than three molecules thick (~ 65% for many cases), water approaches the behavior of bulk solutions. This is certainly true for films ~ 100 microns thick due to the presence of dirt, or deliquescent corrosion products (4,5,15,44,49). Corrosion in this regime may be related to that in bulk electrolytes and similar apparatus may be employed to study it (44). This is the threshold of critical RH, beyond which substantial weight changes are reported and time of wetness monitors indicate substantial corrosion. Below this threshold, weight loss is minor although optical surfaces may be degraded.

3.5 Conclusion. Although much is not known, and quantitative data is scarce, we conclude that a model of the adsorbed aqueous phase provides a perspective on observations made in many different aspects of atmospheric corrosion. The parameter which we have used as a rational gauge of this data in the thickness of the water adsorbed on the oxyhydroxide surface. This must be recognized as a crude beginning, but it is hoped that the model exposes questions which need to be addressed before details of atmospheric corrosion can be understood. Such work will supplement the relatively large number of studies on the protection afforded by particular solid phases.

Acknowledgements

The assistance of C. Breen, V.J. Gupta, and R. Tremoureaux is acknowledged with thanks.

Literature Cited

1. EPA Publication AP-42, U.S. GPO., Wash., D.C., 1973. R.I. Larsen J. Air Pollution Control Association (1976) 26, 325.
2. Ritchie, I.M., "Chemisorption and Reactions on Metal Films," ed Anderson, J.R., Academic Press, 1971.
3. Pourbaix, M., de Miranda, L.R., Cebelcor Rapp. Tech. 227 (1975).
4. Tomashov, N.D., "Theory of Corrosion and Protection of Metals," MacMillan, N.Y. (1966).
5. Sereda, P.J., ASTM (1958), 53 (Bull. No. 228), (1959) 61 (No. 238), (1960) 47 (No. 246), (1968) 326 (No. 435).
6. Mansfeld, F. and Kenkel, J.V., Corros. Sci. 16, 111 (1976).
7. Huber, E.E. Jr. and Kirk, C.T. Jr., Surface Sci. (1966) 5, 447.
8. Jona, F., J. Phys. Chem. Solids (1967) 28, 2155.
9. Krueger, W.H. and Pollack, S.R., Surface Sci. (1972) 30, 263, 280.
10. Tomlinson Fort, Jr. and Wells, R.L., Surface Sci. (1972) 32, 543.
11. Ibid., p. 554.
12. Waclawski, B.J. and Hughey, L.R., Surface Sci.(1970) 19, 464.
13. Bowden, F.P. and Throssell, W.R., Proc. Roy. Soc. (1951) 209, 297.
14. Roberts, M.W. and Wood, P.R., J. Electron Spectrosc. Relat. Phenom., (1977) 11, 431.
15. Klier, K., Shen, J.H. and Zettlemoyer, A.C., J. Phys. Chem. (1973) 77, 1458.
16. Klier, K. and Zettlemoyer, A.C., J. Colloid Interface Sci.(1977) 58, 216.
17. Woessner, D.E. and Snowden, B.S., J. Phys. Chem. (1963) 67, 1590.
18. Ibid., J. Chem. Phys. (1969) 50, 1516.
19. Bass, B.D. and Stejskal, E.O., J Colloid Interface Sci.(1968) 26, 271.
20. McCafferty, E., Pravdic, V. and Zettlemoyer, A.C., Trans. Far. Soc. (1970) 66, 1720.
21. Thorp, J.M., Ibid., p. 1721.
22. Jonscher, A.K., Shahidi, M. and Hasted, J.B., Nature (1975) 258, 595.
23. Sing, K.S.W., Colloques Internationaux du CNRS (1971) 201, 601.
24. Stockbridge, C.O. and Warner, A.W., "Vacuum Microbalance Technique" Vol 2, p. 71, ed R.F. Walker Plenum Press (1962)
25. Brunauer, S., Emmett, P.H. and Teller, E., J. Am. Chem. Soc. (1938) 60, 309.

In Corrosion Chemistry; Brubaker, G., et al.;
ACS Symposium Series; American Chemical Society: Washington, DC, 1979.

26. Brusic, V., this volume.
27. Schwabe, K. and Schmidt, W., Corros. Sci. (1970) 10, 143.
28. Cohen, M., this volume.
29. Foley, C.L., Kruger, J. and Bechtoldt, C.J., J. Electrochem. Soc. (1967) 114, 994.
30. Yolken, H.T., Kruger, J. and Calvert, J.P., Corros. Sci. (1968) 8, 103.
31. Hill, T.L., J. Chem. Phys. (1946) 14, 268.
32. White, L., et al, J. Am. Chem. Soc. (1949) 71, 2593.
33. Ibid., J. Am. Chem. Soc. (1952) 74, 5796.
34. Kwan, T., Freeman, M.P. and Halsey, G.D., J. Phys. Chem. (1955) 59, 600.
35. Adamson, A.W. and Dormant, L.M., J. Am. Chem. Soc. (1966) 88, 2055.
36. Barrer, R.M. and Ruzicka, D.J., Trans. Far. Soc. (1962) 58, 2262.
37. Fripiat, J.J., et al, J. Phys. Chem. (1965) 69, 3294.
38. Basila, M.R. and Kantner, T.R., J. Phys. Chem. (1967) 71, 467.
39. Anderson, J.H. and Parks, G.A., J. Phys. Chem. (1968) 72, 3662.
40. Kawasaki, K. and Hackerman, N., Surface Sci. (1968) 10, 299.
41. Hayward., A.T.J. and Isdale, J.D., J. Phys. D. (1969) 2, 251.
42. Lyklema, J., J. Colloid Interface Sci. (1977) 58, 242.
43. Olejnik, S., Stirling, G.C. and White, J.W., Disc Far. Soc. (1970) 1, 187.
44. Rosenfeld, I.L., "The Atmospheric Corrosion of Metals," NACE, Houston, TX. (1972).
45. Duncan, J.R. and Spedding, D.J., Corros. Sci. (1973) 13, 993.
46. Ibid., (1974) 14, 607.
47. Ibid., (1977) 17, 173.
48. Kroger, F.A., "The Chemistry of Imperfect Crystals," North Holland-American Elserier, New York (1974).
49. Takehara, Z., Saito, A. and Yoshizawa, S., Corros. Sci. (1976) 16, 91.

RECEIVED September 1, 1978.

9

Corrosion Inhibition and Inhibitors

RUDOLF H. HAUSLER

Gordon Lab, Inc., 925 Patton Rd., P.O. Box 605, Great Bend, KS 67580

An Educational Lecture or Paper on Corrosion Inhibition could easily develop into an ambitious undertaking if it were intended to review the vast literature concerned with the chemistry of Corrosion Inhibitors and the multitude of mechanisms proposed as explanations of their action. The past approaches aimed at understanding Corrosion Inhibition have been many, ranging from phenomenological screening of chemical compounds in a given environment to detailed electrochemical adsorption studies. Let me state that the ultimate purpose of inhibitor studies ought to be the development of predictive criteria for inhibitor effectiveness rather than the mere explanation of experimental results or speculation about possible mechanisms. While such predictive criteria have been developed in a few cases it appears that most mechanistic studies have merely contributed to speculative guide lines helpful in the unraveling process of inhibitor action, but have been far from successful in providing a complete understanding of practical inhibition phenomena let alone predictive criteria for more effective molecules.

The reason for this state of affairs may be seen in past emphasis on surface phenomenological studies which attempted to model the metal surface as an array of surface atoms with some valences saturated by subsurface metal atoms and other valences saturated by ions or molecules making up the environment. This model led to the description of the interface in terms of the Helmholz and Guy-Chapman double layer theories, and inhibitors were visualized as interfering with the double layer structure through adsorption on the surface atoms of the metal, thereby altering the electrochemical reaction rates which are governed by the energetics of the double layer. While this model has been

0-8412-0471-3/79/47-089-262$13.85/0

quite successful in explaining changes of electrochemical reaction rates as a consequence of changes occurring in the composition of the electrolyte it has not been successful in describing typical practical inhibition phenomena.

A rather large body of evidence has been accumulated over the past 10 to 15 years indicating that the chemistry of the interphase between the metal per se and the homogeneous bulk of the electrolyte may determine the kinetics of the corrosion process. This interphase must be visualized as being distinctly different in composition from either the metal or the electrolyte and extending from microscopic to perhaps even macroscopic dimensions. As a consequence the overall kinetics of the corrosion process are determined by a complex interplay between the reaction rates at the two interfaces made up by the boundaries of the interphase and transport phenomena in the interphase itself.

If the corrosion process is modeled in this manner, then the corrosion inhibition phenomena must be seen as:

a) the interaction of a chemical substance with the outer surface of the interphase;
b) an interaction with the interphase itself thereby changing its chemical nature;
c) or the formation of a new interphase.

The following discussion will therefore make but a weak attempt to review past approaches to inhibition theory. Rather, emphasis will be placed on the interphase concept. It is hoped that the reader will thus be offered a short introduction to corrosion inhibition as well as being stimulated to further investigative efforts in the field of corrosion inhibition.

The Corrosion Mechanism

Corrosion inhibition is generally described as the interference of a substance foreign to the corrosive medium with the corrosion reaction or reactions, and it is visualized that such interference takes place through the adsorption of the inhibitor on the metal surface. While this concept has been successful in many idealized situations, such as the corrosion of iron in hydrochloric acid (1) its application has been far too general and too prolific in order to advance the understanding of corrosion inhibition in any significant way.

It may therefore be helpful to discuss briefly a kinetic model of the corrosion process itself and then derive from it the various ways in which inhibition can

In Corrosion Chemistry; Brubaker, G., et al.;
ACS Symposium Series; American Chemical Society: Washington, DC, 1979.

take place. This appears all the more necessary as corrosion after more than 50 years of intensive research is still considered in many textbooks to be a purely chemical process, while only special limiting cases such as galvanic corrosion and perhaps pitting are recognized as electrochemical in nature.

Let us emphasize from the beginning that all corrosion (the oxidative conversion of a metal to its metal ions) is electrochemical in nature. This implies the existence of simultaneous anodic and cathodic currents of equal magnitude across the interface of the metal. It is by no means necessary (although sometimes useful), to postulate permanent localized anodes and cathodes as a microscopic concept with fixed space coordinates in order to develop a kinetic model applicable to the rates of the corrosion processes. The corrosion reactions, that is, the anodic oxidation of the metal and the cathodic depolarization by an oxidant, may indeed take place with statistical distribution in time and space on the surface of the metal. The proof of this thesis was given by Wagner and Traud (2) in 1938 by means of the discussion of the limiting case of zinc amalgam dissolution. Liquid zinc amalgam must be considered a completely homogeneous phase where it is impossible to define, in a rigorous thermodynamic sense, local galvanic elements on the surface. The dissolution of zinc amalgam in dilute hydrochloric acid could therefore proceed by a chemical mechanism as shown in equations 1 and 2:

$$Zn + 2H^+ \longrightarrow \{Zn\ H_2\}^{2+} \qquad (1)$$

$$\{Zn\ H_2\}^{2+} \longrightarrow Zn^{+2} + H_2 \qquad (2)$$

This model visualizes that zinc atoms on the surface of the amalgam form a transition complex with two protons which subsequently dissociates into zinc ions and hydrogen. If this mechanism were to prevail, the rate of hydrogen evolution (or oxidation of zinc) would have to depend on the concentration of the transition complex if the second reaction were rate determining, or on the product of the concentrations of zinc and the protons if the first reaction were rate determining. Wagner and Traud, however, have shown that the rate of the hydrogen evolution on a mercury surface is independent of small concentrations of zinc and can therefore be determined electrochemically on a pure mercury electrode. Conversely, the oxidation of zinc from zinc amalgam is essentially independent of the pH and can be measured at high pH without interfering hydrogen evolution. One can therefore determine these two rates

In Corrosion Chemistry; Brubaker, G., et al.;
ACS Symposium Series; American Chemical Society: Washington, DC, 1979.

over a wide potential range and in the case of the hydrogen evolution for different pH's. Since in the "corrosion" of zinc amalgam the oxidation of the zinc and the evolution of hydrogen have to proceed at the same rate in order to preserve the laws of electroneutrality in the system, one can now use the above determined rate characteristics for the two reactions in order to predict the rest potential of corroding zinc amalgam, and to determine its corrosion rate. The result can then be verified independently by determining the rate of hydrogen evolution from zinc amalgam volumetrically and by also analyzing for zinc in the resulting solution. These experiments have indeed been successful and are considered sufficient proof for the postulate of the electrochemical mechanism for the dissolution of zinc amalgam in dilute hydrochloric acid, as shown by equations 3 and 4, where the anodic and cathodic reactions proceed essentially independent from each other. For a more detailed discussion of the dissolution of zinc amalgam the reader is referred to the original literature or a discussion by H. Kaesche (3).

$$Zn \longrightarrow Zn^{+2} + 2e \qquad (3)$$

$$2H^{+} \longrightarrow H_2 - 2e \qquad (4)$$

This verification of the electrochemical nature of the corrosion process also leads to the realization of four distinct and separate basic processes involved in corrosion, which are linked together merely by the necessity of preserving electroneutrality in the overall reaction. These are

a) the anodic or oxidative process;
b) the cathodic or reductive process;
c) the electronic charge transfer process in both directions across the interface;
d) the ionic charge transfer process which is required to maintain electroneutrality on the electrolyte side due to the disappearance of ionic charges in the cathodic process and the formation of ionic charges in the anodic process.

One of these four reactions is usually the slowest, and rate determining for the overall process. Corrosion inhibition takes advantage of this complexity of reactions by attempting to interfere with any of them individually or jointly. Thus a corrosion inhibitor may further slow the rate of the slowest reaction or may bring about a rate limitation of one or the other of the remaining three processes. While it is generally known that corrosion inhibitors may affect the an-

In Corrosion Chemistry; Brubaker, G., et al.;
ACS Symposium Series; American Chemical Society: Washington, DC, 1979.

odic or the cathodic reaction, it is less well known that inhibitive means may affect either the electrolytic conduction or even the electronic conduction process.

Systematic Classification Of Corrosion Inhibitors

The several thousand substances which have in the past been observed to have corrosion inhibitive properties have often been classified in various ways. The starting point for such classification is the point of interference with the above sketched corrosion mechanism either in a phenomenological or in a mechanistic way. A simple system for classification, which will be discussed in more detail later, is based on whether the inhibitor interferes with the anodic or cathodic reaction. Thus inhibitors are classified as anodic or cathodic inhibitors. However, this distinction was shown to be too simplistic and a more complex classification was worked out by H. Fischer (4) on the basis of where, instead of how, in the complex interphase of a metal-electrolyte system the inhibitor interferes with the corrosion reactions. The metal-electrolyte interphase can be visualized as consisting of (a) the interface per se, and (b) an electrolyte layer interposed between the interface and the bulk of the electrolyte. On this basis Fisher distinguished as shown in Table 1, between "Interface Inhibition" and "Electrolyte Layer Inhibition."

Interface Inhibition comes about by substances which position themselves immediately at the surface of the metal and decrease the rates of physical, chemical or electrochemical processes in the corrosion mechanism. Such processes may be:

a) the charge transfer per se;
b) the interruption of the crystal lattice;
c) the partial steps involved in the anodic or cathodic reactions, that is chemical reactions either preceding or following the charge transfer reactions.

Discussing interface inhibition one finds that the pure squeezing out effect (salting out effect), which may concentrate inhibiting neutral molecules at the metal electrolyte interface, will be rather rare. However, it is possible that the activity of ions or molecules taking place in the corrosion reaction is decreased simply by the accumulation of neutral molecules in the vicinity of the metal surface. Such substances could be alcohol, water soluble inert solids in general, or inert ions.

In Corrosion Chemistry; Brubaker, G., et al.;
ACS Symposium Series; American Chemical Society: Washington, DC, 1979.

Table I
(4)
Causes of Interface-Inhibition and Electrolyte-Layer-Inhibition

1. Interface-Inhibition.
   - 1.1 caused by the squeezing out effect.
   - 1.2 caused by adsorption.
   - 1.3 caused by electrosorption.
   - 1.4 caused by coverage with a polymolecular or polymerous layer.

2. Electrolyte-Layer-Inhibition.

   - 2.1 mechanical E. caused by
     - 2.11 colloids or suspensions.
     - 2.12 viscous solutions.
     - 2.13 pores in polymolecular or polymerous layers.
   - 2.2 chemical E. caused by substances reacting with components of homogeneous partial reactions of the electrode reaction.
   - 2.3 electrochemical E. caused by changes of the potential in the diffuse double layer dependent on a coverage of the interface with ions

Mostly however, these and other molecules as well as ions or ion pairs coming from the electrolyte may be adsorbed on the metallic (or semiconductive) part of the interface. Disregarding the special case of the potential of zero charge at the metallic surface, the conductor will usually carry a positive or negative charge which may favor its coverage with charged or polar substances occuring near the interface. It is very difficult, however, to distinguish between pure adsorption of neutral molecules on the surface of the corroding metal by means of Van der Waals or a chemical forces, and electrosorption which takes place by potential dependent electrostatic forces. Often the two mechanims operate in conjunction. It has been shown for instance, that organic amines become much more effective corrosion inhibitors in acid medium if a halide is present. Halide ions, particularly iodide, are strongly adsorbed on metal surfaces thus forming a negatively charged layer on the metal surface onto which protonated organic amines adsorb subsequently, with a resulting inhibition of corrosion reactions.

Finally, one can talk about an interface effect which is caused by coverage of the metal surface with a polymerous layer. Some authors think that certain

In Corrosion Chemistry; Brubaker, G., et al.;
ACS Symposium Series; American Chemical Society: Washington, DC, 1979.

inhibitors such as the acetylenic ones form a polymer layer on the surface of the metal. In other words, the monomeric inhibitor molecules undergo either chemical or electrochemical reaction on the metal surface such that a polymeric two dimensional system is formed which tightly adheres to the metal surface and interferes with the rates of the corrosion reactions.

All of the above inhibition phenomena are visualized as taking place immediately on the metal surface of the corroding specimen. Apparently, there are ways that one can affect corrosion reactions by interfering with processes which are not on the surface, but those in the vicinity of the surface, namely in the electrolyte layer closest to the surface. Electrolyte layer inhibition may hinder the following partial steps of electrode reactions:

1) Transport of components of the electrode reactions to or from the interface;
2) Partial steps of the homogeneous chemical reactions within the electrolyte layer. This can be accomplished by:
   a) purely mechanical obstacles assembled in the electrolyte layer (mechanical electrolyte layer inhibition);
   b) by chemical reactions of components of the electrode reactions with substances assembled in the electrolyte layer (chemical electrolyte layer inhibition);
   c) by electrochemical effects such as a change of the zetapotential in the diffuse part of the double layer which controls the migration of components of electrode reactions. This is called the electrochemical electrolyte layer inhibition.

For more detailed discussion of the various phenomenological inhbition mechanism the reader is referred to the original literature. (4)

It is obvious now that corrosion inhibition is not a simple phenomena, and a decision may have to be made whether it may be more useful to discuss corrosion inhibition along mechanistic lines or by means of a tabulation of chemical compounds which have been found effective under specific circumstances. However, the digestion of exhaustive tables of chemical compounds and their application as corrosion inhibitors as presented in C. Nathan's book (5) leaves the reader as dissatisfied and puzzled as do elaborate classification systems of corrosion inhibitors which invariably lack experimental substantiation and have at this stage little predictive value.

In Corrosion Chemistry; Brubaker, G., et al.;
ACS Symposium Series; American Chemical Society: Washington, DC, 1979.

As a consequence it is judged to be more useful for the novice in the field of corrosion inhibition to familiarize himself with some of the fundamental investigative means and subsequently be confronted with some special cases of corrosion inhibition which may or may not lend themselves to generalization.

Experimental Observation of Corrosion Inhibition

The study of corrosion processes in recent years has been almost entirely based on the so called Evans diagram. Considering how often this diagram has been misused or misrepresented suggests that a brief discussion may again be in order at the risk of being repetive or trivial.

The Evans diagram (1) is a graphical presentation in semilogarithmic coordinates of the anodic and cathodic reaction rates expressed as partial currents dependent on potential. The basis for the Evans diagram is the corrosion model discussed above:

$$Me \longrightarrow Me^{n+} + ne \qquad (5)$$

$$Ox + ne \longrightarrow Red^{n-} \qquad (6)$$

These partial reactions proceed with equal reaction rates when the metal is freely corroding. In order to express the reaction rates in terms of a current, the conversion per time is multiplied by the Faraday constant according to the following equation:

$$J = Q^{\cdot} \cdot F \cdot n \qquad (7)$$

Where J equals current, n number of electrons transferred per molecule, F equals Faraday constant and $Q^{\cdot}$ is the rate of the reaction expressed in terms of moles per unit time. If the above equation is divided by the surface area the current density can be expressed as follows:

$$\frac{J}{A} = i = Q^{\cdot} \cdot \frac{F \cdot n}{A} \qquad (8)$$

The partial anodic (i_a) and cathodic (i_c) current densities are then expressed as exponential functions of the over-potential (η_a, η_c) which is the difference between the operating potential (ε) and the equilibrium potential (E_a, E_c) of the particular partial reaction. These relationships are shown graphically and explicitly in Fig.1. Thus by defining the anodic and cathodic current potential relationships for a corroding system

In Corrosion Chemistry; Brubaker, G., et al.;
ACS Symposium Series; American Chemical Society: Washington, DC, 1979.

and by plotting them as shown in a potential vs log i diagram, one quickly finds the point where the two lines intercept, which is the potential at which anodic and cathodic reaction rates are equal. The current at this point becomes corrosion current or corrosion rate while the corresponding potential is the corrosion potential.

It must be realized that in a corroding system the partial currents cannot be directly observed. If a corroding piece of metal is made an electrode in an electrochemical cell the corrosion reactions already proceed with a given rate. The metal will therefore assume the corrosion potential (ε_{corr}) and the system is in a steady state condition as opposed to an equilibrium state. No current will flow in the external circuit at this point. If now by means of an external circuit the potential of the corroding metal is moved in the anodic or cathodic direction, the anodic or cathodic current will flow in the external circuit ($\pm i_{ext}$). This observed external current is the equivalent of the algebraic sum of the anodic and cathodic partial currents and can therefore be predicted from the individual characteristics as shown in Fig.1. If the operating potential is sufficiently negative of the corrosion potential, the current-potential behavior of the external current will resemble the partial cathodic characteristic because under these conditions the anodic current has become extremely small. The potential regions where either of the partial reactions is negligibly small with respect to the other are called the Tafel regions. The current potential behavior in the Tafel regions of an actively corrosing piece of metal are often used to draw conclusions with respect to the mechanism of the partial corrosion reactions. It is therefore in principal possible to establish the Evans diagram from fundamental knowledge of the individual reactions or experimentally by studying the polarization behavior of a corroding piece of metal in a given environment. For more detailed derivation of electrochemical rate equations see (6).

It is important to remember that some assumptions have been made in the derivation of Fig.1. First, the equations given there are applicable only if the electron transfer is the rate determining step in the partial corrosion reactions. This is important with respect to the calculation of the Tafel slope ($RT/\alpha nF$) or the interpretation of an experimental one. It is further assumed that during the polarization of the test electrode (corroding piece of metal) the composition of the solution in the vicinity of the electrode remains

In Corrosion Chemistry; Brubaker, G., et al.;
ACS Symposium Series; American Chemical Society: Washington, DC, 1979.

constant. This is often not the case since the consumption of an oxidant (oxygen or protons) during cathodic polarization rapidly leads to diffusion limitation (diffusion over-potential) while secondary reactions during polarization in the anodic direction often lead to precipitation of metal hydroxides and consequently passivation phenomena.

In spite of such experimental difficulties the Evans diagram has been extremely useful in determining certain characteristics of inhibitors. In acid solutions for example, the electrode reactions follow a behavior which is quite predictable on the basis of the electron transfer being the rate determining step. Thus Hackerman (7) and Nobe (8) have studied such systems extensively and found that the effectiveness of certain amine inhibitors can be explained by their adsorption behavior. The adsorption isotherms in turn proved to be predictable on the basis of molecular structure and configuration.

In neutral or alkaline solution, or solutions of low conductivity, however, one finds very small Tafael regions, or the Tafael regions are essentially nonexistent. The reasons for such behavior are many:

a) Stern (9) for example has shown that the cathodic polarization curves for iron corroding in oxygen free sodium chloride solution show hydrogen ion diffusion limitation at a current of 10^{-4} a/cm^2 at a pH of 2. Thus in such systems above a pH 1.5 essentially no Tafel region is observed due to a diffusion over-potential.

b) Resistances or over-potentials other than those determining the rate of the electron transfer reaction are often included in the current potential measurement. The most frequent situation is the inclusion of an ohmic resistance which occurs between the working electrode and the reference electrode. Such ohmic electrolyte resistances can easily be determined by positioning the reference electrode at varying distances from the working electrode, or by various mathematical procedures including automatic iR-drop compensating electronic devices. Mansfeld has recently discussed the effect of such resistance on current potential curves (10). A more serious resistance often influencing the potential determination in polarization studies is caused by the formation of a corrosion product layer on the surface of the corroding test electrode. This situation is considerably more complex because, first, this additional resistance is most likely not ohmic in nature due to the semiconducting properties of the corrosion product layer and second, anodic and cathodic

In Corrosion Chemistry; Brubaker, G., et al.;
ACS Symposium Series; American Chemical Society: Washington, DC, 1979.

reactions do not necessarily take place at the same location. Thus the anodic reaction can be visualized as taking place at the metal-scale interface while the cathodic reaction may take place at the scale-electrolyte interface. The resultant polarization diagram is shown in Fig. 2. Note that not only the external current is subject to an iR drop (the case most often discussed) but the partial currents are also subject to a distortion caused by the additional resistance. It must further be remembered that the resitance may be different in magnitude for the cathodic and anodic partial currents. This situation was discussed by Hausler (11) in some detail.

Effect Of Inhibitors On Polarization Behavior

One of the most interesting and perhaps most difficult to understand phenomena in corrosion inhibition is in fact that inhibitors do not affect anodic and cathodic reactions to the same degree. Thus one finds, as shown in Fig.3 that in some instances the cathodic reaction rate is reduced while the anodic reaction rate remains the same or vice versa. As can readily be understood from the diagram in Fig.3, this distinction can be made on the basis of a shift in the corrosion potential and if more detailed information is required from a complete study of the polarization curves. A brief remark maybe in order here with respect to the terminology used in such cases, as it is often confusing: Cathodic inhibition results in a shift of the corrosion potential in the anodic or negative direction while anodic inhibition results in a potential shift in the cathodic or more positive direction. It has been shown in the literature many times that some systems are classically behaved as will be discussed in more detailed below, while others may show both effects, that is, a combination of anodic and cathodic inhibition in varying degrees. Therefore, while the corrosion potential may give a preliminary indication of the inhibitor mechanism, polarization curves should be recorded for more complete assessment of its mode of action. This is all the more important since a reduction of the anodic reaction rate, for instance, coupled with an acceleration of the cathodic reaction rate may result in a large cathodic potential shift with no change in the overall corrosion rate. Conversely, if both anodic an cathodic reaction rates are reduced to the same extent as shown in Fig.4, no shift in the corrosion potential is observed while the inhibition effect is the largest possible. Table 2 il-

In Corrosion Chemistry; Brubaker, G., et al.;
ACS Symposium Series; American Chemical Society: Washington, DC, 1979.

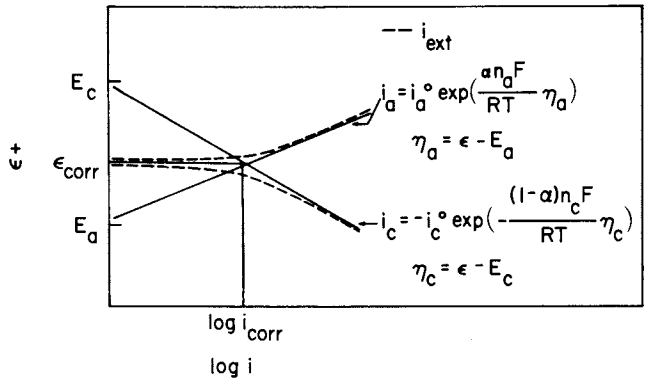

$$i_{ext} = \Sigma i_a, i_c$$

$$i_{ext} = i_{corr}\left[\exp\left(\frac{\alpha n_a F}{RT}\eta_{corr}\right) - \exp\left(\frac{-(1-\alpha)n_c F}{RT}\eta_{corr}\right)\right]$$

Figure 1. Anodic and cathodic current–potential relationships in a corroding system

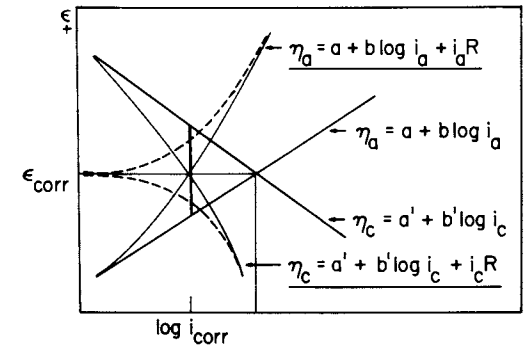

$$\text{----}: i_{ext} = i_{corr}\left[\exp\left(\frac{\alpha nF}{RT}\{\eta_{corr} - i_a R\}\right) - \exp\left(\frac{-(1-\alpha)nF}{RT}\{\eta_{corr} - i_c R\}\right)\right]$$

Figure 2. Effect of electrolyte resistance

In Corrosion Chemistry; Brubaker, G., et al.;
ACS Symposium Series; American Chemical Society: Washington, DC, 1979.

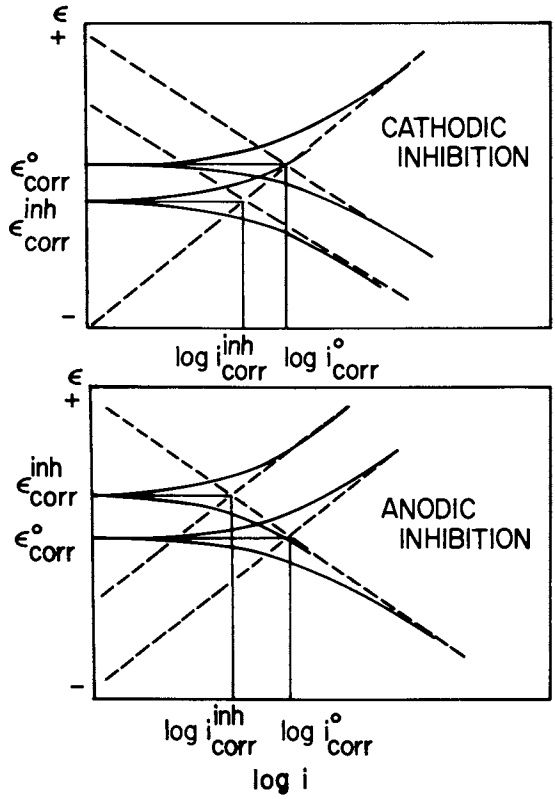

Figure 3. Inhibition: (top) *cathodic inhibition;* (bottom) *anodic inhibition*

In Corrosion Chemistry; Brubaker, G., et al.;
ACS Symposium Series; American Chemical Society: Washington, DC, 1979.

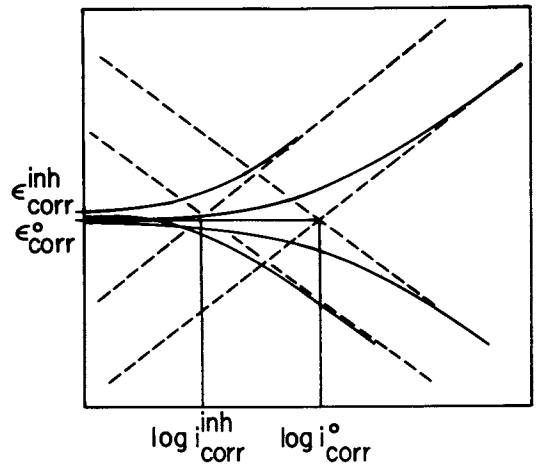

Figure 4. Inhibition, both anodic and cathodic

Table II

WEIGHT LOSS MEASUREMENTS OF CARBON STEEL IN 10% SULFURIC ACID AS A FUNCTION OF TYPE AND CONCENTRATION OF INHIBITOR AT 25 C.

Inhibitor	Concentration of Inhibitor (mol/l)	Weight loss mg/25cm^2. day	Corrosion Potential mV vs. H_2
Blank	0	956	- 235
Aniline	0.0063	943	- 233
Diethylaniline	0.0063	513	- 209
p-Phenylene diamine	0.0063	886	- 225
β-Naphthyl-amine	sat.sol.	374	- 210
Phenyl-α-naphthyl amine	sat.sol.	938	- 234
Pyridine	0.0063	863	- 232
Quinoline	0.0063	370	- 201
Quinoline	0.063	122	- 181
α-Naphthoquinoline	0.0063	78	- 177
α-Naphthoquinoline	0.063	59	- 172
β-Naphthoquinoline	0.0063	73	- 178
β-Naphthoquinoline	0.063	58	- 172
2,4,-Dimethylquinoline	0.0063	321	- 192
2,4,-Dimethylquinoline	0.063	178	- 176
2,6-Dimethylquinoline	0.0063	175	- 192
2,6-Dimethylquinoline	0.063	64	- 170
Ethylquinolinium bromide	0.0063	63	- 184
Acridine	sat.sol.	404	- 227
Acridine orange	sat.sol.	24	- 201
Acridine red	sat.sol.	61	- 184
Acriflavine	sat.sol.	112	- 196
Water soluble Petroleum sulfonate	sat.sol.	170	- 212
Sulfonated oil	sat.sol	23	- 227
Commercial Inhibitor A	sat.sol.	23	- 227
B	sat.sol.	44	- 216
C	sat.sol.	85	- 218
D	sat.sol.	51	- 223

In Corrosion Chemistry; Brubaker, G., et al.;
ACS Symposium Series; American Chemical Society: Washington, DC, 1979.

lustrates these points in a survey of potential shifts and corrosion rates for various inhibitors on carbon steel in sulfuric acid. Such relatively simple electrochemical techniques therefore can be considered useful tools for the rapid assessment of inhibitor activity and for the purpose of obtaining preliminary information on a possible inhibition mechanism. However, polarization measurements, either in the form of "Linear polarization measurements" or Tafel-slope determinations are fraught with peril (c.f. Hausler 11). Even if a system is relativly well behaved, the informational value obtained from polarization curves is relatively small and should be combined with more extensive determination of the electrode kinetic parameters, adsorption studies and mass transfer studies in order to elucidate the mechanism of a particular corrosion inhibitor or class of compounds exhibiting inhibitive effects. In short only a complete description of the interphase chemistry will eventually lead to the predictive criteria for inhibitor behavior.

Very few such investigations have been carried out in the past. It appears that investigators were mostly satisfied with demonstrating the inhibitory effect of chemical substances and subsequently forcing those substances into one or the other simple mechanistic concepts. The few investigations which have pinpointed vastly more complex behavior, have mostly been overlooked. In the interest of stimulating more research in the field of inhibitor chemistry, this review shall stress the more exotic investigations. In particular it will be suggested that chemical reactions of inhibitors occuring in the interphase between corrosion products and the inhibitor are a more general and widespread phenomenon than has generally been believed in the past.

Inhibition By Thiourea And Quinoline Derivatives

A large number of investigations in acid media have led to the conclusion that the inhibition effect caused by relatively small and simple molecules is due to their adsorption on the metal surface. Compounds of this nature usually contain sulfur and nitrogen, or are of the groups of higher alkyl-alcohols and fatty acids. Typical compounds to be discussed here in more detail are quinoline and thiourea derivatives. Fig. 5 shows a comparison of the effectiveness of several such compounds determined by means of weight loss measurements on carbon steel in 5% sulfuric acid at 40° C. as a function of the inhibitor concentration. A cur-

In Corrosion Chemistry; Brubaker, G., et al.;
ACS Symposium Series; American Chemical Society: Washington, DC, 1979.

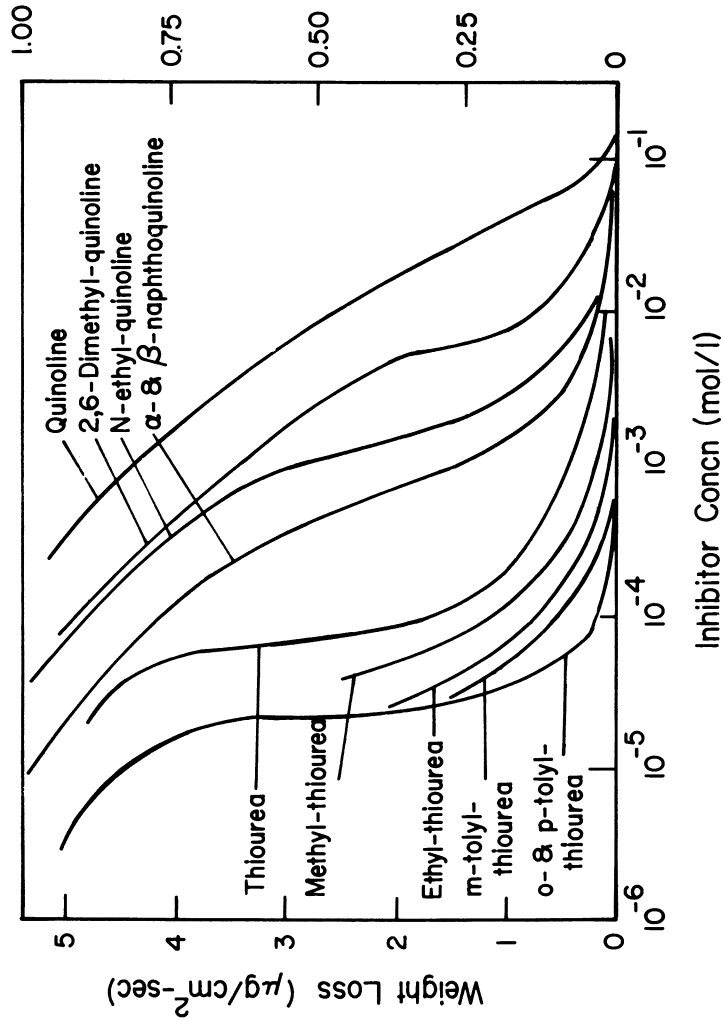

Figure 5. Weight loss of 0.1% C–steel in 5% aqueous H_2SO_4 at 40°C as a function of concentration of various quinoline and thiourea inhibitors (3)

sory examination of Fig.5 might lead to the conclusion that the relationships of corrosion rate vs. inhibitor concentration are basically quite similar for the two classes of compounds and differ only quantitatively with respect to the efficiency. It will be shown however, that there are indeed profound differences between the two classes of inhibitors. Hoar and Holiday (12) found relatively simple conditions as a result of their investigation of the corrosion inhibition of iron in 5% sulfuric acid by 2,6-dimethylquinoline. These authors determined first the external current-potential curves in the unihibited solution and then the anodic partial current-potential curves at different inhibitor concentrations and the quantity of dissolved iron in the electrolyte at certain electrode potentials. The difference between the anodic external current and the independently determined anodic partial current (dissolved Fe) is the cathodic partial current density. The results as obtained by Hoar and Holiday are shown in Fig.6. The dashed curve represents the external polarization behavior in the absence of inhibitor and the black lines are the Tafel slopes for the anodic partial current density (the metal dissolution) for different inhibitor concentrations. The cathodic partial current density (hydrogen eveolution) is found for all values of the inhibitor concentrations in the shaded area. Therefore, it is obvious that the inhibitor in this case acts exclusively by reducing the anodic reaction rate but not the cathodic one.

Kaesche and Hackerman (13) have investigated the inhibition of several aliphatic and aromatic amines on pure iron corroding in 1N hydrochloric acid. These authors observed in thirteen out of fourteen cases that the inhibition was both anodic and cathodic, albeit predominantly anodic. The exception was methylamine which acted only cathodically. In the case of the corrosion inhibition on pure iron by β-naphthoquinoline in sodium sulfate/sulfuric acid solution (13), one observes a simple parallel shift of the anodic and cathodic Tafel lines towards smaller values of current density. Here the effect is almost symetrical, indicating that this inhibitor acts to the same extent upon anodic and cathodic reaction rates. Therefore, the effect of β-naphthoquinoline can be explained on the basis that its adsorption blocks a fraction θ of the metal surface for all electrode reactions. If equation 9 describes the external polarization behavior in terms of a function of the partial current potential relationship for the anodic and cathodic reactions in the usual terms:

In Corrosion Chemistry; Brubaker, G., et al.;
ACS Symposium Series; American Chemical Society: Washington, DC, 1979.

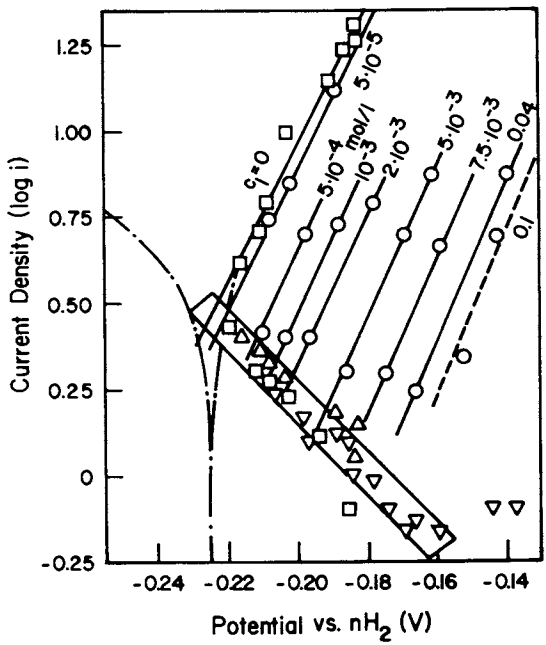

Springer–Verlag

Figure 6. Current–potential diagram for 0.1% C–steel in 5% aqueous H_2SO_4 at 40°C for various concentrations of 2,6-dimethylquinoline (3)

$$(i_{ext})_o=(i^o_{an})_o \cdot \exp\{\varepsilon/(B_{an})_o\} - (i^o_{cath})_o \cdot \exp\{-\varepsilon/(B_{cath})_o\} \quad (9)$$

where: i^o = exchange current density
ε = electrode potential
B_{an} = anodic Tafel slope
B_{cath} = cathodic Tafel slope
then equation 10 describes the polarization behavior of inhibited electrodes in the same terms:

$$(i_{ext})_I=(i^o_{an})_I \exp\{\varepsilon/(B_{an})_I\} - (i^o_{cath})_I \cdot \exp-\{\varepsilon/(B_{cath})_I\} \quad (10)$$

If the inhibitor does not affect the Tafel slopes (see β-naphthoquinoline),

$$(B_{an})_o = (B_{an})_I; \quad (B_{cath})_o = (B_{cath})_I \quad (11)$$

the inhibited anodic current density is a simple fraction of the uninhibited anodic current density as shown in equation 12.

$$(i^o_{an})_I = (i^o_{an})_o \ (1-\theta) \quad (12)$$

and for the cathodic partial current

$$(i^o_{cath})_I = (i^o_{cath})_o \ (1-\theta) \quad (13)$$

It follows that the inhibited external current is a similar fraction of the uninhibited external current as indicated in equation 14

$$(i_{ext})_I = (i_{ext})_o \ (1-\theta) \quad (14)$$

It also follows that the degree of inhibition in this case is directly proportional to the fraction of the surface covered with adsorbed inhibitor:

$$P = \frac{I^o_{corr} - I^{inh}_{corr}}{I^o_{corr}} = \theta \quad (15)$$

In general, however, these equations are not applicable since symmetrical anodic and cathodic inhibition is a rare case. In the case of dimethylquinoline which, as shown in Fig.6, does not affect the cathodic hydrogen evolution, Hoare and Holiday (12) have proposed a different approach. One can assume that two kinds of

In Corrosion Chemistry; Brubaker, G., et al.;
ACS Symposium Series; American Chemical Society: Washington, DC, 1979.

atomic sites occur on the steel surface. There might be a site S_1 occurring at a frequency N_1 where the anodic metal dissolution occurs, and all other sites, S_2 occurring with a frequency N_2. One further assumes that N_1 is much smaller than N_2 and that the cathodic hydrogen evolution occurs on all sites S_1 and S_2. Adsorption now occurs to a different degree on the sites S_1 with a coverage θ_1 and a coverage θ_2 on the sites S_2. If we then further neglect the cathodic hydrogen evolution on the sites S_1 because of their negligible contribution, equation 16 results:

$$(i_{ext})_I = (i^o_{an})_o\ (1-\theta_1)\ \exp\{\varepsilon/(B_{an})_o\} - (i^o_{cat})_o \cdot (1-\theta_2)\ \exp\{-\varepsilon/(B_{cath})_o\} \qquad (16)$$

Since dimethylquinoline is only a marginal corrosion inhibitor it is probably only marginally or weekly adsorbed. One can further speculate that the adsorption occurs only on the sites S_1, that is the lattice dissolution sites which will favor the adsorption of foreign molecules from an energetic point of view. Therefore, θ_2 will be approximatly zero. Equation 16 then reduces to equation 17:

$$(i_{ext})_I = (i^o_{an})_o\ (1-\theta_1)\ \exp\{\varepsilon/(B_{an})_o\} - (i^o_{cath})_o \cdot \exp\{-\varepsilon/(B_{cath})_o\} \qquad (17)$$

By proper adjustment of the parameter θ_1 the curves in Fig.6 can then be calculated.

Similar calculations have been carried out for the inhibition of iron corrosion in hydrochloric acid by Victoria blue which, according to Elze and Fischer (14) does not affect the Tafel slopes, but reduces both the anodic and cathodic partial reactions to a different degree. In this particular case θ_1 and θ_2 have to be adjusted by way of a trial and error calculation.

This simple model of the inhibitor action which is based essentially on the potential independence of the inhibitor adsorption is, however, often not applicable. Kaesche (15) indicates that the corrosion inhibition of pure iron in sulfuric or perchloric acid by phenyl-thiourea strongly affects the slopes of the polarization curves, leaving the corrosion potentials almost unchanged Fig.7. In fact, the polarization curves for the inhibited situation do not exhibit real Tafel behavior. This behavior finds a partial explanation in the fact that the mechanism of the hydrogen evolution appears to be changed in the presence of

In Corrosion Chemistry; Brubaker, G., et al.;
ACS Symposium Series; American Chemical Society: Washington, DC, 1979.

phenylthiourea. Specifically, it appears the electrochemical desorption of hydrogen is greatly hindered. This mechanism may possibly find confirmation in the independently observed fact that in the presence of phenylthiourea considerably more hydrogen diffuses into the metal. However, the inhibition mechanism of phenylthiourea is probably considerably more complicated than that, as can be seen from the very complex relationship of the corrosion potential with the inhibitor concentration. This is shown in Fig.8, in comparison with a similar relationship for β-naphthoquinoline. Hoar (16) found that in the corrosion inhibition of iron in hydrochloric acid by β-naphthoquinoline, the corrosion potential increases monotonically with increasing inhibitor concentration, while in the case of o-tolylthiourea one observes first a decrease of the corrosion potential followed by an increase at higher inhibitor concentrations. A similar predominant inhibition of the cathodic partial reaction at small inhibitor concentrations is exhibited also by phenylthiourea according to Kaesche. Furthermore, in the series of the thiourea derivatives one often finds corrosion acceleration at small concentrations, as for instance in the case of phenylthiourea at concentrations of 10^{-7} moles per liter. This appears to be due to a small cathodic decomposition of thiourea and its derivatives in the course of which hydrogen sulfide is formed. As is well known, hydrogen sulfide tends to accelerate corrosion, in particular the anodic partial reaction of dissolution of iron, which has been demonstrated independently by other authors (17).

It is generally assumed that ions which can accelerate either or both partial reactions in a corrosion process are capable of being adsorbed on the iron surface. Thus it is known that hydrogen sulfide ions which accelerate both partial reactions of acid corrosion (although predominantly the anodic one), and formic acid molecules which catalyze the cathodic partial reaction but inhibit the anodic one, as well as commercial inhibitors which reduce both partial reactions, are in fact adsorbed on the iron surface. As a consequence the mere fact that adsorption takes place cannot be used to predict an expected change in corrosion rate as it is also known that halide ions catalize the anodic dissolution of indium, while hydroxyl adsorption catalyzes the anodic dissolution of iron. Furthermore, it is also known that certain ions can act either as a catalyst or an inhibitor when adsorbed on the metal surface depending on the type of metal considered. Kolotyrkin (18) observed that the adsorp-

In Corrosion Chemistry; Brubaker, G., et al.;
ACS Symposium Series; American Chemical Society: Washington, DC, 1979.

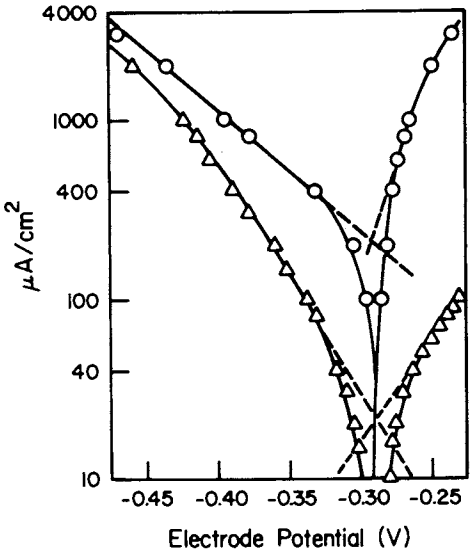

Springer–Verlag

Figure 7. Polarization of carbonyl iron in 1N $NaClO_4/HClO_4$ at pH 2, 25°C deaerated, with and without 7 · 10^{-5} mol/L phenylthiourea (3)

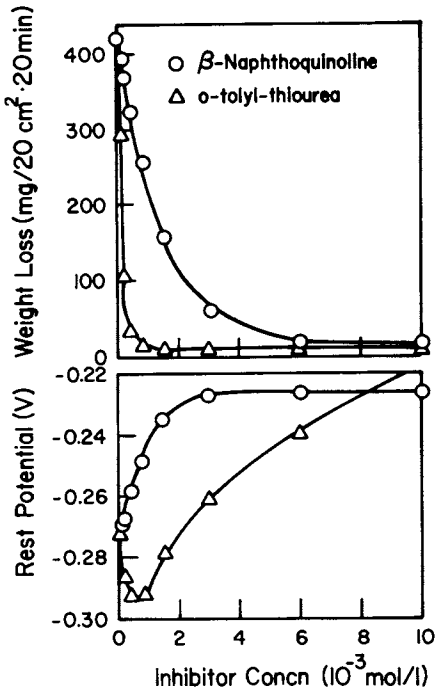

Springer–Verlag

Figure 8. Weight loss and rest potential of mild steel in 10% H_2SO_4 as a function of the concentration of β–naphthoquinoline and o–tolylthiourea (3)

tion of iodine ions consistently increases the hydrogen over-voltage on silver but decreases it on mercury. On lead one observes that small amounts of adsorbed iodine increase the hydrogen over-potential, larger amounts, however, decrease it. In the case of the hydrogen evolution it is probably the heat of adsorption of the atomic hydrogen on a particular metal which controls the acceleration or inhibition of this reaction upon adsorption of a foreign ion. With respect to the kinetics of the anodic dissolution of metal, however, the important parameter is most likely the strength of the complex formation between surface metal atoms and the adsorbed particle. If the complex formation is weak, therefore hardly affecting the bonding forces holding the surface atoms in the metal lattice, one would expect inhibition through simple blocking of the dissolution sites. Conversely, if strong ligand forces act between the surface metal ions and the adsorbed particle, one would expect catalysis of the metal dissolution. Along these lines one also has to consider the possibility that one kind of adsorbed particle can be displaced by a different kind. One would therefore suggest that increasing the concentration of thiourea derivatives eventually leads to corrosion inhibition because of competitive adsorption with the hydrogen sulfide ion which causes acceleration of corrosion.

Acceleration of corrosion has been demonstrated with strong complexing agents such as EDTA salts. However, as EDTA is substituted with longer alkyl chains, the catalytic effect is gradually lost and inhibition is obtained. This strongly suggests that the adsorption of the inhibitor particle on the metal surface, a purely interfacial phenomenon, is not the predominant feature to be studied, but that in fact the chemistry in the interphase, in particular, the formation of corrosion products and corrosion product layers has to be given more consideration.

A case in point is a study made by Ross (19) on the dissolution of iron in 0.5 molar sulfuric acid in the presence of thiourea at 40° C. The results of this study, which was conducted as a function of the flow rate, are shown in Fig.9. It appears that the uninhibited dissolution of iron follows expected mass transfer behavior both in the laminar and turbulent regions. However, at two inhibitor concentrations marked deviations from the expected mass transfer behavior are observed. Ross attempted to explain these results on the basis that different inhibitor concentrations affect the anodic and cathodic polarization in different ways, taking also into consideration that at small

In Corrosion Chemistry; Brubaker, G., et al.;
ACS Symposium Series; American Chemical Society: Washington, DC, 1979.

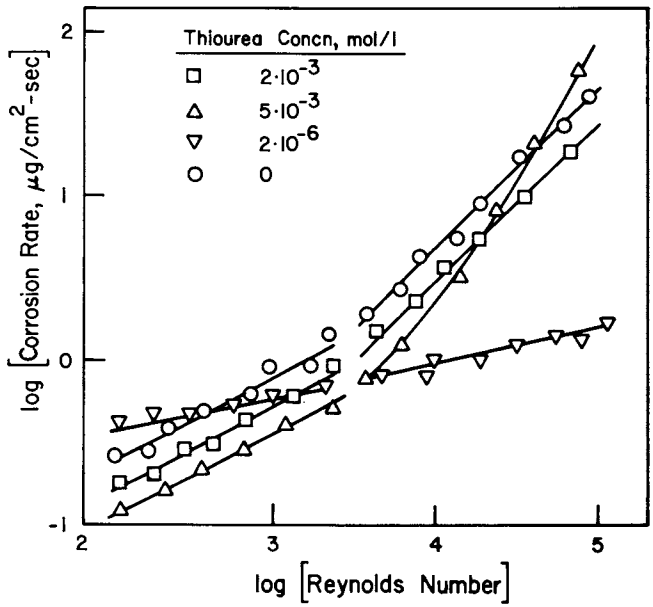

Figure 9. Corrosion rate of mild steel tubes in plain 0.5N H_2SO_4 at various Reynolds Numbers and in the presence of thiourea

In Corrosion Chemistry; Brubaker, G., et al.;
ACS Symposium Series; American Chemical Society: Washington, DC, 1979.

thiourea concentrations hydrogen sulfide is formed on the surface of the metal catalizing the anodic reaction, thereby achieving a corrosion rate which is higher than the blank corrosion rate. However, Ross's explanation leaves many ends untied. One has to explain first of all the mass transfer behavior for the uninhibited dissolution of iron in sulfuric acid. At a proton concentration of one normal and at corrosion rates as measured, proton diffusion cannot be rate controlling. Second, the iron diffusion away from the metal surface is not expected to be rate limiting, since iron can in fact diffuse away from the surface as fast as it is formed, a fact that has been experimentally verified by this author (see below). One must then assume that the observed mass transfer behavior is caused by a secondary reaction most likely the dissolution of a corrosion product. It is known that certain iron sulfates are quite insoluble in water, such as the monohydrate of the ferrous sulfate, and ferric sulfate. In Ross's experiment oxygen was present since the author does not mention any precautions for keeping oxygen out of the experimental system.

At low thiourea concentrations ($2 \cdot 10^{-6}$ molar) it is observed that the corrosion rate varies approximately with the 1/5 power of the flow rate. This author has observed that, in hydrogen sulfide saturated solutions at 70° C in the presence of small amounts of ammonium chloride, the cathodic partial reaction for iron corrosion varies with the 1/6th power of the flow rate. This maybe a coincidence; however, since the formation of hydrogen sulfide and iron sulfide on corroding iron surfaces in acid thiourea containing media has been observed independently by other authors, it is quite likely that the abnormal mass transfer behavior observed by Ross for the small thiourea concentration is in fact caused by an iron sulfide layer on the surface of the metal. At higher thiourea concentrations there may well be competition between the thiourea molecule and the hydrogen sulfide in the complexing reaction with iron. It should be noted, that the next higher thiourea concentration is three orders of magnitude larger but achieves only a marginal inhibition effect. One would therefore assume that thiourea is in competition with sulfate or water for ligand positions around the iron. Since thiourea is a neutral molecule, it is quite understandable that it will reduce the dissolution rate of iron sulfate merely by blocking access of water molecules to the iron sulfate surface. A complete explanation of Ross's scanty data is complicated by the presence of oxygen which

In Corrosion Chemistry; Brubaker, G., et al.;
ACS Symposium Series; American Chemical Society: Washington, DC, 1979.

will interfere with the corrosion and complexing reactions on the surface of the metal. Nevertheless, this particular investigation is of great value in that it points out the importance of studying inhibitor effectiveness under dynamic flow conditions, and in underlining further the importance of the chemistry occurring in a phase immediately adjacent to the metal surface but distinctly different from the bulk of the corrosive medium.

Acetylenic Inhibitors

Acetylenic compounds have long been known as effective corrosion inhibitors in hydrochloric acid. Tedeschi and coworkers (20,21) have presented over the past 10 years extensive investigations of these compounds. Their results are summarized in Tables 3, 4 and 5. Some of the basic features of these comparisons are the position of the hydroxyl group and the position of the triple bond. Thus it appears that the hydroxyl group has to be in α-position to the acetylenic function and optimum efficiency is obtained if the acetylenic function is terminal. These two effects can be explained on the basis of the tautomerism shown in equation 18.

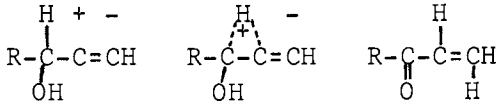

(18)

This formalism implies that the polarization of the triple bond can be stabilized first by a nonclassical carbonium ion and further by an α-keto-double bond confirguration which is known to complex strongly with transition metal ions. It is noted that the hydroxyl group has to be located not only in α-position but on a secondary carbon atom for strong corrosion inhibition to result. This is to be expected, since protons are much more apt to form nonclassical carbonium ions than methyl groups. However, if the terminal proton on the triple bond is substituted with a strong electrophilic group, the polarization of the triple bond becomes strong enough to involve the above indicated tautomerism.

One can further rationalize that a compound with a non-terminal triple bond experiences some steric hindrance in the formation of complexes with transition metal ions. Thus, the effect indicated in Table 3 which Tedeschi ascribed to steric hindrance is rather a kinetic effect concerning the intra-molecular shifts

In Corrosion Chemistry; Brubaker, G., et al.;
ACS Symposium Series; American Chemical Society: Washington, DC, 1979.

Table III

Decreasing Inhibition

1. Location of Triple Bond:

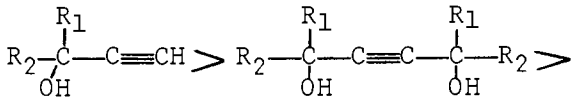

R_1 = H or CH_3
R_2 = $CH_3 \rightarrow C_5H_{11}$

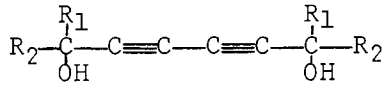

2. Sterichindrance:

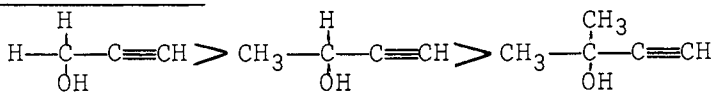

3. Alkyl Chain Length:

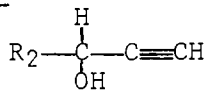

R_2: $C_5H_{11} > C_4H_9 > C_3H_7$, 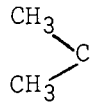 $> C_2H_5 > CH_3$

4. Position of Triple Bond and Hydroxyl Function:

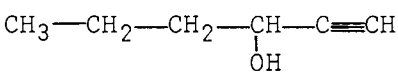

INHIBITOR

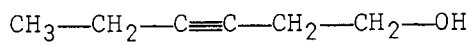

NO INHIBITOR

In Corrosion Chemistry; Brubaker, G., et al.;
ACS Symposium Series; American Chemical Society: Washington, DC, 1979.

Table IV

Formula	Type OH	Chain Length	Corrosion Rate
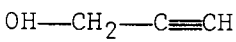	1°	3	0.026
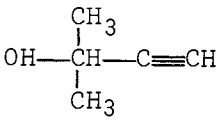	3°	4	>1.6
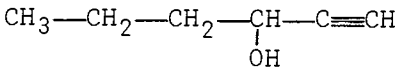	2°	6	0.002
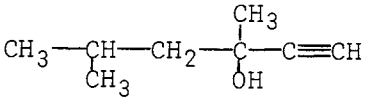	3°	6	>1.6

Table V

Formula	Temperature	Concentration	Corrosion Rate
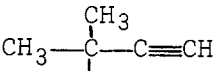	200	0.2	>1.8
	175	0.3	0.221
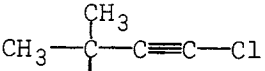	200	0.2	>1.8
	175	0.3	0.243
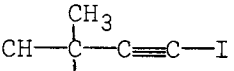	200	0.4	0.004
	175	0.4	0.002
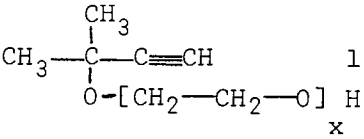	175	0.1	Some Activity

In Corrosion Chemistry; Brubaker, G., et al.;
ACS Symposium Series; American Chemical Society: Washington, DC, 1979.

necessary for complex formation. It is also interesting to note that substituted propargyl alcohols become more effective as the alkyl chain increases. This effect most likely has to do with the nature of the "adsorbed layer" in that increasing length of the alkyl chain imparts greater hydrophobicity to the interfacial layer, thus squeezing out water molecules from the interphase. Quantitative results for this effect are shown in Table 4.

The temperature effect of some acetylenic derivatives is quite surprising. Dimethyl-propargyl alcohol loses its efficiency as the temperature rises from 175° to 200° F. The fact that this is no longer true for the iodine-substituted compound is in support of the above mechanism. Furthermore, if the hydroxyl group on the dimethyl propargyl alcohol is blocked by a polyol group, the corrosion inhibition is almost lost, underlining the importance of the hydroxyl group as an integral part of the inhibition mechanism. It should further be noted, that the equivalent compounds containing double bonds instead of the triple bond show no corrosion inhibition whatsoever. Tedeschi's attempt to formalize the inhibition mechanism of acetylenic compounds has recently been published, (22) and is shown in Table 6. Here the interaction of protonated alkynols such as methyl-butynol and hexynol with themselves and the metal surface is illustrated in the building up of a complex inhibitor multilayer. Such a charged molecular barrier is analogous to a three-dimensional polymer in which a large excess of protons is kept from the metal by repulsion of like charges or by interaction with the basic π- field of the triple bond.

According to Poling (23) IR studies have indicated that such films may be up to 200Å thick. If the average molecule is estimated at about 4Å in diameter, then a barrier of up to fifty molecules thick is possible. The ability of the triple bond to function as a Broensted base in hydrogen bonding with either acidic ethynyle protons or hydroxylgroups has also been proved by IR studies (23).

The formation of such a space charge layer is intuitively appealing, although it is unlikely to extend very far. If protons were to play a role in the build-up of a large three-dimensional polymerous network of the kind shown in Table 6, then necessarily some negative counter ions would have to be built into such a layer. However, a more serious flaw of this model is that it cannot account for the migration of two or three valent metal ions through such a polymer layer.

In Corrosion Chemistry; Brubaker, G., et al.;
ACS Symposium Series; American Chemical Society: Washington, DC, 1979.

Table VI

Methyl Butynol (MB) - Hexynol (H)

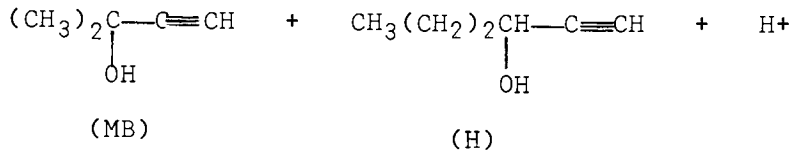

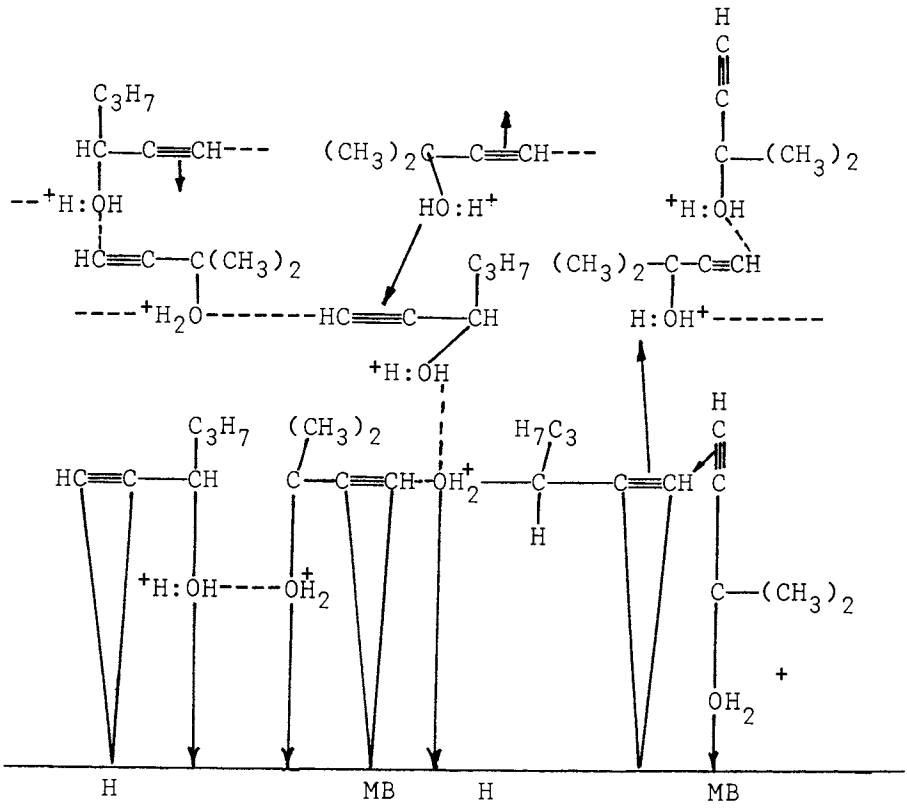

FORMATION OF POLYMEROUS LAYERS WITH ACETYLENIC COMPOUNDS IN HYDROCHLORIC ACID ON METAL SURFACES

In Corrosion Chemistry; Brubaker, G., et al.;
ACS Symposium Series; American Chemical Society: Washington, DC, 1979.

In hydrochloric acid for instance at room temperature the corrosion rate at 95% inhibition is still several hundred mpy's. Therefore, under steady state conditions there is a flux of iron ions across the interphase which must be accommodated in the inhibition mechanism. This could be done more easily by assuming a corrosion product layer of discrete thickness composed of a complex formed from metal ions and inhibitor. Details of this model will be discussed below.

Thus, it is important to point out that any model of the inhibition mechanism has to include not only an explanation of the interference with the surface kinetics but also with the charge transfer processes across the boundry layer.

The study of such transfer processes was one of the purposes of a fairly extensive investigation of the inhibition of corrosion of iron in hydrochloric acid by acetylenic corrosion inhibitors. The parameters of this investigation were: the concentration of the acid, the concentration of the inhibitor, the flow rate and the oxygen concentration in the corrosive medium. While most of the experimental data were obtained by means of the so called resistance probe, polarization measurements were carried out in order to elucidate some of the more peculiar results. The experimental arrangement is more fully explained in (24).

Originally it had been intended to find a correlation between inhibitor constitution and inhibitor activity. The approach taken in evaluating the data essentially followed the thinking of other investigators in the field. It was assumed that the parameters of an adsorption isotherm would be a means to correlate chemical structure with inhibitor performance (25).

If one assumes that the blank corrosion rate (I^{o}_{corr}) represents the total number of "active sites" on the surface of a corroding metal and that the inhibited corrosion rate (I^{inh}_{corr}) represents the total number of active sites minus the inhibited sites, then equation 15 is an expression for the fraction of the surface which is covered by inhibitor molecules. Thus, as explained previously, θ stands for the fractional coverage of the surface with inhibitor and is, of course, equal to the percent protection as defined by equation 15. The dependence of coverage θ on the concentration of the inhibitor, within the assumptions and restrictions made previously, is given by the adsorption isotherm of a particular inhibitor. A typical adsorption isotherm was derived by Langmuir and is given in equation 19:

In Corrosion Chemistry; Brubaker, G., et al.;
ACS Symposium Series; American Chemical Society: Washington, DC, 1979.

$$\theta = \frac{KC_{inh}}{1 + KC_{inh}} \qquad (19)$$

where K is the Langmuir adsorption constant. Rearranging equations 15 and 19 give equation 20, which shows the relationship between the percent protection and inhibitor concentration discussed earlier:

$$C_{inh} = \frac{P}{K\ (1-P)} \qquad (20)$$

It is necessary to discuss some of the inherent assumptions of this approach. It has been pointed out earlier that an inhibitor does not necessarily block both anodic and cathodic reaction sites. Adsorption isotherms are nonetheless useful if the blank corrosion current (I^{o}_{corr}) is in fact proportional to the total number of sites that can possibly adsorb inhibitor. This, however, is not necessarily so, as it has been shown that often a substantial corrosion rate is observed at saturation coverages by the inhibitor.

A number of adsorption isotherms have been proposed in the literature and have been used for such correlation purposes. Of these the Langmuir adsorption isotherm shown in equations 19 and 20 is the simplest one. It is based on the assumption that all sites are energetically equal, that is the heat of adsorption is independent of coverage. It can be seen from equation 20 that, if the logarithm of the inhibitor concentration is plotted against the logarithm of P/(1-P), a straight line with unit slope should result. Hence, this criterion can be used to test the Langmuir assumptions.

Another adsorption isotherm was derived by Freundlich and is shown in equation 21. Here the logarithm of coverage is directly proportional to the logarithm of the inhibitor concentration. This isotherm is only valid at low coverage. It assumes exponential dependence of adsorption energy on coverage.

$$\log \theta = k \cdot \log \cdot C_{inh} + k^{1} \qquad (21)$$

A still further isotherm (equation 22) is attributed to Tempkin and assumes a linear dependence of the adsorption energy on fractional coverage.

$$\theta = \frac{1}{a} \cdot \log C_{inh} + \text{const} \qquad (22)$$

In Corrosion Chemistry; Brubaker, G., et al.;
ACS Symposium Series; American Chemical Society: Washington, DC, 1979.

This assumption is supported if a plot of P vs $\log C_{inh}$ yields a straight line. In this case, as in the case of the Freundlich isotherm, competitive adsorption between inhibitor molecules and either water or other constituents of the corrosive medium is part of the assumptions. Thus, except in the case of the Langmuir isotherm, competitive adsorption is recognized as important, hence the Langmuir isotherm seems somewhat ideal, not withstanding the fact discussed earlier, that the adsorption may be highly selective with respect to the electrode reaction and may furthermore be potential dependent. Hence, isotherm plotting is at best only a means to correlate data and to register possible chemical effects of the system on a purely comparative basis. For a more detailed discussion of adsorption isotherms in electrolyte systems, the reader is referred to the pertinent literature published by Parsons (26) Delahay (27) and Bockris (28).

In the course of studying some acetylenic inhibitors in hydrochloric acid, a number of different isotherm type correlation were found. Thus Fig.10 shows a Langmuir plot for 2-butyne-1,4-diol in 6N hydrochloric acid under aerated conditions. Two different commercial products of this compound were used. It is shown that the straight line relationship is obtained with a good reproducibility over three orders of magnitude of inhibitor concentration. In the light of what was said above, this was a surprising result, however, it corresponds to other similar observations reported in the literature.

Fig.11 shows the same type of plot for the identical inhibitor in hydrochloric acid of different concentrations. It can now be seen that in weaker hydrochloric acid the linear relationship is not retained. At the higher inhibitor concentrations inhibition is reduced with respect to 6N hydrochloric acid, while at the lower concentrations the inhibitor seems to be more effective in 4N than in 6N hydrochloric acid. The decrease of inhibitor efficiency with decreasing acid concentration is unexpected. No similar results seem to have been reported elsewhere.

An interesting effect is observed, Fig.12, when the six normal hydrochloric acid solution is deaerated with nitrogen. It is seen that the absence of oxygen reduces the efficiency of the inhibitor considerably.

Finally Fig. 13, shows a comparison of 2-butyne-1, 4-diol, in 4N hydrochloric acid under aerated and deaerated conditions. While at lower concentrations the presence of oxygen does not seem to be important at higher concentrations better inhibitor efficiency is

In Corrosion Chemistry; Brubaker, G., et al.;
ACS Symposium Series; American Chemical Society: Washington, DC, 1979.

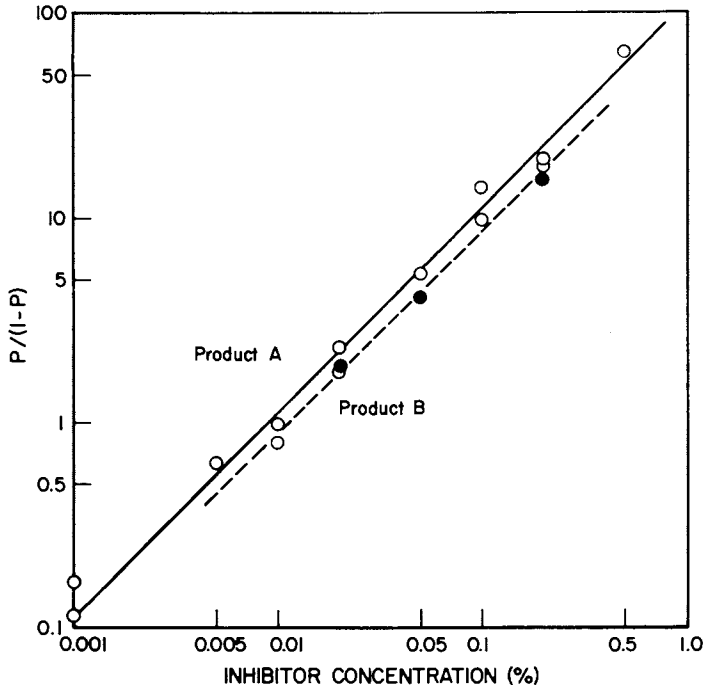

Figure 10. Inhibition of iron corrosion by 2–butyne–1,4–diol in 6N HCl aerated

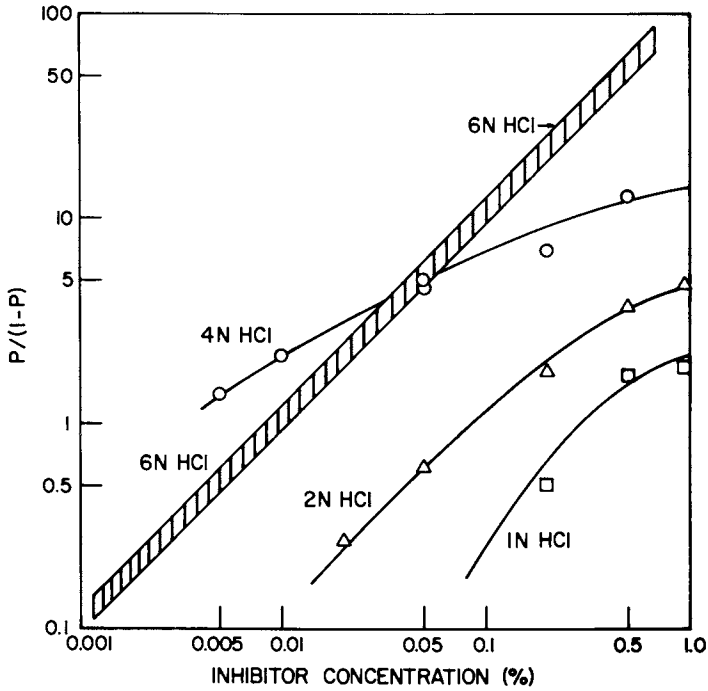

Figure 11. Inhibition of iron corrosion by 2–butyne–1,4–diol aerated

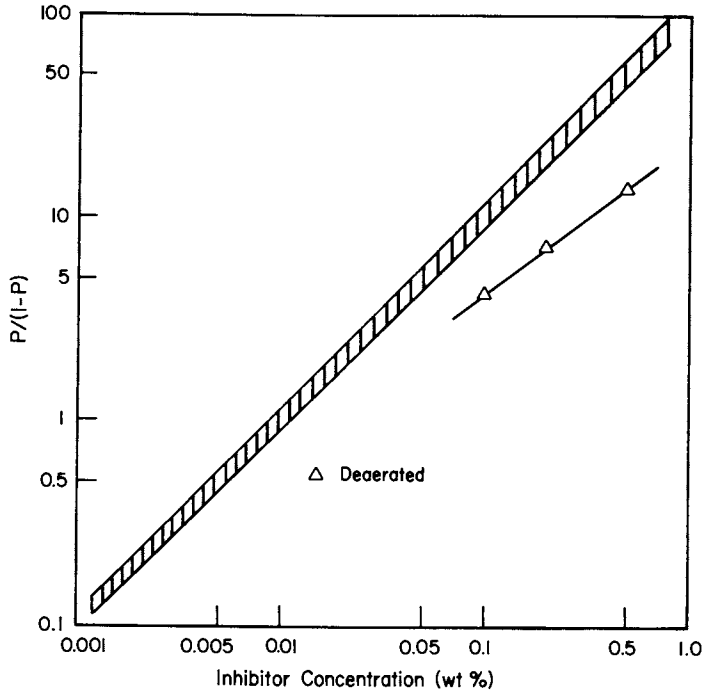

Figure 12. Inhibition of iron corrosion by 2–butyne–1,4–diol in 6N HCl

In Corrosion Chemistry; Brubaker, G., et al.;
ACS Symposium Series; American Chemical Society: Washington, DC, 1979.

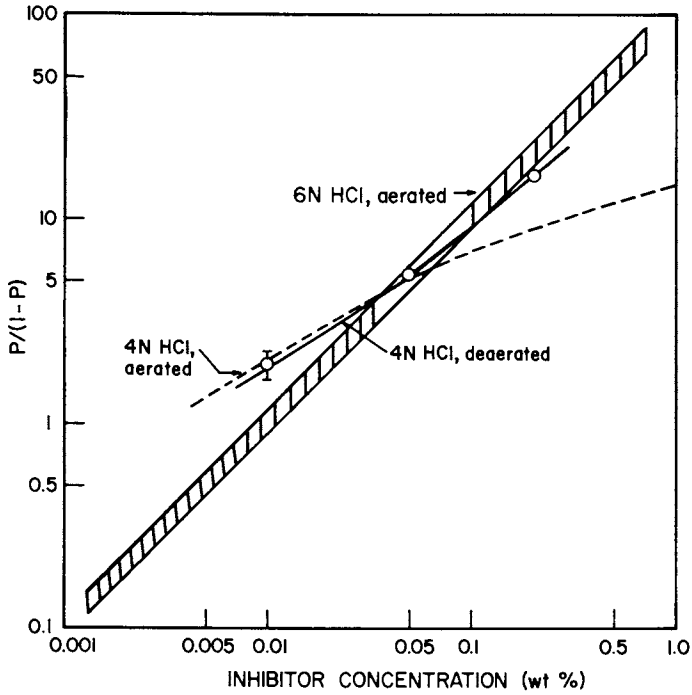

Figure 13. Inhibition of iron corrosion by 2–butyne–1,4–diol

observed in deaerated vs aerated hydrochloric acid, or in other words, the reverse of the effect observed in 6N hydrochloric acid.

Similar experiments with propargyl alcohol are shown in Fig.14. This series of experiments was carried out in 4N hydrochloric acid under aerated and deaerated conditions. Apparently a different mechanism applies for propargyl alcohol because the curvature of the relationship between protection and inhibitor concentration plotted in Langmuir type fashion is reversed from what was observed for butyne-diol. While the oxygen effect with butyne-diol in 4N hydrochloric acid was significant only at higher inhibitor concentrations, it becomes evident that for propargyl alcohol oxygen reduces the inhibitor efficiency over a large concentration range. Most importantly propargyl alcohol is more effective than butyne-diol.

In summary, indirect "adsorption measurements" indicate some surprizing results. First a rather large effect of small changes in acid concentration is observed for the butyne-diol. It would be rather difficult to explain this in terms of adsorption theory because the adsorption isotherm in 4N hydrochloric acid crosses the one obtained in 6N hydrochloric acid.

The pronounced and complex effect of oxygen is even more unexpected in terms of adsorption theory, because oxygen is not thermodynamically stable under the conditions of iron corrosion in hydrochloric acid. Note also, in this context, the oxygen effect in 6N hydrochloric acid is exactly opposite from 4N hydrochloric acid. And, finally, in 4N acid we find that the oxygen effect is in the same direction for propargyl alcohol and butyne-diol, with propargyl alcohol being much stronger affected. In terms of adsorption theory one would expect the better inhibitor to be adsorbed more strongly and hence less affected by competitive adsorption. The experimental results indicate the opposite.

A complete and extensive rational for the rejection of adsorption theroy in the present case would easily go beyond the frame work of this paper. However, since in the area of acetylenic inhibitors the build-up of surface films up to 200 Å has already been observed (25), it maybe more fruitful to follow this line of reasoning. Further experimental effort, of course, ought to attempt to clarify the nature of this surface film. The above described effects such as the acid and the oxygen effect are not immediately obvious if such a surface film is of the nature shown in Table 6. However, some observations involving the de-

In Corrosion Chemistry; Brubaker, G., et al.;
ACS Symposium Series; American Chemical Society: Washington, DC, 1979.

pendence of inhibited corrosion rates on flow rate may shed further light on this problem.

Fig.15, shows the corrosion rate of iron in 4N hydrochloric acid under aerated conditions as a function of flow rate and different inhibitor concentrations. It is noted that the blank corrosion rate increases slightly with flow rate while a somewhat stronger dependence is observed for 0.01 and 0.02 per cent inhibitor solutions. At the stronger inhibitor concentration (0.1%) the flow dependence becomes complex.

Since these experiments were not carried out under ideally defined flow conditions the dependence of corrosion rate on flow rate will be discussed only in a qualitative manner. Under laminar flow conditions and mass transfer control one would have expected the corrosion rate to increase with the square root of the velocity while under turbulent conditions proportionality would prevail. However, in Fig.15 one finds that the corrosion rate varies approximately with the 0.2 to 0.3 power of the flow rate. It appears therefore that the observed dependence on the flow rate does not obey conventional mass transfer theory. A flow effect might be expected in uninhibited hydrochloric acid because hydrogen bubbles, formed on the surface of the metal, are faster and more easily removed at higher flow rates. While this argument could be applied in discussing Fig.15, we find in Fig.16 that the flow effect at similar corrosion rates is much less pronounced under deaerated conditions. We therefore have to conclude that the observed flow effect is not mechanical and cannot be related to pure mass transfer control either. In Fig.17, the flow dependence of the corrosion rate is shown for 2-butyne-1,4-diol in deaerated 4N hydrochloric acid. Note that the corrosion rate appears to be noticeably affected only at the higher flow rates. Finally, in Fig.18, we observe that increased flow rate can either increase or decrease the corrosion rate in the presence of an inhibitor. This effect was observed reproducibly only in 6N hydrochloric acid with 2-butyne-1,4-diol under deaerated conditions for 0.2% and 0.1% inhibitor concentration. This behavior indicates that the corrosion rate is controlled by the superposition of two partial reaction rates each of which is mass transfer dependent to a certain extent. In terms of the model delineated in Table 6, it is suggested that the three-dimensional polymeric layer made up by inhibitor molecules is in fact a three-dimensional chelate made up of iron ions and inhibitor molecules. The corrosion rate is then

In Corrosion Chemistry; Brubaker, G., et al.;
ACS Symposium Series; American Chemical Society: Washington, DC, 1979.

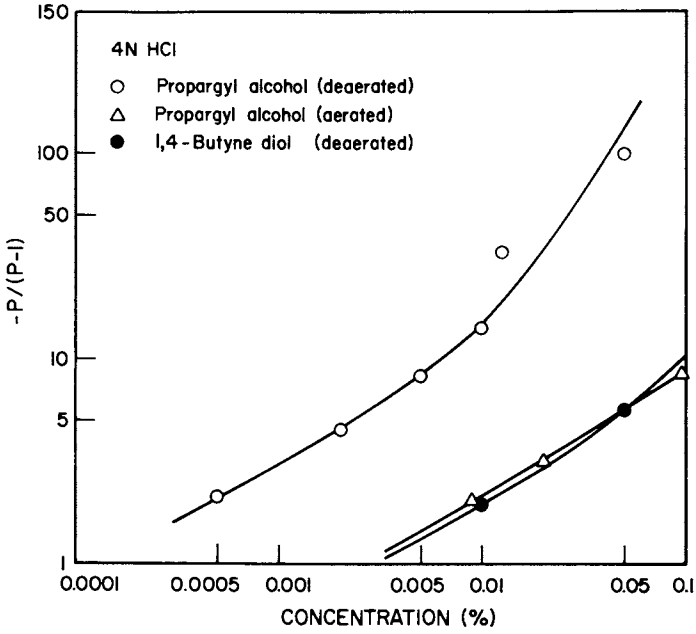

Figure 14. Effectiveness of acetylenic inhibitors

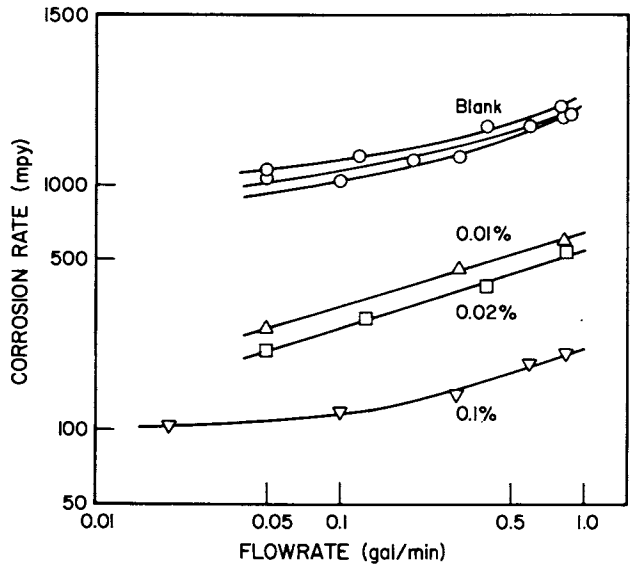

Figure 15. Corrosion of iron in 4N HCl, propargyl alcohol aerated

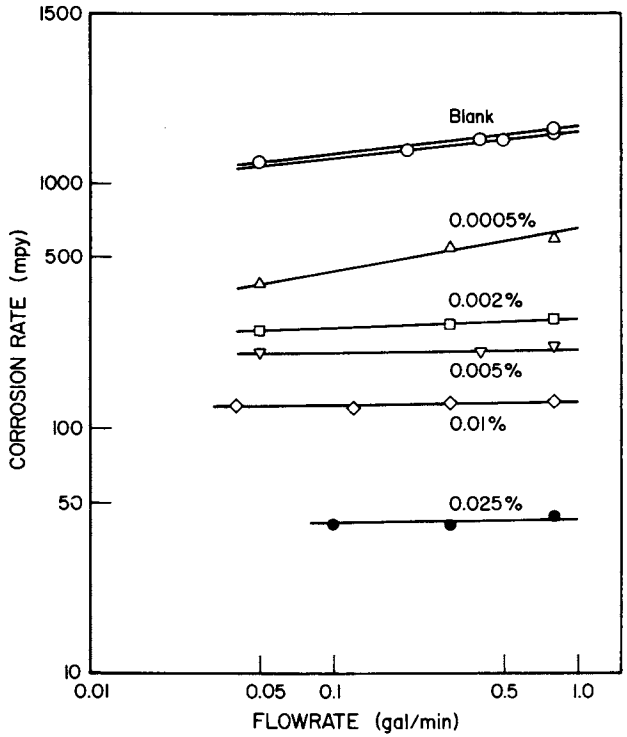

Figure 16. Corrosion of iron in 4N HCl, propargyl alcohol deaerated

In Corrosion Chemistry; Brubaker, G., et al.;
ACS Symposium Series; American Chemical Society: Washington, DC, 1979.

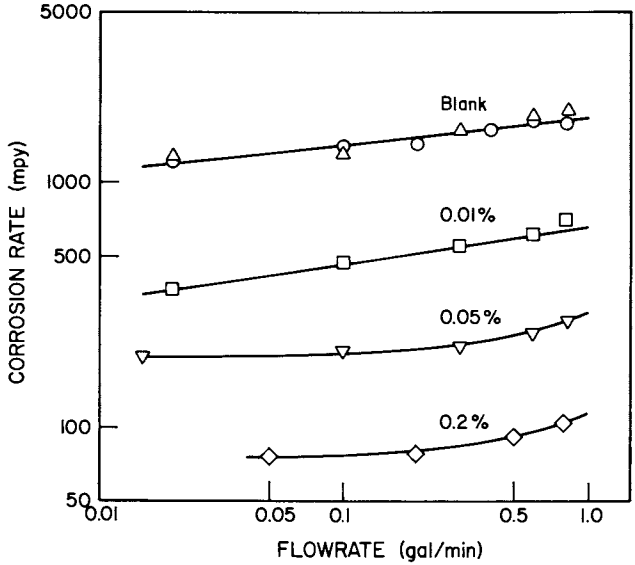

Figure 17. Corrosion of iron in 4N HCl, 2-butyne-1,4-diol deaerated

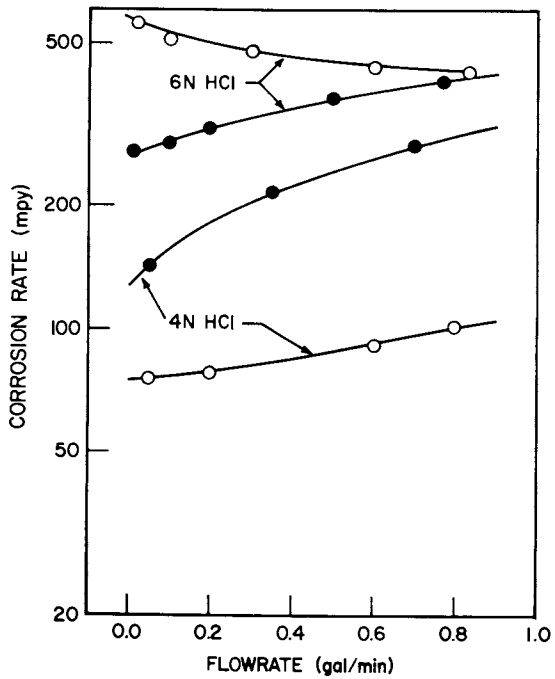

Figure 18. 2-Butyne-1,4-diol, 0.2%; (○) deaerated; (●) aerated

controlled by the thickness of this layer which, in turn, is dependent on the formation rate of the chelate as well as its dissolution rate. This suggested model is naturally based on a number of assumptions, such as a partially soluble chelate between the acetylenic inhibitor and iron, and a different chemistry of the 2-valent from the 3-valent chelate, in order to explain the oxygen effect. Since this chelate has a finite solubility and is constantly formed during the corrosion process, one can understand that in one instance its dissolution rate is rate determining, while in the other instance its formation rate maybe rate determining, the latter being controlled by the mass transfer of the inhibitor from the bulk of the solution to the surface of the metal. While many questions in this model have to be left open at this stage and await further investigation, the polarization behavior of an inhibited iron electrode may shed further light on the nature of the surface corrosion product layer and hence the interphase chemistry defined above. Fig.19 shows typical polarization curves obtained in 4N hydrochloric acid under aerated and deaerated conditions and with 0.5% propargyl alcohol (24). The results indicate the time dependence of the polarization curves as well as the dependence on scan rate. The blank corrosion rates, which can be seen to increase with time, are an indication of the progressively larger surface area. The anodic Tafel slopes are quite independent of scan rate while the cathodic Tafel slopes appear to increase slightly with faster scan rates. This last effect may be an indication of adsorption of a small impurity in the electrolyte. The inhibited corrosion rates decrease with time and become essentially constant after about two hours. These slopes are not dependent on scan rate or on corrosion rate. The most interesting effect is observed when the inhibited hydrochloric acid solution is aerated: the anodic Tafel slope increases while the cathodic Tafel slope decreases dramatically. As would have been expected from the resistance probe measurement the corrosion rate in the aerated inhibitor solution increases. These observations have been found to be of general nature in different hydrochloric acid as well as varying propargyl alcohol concentrations. While most of the observed effects in Fig.19 could be explained in terms of conventional electrochemical kinetics, the fact is that in the presence of oxygen and propargyl alcohol the cathodic curve shows a limiting current behavior and is rather difficult to understand. However, if one were to assume an iron - inhibitor chelate film

In Corrosion Chemistry; Brubaker, G., et al.;
ACS Symposium Series; American Chemical Society: Washington, DC, 1979.

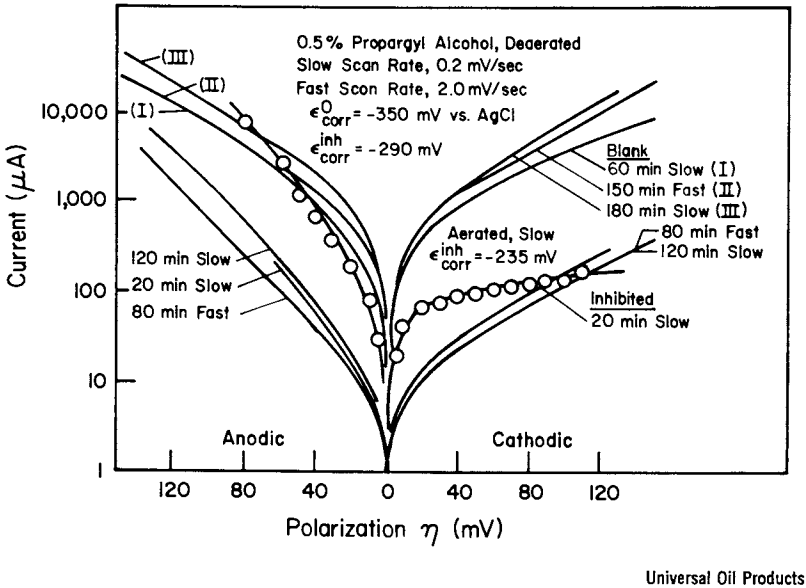

Figure 19. Corrosion of iron in 4N hydrocaloric acid, aerated and deaerated with propargyl alcohol as inhibitor

Table VI

METAL	PROTECTIVE COMPLEX	HYDRODYNAMIC BOUNDARY LAYER	BULK FLUID
$Fe \rightarrow Fe^{++} + 2e$		$2H^{+} + 2e \rightarrow H_2$	$C^{\circ}_{Fe^{++}}$
	$\gamma_{Fe^{++}} \Delta C_{Fe^{++}}$	$D_{Fe} \cdot \Delta C_{Fe}$	
	$\gamma_{e} \cdot \Delta C_{e}$ or		C°_{Inh}
		$D_{Inh} \cdot \Delta C_{Inh}$	
	$\gamma_{Fe_O} \cdot \Delta C_{Fe_O}$		
		$Fe^{++} + Inh \rightarrow \{FeInh\}$	
		$D_{\{\}} \cdot \Delta C_{\{\}}$	

on the surface of the metal, which is more soluble if the iron is in the three valent rather than the two valent state one, can readily understand that a cathodic current will be passivating while anodic current will progressively decrease inhibition.

There is therefore a certain amount of evidence indicating the build up of a discrete phase on the surface of the metal consisting most likely of a metal inhibitor-chelate structure. In order to further rationalize the model, Table 7 indicates the different processes and parameters which control the chemistry in this interphase. The iron oxidation takes place at the interface of the metal-chelate layer (protective complex). This then requires metal ions to migrate through the chelate layer. The mechanism which permits this process to take place is borrowed from semiconductive physics in postulating the existence of iron ion vacancies or excess iron ions in the chelate layer. Simultaneously, electron holes or free electrons have to be present to preserve the electroneutrality. The cathodic reaction may take place at the chelate-layer/hydrodynamic-boundary layer interface, or at the metal surface. Furthermore, at at the chelate layer/hydrodynamic-boundary layer interface iron ions react with the inhibitor to form the chelate. It is further assumed that the thickness of the chelate layer is rate controlling with respect to migration of charges through it. The thickness in turn is determined by the iron ion concentration and the inhibitor concentration gradient through the hydrodynamic-boundary layer. Thus one can readily understand, at least qualitatively how a very complex superposition of mass transfer rates in the hydrodynamic-boundary layer and charge transfer rates in the chelate layer combine to generate the above discussed results. Taking furthermore into consideration that the chemistry of the chelate layer is dependent on the valence state of iron, one can understand the effect of oxygen. While at this stage, this model is perhaps only a rationale for the above discussed effects, it is considered a more useful model than the old and antiquated adsorption theories, leading to new diagnostic experiments.

Corrosion Inhibition In The Presence Of Hydrogen Sulfide

Introduction. The need for corrosion protection in the presence of hydrogen sulfide arises most prominently in the petroleum industry, specifically pro-

duction of crude oil and the refining of it. The process streams in these fundamental operations are characterized in that they consist of an aqueous and a hydrocarbon phase in various proportions. Although the corrosion is caused by the aqueous phase and its constituents, corrosion inhibitors used in this industry are both water and hydrocarbon soluble. It is interesting to note that the hydrocarbon soluble corrosion inhibitors have in the past given the best results and their use is still predominant, a recent NACE survey not withstanding.

The importance of the use of corrosion inhibitors in the petroleum industry as a whole can be gauged by recent literature and patent reviews (29,30 and 31). There are basically two types of oil soluble inhibitors which have played a predominant role, these are fatty acids and fatty amines. It is a confusing feature of the voluminous patent literature that, for obvious reasons, no distinction is made with respect to the specific use of these two classes of inhibitors. Nevertheless, one finds that the fatty amines are predominantly used in hydrogen sulfide containing media while the fatty acids have found application as corrosion inhibitors in media containing oxygen and carbon dioxide but no hydrogen sulfide. Since the reality of industrial systems hardly ever fits such neat classifications, it is not surprizing that commercial inhibitors are often mixtures or salts of fatty amines and fatty acids, and that claims of synergism are often found.

Both fatty amines and fatty acids are known to be surface active, that is they adsorb on metal surfaces thereby forming a hydrophobous film which forms a water impenetrable barrier. Keeping water molecules away from the metal interphase by a thin film of fatty amines would reduce the oxydation of the metal. This simple mechanism has lead to the term "filming amines" as a generic descriptor for this group of corrosion inhibitors. The experimental evidence for this simple concept can be seen in the practice of periodic inhibitor application resulting in good corrosion inhibition over extended periods of time. For instance, in the oil field, better results are obtained by treating subsurface equipment such as insert pumps, oil well tubing and sucker rods periodically with a certain quantity of "filming amine" inhibitor, rather than using such compounds on a continuous basis. Many studies have been published detailing the frequency of the treatment as well as the quantity of inhibitor used per treatment as a function of oil well parameters (32

In Corrosion Chemistry; Brubaker, G., et al.;
ACS Symposium Series; American Chemical Society: Washington, DC, 1979.

and 33). However, if one looks at a subsurface structure which was pulled from an oil well, one finds that the surface is not only hydrophobic but looks black instead of metallic, as one might expect from laboratory experiments. This has subsequently led to the idea that the "filming amine" inhibitor is not adsorbed on the metal surface but on an iron sulfide film covering the metal surface. While the result of a hydrophobic surface is the same, the latter concept leads to a more rigorous discussion of the inhibition mechanism and avoids some of the confusion which has been generated by diagnostic tests which were based on surface activity or wetting angle measurements performed on a clean metal surface.

The proof of the importance of iron sulfide in the interaction between the corrosion inhibitor and the metal surface was brought in 1970 when it was shown (34) that corrosion inhibition was considerably enhanced and prolonged when the corrosion inhibitor was adsorbed on a presulfided specimen rather than on the nonsulfided surface. These measurements were made electrochemically and gave support to the practical well-known fact that periodic "filming" could inhibit the corrosion for relatively long periods of time.

In order to understand the iron sulfide-inhibitor interaction, it will be necessary to review briefly the corrosion mechanism of iron in the presence of hydrogen sulfide in a two-phase medium.

Corrosion Of Iron In The Presence Of Hydrogen Sulfide

It has been known for a long time that iron corroding in the presence of hydrogen sulfide will be covered by an iron sulfide film. One would therefore have expected that this film somehow affects the kinetics of the corrosion process. Sardisco and coworkers (35) carried out classical investigations of the corrosion kinetics of iron as a function of the partial pressure of hydrogen sulfide and carbon dioxide. The authors measured the overall kinetics of the corrosion as well as the rate of iron sulfide film formation and came to some conclusions with respect to the protectiveness of the iron sulfide film. The results, however, were rather confusing and could not be fitted into conventional rate theory.

If in fact the iron sulfide building up on the surface of the metal represents a resistance to the corrosion processes, then one would expect that the corrosion rate decreases as the iron sulfide film increases. In other words the corrosion kinetics would

In Corrosion Chemistry; Brubaker, G., et al.;
ACS Symposium Series; American Chemical Society: Washington, DC, 1979.

not be linear (constant corrosion rate) but parabolic (linearity between the corrosion rate and the square root of time).

It was shown, however, that the parabolicity of sulfide corrosion is extremely sensitive to the presence of minute quantities of oxygen. It is believed that many of the earlier results may have been affected by the incomplete elimination of air from the corrosive medium or its inadvertent presence.

Careful measurements of the corrosion rate in the presence of hydrogen sulfide under rigorous exclusion of air showed almost perfect parabolic corrosion kinetics, indicating the rate controlling factor of an iron sulfide film (36). It was subsequently also shown in (37) that minute quantities of oxygen, as little as 400 ppm in the gas phase in equilibrium with the corrosive media, accelerate the corrosion rate from 5 to 10 times resulting in essentially linear corrosion kinetics. Further studies (38) indicated that the thickness of the rate controlling iron sulfide film becomes constant although the total iron sulfide scale maybe much larger than that. This was confirmed by electrochemical measurements over long periods of time. By actually weighing the amount of iron sulfide built up on the corroding specimen as a function of pH and oxygen concentration (38), it was shown that the "protectiveness" of the rate controlling iron sulfide film increases with increasing pH and decreases with increasing oxygen concentration. However, the concentration of dissolved sulfidic sulfur has essentially no effect on iron sulfide film in the region of 1500 to 25,000 ppm (37).

A most surprising behavior was found when the polarization current of a corroding specimen was observed as a function of flow rate. Fig.20 shows the results which were obtained. Anodic and cathodic polarization currents in milliamps at potentials of $\pm$ 50 millivolts from the corrosion potential are plotted against flow rate. In several runs reproducible behavior was observed. The cathodic current varies with flow rate to the $\frac{1}{5}$ th power, while the anodic current varies with flow rate to the $\frac{1}{11}$ th power. This relationship holds true over more than one decade of flow rates. It is very difficult to explain such results in terms of conventional mass transfer limitations. It is well known that the diffusion limited current varies approximately proportionally to the flow rate in the turbulent region and with the square root of flow rate in the laminar region. If on the other hand the polarization current was transport limited across the corrosion

In Corrosion Chemistry; Brubaker, G., et al.;
ACS Symposium Series; American Chemical Society: Washington, DC, 1979.

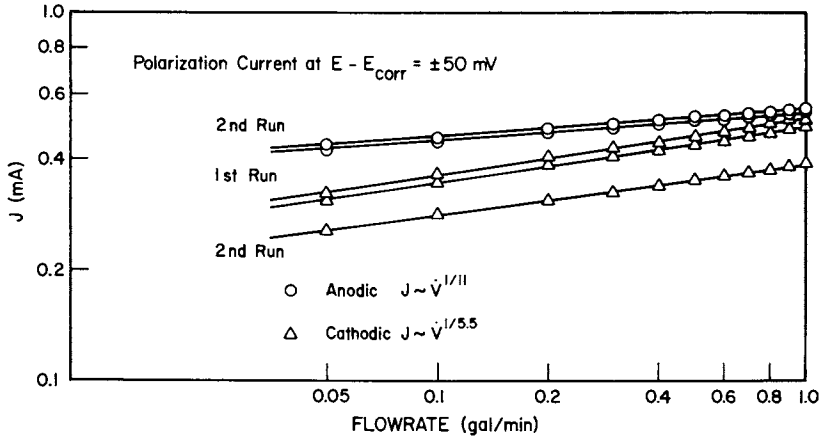

Figure 20. Iron corroding in H_2S containing medium

Table VIII

METAL	SCALE	LIQUID
Corrosion:	$Fe \rightarrow Fe^{++} + 2e$	$H_2S \rightleftharpoons Fe_O'' + 2\oplus + FeS + H_2$
		$2H^+ \rightleftharpoons H_2 + 2\oplus$
		$\{H_2S + 1/2\ O_2 \rightleftharpoons H_2O + S^= + 2\oplus\}$
	$2e + 2\oplus \rightarrow \epsilon$	
	$Fe^{++} + Fe_O'' \rightarrow \epsilon$	
	Solid State Transfer	Liquid Transfer
	$\frac{\partial(Fe_O'')}{\partial x}$	$D_{H^+}\frac{dC_{H^+}}{\delta}$
	$\frac{\partial(\oplus)}{\partial x}$	$\{D_{O_2}\frac{dC_{O_2}}{\delta}$

In Corrosion Chemistry; Brubaker, G., et al.;
ACS Symposium Series; American Chemical Society: Washington, DC, 1979.

product layer, no dependency on flow rate should be found.

It is therefore necessary to postulate a more complex mechanism, such as is suggested in Table 8. Since the corroding metal is covered by a corrosion product layer, the following reactions have to take place at the metal/scale interface: a. oxidation of iron; b. the consumption of electron holes by electrons (or possibly discharge of protons with subsequent solution of hydrogen in the metal); c. the combination of iron ion vacancies with newly formed iron ions. The latter two processes take place with the release of energy. These reactions necessitate a concentration gradient through the corrosion product layer of iron ion vacancies and electron holes. (It is understood that the mechanism could be written in terms of iron ions moving interstitially, in which case the scale would be an electron conductor. This mechanism seems less likely however). Since the corrosion process takes place with formation of iron sulfide the following reactions have to take place at the scale liquid interface: a. formation of iron sulfide and iron ion vacancies; b. discharge of protons to form hydrogen and electron holes; c. if oxygen is present, the electron holes can be formed by reduction of oxygen. The formation of hydrogen from protons also necessitates a proton concentration gradient in the liquid phase (if oxygen is present, the corresponding oxygen concentration gradient would have to exist as well). The reactions taking place at the scale liquid interphase can be visualized as equilibrium reactions. This means that the sulfide concentration influences the iron ion vacancy concentration in the scale, and the proton concentration in the liquid affects the electron hole concentration in the scale. Since the nature of the scale determines the rate of the solid state transfer phenomena, and the flow rate determines the liquid boundary layer concentration gradient, hence the liquid-solid interfacial proton, H_2S and oxygen concentrations, it follows that liquid and solid state mass and charge transfer are linked together by the chemical equilibria established at the scale-liquid interface.

An attempt was made to formulate these relationships analytically, in order to confirm the dependence of corrosion rate on flow rate observed in Fig.20. Thus equation 23 restates the formation of iron ion vacancies and electron holes at the scale/liquid interface.

$$H_2S \xrightarrow{K_1} Fe''_{\square} + 2\,\oplus + FeS + H_2 \qquad (23)$$

In Corrosion Chemistry; Brubaker, G., et al.;
ACS Symposium Series; American Chemical Society: Washington, DC, 1979.

$$2H^+ \xrightarrow{K_2} 2H_\delta + Fe'' \qquad (24)$$

$$2(Fe''_\square) = (H_\delta) + (\oplus) \qquad (25)$$

It is also assumed, following Simkovich (39), that protons can dissolve interstitially in the iron sulfide lattice (equation 24). The requirement for electroneutrality in the iron sulfide lattice leads to equation 25. Assuming the ratio of hydrogen partial pressure to hydrogen sulfide partial pressure to be constant, equations 23 through 25 can be rearranged to:

$$\frac{2\,K_1^*}{(\oplus)^3} = 1 + \sqrt{\frac{K_2}{K_1}}\,(H^+) \qquad (26)$$

and

$$(\oplus)^3 = \frac{1}{A + B\,(H^+)} \qquad (27)$$

indicating the cube of the electron hole concentation to be inversely proportional to the proton concentration. According to Bennett and Meyers (40) the mass flux accross the liquid boundary layer can be formulated as follows:

$$i_{cath} = N_{H^+} = K_3\,(C_H^\circ - C_{H^+})\,Re_L^{\frac{1}{2}} \cdot (Sc)^{1/3} = K_4\,(C_H^\circ{}^+ - C_{H^+})\,(Um)^{\frac{1}{2}} \qquad (28)$$

where $(C_H^\circ{}^+ - C_{H^+})$ = Proton gradient in liquid boundary layer
Re_L = Reynolds number
Sc = Schmitt number
Um = Average flow velocity
K_4 = combined constants

Since in the system investigated only the linear velocity changes, all other variables and constants are lumped together in K_4. Assuming now that the electronic conductivity of the scale is the limiting factor rather than the ionic one, the cathodic current can be set to be proportional to the electron hole concentration times the electron hole mobility:

$$i_{cath} = \gamma_\oplus \cdot (\oplus) \qquad (29)$$

Substituting equation 27 into equation 29

In Corrosion Chemistry; Brubaker, G., et al.;
ACS Symposium Series; American Chemical Society: Washington, DC, 1979.

$$(i_{cath})^3 = \gamma_{\oplus}^3 \frac{1}{A+B(H^+)} \qquad (30)$$

and finally with equation 28 one obtains

$$(i_{cath})^3 = \frac{K_4 \cdot U_m^{1/2}}{CU_m^{1/2} - B\, i_{cath}} \qquad (31)$$

It is difficult to estimate all the constants in quation 31 in order to arrive at a quantitative evaluation. However, since the current increases with increasing mean velocity, it might be said the effects nearly cancel in the denominator of equation 31. This would mean that indeed the cathodic current becomes almost proportional to the mean velocity with the 1/6 power. Even though this argument is not strictly quantitative, it still suggests a reasonable explantion for the rather unusual mass transfer effect observed in Fig.20. The above rationale applies only to the cathodic current, however, a similar derivation can be used to calculate the anodic current dependence on flow rate.

Inhibitor Interaction With The Iron Sulfide Surface

Since protons are discharged in the corrosion process, and since these protons are furnished from the corrosive medium, there must exist some mechanism for proton adsorption on the iron sulfide surface. It is reasonable to assume that on the iron sulfide surface there are sulfide groups, the valences of which are not totally neutralized by iron molecules. These partially neutralized sulfide centers can adsorb protons. This leads to the postulation of a protonated iron sulfide surface group: $-\text{FeS}\!-\!\!-\!\text{H}$. This surface group facilitates the discharge of hydrogen according to equation 32.

$$2\,\{\text{FeS} - \text{H}\} - 2\oplus \rightleftharpoons 2\,\{\text{Fe-S}^-\} + \text{H}_2 \qquad (32)$$

where:

$\oplus$ = electron hole; positive charge

In order to stop the corrosion process this reaction has to be impeded. This can be achieved if the proton adsorbed on the surface containing the iron sulfide species is replaced by a cation, the reduction of which is not as easily accomplished as the reduction of the proton. It is suggested that the alkyl ammonium

In Corrosion Chemistry; Brubaker, G., et al.;
ACS Symposium Series; American Chemical Society: Washington, DC, 1979.

ion can displace the proton via an ion exchange mechanism described in equation 33, the equilibrium constant of this reaction being designated as K_4:

$$\{FeS\text{-}H\} + RNH_3^+ \overset{K_4}{\rightleftharpoons} \{FeS\text{-}RNH_3\} + H^+ \quad (33)$$

where:

$\{FeS\text{-}RNH_3\}$ = surface complex

It should be noted that this is not a simple adsorption of the alkyl ammonium ion on the surface of the iron sulfide but can be considered as an ionic reaction in which a proton is being set free. It is now reasonable to consider the factors which may influence the concentration of the surface complex formed from iron sulfide and the alkyl ammonium ion. Going through a simple series of equilibrium calculations, it is found that the concentration of the surface complex equals the product of a series of equilibrium constants times the proton concentration of the medium, as shown in equation 34.

$$(\{FeS\text{-}RNH_3\}) = K_4 \cdot K_1 \cdot K_2 \cdot (H^+) \cdot C_N \cdot C_S \quad (34)$$

where:

K_4 = formation constant
K_1 = dissociation constant of surface FeS-H
K_2 = dissociation constant of amine
(H^+) = proton concentration
C_N = concentration of amine
C_S = concentration of surface-sulfide

$$\{Fe\text{-}S^-\} + \{Fe\text{-}SH\}$$

The two main factors which affect the concentration of the surface complex are its formation constant K_4 and the pH. The latter has been shown to be true experimentally (Table 9).

Chemistry Of Corrosion Inhibitors. There are two questions which arise with respect to K_4. These are

1. How can the formation constant of the surface complex be increased?
2. Why isn't the adsorption process reversible?

That is to say, why do small concentrations of amine (0.25 ppm) lead to large surface coverage and consequently large inhibitor efficiency?

Although water molecules do not appear in Equation 34, it is nevertheless reasonable to assume that

In Corrosion Chemistry; Brubaker, G., et al.;
ACS Symposium Series; American Chemical Society: Washington, DC, 1979.

Table IX

Concentration in ppm for 90-95% Protection

Inhibitor	pH 4.2-4.5	pH 6-6.5	pH 7-7.2
Armand	2.5	10-15	20
Kathy	2.5-3	10	20
Norman	3-4	7-10	20
Dora Talbot	0.3-0.5	10-15	20
Peter E.	0.2	n.a.	n.a.
Conny E.	0.25-0.5	2	5
Teddy E.	0.2-0.3	2	2-3

the iron sulfide surface is covered with a layer or more of water molecules, because the proton adsorbed on the surface iron sulfide has a tendency to dissociate and, therefore, needs to be solvated. The free alkyl ammonium ion and its counter ion, e.g., a bisulfide ion, are both solvated by water. In the adsorption step an electronically neutral surface complex is formed. Thus, a proton solvated by water and its counter ion, the bisulfide ion, are set free. The essentially neutral surface complex, does not require solvation and because of its hydrophobic nature will have a tendency to displace water molecules from the iron sulfide surface. Since the desorption process would again require solvation of the iron sulfide surface, it can no longer take place because water molecules are permanently displaced from the surface by the hydrophobic nature of the surface complex. As a consequence it can be predicted that an inhibitor with a higher lipophilic character will be more permanently adsorbed.

It is known that amines become more lipophilic, or water insoluble, with increasing alkyl chain length. Thus water soluble amines such as morpholine (Table10) show no inhibition efficiency at these small concentrations because their adsorption is as easy as their desorption.

In Corrosion Chemistry; Brubaker, G., et al.;
ACS Symposium Series; American Chemical Society: Washington, DC, 1979.

Table X

Effectiveness of Various Alkyl Propylenediamines and Water Soluble Amines as Process Corrosion Inhibitors

Conditions: Toluene-Water, Saturated with H_2S
200 ppm Cl^-
70°C
Carbon Steel, linear velocity 7 ft/sec

Tallow Propylenediamine		C_{15} Alkyl Propylenediamine		C_{11} Alkyl Propylenediamine		Morpholine	
Concentration ppm	Protection %	Concentration ppm	Protection %	Concentration ppm	Protection %	Concentration ppm	Protection %
0.062	0	0.5	30	0.5	0	5	0
0.125	56	1	100	2	81	10	0
0.25	97			5	97		
0.5	99						
0.75	100						

In Corrosion Chemistry; Brubaker, G., et al.;
ACS Symposium Series; American Chemical Society: Washington, DC, 1979.

Table 10 also shows a comparison between different propylenediamine derivatives with decreasing molecular weight. A tallow propylenediamine (C_{18}) which has been proposed as a process corrosion inhibitor in the literature many times, is a very efficient material. As the molecular weight decreases due to a reduction of the alkyl chain length to 15 C-atoms and 11 C-atoms the corrosion inhibiting tendency decreases gradually. This would have been expected because the water solubility of these compounds increases with decreasing alkyl chain length.

Yet another way to vary the formation constant of the surface complex is to change the number of amine groups in the molecule. One of the first process corrosion inhibitors proposed in the literature was oleylamine. As has been shown in (37), oleylamine is quite effective in the range of 3-4 ppm. The tallow propylenediamine derivative which has about the same molecular weight is, however, at least ten times as active as oleylamine.

This concept represents a new theory for the action of process corrosion inhibitors. In contrast to the old filming amine theory the new one is based on a specific adsorption mechanism involving an ion exchange step. It can correctly predict the decrease of protection efficiency with increasing pH. It also explains structural differences between inhibitors such as increased efficiency of propylenediamine derivatives over primary amines and decreased efficiency with decreasing molecular weight of the amine group compound.

Literature Cited

1. Annand, R.R., Hurd, R.M., Hackerman, N., J. Electrochem. Soc., 112, 138, (1965).
   Parsons, R., 3rd European Symposium on Corr. Inhib., Ferrara, Italy, 1970, Proceedings p. 3 (1971).
2. Wagner, C., Traud, W., Z. Electrochemie 44 391 (1938).
3. Kaesche, H., Die Korrosion der Metalle, Springer Verlag, Berlin 1966, p. 68.
4. Fischer, H., 3rd European Symposium on Corr. Inhib., Ferrara, Italy, 1970 Proceedings, p. 16(1971).
5. Nathan, C., Corrosion Inhibitors, National Association of Corrosion Engineers, Houston, Texas, 1973, c.f. Riggs, O.L. p. 7.
6. Vetter, K., Electrochemical Kinetics, Academic Press, New York, London, 1967.

In Corrosion Chemistry; Brubaker, G., et al.;
ACS Symposium Series; American Chemical Society: Washington, DC, 1979.

7. Hackerman, N., Corrosion/74, National Meeting of the NACE, Chicago, Ill., paper 73,(1974).
8. Nobe, K., Hussein, N., Corrosion/73, Annual Meeting NACE, paper #26 (1973).
9. Stern, M., J. Electrochem. Soc. 102 609 (1955).
10. Mansfeld, F., Corrosion, 32 (4) 143 (1976).
11. Hausler, R.,., Corrosion, 33 (4) 117 (1977).
12. Hoar, T.P., Holliday, R.D. J. Appl. Chem. 3 502 (1953).
13. Kaesche, H., Hackerman, N., J. Electrochem. Soc. 105, 4, (1958).
14. Elze, J., Fischer, H., J. Electrochem. Soc. 99, 259 (1952).
15. Kaesche, H., Z. Electrochemie 63, 492 (1959).
16. Hoar, T.P., Pittsburgh Intern. Conf. Surface Reactions, p. 127, Pittsburgh Corrosion Publications Company (1948).
17. Bartonicek, R., Proc. 3rd Internat'l Congr. on Mettallic Corrosion, Moscow, 1966 Vol. 1 p. 119 (1969).
18. Kolotyrkin, Y.,., Trans. Faraday Soc. 55, 455 (1959).
19. Ross, T.K., Jones, D.H., J. Applied Chem. 12, 317 (1962).
20. Tedeschi, R., Proceedings of the 25th Conference, NACE, March, 1969, p. 173, (1970).
21. Tedeschi, R., National Conference NACE, Annaheim Calif. 1973, paper #24.
22. Tedeschi, R., Corrosion, 31 (4) 130, (1975).
23. Poling, G.W., J. Electrochem. Soc. Vol. 114, 1209 (1967).
24. Hausler, R.H., Corrosion, 33 (4) 119 (1977).
25. Gardner, G., Corrosion Inhibitors, C. Nathan editor, National Assoc. Corrosion Engineers, Houston, Texas (1973).
26. Parsons, R., Advances in Electrochemistry and Electrochem. Eng. Vol. 1, ed. Delahay p. 65 Interscience, New York, (1961).
27. Delahay, P., Double Layer and Electrode Kinetics, Wiley, New York, (1965).
28. Bockris, M., Modern Electrochemistry, Plenum Press (1972).
29. Ranney, M.W., Corrosion Inhibitors, Manufacture and Technology, Noyes Data Corporation, Park Ridge, N.J. (1976).
30. Bregman, J.I., Corrosion Inhibitors, The Mac Millan Co., New York, N.Y., p. 198 (1963).
31. Nathan, C., Corrosion Inhibitors, National Assoc. Corr. Engineers, Houston, Texas, 1973 c.f.p.42

In Corrosion Chemistry; Brubaker, G., et al.;
ACS Symposium Series; American Chemical Society: Washington, DC, 1979.

32. Larrison, K.L., Use of Polarization Data In the Field Evaluation of Oil Well Corrosion Treatment, paper presented at the NACE South Central Region, Conference, Oct. 18, 1966.
33. Frank, W.J., The Oil and Gas Journal May 31, p. 63 (1976).
34. Hausler, R.H., Proceedings 3rd. European Symposium Corr. Inhibitors, Ferrara, Italy, (1970) p.399 (1971).
35. Sardisco, T.B., Corrosion 19 354 (1963), Corrosion 21 69 (1965).
36. Hausler, R.H., Materials Performance, 13, (9), 16 (1974).
37. Hausler, R.H., et.al., Corrosion/74, Annual NACE Meeting, Chicago, Ill., paper #123 (1974).
38. Hausler, R.H., NACE Annual Meeting, Philadelphia P.A., paper #63 (1970).
39. Simkovich, G., et.al. paper 12-69, 34th Midyear Meeting API, Div. Refining, Chicago, Ill. May 12, (1969).
40. Bennet, C.O., Meyers, J.E., Momentum, Heat and Mass Transfer, McGraw Hill Publishing Co.,(1975).

RECEIVED September 1, 1978.

10

Stress-Corrosion Cracking

J. C. SCULLY

Department of Metallurgy, University of Leeds, Leeds LS2 9JT, England

Stress corrosion cracking is the phenomenon by which alloys fail by cracking when simultaneously stressed and exposed to certain environments. Failures occur at stress levels well below that which would cause failure in air. While the application of the stress may be multi-axial, it is necessary for it to have a tensile component and cracking will usually occur perpendicularly to it. Stress corrosion cracking represents the most highly localized form of corrosion that is ever encountered.

While the discussion in this chapter is confined to metallic alloys, stress corrosion cracking is part of a larger range of phenomena, since similar failures occur in nonmetallic materials, e.g., glass in H_2O, organic polymers in polar solvents, alumina in H_2O. Furthermore, while most of the discussion is confined to alloys cracking in aqueous environments, similar cracking in some alloys occurs in organic liquids, steam, dry gases and in both liquid and solid metals. The amount of corrosive may be quite small. Failures have been caused, for example, by the perspiration residue of a single fingerprint. Within the confines of a short chapter, it is not possible to discuss every example of such failures. The descriptions below are confined mainly to stress corrosion cracking in aqueous media.

As an industrial problem stress corrosion cracking is of considerable importance. There is a long history of major and minor failures, particularly in the chemical industry and in the transport industry, particularly of components in ships and planes. It is a major potential source of failure in the nuclear power industry in which, for example, austenitic stainless steels may fail in high purity water containing oxygen and chloride ions at the level of ppb.

0-8412-0471-3/79/47-089-321$07.50/0

A large amount of research effort has been devoted to the subject and the published literature is quite immense. Many conferences have been held. Anyone concerned to learn more about the subject can find his way by taking (1,2,3,4,5) as a starting point.

There comes a point with most technological problems when sufficient is known about a subject to enable predictions to be made. These may be made possible by a fundamental understanding of the problem or by the development of empirical relationships which have been discerned without an a priori understanding. To the practising metal user either background is acceptable provided that it gives sufficient predictive capacity with which to avoid or at least reduce the incidence of failures. This stage has not been reached with stress corrosion cracking. A lot is known about the problem but it is not always possible to know with certainty when or even whether a failure will occur. It is hoped to show below why this uncertainty exists. It must also be added that the method of testing becomes important. This, too, is therefore discussed.

In this chapter some general remarks are made about the problem. This is followed by a detailed discussion of mechanisms, and at the end preventative measures are indicated.

General Features of Stress Corrosion Cracking

Stress corrosion cracking is a complicated subject. Unless that is emphasized at the beginning, then the fine details of phenomenological and mechanistic factors will not be appreciated. In order to gain some understanding of stress corrosion cracking, it is necessary to realize that three different disciplines are at work in any stress corrosion situation. These are physical metallurgy, electrochemistry and fracture mechanics.

Physical Metallurgy. All commerical metal components are polycrystalline and all metal lattices contain both point and line faults. Heat treatable alloys frequently contain precipitates which may be very small (< 5 pm dia). All alloys contain major alloying elements but they contain also a range of nondeliberate elements, both metallic and nonmetallic in nature. It is possible to show that all these factors, as well as surface finish, residual cold work and metallurgical history (what was done to the alloy in bringing the component to its present shape) may have an effect on

In Corrosion Chemistry; Brubaker, G., et al.;
ACS Symposium Series; American Chemical Society: Washington, DC, 1979.

stress corrosion cracking, making an alloy more susceptible or less. Different batches of one alloy, both meeting the same alloy specification may exhibit markedly different levels of susceptibility, which is merely to say that specifications, embodying as they do ranges of alloying elements acceptable to the industry, arise usually from processing and manufacturing considerations, and not from stress corrosion considerations. A lack of appreciation of such points, with which a metallurgist will usually be conversant, can cause much frustration and bewilderment to nonmetallurgists. Grain size is of importance, an alloy generally becoming more susceptible as the size is increased. Grain shape is also of importance. After a manufacturing process during which grain growth occurs in one direction more than in another, susceptibility in one direction of a component may be greater in one direction then in another. Such considerations come under the general heading of texture. Plastic deformation increases the density of dislocations and these may play an important role in crack propagation. For heat treatable alloys that suffer from stress corrosion, susceptibility is usually increased by increasing the strength. Finally, the path of a crack may be transgranular or intergrandular. In some alloys it is predominently one, in others mixed, in other dependent upon the environment or the level of stress. Observations in crack path provide information about the mechanisms since they indicate the relative importance of stress, chemistry, alloy composition, etc.

Electrochemistry. In aqueous solutions containing dissolved, charged species, electrochemical reactions occur on metal surfaces and the rates at which they occur will affect the susceptibility of an alloy to stress corrosion cracking. The most important variable is the corrosion potential of the specimen, arising from polarization of the separate anode and cathode reactions to a common value. Changes in potential will always affect stress corrosion reactions. Conductivity, pH, O_2 levels, solution composition and temperature are also important.

Fracture Mechanics. The manner in which a specimen is stressed may affect stress corrosion susceptibility. A condition of plane strain, achieved when the specimen thickness is above a certain value which is related to its strength (5), may sometimes promote greater susceptibility than is observed in specimens below that thickness. Crack branching can sometimes be

In Corrosion Chemistry; Brubaker, G., et al.;
ACS Symposium Series; American Chemical Society: Washington, DC, 1979.

predicted from consideration of strain energy release rate (2). The sharpness of cracks (notch root radius) is important. Blunt cracks can be expected to propagate less readily than sharp cracks. Crack or notch depth is also important from the viewpoint of stress concentration. The application of a critical flaw depth criterion is sometimes attempted. Loading mode is also critical, being the relation between the directions of applied stress and the plane of cracking.

Systems of Stress Corrosion Cracking

Stress corrosion cracking is often described as arising between an alloy and a specific environment. Failures of α-brass in ammoniacal solutions would be a typical example. However, it has become increasingly clear in recent years that, for any given alloy, stress corrosion cracking can occur in more than one environment. The specific aspect of the corrodent is therefore no longer true. Nevertheless, only a small number of corrodents cause stress corrosion in any alloy. What needs to be explained is what property or action of a corrodent is necessary to promote stress corrosion. An attempt to answer this question is made below in the discussion on mechanisms. With these reservations, a list of stress corrosion cracking systems (alloy + corrodent) is given in Table I, which is not intended to be complete, merely to indicate the more commonly observed types of failures.

Testing for Stress Corrosion Susceptibility

Most stress corrosion service failures occur from the influence of residual stresses. These arise during component manufacture, and plant assembly, including welding. In laboratory work the stress is usually applied externally since it is then much easier to control and measure. The oldest and simplest test is to measure how long a specimen takes to break -- the time-to-failure, t_f. Typical specimens might be loaded in tension and surrounded by the corrodent or bent into a U, clamped and then immersed. Typically, the value t varies as shown in Figure 1. Two points can be made. First, the t_f changes less markedly at stresses above the 0.1% proof stress than below it. Secondly, it is not always clear whether a threshold stress exists below which stress corrosion failures will not occur. This is of obvious importance but it has proved a

In Corrosion Chemistry; Brubaker, G., et al.;
ACS Symposium Series; American Chemical Society: Washington, DC, 1979.

Table I Alloy/Environment Systems Exhibiting Stress Corrosion Cracking

Alloy	Environment
Mild steel	Hot nitrate, hydroxide, and carbonate/bicarbonate solutions
High strength steels	Aqueous electrolytes, particularly when containing H_2S
Austenitic stainless steels	Hot, conc. chloride solutions, chloride-contaminated steam
High Ni alloys	High purity steam
α-brass	Ammoniacal solutions
Al alloys	Aqueous, Cl^-, Br^- and I^- solutions
Ti alloys	Aqueous Cl^-, Br^- and I^- solutions; organic liquids, N_2O_4
Mg alloys	Aqueous Cl^-/CrO_4^{2-} solutions
Zr alloys	Aqueous Cl^- solutions; organic liquids, I @ 350°C

difficult point to establish. Some stress corrosion systems have such a threshold, others do not. The point is further discussed below.

In examining all the metallurgical and electrochemical variables that together determine susceptibility, the measurement of t_f is not altogether satisfactory since changes in t_f can arise for two different reasons. Time-to-failure is made up of two components, the time for the crack to initiate (t_i) and the time for it to propagate (t_p) so that

$$t_i + t_p = t_f \quad (1)$$

Whether the effect of a changed variable on t_f arises from alterations to t_i or t_p may be of fundamental significance and it is therefore important under some circumstances to distinguish such an effect between the components of t_f. It might be supposed that t_i is of greater consequence than t_p (a) because it is frequently the case that $t_i >> t_p$, and (b) because it would seem self-evident that what cannot initiate cannot propagate. In practice, however, such considerations are too simple. It is generally well recognized that engineering structures composed of a number of metal components always contain a multiplicity of surface cracks and flaws. These arise during fabrication and assembly. If any of these is an incipient stress corrosion crack, the considerations of initiation are unimportant because they are irrelevant. What then becomes important is whether the crack will propagate and at what rate.

Such considerations have given rise to the use of precracked notched specimens, like those that are used in measuring a metallurgical factor known as Fracture Toughness (5). The dimensions of such specimens are determined by considerations of Fracture Mechanics. This approach tends to be limited to high strength alloys since these often have mechanical properties that are closest to the ideal required and because of their engineering importance. The type of specimem employed takes into account the stress concentration arising from the presence of a crack in a specimen and employs a measured component K, the stress intensity factor, which is obtained from the applied stress $\sigma \times c^{1/2}$, where c is the crack depth. It has units $MN \cdot m^{-3/2}$. If such specimens are now tested as a function of time-to-failure, the results obtained are of the kind shown in Figure 2. Again, the question arises of a threshold which is such specimens is termed K_{Iscc} where the subscript I refers to the loading mode(5). The whole term represents that value of K below

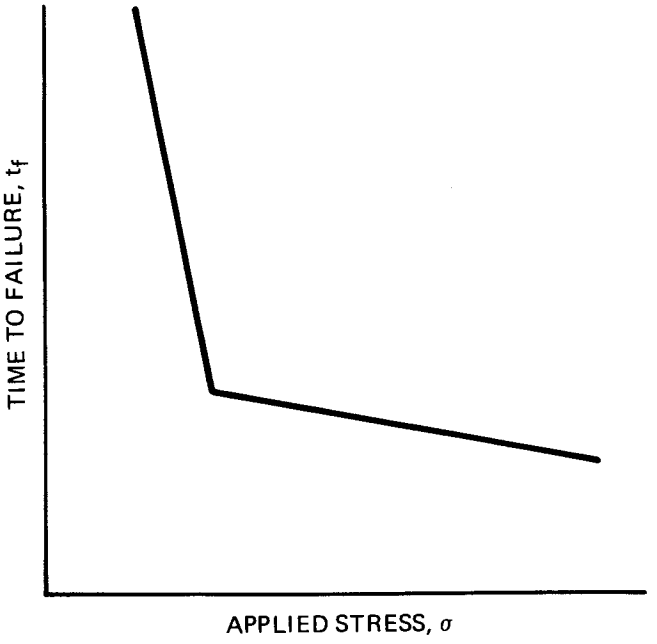

Figure 1. Relationships between time-to-failure (t_f) and applied stress (σ) commonly observed in stress-corrosion cracking

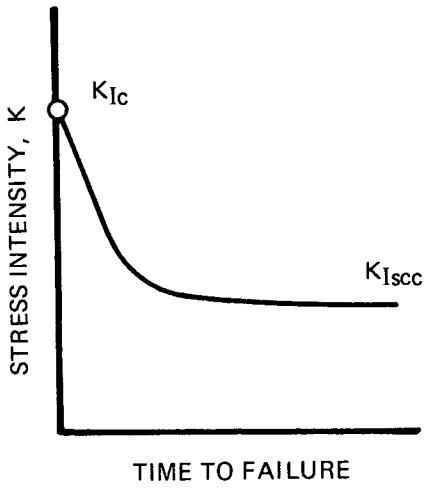

Figure 2. Relationship between t_f and initial value of stress intensity factor (K)

which failure does not occur. Since the initiation time is very small in relation to t_f (the reverse of the type of experiment to which Figure 1 applies), this test gives a good indication of stress corrosion crack propagation resistance. The ratio of K_{Iscc} to K_{Ic} (the fracture toughness in air) is a useful ratio of relative susceptibility. For Ti alloys, for example, it varies between 0.2-0.9, which could be said to describe alloys that are very susceptible to those that are scarcely susceptible.

Since this type of test is mainly concerned with propagation, attention was subsequently focused upon measuring velocity v as a function of K. A general schematic picture of results obtained is shown in Figure 3. A maximum of 3 stages of cracking may be observed. Stage I (the extent of which will be determined by the difference between K_{Iscc} and the K value at the Stage I/II transition) shows a logarithmic dependence of crack velocity v upon K. For Al and Ti alloys an activation energy for this stage of 112 $kJ \cdot mol^{-1}$ has been determined (2). Stage II, sometimes referred to as the plateau velocity, is generally interpreted as being caused by the chemical or electrochemical reaction at the crack tip being limited by diffusion of a critical reactant or product within the solution. The idea is supported by observations (2) that increasing the solution viscosity lowers the plateau velocity. An example of this is shown in Figure 4 (2). An activation energy of 12-21 $kJ \cdot mol^{-1}$ for this region has been obtained both for Al and Ti alloys. Stage III is rarely observed and arises mainly for mechanical reasons. For many alloys, therefore, Figure 3 would consist of Stages I and II only.

This type of experimental data has been of considerable value. It has become possible to examine all the major variables, one at a time, for their effect upon crack velocity. As a result, it becomes possible, if required, to determine in detail the effect of minute variations in composition, changes in heat treatment, electrochemical variables and changes to the environment. Typical examples are shown in Figures 5, 6, and 7 (2).

When such data are available, they can be used in alloy selection. Stress corrosion situations cannot always be avoided. Under such circumstances alloys which have a low plateau maximum velocity can be chosen in preference to alloys with a high plateau velocity under circumstances where the same alloys are metallurgically equivalent or interchangeable. Examples of this have been given in the literature (5).

In Corrosion Chemistry; Brubaker, G., et al.;
ACS Symposium Series; American Chemical Society: Washington, DC, 1979.

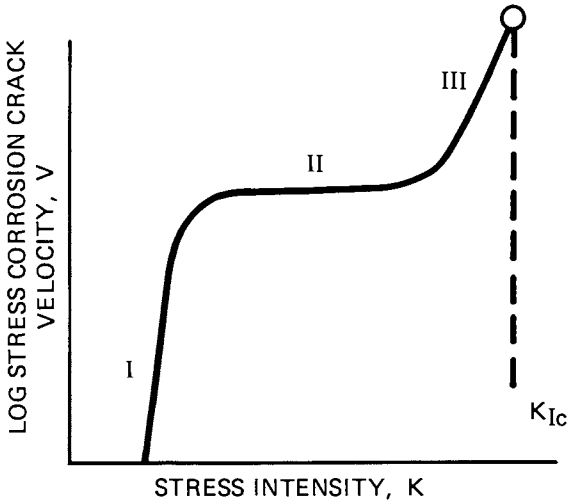

Figure 3. General relationship between stress-corrosion-crack velocity (v) and stress intensity factor (K)

In Corrosion Chemistry; Brubaker, G., et al.;
ACS Symposium Series; American Chemical Society: Washington, DC, 1979.

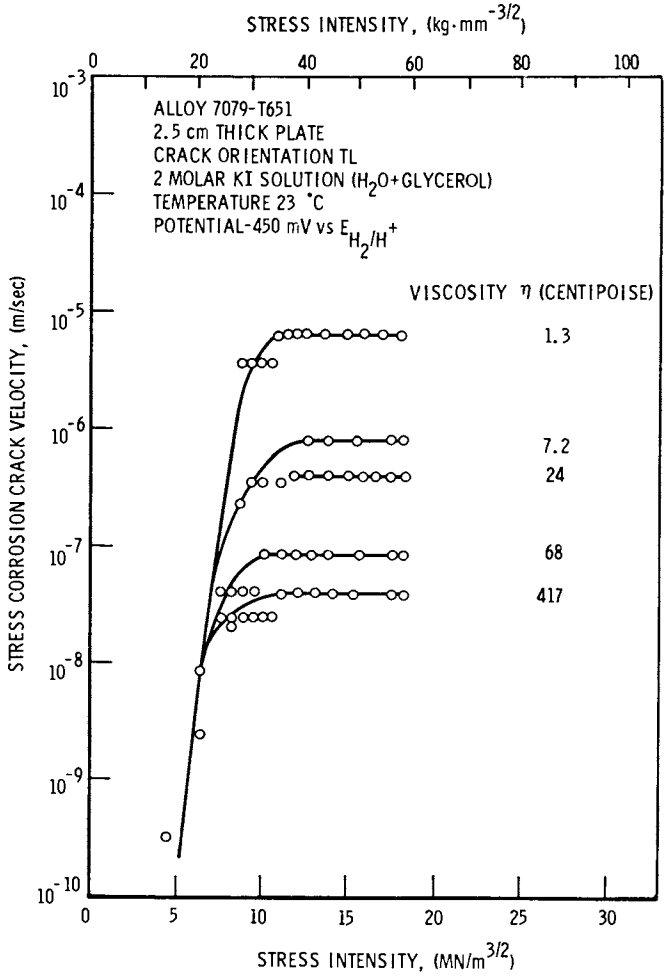

Figure 4. The effect of solution viscosity upon the log v:K relationship of an aluminium alloy (2)

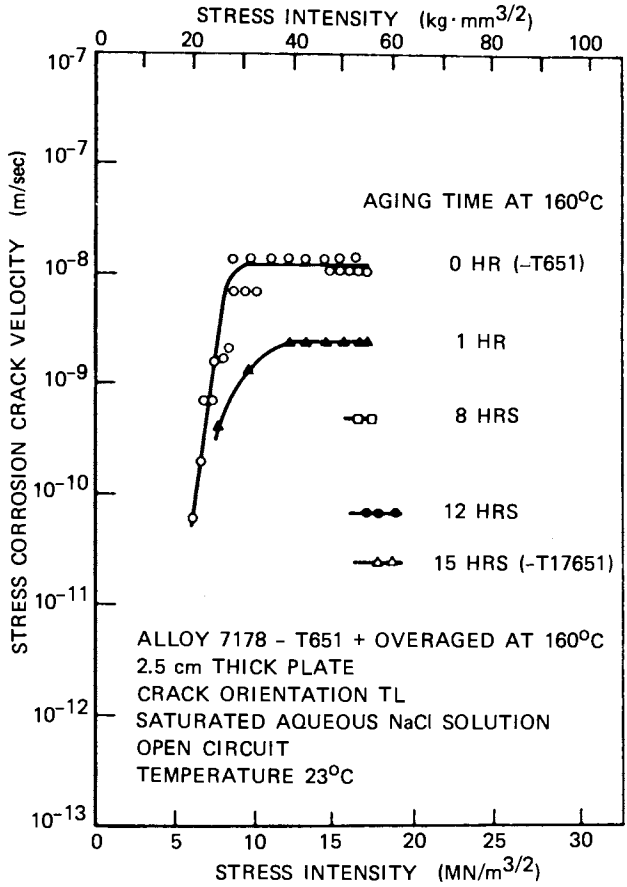

Figure 5. Effect of overaging on stress-corrosion-crack velocity in an aluminum alloy (2)

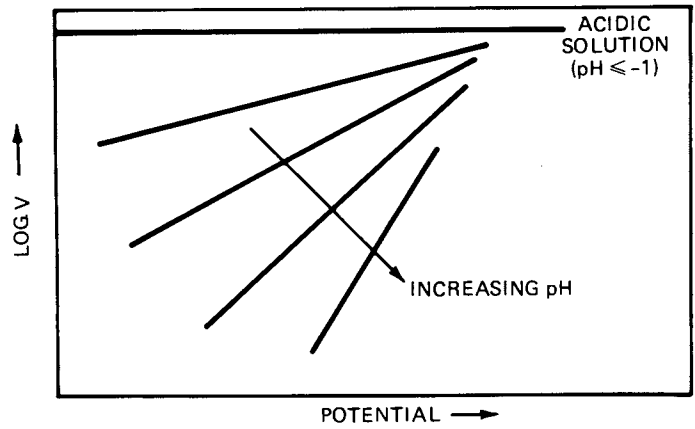

Figure 6. Schematic of the influence of pH on stress-corrosion-crack velocity in titanium alloys (2)

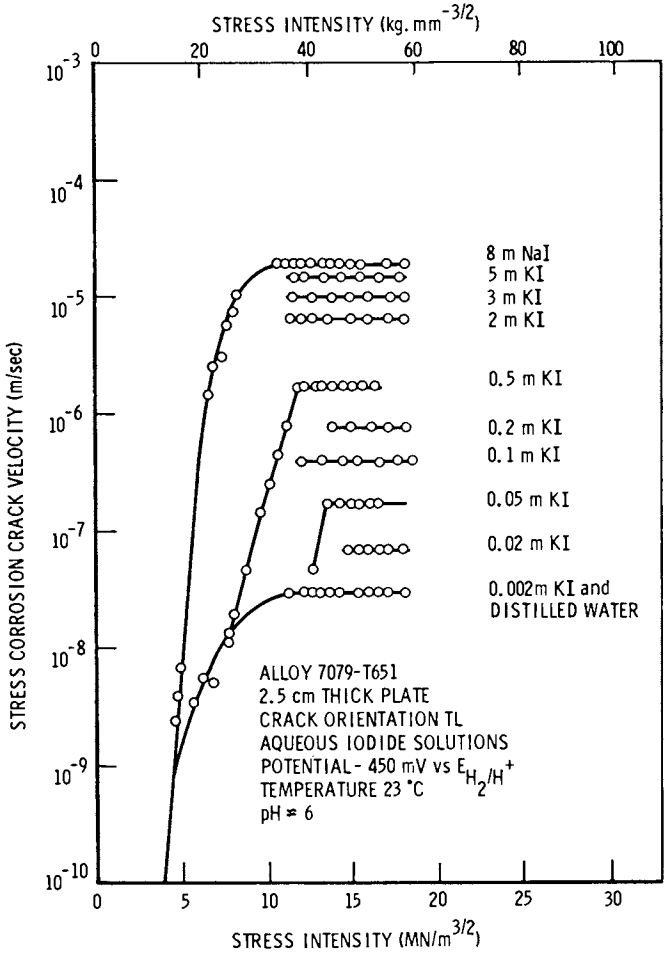

Figure 7. Effect of solution concentration upon stress-corrosion-crack velocity in an aluminum alloy (2)

The Importance of Repassivation

In many of the alloy systems shown in Table I, the stable configuration of the alloy surface is that it is filmed. Many of the alloys, e.g., stainless steels, Al, Ti, Zr and Mg alloys are only usable in such a condition. Such a consideration applies not only to these alloys covered with a thin passive film but also to those on which relatively thick films are formed. The possible mechanisms by which stress corrosion cracking occurs are concerned with reactions between unfilmed metal and the environment. Before consideration of these it is necessary to consider how these various types of film break down initially. While many of the alloys exhibit pitting, it is not necessary for pitting as such to precede crack propagation. Pitting is associated with static unstressed metals whereas cracking is associated with a metal whose surface is stressed. The application of a stress creates a surface strain-rate (or creep strain-rate, since it is very low). Of fundamental importance is the interaction of the deforming surface and the reactions on the metal surface. The subject is not a simple one, but the main points can best be envisaged by attempting to draw the repetitive segment of events occurring at a crack tip or at the base of a surface flaw. This is attempted in Figure 8. The application of a stress creates a slip step which breaks the passive film which is in equilibrium with the solution. There is abundant experimental evidence that such events take place (e.g., 6). The slip step height will usually be very much greater than the film thickness and the film is usually relatively brittle. Both these would appear to be necessary conditions for the situation depicted in Figure 8. After film fracture, reaction then occurs between the newly created metal surface and the environment. The specific type of reaction will be considered below since it is the important process that determines crack propagation. But the time available for this reaction to occur will be determined by the repair time of the film, commonly referred to as the repassivation time (7). As soon as the film fractures, it will start to reform since the equilibrium condition of the surface is that it is filmed. It has been argued (7) that the delay in repassivation is of crucial importance. If repassivation occurs too rapidly, there will not have been time for enough reaction to occur to cause an increment of crack growth. If repassivation occurs too slowly, then too much reaction may have occurred, giving rise to crack blunting and pitting.

In Corrosion Chemistry; Brubaker, G., et al.;
ACS Symposium Series; American Chemical Society: Washington, DC, 1979.

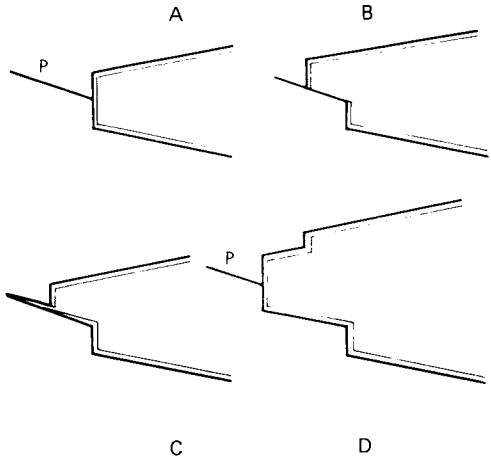

Figure 8. Schematic of the sequence of events occurring at the tip of a propagating stress-corrosion crack. The film is fractured (B) and immediately starts to repair (C) while dissolution is occurring. Complete repassivation occurs at D by which time the crack has extended.

In Corrosion Chemistry; Brubaker, G., et al.;
ACS Symposium Series; American Chemical Society: Washington, DC, 1979.

The important factor is the repassivation time since it determines for how long the metal and environment can react together.

Figure 8 can be considered in a more general sense. The plastic deformation that creates the slip step can be considered as a strain-rate that, in the most general way, is creating new, unfilmed, metal surface. It will be governed by mechanical and metallurgical factors. The process that causes film formation is electrochemical and it will be dependent upon the potential and all other electrochemical factors. It is possible to consider that stress corrosion cracking occurs when there is a critical imbalance between these two rate processes -- one creating fresh metal area, the other filming that area. Thus, the situation depicted schematically in Figure 8 is not merely that of a film broken by an emergent slip step since that could be expected, and is indeed observed, of nonsusceptible alloys and metals in environments that are known not to cause stress corrosion cracking. What is envisaged in Figure 8 is a particular set of circumstances in which passivation is delayed for a narrow range of time intervals.

A good example of the importance of repassivation is shown in Figure 9 (8). A titanium alloy, Ti-5 Al-2.5 Sn, in the form of tensile specimens is strained dynamically in two different solutions. In aqueous NaCl solution Ti does not corrode and repassivation can be expected to occur. At high crosshead speeds the test is over in a very short time and there is no time for crack initiation. A fracture is observed fractographically with the elongation to fracture ε_f and the texture the same as in air. At lower crosshead speeds stress corrosion crack propagation occurs with a consequent reduction in ε_f and characteristic cleavage fractography. At the lowest crosshead speeds the relatively slow strain-rate induced on the surface is such that repassivation predominates over cracking and no crack propagation occurs. Fractographically, air fracture is seen and ε_f is high. Thus, in the aqueous solution cracking is confined to a narrow range of speeds. This behavior can be contrasted with that observed for the same alloy exposed to a CH_3OH + 1 vol. % conc HCl mixture which is corrosive to Ti and in which, therefore, no repassivation might be expected. At high crosshead speeds the same behavior is seen as that observed in the aqueous solution. At the lowest crosshead speeds, however, because no repassivation is possible, cracking is observed and because the test takes increasingly long times as the crosshead speed is

In Corrosion Chemistry; Brubaker, G., et al.;
ACS Symposium Series; American Chemical Society: Washington, DC, 1979.

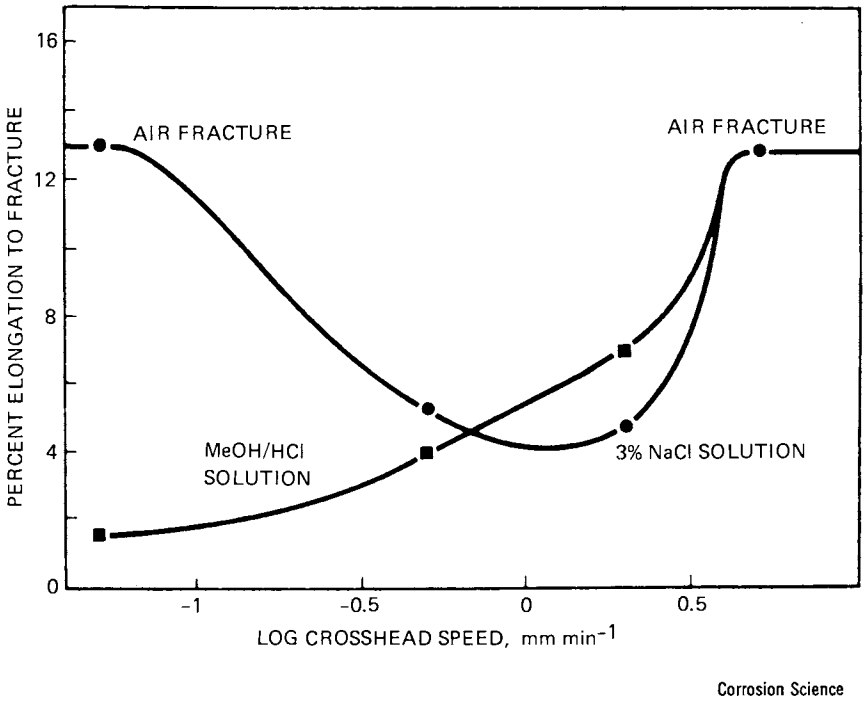

Figure 9. The relationship between elongation-to-failure (ϵ_f) and crosshead speed for a Ti–5Al–2.5Sn alloy exposed to (1) aqueous NaCl, and (2) a CH_3OH/HCl mixture (8)

lowered, the ε_f falls continually. It can be expected that the crack velocity would fall until it became similar to the corrosion rate of the unstressed alloy which, in this example, is selectively intergranular. In the CH_3OH solution no K_{Iscc} or any other threshold can be anticipated and it is not found. In the aqueous solution a K_{Iscc} can be expected, corresponding to that value of K that results in so low a surface strain-rate that repassivation can occur. This strain-rate has been characterized $\dot{\varepsilon}_r$ (9). K_{Iscc} is commonly observed in Ti alloys exposed to aqueous chloride solutions. From Figure 9 and all that has been described, it can be appreciated that K_{Iscc} is not a material constant. For a given alloy it varies according to the environment in which it is measured. It is not an alloy that has a threshold; it is the alloy + environment which may exhibit one.

The type of experiment encompassed in Figure 9 has become increasingly important as a method of testing. The conditions are severe, the tests are rapid and the imposed conditions of a slow strain-rate are similar to those occurring at a crack tip. For reasons discussed below, experiments should be done potentiostatically. A recent conference (10) was devoted to the constant extension rate test, organized by A.S.T.M.

The importance of repassivation and the interaction of this process with a straining metal surface probably constitutes the essense of many stress corrosion cracking mechanisms. Since repassivation is an electrochemical phenomenon, it might be expected that the necessary imbalance to achieve stress corrosion, referred to above, will occur only over a narrow range of potential, corresponding to a narrow range of repassivation rates. Such rates can be expected to change markedly in those regions of potential where the passive range changes to a pitting range or to an active range, i.e., where the film is changing from being the stable surface configuration to where it is an unstable configuration. The zones of potential where cracking might be expected are shown in Figure 10. There are examples in the literature of cracking occurring in such regions (2). The site of these regions depends upon a number of electrochemical factors. Stress corrosion failure occurs under open-circuit conditions when the corrosion potential of an alloy lies within the potential range for cracking of that alloy in the particular environment. Systems described in Table I fall into this category. It must be emphasized that under controlled potential conditions stress corrosion failure may occur in alloys exposed to

In Corrosion Chemistry; Brubaker, G., et al.;
ACS Symposium Series; American Chemical Society: Washington, DC, 1979.

environments which do not cause failure under open circuit conditions. α-brass fails in ammonia under open circuit conditions, as is indicated in Table I. When anodically polarized, it also cracks in nitrate and sulfate solutions. Thus, the uniqueness of ammonia lies only in its ability to cause cracking under open circuit conditions under a wide range of solution pH conditions (other solutions, e.g., tartrate solutions, can also cause cracking over a narrow range of pH). This type of observation applies to other systems too and its importance cannot be exaggerated. It has a bearing both on mechanistic ivestigations and on testing proceudres. It is foolish to test only under open circuit conditions since, if cracking occurs in a potential range not including the open circuit potential, susceptibility will be missed in laboratory conditions. If in service use the open circuit potential moves into the cracking range, cracking will occur. This may appear to be a simple point, but such problems do arise and cause confusion. Testing should always be done over a range of potential larger than that likely to be encountered in service under the most extreme conditions.

Repassivation processes have become an important subject in stress corrosion studies and also in other forms of corrosion, e.g., pitting corrosion and corrosion fatigue. A range of scratching and straining electrode techniques have been employed. While it is not possible to go into detail, the results have to be examined in relation to the techniques employed, e.g., has repassivation started before the scratching or straining has stopped? It is important also to know whether the current measured under potentiostatic conditions is a complete anode current or the difference between an anode current and a cathode current (most commonly due to H^+ ion reduction). Typical repassivation rates correspond to an equation (11) of the type:

$$i - i_0 = (i_1 - i_0)t^{-b} \qquad (2)$$

where i = current after time t, i_0 = current after complete repassivation, i_1 = current after one second and b is a constant. The constant b varies with potential. Under certain condition (11) the relationships is given by

$$i = i_{max}\exp(-\beta t) \qquad (3)$$

In Corrosion Chemistry; Brubaker, G., et al.;
ACS Symposium Series; American Chemical Society: Washington, DC, 1979.

where β is a constant, and i_{max} is the initial maximum value of the current after destruction of the film. When a film is broken, the initial monolayer adsorbs within 20-50 ms (12). The measured current is made up partly of dissolution and partly of film formation, the ratio between them falling with time.

Stress Corrosion Mechanisms

The circumstances under which the film is broken and repaired have been described at length since they control the subsequent reaction time during which the crack actually grows. It has been strongly emphasized since unless this point is understood confusion can arise because the alteration of an experimental variable, e.g., potential or pH, may have a greater effect on repassivation then on the cracking reaction. Unless that possibility is appreciated, ambiguity in interpretation is likely to arise on occasion. An example is given below with respect to the effect of cathodic polarization on stress corrosion cracking of Ti alloys in aqueous chloride solutions. It is a general point and is not often emphasized.

The Mechanism of Cracking

Why does cracking occur? This is the most difficult question to answer. Many explanations have been put forward and with stress corrosion cracking occurring in so many alloys it is not unlikely that some very specific points apply here and there. An example might be the action of voluminous corrosion product in wedging open a crack for which there is evidence in isolated cases. Overriding many such tiny phenomenological points, cracking mechanisms can be divided into (1) active path, (2) hydrogen embrittlement, (3) stress sorption and (4) corrosion film fracture.

It is now intended to discuss the essential features of these mechanisms. It must be emphasized that these are general categories and much subdivision is possible, particularly in the case of hydrogen embrittlement. There is no reason that cracking should not occur by a mechanism that traverses more than one of the above, e.g., a combination of anodic dissolution and hydrogen embrittlement. These four categories are in no way exclusive from each other.

Active Path. Since the term stress corrosion cracking implies corrosion, it is not surprising that the first mechanism ever proposed was that cracking

In Corrosion Chemistry; Brubaker, G., et al.;
ACS Symposium Series; American Chemical Society: Washington, DC, 1979.

occurred by preferential dissolution over a narrow preferred front along a path that was pre-existing (13). This was probably true for the particular system being investigated, but since cracking occurs in alloys which most certainly do not have a pre-existing path, more recent ideas have attempted to explain the localized corrosion by a process involving repassivation of the crack sides, thus concentrating the current at the tip where various forms of directional localized dissolution occurs. The possible preferential corrosion of dislocations piled up at the crack tip as a result of the acting stress has been considered at length over many years. The strain energy associated with such pile-ups of dislocations provides little additional driving force for dissolution (14). As a result attention has focused on minute compositional changes in a metal lattice occurring around dislocation pile-ups which may cause significant directional differences in dissolution on an atomistic scale (15). These ideas were originally associated with electron microscope observations of the edges of electropolished thin foils where regions of dislocation pile-ups showed. very directional dissolution (16). Such processes give rise to unusual morphological effects (17) and may cause tunnel corrosion (18).

At some stage it is necessary to know whether the current flowing is sufficient to account for the maximun velocity of the crack, a requirement sometimes referred to as 'faradaic equivalence'. From the application of Faraday's laws and assuming that dissolution accounts for 100% of the crack propagation then:

$$v = \frac{J}{F\rho} i \qquad (4)$$

where v = crack velocity, J - chemical equivalent, F = the Faraday, ρ = alloy density and i = dissolution current density.

For a number of stress corrosion cracking systems, e.g., mild steel, austenitic stainless steels, measured bare surface current densities appear to be of the right order of magnitude (3). For other alloys, e.g., Ti alloys, in which the crack velocities are very much higher than in steels, much higher current densities are required, of the order required for electrochemical machining. Their existence has been claimed (2).

Reference to Figure 8, together with the concept of repassivation, indicates during the propagation of cracks the current should consist of a number of successive transients. One is shown in Figure 11, which might be taken to correspond to the sequence of events

In Corrosion Chemistry; Brubaker, G., et al.;
ACS Symposium Series; American Chemical Society: Washington, DC, 1979.

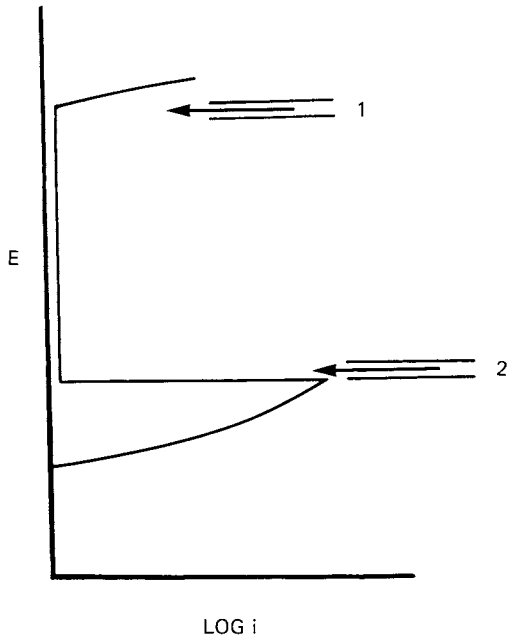

Figure 10. Schematic polarization curve for an alloy exhibiting passivity and pitting. Two zones are indicated where stress-corrosion cracking might be expected to occur.

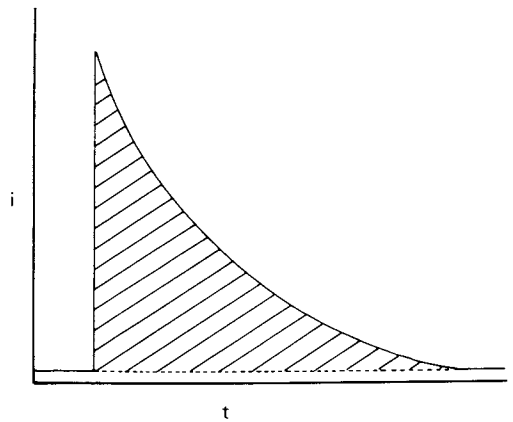

Figure 11. A general schematic of the current transient during the sequence of events drawn in Figure 8. The hatched area represents the total charge flowing.

In Corrosion Chemistry; Brubaker, G., et al.;
ACS Symposium Series; American Chemical Society: Washington, DC, 1979.

described in Figure 8. What is important is the total amount of corrosion, represented by the charge, which is hatched in Figure 11. It has been argued (9) that stress corrosion crack propagation occurs as a result of the passage of a constant charge Q_{min}, which then initiates the next increment of crack growth. Crack arrest occurs if repassivation occurs before Q_{min} has passed. From such considerations, with integration of the appropriate repassivation rate equation over the time limits between successive slip step events, it has been possible to derive the shape of the corrosion current: time curves of Stages I and II shown in Figure 3 (9).

Hydrogen Embrittlement. At the crack tip in many alloys local acidity and low potentials ensure that hydrogen ion discharge occurs. This is true for Al, Ti, Zr alloys and for stainless and high strength plain carbon steels and also for Mg alloys in which the crack tip solution is alkaline. The question is whether any of these alloys crack as a result of H adsorption which occurs after neutralizaton has occurred

$$H^+ + e = H_{ads} \quad (5)$$

and before desorption has occurred by either

$$H_{ads} + H^+ + e = H_2 \quad (6)$$

or

$$H_{ads} + H_{ads} = H_2 \quad (7)$$

in acidic solutions and the equivalent reactions appropriate for alkaline solutions in the case of Mg alloys. Some proportion of H_{ads} will be absorbed by the alloy in any situation. An important ratio is H (absorbed/ H (evolved) and this is likely to be very sensitive to cathodic poisons in the solution and to certain elements within the alloy. Cracking in Al and Ti alloys and in high strength steels is accelerated by the presence of cathodic poisons. This is very strong evidence that H plays a role in the cracking process.

After entering the metal it may collect inside traps and cause decohesion. It may combine around inclusions and cause local regions of very high pressure, resulting in blistering and possibly even fissioning. In Ti and Zr alloys it may form hydrides which interact with the lattice, promoting cleavage by impeding

In Corrosion Chemistry; Brubaker, G., et al.;
ACS Symposium Series; American Chemical Society: Washington, DC, 1979.

the movement of dislocations. The effects of H on the mechanical properties of metals is a very complex subject and no attempt has been made other than to indicate several possible general effects. Another area of some difficulty is that the diffusion rates of H often appear to be too slow to account for the observed crack propagation rates. The reconciling of these contrary observations calls for considerable care.

Stress Sorption. This mechanism supposes that the reaction between a species in the environment and the metal atoms at the crack tip can cause a redistribution of electrons in the orbits of the atoms so that the bond between them is weakened (19). It is not possible to cite experimental data that would support this concept for the fracture of metals although the absence may merely reflect the difficulties of obtaining such data.

Corrosion Film Fracture. At various times it has been suggested that the fracture of corrosion product films at the crack tip with their subsequent reformation constitutes the main forward movement of the crack. The evidence for such a mechanism is not terribly clear. Thick film formed on steels and brasses, for example, may form by precipitation from solution rather than by direct corrosion of the metal to a solid compound. Where this occurs, the initial dissolution that precedes the precipitation would appear to fit into the active path category. If fracture of the precipitated film is necessary, then it becomes a matter of choice whether this constitutes a separate category or a special case of the active path mechanism. For mild steel and brasses this type of explanation is commonly associated with intergranular cracking. What needs to be explained is why preferential corrosion of the grain boundary occurs. Often this is attributed to the presence within the grain boundary of an unidentified element in solid solution which alters the dissolution kinetics. It is a requirement that the film is sufficiently protective to reduce the reaction rate to an insignificant value so that its fracture is necessary for the crack propagating reaction to be reinitiated. On brass, for example, in ammoniacal solutions thick films form over a wide range of pH but it is only over a narrow range that this type of mechanism may apply (2), corresponding to the formation of a relatively protective film.

In Corrosion Chemistry; Brubaker, G., et al.;
ACS Symposium Series; American Chemical Society: Washington, DC, 1979.

Distinguishing between the various mechanisms and how they apply to various alloy systems is not an easy matter. It is difficult to design experiments that give clear unambiguous answers. Rather elementary points can be made in order to show some of the difficulties.

Anodic polarization will frequently shorten t_f and also raise the crack velocity to a maximum associated with the onset of simultaneous pit propagation. These effects are not necessarily evidence that an active path mechanism is operative. If the potential of the crack tip is such that H^+ ion discharge can occur then the greater ease of acidification at the crack tip as a result of the application of anodic polarization may increase the amount of hydrogen absorption and thereby increase the crack velocity if a hydrogen embrittlement mechanism is operative. Conversely, anodic polarization when applied to brass results in a lower crack velocity in neutral solutions (20) when the potential is raised into the region where the film that forms under open circuit conditions is unstable. The same current is thereby spread over a much wider area, giving rise to a much higher crack denisty. The crack velocity is therefore reduced. In this system an active path mechanism is operative, yet crack velocity is reduced by anodic polarization. Such contrary interpretations need not be confusing. They serve to underline that it is necessary to look closely at the consequences of a given experimental technique. This can be particularly important for workers attempting to interpret results obtained with one technique on two quite different alloys.

Cathodic polarization will generally shorten t_f for alloys that are susceptible to hydrogen embrittlement. This is not universally true, however. If cracking is occurring just below E_{pit} (Figure 10), then cathodic polarization will accelerate the repassivation process. This is not a case of cathodic protection lowering the corrosion potential to the equilibrium potential of the anode reaction. For Ti alloys the absorption of hydrogen occurs readily on unfilmed surfaces. On filmed surfaces hydrogen entry is very much reduced because the passive film has a low hydrogen permeability. Also, the passive film is not readily reduced cathodically. Thus, cathodic polarization of Ti alloys in neutral chloride solutions arrests crack propagation and prevents crack initiation even though the mechanism of cracking is that of hydrogen embrittlement. This is an example in

In Corrosion Chemistry; Brubaker, G., et al.;
ACS Symposium Series; American Chemical Society: Washington, DC, 1979.

which the role of the potential on the repassivation process is more important then its role on the mechanistic reaction occurring on the unfilmed metal surface. In very strong acid solutions, in which the film is unstable and repassivation will not therefore occur, cathodic polarization has no effect on crack velocity (21,2). Where an active path mechanism is operative, cathodic polarization will always lengthen t_f and lower the crack velocity, eventually causing crack arrest.

Some alloys exhibit reversible embrittlement, e.g., Mg (22), Al (23), Ti (24) and Zr (25) alloys. For each alloy, experiments have been done in which specimens were exposed unstressed, to solutions that can cause cracking, under a variety of conditions. If broken in air immediately after removal from the solution, specimens exhibited a low value of ε_f and fracture surfaces characteristic of stress corrosion cracking. If lapse of time occurs between removal from solution and stressing, specimens exhibited increased values of ε_f and decreased amounts of stress corrosion-type fracture with increasing length of lapse of time. This behavior is characteristic of hydrogen embrittlement fracture and has been interpreted as such for the four types of alloys described. These are simple but very clear experiments.

Preventative Measures

It is clearly important to know how to avoid, or at least minimize the incidence of the occurrence of such a widespread type of failure. The choices are relatively few in number and can be conveniently considered under the headings of the words that make up name of the problem.

Stress. From Figures 1 and 2 it has already been stated that stress corrosion cracking can be reduced or abolished altogether by reducing the stress level, depending upon whether the system exhibits a threshold stress or K value. In practice this may mean ensuring that components are stress relief annealed, e.g., brass tubes after drawing, or that welds are given post-weld heat treatements, since it is residual stress that is often the problem. To minimize failures in steel tube assemblies handling sour oil wells, for example, it is recommended that all welds be kept below a certain hardness level (26). The hardness can be measured in situ. Design can help in reducing operating stress levels also. Critical flaw depth has

In Corrosion Chemistry; Brubaker, G., et al.;
ACS Symposium Series; American Chemical Society: Washington, DC, 1979.

also been mentioned. Controlling flaw depth is easier to describe then to achieve but care should be taken to prevent large flaw depths, particularly where a K_{Iscc} level exists. There are examples of tanks being operated containing liquids that cause stress corrosion cracking with residual and operating stresses controlled so that K_{Iscc} is not exceeded. For high strength alloys overtempering or overaging will often give a much more acceptable life time at the cost of a lower alloy strength. Such considerations call for a balance between the requirements of the plant operator and the demands of the plant designer.

Corrosion. Reducing corrosion by the use of inhibitors will commonly reduce or even eliminate stress corrosion cracking, possibly by moving the corrosion potential outside the range of cracking. Sometimes these are referred to as dangerous inhibitors since, if this is their sole function, cracking will occur if the corrosion potential moves back into the cracking range. The contrast is made with safe inhibitors which reduce or prevent cracking even if the corrosion potential is in the cracking range. In practice the use of inhibitors of either category may be restricted by (1) solubility problems, (2) economic aspects and (3) practicality limits. Many failures occur in steam or under condensation conditions. In both of these cases the transport of inhibitors to sites of crack initiation is not feasible. With other systems, however, quite small additions or changes may eliminate problems, e.g., 1-2% H_2O to CH_3OH/HCl mixtures, using impure N_2O_4 rather than pure N_2O_4, both for Ti alloys. Cathodic protection may also achieve the same effect of a lowered corrosion rate. As with inhibitors its use is limited and for much the same reasons. Mention must be made of current stress corrosion cracking problems in gas trunk transmission lines in the U.S.A. and elsewhere. A number of failures have occurred in these lines as a result of certain carbonate/bicarbonate mixtures being generated in the alkaline liquid adjacent to the pipe by the application of cathodic protection (4). This is in no way an argument against the use of such a protection method. It is merely a warning about possible effects. These failures also underline some of the difficult technical/economic decisions attendant upon such failures. There are two quite different questions to be settled: (1) what can be done to reduce the incidence of cracking in existing pipelines? and (2) what can be done to reduce the possibility of cracking in pipelines to be installed in the future? Both technically and economically the

In Corrosion Chemistry; Brubaker, G., et al.;
ACS Symposium Series; American Chemical Society: Washington, DC, 1979.

questions pose a number of different problems. This is in some ways typical of all preventative measures. There are many factors to be considered before settling upon an acceptable solution.

The use of paintings and coatings must be mentioned. They are usually applied for other reasons -- to reduce the rate of general corrosion and the cost of cathodic protection. To the extent they are successful, they will frequently minimize the incidence of stress corrosion failures. Coatings always have faults in them and depending upon coatings alone is usually unwise. It is in their use with systems of cathodic protection that they are to be judged, together with ability to withstand service conditions, e.g., continual temperature fluctuations.

Increasing the corrosion rate might appear to be a rather drastic counter measure against stress corrosion cracking. Since it is a form of highly localized corrosion, extending corrosion over the whole of the surface will usually lessen the probability of such failures. This approach is unlikely ever to be a permanent remedy. It is employed in making up mixtures containing HCl to clean austenitic stainless steel parts in chemical plant: the corrosion rate is maintained > 10 mpy (27).

Cracking. Possible effects of plane stress/plane strain transitions have already been indicated. The effectiveness of the strain-rate in promoting cracking can be important where engineering structures are subject to periodic straining, e.g., pipelines. It is possible to have interrupted loading stress corrosion cracking in which case the stress combines to produce a strain transient that generates a crack increment. This is different from corrosion fatigue and the interface between the two has been discussed (28). Interrupted loading stress corrosion cracking can be of particular importance where the system exhibits a threshold under constant load laboratory testing conditions. A small fluctuation in load (±1-2%) can reduce the threshold by 50% (3). Unless laboratory tests simulate accurately service conditions, confusion and a lack of confidence are likely to ensue.

Since a tensile component of stress is required, stress corrosion cracking can be prevented by putting the surface of a component into compression, e.g., by short-peening. Where this is practicable, it is desirable. The treatment needs to be applied uniformly. It will not be effective if pitting occurs on the compressed layer.

In Corrosion Chemistry; Brubaker, G., et al.;
ACS Symposium Series; American Chemical Society: Washington, DC, 1979.

Cracking may be avoided by using a nonsusceptible or less susceptible alloy. This usually entails using a more expensive alloy or a greater volume of a lower strength alloy. From what has been discussed above, such a choice depends upon a reliable test having been made in the environment under consideration.

Concluding Remarks

Stress corrosion cracking is a complicated subject and it is necessary to be very careful in making simplifications. Certain points have been emphasized in the description presented above. The simple idea of an imbalance between creep strain-rate and repassivation rate does seem to be an accurate description of an essential process occurring during the propagation of a stress corrosion crack. To appreciate the subtleties of this interaction does require both a metallurgical and electrochemical approach. In this subject a dual approach is always required. To do accurate tests, potential control is necessary and the investigation of a range of potentials is always required. Commercial metallurgical alloys are complicated heterogeneous assemblies of atoms. Some of these heterogeneities are responsible for cracking.

Some points have been neglected because of the limitations of space and time. Why is the chloride ion so prevalent in Table I, for example? The answer almost certainly lies in its effect upon delaying repassivation as a result of metal ion hydrolysis and the low pH of many metal chlorides. In addition, it promotes the initial breakdown, probably in much the same way. With this and other points completely clear answers and explanations are not yet arrived at. Progress is being made, however, and eventually a good if not perfect, predictive capacity will be achieved over what remains a facinating and irritating phenomenon.

Literature Cited

1. Staehle, R.W., Forty, A.J. and Van Roogen, D., Editors, "Fundemental Aspects of Stress Corrosion Cracking," N.A.C.E., Houston, Texas, 1969.
2. Scully, J.C., Editor, "The Theory of Stress Corrosion Cracking in Alloys," N.A.T.O. Brussels, 1971.
3. McCright, R.D., Slater, J.E. and Staehle, R.W., Editors, "Stress Corrosion Cracking and Hydrogen Embrittlement of Iron Base Alloys," N.A.C.E.,

In Corrosion Chemistry; Brubaker, G., et al.;
ACS Symposium Series; American Chemical Society: Washington, DC, 1979.

4. Swann, P.R., Ford, F.P. and Westwood, A.R.C., "Mechanisms of Environment Sensitive Cracking of Materials," Metals Society, London, 1977.
5. Brown, B.F., Editor, "Stress Corrosion Cracking in High Strength Steels and in Titanium and Aluminium Alloys," N.R.L., Washington, D.C., 1972.
6. Engseth, P. and Scully, J.C., Corrosion Science (1975) 15, 504.
7. Scully, J.C., Corrosion (1975) 15, 505.
8. Scully, J.C. and Powell, D.T., Corrosion Science (1970) 10, 371.
9. Scully, J.C., Corrosion Science (1975) 15, 207.
10. Scully, J.C., "Stress Corrosion Cracking -- The Constant Strain Rate Technique," A.S.T.M., Philadelphia, in press.
11. Barbosa, M. and Scully, J.C., "Environment Sensitive Fracture of Engineering Materials," A.I.M.E., to be published.
12. Ambrose, J.R. and Kruger, J., Corrosion (1972) 28, 30.
13. "Symposium on Stress Corrosion Cracking of Metals," A.S.M./A.I.M.E., Philadephia, 1945.
14. Tromans, D. and Nutting, J., Corrosion (1965) 21, 146
15. Swann, P.R., Corrosion (1963) 19, 102.
16. Swann, P.R. and Nutting, J., J. Inst. Met. (1959/60) 80, 478.
17. Scamans, G. and Swann, P.R., Corrosion Science, in press.
18. Swann, P.R. and Embury, J.D., "High Strength Materials," Editor Zackey, V., Wiley, New York, 1965, p. 327.
19. Coleman, E.G., Weinstein, D. and Rostoker, W., Acta. Met. (1961) 9, 491.
20. Kermani, M. and Scully, J.C., Corrosion Science, in press.
21. Powell, D.T. and Scully, J.C., Corrosion (1968) 24, 151.
22. Chakrapani, D.G. and Pugh, E.N., 6th International Congress on Metallic Corrosion, N.A.C.E., Houston, to be published.
23. Scamans, G.M., Alani, R. and Swann, P.R., Corrosio ence (1976) 16, 443.
24. Adepoju, T. and Scully, J.C., Corrosion Science (1976) 16, 789.
25. Majumdar, P. and Scully, J.C., Corrosion Science, in press.
26. N.A.C.E. Standard RP-04-72.
27. Laque, F.L. and Copson, H.R., "The Corrosion Resistance of Metals and Alloys," Reinhold, New York, 1963, p. 392.
28. Parkins, R.N. and Greenwell, B.S., Met. Sci. (1977) 11, 405.

RECEIVED September 21, 1978.

11

Industrial Problems: Cooling Water and Cooling-Water Treatment

J. FRED WILKES

Consulting Chemical Engineer, 143 Seventh Avenue, La Grange, IL 60525

The ability to dissipate unwanted heat through cooling systems is vital to operation of power generating stations and most industrial or commercial installations. Open recirculating towers and closed cooling systems are assuming a steadily increasing proportion of utility and industrial cooling loads, as water shortages continue to limit availability of once-through cooling water sources.

Cooling water treatment programs all have similar objectives: 1) to maintain heat transfer efficiency. 2) To preserve operating efficiency of the overall system. 3) To prolong service life of equipment.

Protection of cooling system metals involves complex interrelated problems of scale and deposit prevention, control of microbiological growths and other fouling sources, in addition to corrosion mitigation by inhibitors. Corrosion control programs may be expected to vary considerably between systems, since each installation presents different environmental factors and operating problems which affect response.

Those of us who own or drive automobiles recognize the need for cooling systems to remove excess engine heat and maintain safe operating temperatures. Industrial cooling systems must accomplish similar jobs of heat rejection. They include many different types and mechanical designs. In a major refinery or chemical process plant, residual heat in process fluids and gases may be employed for generation of high pressure steam, in heat exchangers of special design called waste heat boilers. A waste heat boiler dissipates unwanted process heat while recovering its thermal energy in the form of useful steam.

We live or work in air conditioned buildings which are totally enclosed and don't have windows that can be opened. Such buildings accumulate heat from humans;

0-8412-0471-3/79/47-089-351$10.00/0

from sunlight; and from lighting systems. This heat must be disposed of, so that we can live and work in comfort. Air conditioning systems employ mechanical refrigeration units. The heat developed in compression of refrigerants used to remove building heat must be disposed of by external means such as cooling towers, evaporative condensers and spray ponds.

Most cooling towers are open-recirculating types in which heat rejection mainly is accomplished by evaporation of water. There also are closed cooling systems (of which an automobile radiator would be typical), from which heat is dissipated by the forced flow of air across radiation sections. In some combination systems, heat from closed cooling circuits is transferred through heat exchangers into circulating water which is cooled by evaporative systems.

Open Recirculating Cooling Systems

Figure 1 shows a typical induced draft cooling tower of wood construction. Powerful fans at the top draw air through louvers at the tower base, across the tower fill, and discharge it through fan stacks. From distribution troughs located above the tower fill section, incoming hot water from a building or plant flows downward over the fill (packing), partially evaporates, and is cooled both by evaporation, convection and conduction.

Figure 2 is a schematic of a natural draft, atmospheric tower. Warm water is distributed at the top, and moves down by gravity across wood fill. Air is drawn in by chimney effect. Figure 3 shows a long bank of atmospheric towers, functioning like the one shown in the schematic. Figure 4 illustrates major characteristics of a cooling system combining a closed cooling section with an open (evaporative) cooling tower. This double recirculating system might be used to reject unwanted heat from an internal combustion engine or process unit. Figure 5 shows another configuration of a double recirculating system in which a closed system heat exchanger in the bottom of the tower is cooled by evaporating water flowing down over it.

Let us consider how cooling towers work. What is the relationship of evaporation to cooling tower operation? By comparison, in the process of generating steam, after heating feedwater to its boiling temperature one must add roughly 1,000 British thermal units (Btu) of heat energy for every pound of water, to cause a change of state from liquid water to water vapor (steam). An evaporative cooling system also requires

In Corrosion Chemistry; Brubaker, G., et al.;
ACS Symposium Series; American Chemical Society: Washington, DC, 1979.

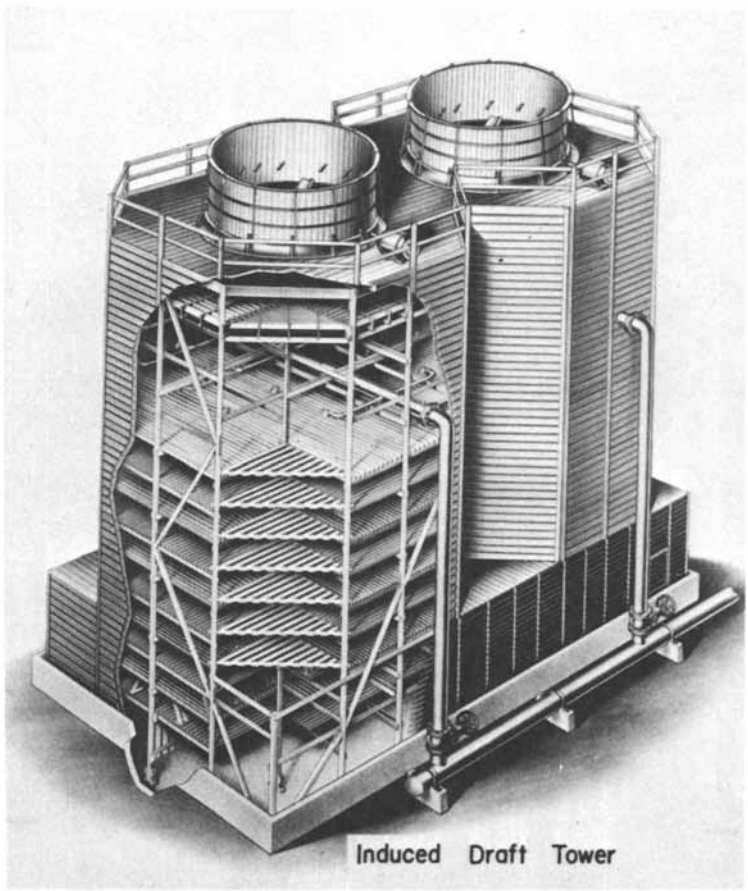

Figure 1. Cutaway section of induced draft cooling tower

In Corrosion Chemistry; Brubaker, G., et al.;
ACS Symposium Series; American Chemical Society: Washington, DC, 1979.

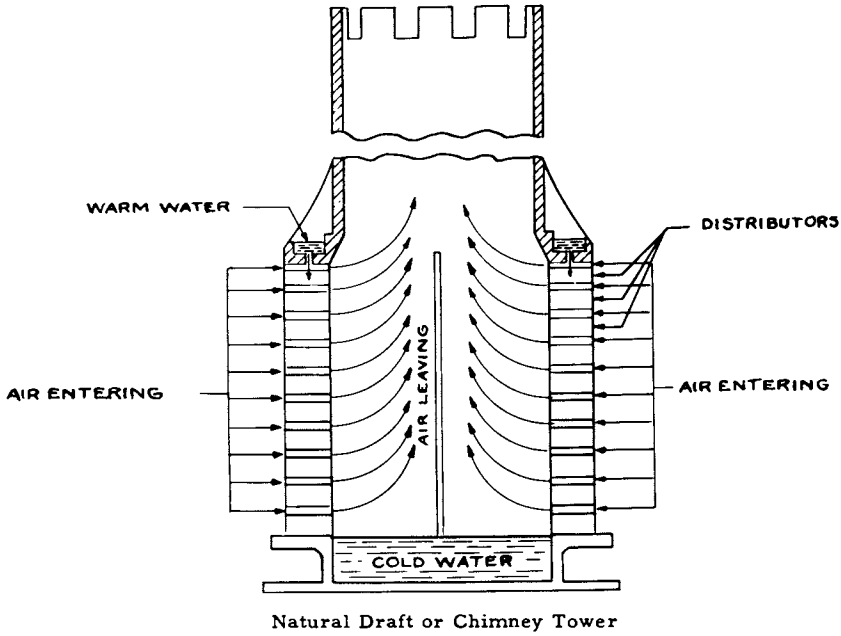

Figure 2. Schematic of a natural draft cooling tower

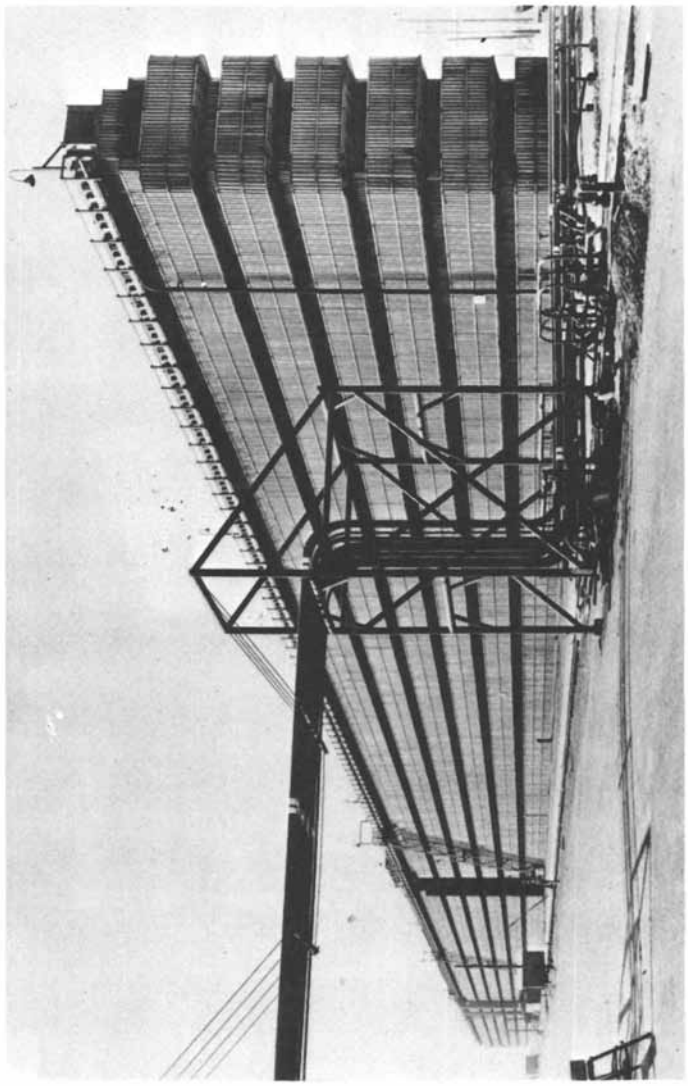

Figure 3. Multicell, natural draft (atmospheric) cooling tower

In Corrosion Chemistry; Brubaker, G., et al.;
ACS Symposium Series; American Chemical Society: Washington, DC, 1979.

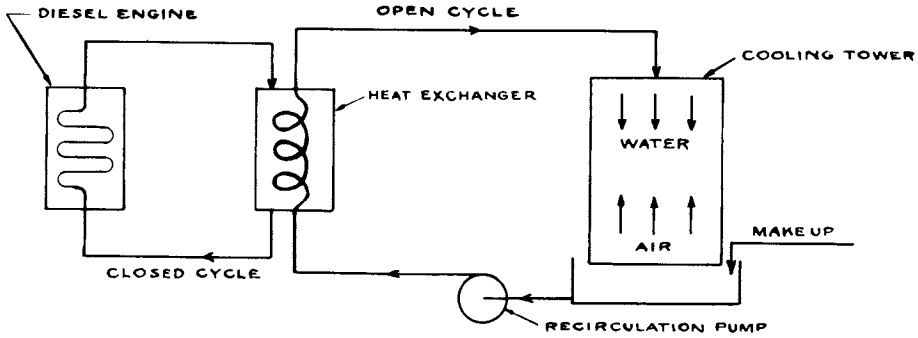

Figure 4. Schematic of a double recirculating cooling system

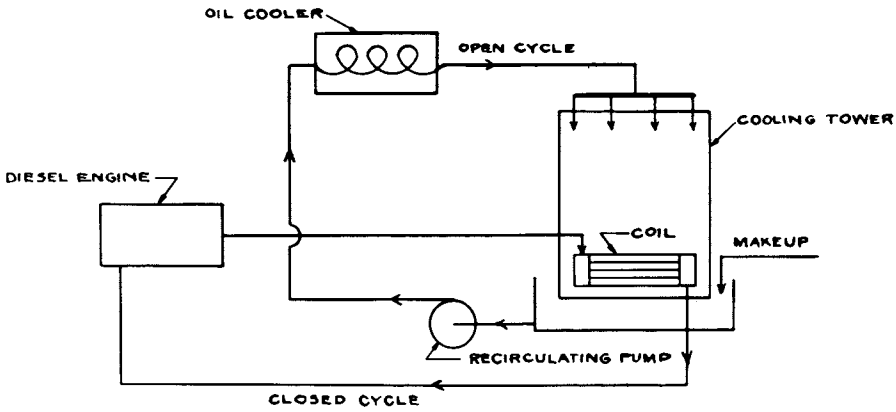

Figure 5. Schematic of a double recirculating cooling system showing heat exchanger in bottom of cooling tower

In Corrosion Chemistry; Brubaker, G., et al.;
ACS Symposium Series; American Chemical Society: Washington, DC, 1979.

equivalent heat input. To cause one pound of water to evaporate, we must supply about 1,000 Btu of heat energy from some source. In a cooling system we transfer unwanted heat from a piece of equipment into cooling water, and cause part of that water to evaporate. In the process we will reject about 1,000 Btu for every pound of water caused to evaporate. Practically speaking, when hot water is passed through a cooling tower, about one percent of the water being circulated must evaporate for each 10 degrees F. temperature drop accomplished in the tower. In a cooling tower circulating 20,000 gallons per minute and operating with 100 degrees F. water coming in at the top, and 80 degrees F. water discharged at the bottom, (a 20 degree temperature drop) we will have evaporated 2% of the water circulating, at every pass through the tower.

What should happen when water containing hardness, alkalinity and other dissolved minerals is added to a cooling system and caused to evaporate and concentrate? Once the limit of solubility of the dissolved minerals or salts in that water is reached, they would begin to come out of solution and crystallize in solid form. To the extent that dissolved salts include calcium and magnesium which could combine with silica, sulphate and carbonate, the end result might be insoluble scale deposits on heat transfer surfaces. We don't like such deposits in boilers. They are equally destructive in cooling system heat exchangers, where ability to reject heat is essential to continuation of process operations, refrigeration and air conditioning systems. So by the evaporation of cooling water, we accomplish the bulk of the industrial cooling job. Such systems also dissipate some heat by radiation and convection. But the major reduction of heat is accomplished by evaporation. As we evaporate and concentrate cooling water, dissolved minerals soon would reach levels at which scale deposits would form, in the absence of corrective measures. Calcium carbonate scale control is a major concern.

One way to prevent $CaCO_3$ scale in cooling system exchangers is to convert carbonate and bicarbonate ions to some other form having greater solubility in heated water. $CaCO_3$ has a very low solubility in water; not more than 20 to 30 mg/liter. Like most other materials that form scale *in situ* on heated surfaces, it has a negative solubility curve, (solubility goes down as temperature goes up). Other salts like sodium chloride, sodium carbonate, sodium sulfate get more soluble as temperature rises.

Among the early efforts made to prevent $CaCO_3$

In Corrosion Chemistry; Brubaker, G., et al.;
ACS Symposium Series; American Chemical Society: Washington, DC, 1979.

scaling and corrosion of cooling surfaces and heat transfer units was application of chemical equilibrium principles (the Calcium Carbonate Saturation Index) developed by W. F. Langelier. (1, 2) Langelier showed that each natural water supply would be completely stable with respect to $CaCO_3$ at a certain pH, which he identified as pH_s. The water would be exactly saturated with calcium carbonate, neither unsaturated nor supersaturated. The pH_s of a given water could be calculated from simple data, including calcium content, total alkalinity, temperature and total dissolved solids. Simple charts and nomographs were developed to simplify determination of pH_s. Langelier also proposed the Saturation Index, to show whether a water supply would be stable or unstable (with respect to $CaCO_3$ solubility) at any given temperature and pH.

Having determined pH_s (the saturation pH) by nomographs or calculations, we then compare pH_s with the actual pH of the water. Subtract pH_s from the actual pH; if the result is a positive number this indicates a scaling water, with more calcium carbonate in solution than can be held. The higher the positive saturation index rises, the greater will be the scaling tendency. What if the Saturation Index, $(pH - pH_s)$, is a negative number? This indicates a water that is undersaturated with calcium carbonate, and hungry to dissolve more. If there is no calcium carbonate handy to be dissolved, the water will attack the metals of the system. In other words, a negative pH_s indicates a corrosive water. The more negative the Saturation Index, the more corrosive the water will be.

John Ryznar of NALCO developed a useful modification called the Stability Index, based on empirical data from field locations. The Saturation pH is determined exactly the same way, but the Index is obtained differently. The Stability Index is calculated from $(2\ pH_s - pH)$. It always will be a positive whole number. Stability Index numbers around 7 show the water is quite stable, neither corrosive nor scaling. As the Stability Index drops below 6, water becomes progressively more scaling. On the other hand, as the Stability Index rises above 7, water becomes progressively more corrosive. A cooling water with a Stability Index of 10 might produce severe to intolerable corrosion conditions.

Some pioneers in cooling system water treatment attempted to control corrosion by Saturation Index adjustments alone, without addition of chemical inhibitors. Unfortunately, most cooling systems include heat exchangers with wide temperature variations. A cooling

In Corrosion Chemistry; Brubaker, G., et al.;
ACS Symposium Series; American Chemical Society: Washington, DC, 1979.

water completely stable and non-corrosive at 70 degrees F. might become either scaling or corrosive, when passed through an exchanger where temperature was raised to 130 degrees F. Therefore, corrosion control by Saturation Index adjustment alone rarely offered a practical solution.

The next approach to scale control was reduction of potential calcium carbonate by acidification of makeup water. Sulfuric acid is added to reduce alkalinity and convert most of the calcium bicarbonate to calcium sulfate. Calcium sulfate is soluble up to about 1,700 parts per million in cooling waters at ordinary temperatures, whereas calcium carbonate solubility is less than 30 ppm. So by slightly acidifying makeup water we greatly reduce tendency for calcium carbonate deposition. The calcium sulfate level in concentrated cooling water is controlled by bleed-off adjustment--manually or automatically.

Obviously when we deliberately add sulfuric acid to cooling water, we reduce alkalinity and also depress pH. This increases corrosivity of the circulating water, which is saturated with dissolved oxygen, contacts many dissimilar metals, and is elevated in temperature. In the process of acidification to prevent scale deposition so heat transfer equipment will function efficiently, we knowingly build in added corrosion factors and increase corrosion control difficulty. Now we need to find corrosion inhibitor combinations which will be practical for use in industrial systems; can be tolerated from the viewpoints of toxicity and pollution controls and will effectively protect these multimetal circuits during their normal service life of 20 to 30 years.

One early approach for cooling water corrosion inhibition was the use of inorganic polyphosphates. These complex molecularly dehydrated phosphates came into widespread industrial use beginning in the 1930's. There is some disagreement about how polyphosphates function as corrosion inhibitors. Generally accepted theory is that, in an aerated system, they cause formation of a protective surface film which contains both iron oxide and phosphorus, perhaps an iron phosphate. Polyphosphates will not work in a system that is devoid of oxygen, nor in a stagnant system. Polyphosphate corrosion inhibition required flow, to replace the iron-phosphate film as fast as it is removed or depleted. Polyphosphates are unstable and subject to problems in high temperature circuits, or where pH fluctuation occurs. Ecological considerations also are involved, because of possible pollution contributions of residual

In Corrosion Chemistry; Brubaker, G., et al.;
ACS Symposium Series; American Chemical Society: Washington, DC, 1979.

phosphates in cooling tower discharges to surface waters--lakes, streams, etc.

In the early 1950's, combinations of alkali chromate (an anodic inhibitor) and polyphosphate (generally accepted as cathodic) came into prominence for cooling system corrosion inhibition. The combination of chromate with phosphates proved highly efficient in comparison with straight phosphate or straight chromate, and could be used at substantially lower concentrations. For example, a cooling system that had been treated with 400 ppm alkali chromate, with cooling water pH adjusted to the neutral range of pH 7 to 8, could be equally well protected by a combination of chromate and polyphosphate, with chromate concentration of 30 to 40 ppm, and phosphate at 10 to 20 ppm.

In the late 1950's, chromate-phosphate systems incorporating zinc as another cathodic inhibitor were introduced, followed by zinc-chromate inhibitors, without phosphate. Using chromate-zinc, or polyphosphate-chromate-zinc inhibitors it was possible to cut working concentrations still further. It was necessary to control pH to make this inhibitor system function effectively. At increased pH (above pH 7.5) tendency for zinc loss by precipitation increases. Furthermore, pH rise may cause heat exchangers to become fouled by zinc hydroxide slimes or zinc phosphate.

We have mentioned relationship of scaling and deposition to corrosion control. When considering deposition causes, we're concerned not only with calcium carbonate and calcium phosphate, but also with dust and other impurities. The cooling tower acts as an efficient scrubber for such solids, and for combustion gases such as sulphur dioxide which are potent reducing agents for chromates. We must also consider microbiological growths which form slimy deposits and interfere with heat transfer. In short, we must be concerned about all causes of fouling including deposition of inhibitor reaction products, process leakages and corrosion products. All of the preceding impurities must be dealt with effectively so that cooling water corrosion inhibitors can function. Unless the metal surfaces in the system are kept clean and accessible to the inhibitor, then the corrosion inhibitor cannot be expected to function. If we permit growth of microbiological layers on a surface, both heat transfer and corrosion inhibition will suffer.

The need to keep metal surfaces clean led to the development of additives called antifoulants and dispersants. Many natural organics such as tannins and lignin derivatives have been used as dispersants. As an

In Corrosion Chemistry; Brubaker, G., et al.;
ACS Symposium Series; American Chemical Society: Washington, DC, 1979.

outgrowth of work originated in the boiler water chemistry field, it became apparent that synthetic compounds based on acrylic or methacrylic acid also were useful as antifoulants in cooling circuits. (3, 4, 5, 6) They aid in dispersion of silt, corrosion products, residues from bacterial growth and other foulants. Other synthetic dispersant-antifoulants include phosphated polyalcohols. A variety of chelant/sequestrants also have been used, particularly phosphonic acid derivatives having structures analogous to the nitrogen-based chelants EDTA and NTA. In practice the later chelants are rarely used because of their tendency to complex and remove protective oxide layers from heat exchanger surfaces, particularly at lower pH levels commonly maintained in cooling water.

Earlier the standard industrial approach to prevention of calcium carbonate scaling by addition of sulfuric acid was described. Objectives were to reduce bicarbonate alkalinity, convert calcium carbonate to calcium sulfate, and regulate sulfate concentration by bleedoff. Corrosion inhibitors were added to protect system metals. A new approach to industrial cooling system treatment does not require addition of sulfuric acid. It involves application of phosphonate sequestrants, dispersants and special corrosion inhibitors, and provides deposit control equal to that obtainable when using sulfuric acid. Availability of phosphonate sequestrants makes possible combination scale control and corrosion inhibitors that can be used without the necessity of reducing cooling water alkalinity by acid feed.

Alkalinity and calcium hardness of circulating water build up to a level determined by allowable operating concentrations. System pH usually plateaus in the stabilization range of pH8 to 9. So long as the Langelier Saturation Index of concentrated cooling water can be kept below +2.0 by bleedoff, supplemental acid feed is not required for scale control.

For many locations, the phosphonate/dispersant combination provides effective scale control without necessity of acidification. How does this type of treatment function as a corrosion inhibitor? One possible explanation is that if a surface is clean, free from deposits of any type that can set up local concentration cells, then any corrosion occurring will be uniformly distributed and reduced in severity. This permits normal service life of system equipment. This approach to corrosion control is called the "clean system concept." Copper inhibitors (thiazoles and triazoles) function well in these combinations. Addi-

In Corrosion Chemistry; Brubaker, G., et al.;
ACS Symposium Series; American Chemical Society: Washington, DC, 1979.

tional corrosion suppression is provided by increased alkalinity and pH in non-acidified systems, plus inhibitor properties of the phosphonate sequestrants. It has also been discovered that other inhibitors such as chromate can be used in combination with specially selected sequestrants to obtain improved corrosion inhibition.

This presentation will not attempt detailed discussion of microbicides, which are essential to maintenance of clean metal surfaces needed for effective corrosion inhibition. All of the previously discussed needs also must be met, including deposit control, antifoulants to prevent localized accumulations of suspended, insoluble contaminants, and addition of corrosion inhibitors. The contributions of microbiicides and associated antifoulants to corrosion prevention in cooling systems cannot be minimized. We are concerned not only with visible microbiological growths (algae and slimes) which are unsightly and interfere with uniform water distribution through the tower, but also with slime formers that deposit inside heat exchanger tubes, and which reduce efficiency of heat transfer just as would scale deposits. Biocides also play a key role in protection of wood structural members and wood fill sections against destruction by rot or fungal microorganisms.

The way in which aquatic growths and microorganisms can interfere with uniform circulation, or screen off part of heat exchange surfaces from uniform contact with cooling water and corrosion inhibitors can be visualized from Figure 6. This shows a sizeable accumulation of aquatic weeds on the inlet to a large heat exchanger. Some tubes are totally blocked. Active corrosion may be expected beneath deposits where metal surfaces are screened from free contact with inhibited cooling water.

Closed Recirculating Cooling Systems

In open recirculating systems evaporation is the major factor in heat disposal. In these evaporative systems circulating water is continuously scrubbed with air, therefore saturated with dissolved oxygen. In contrast, water in closed recirculating cooling systems usually will contain minimum dissolved oxygen, even though the systems may include vented expansion tanks.

Closed cooling svstems operate at appreciable pressure, often 30 pounds per square inch or higher. They are essential for temperature control of internal combustion engines used in automobiles, tractors, trucks, buses and railway locomotives. Diesel engines also provide motive power for river and lake vessels and are

In Corrosion Chemistry; Brubaker, G., et al.;
ACS Symposium Series; American Chemical Society: Washington, DC, 1979.

Figure 6. Cooling system heat exchanger partly clogged by aquatic weeds and shellfish

In Corrosion Chemistry; Brubaker, G., et al.;
ACS Symposium Series; American Chemical Society: Washington, DC, 1979.

used to drive electric generators in power plants, both for full time and emergency stand-by use.

In typical railway diesel engines, cooling water is pumped through water jackets or cored liners in which the pistons work. It then passes through the cylinder heads which must dissipate tremendous heat created by combustion of diesel fuel under pressure; finally it returns to an expansion tank via fan-cooled radiator sections. A parallel cooling flow passes through lubricating oil heat exchangers to remove additional heat.

In the design of railway Diesel engines the builders apparently, did not recognize that there could be corrosion problems within the cooling circuits. This may explain why some cooling systems included as many as twelve dissimilar metals, all electrically coupled together. Metals used included cast iron, copper, brass, Admiralty, phosphor bronze, galvanized steel, cast and wrought aluminum, tin-plated Admiralty, solder and others--in a variety of dangerous couples.

The railroads were told by locomotive builders that when they bought Diesels to replace steam locomotives, they could forget about water problems. Unfortunately the designers were not corrosion engineers, and didn't design cooling systems to withstand continuous contact with high temperature cooling water. There was an added need for boiler feedwater, since Diesel-powered trains still required steam for heating cars, for lavatories and for dining cars. This required compact steam generators of unique design, small enough to be installed aboard Diesel locomotives, yet capable of generating 3,000-5,000 lbs. steam/hour. These boilers required mineral-free feedwater supplemented by corrosion inhibitors. Cooling systems also needed high-quality makeup water, plus special corrosion inhibitors to protect the multimetal circuits.

At some locations where Diesel engines were used to drive electric generators, attempts were made to recover part of the heat in recirculating cooling water. Engine coolant circulating at 30 pounds pressure and temperatures of 240 to 250 degrees F. was allowed to pass through an orifice into an expansion chamber. Part of the water would flash into low pressure steam, which could be used for building heating. Theoretically, all the steam condensed in space heaters and radiators would be recovered as condensate and returned to the engine cooling system. Unfortunately, heating systems are never completely tight, so losses of steam and condensate occurred. This created a need for continuous makeup to the cooling system--which in effect had become

In Corrosion Chemistry; Brubaker, G., et al.;
ACS Symposium Series; American Chemical Society: Washington, DC, 1979.

a steam generator. Since it was operating as a steam generator, the cooling system now required blowdown (to control build-up of dissolved solids), plus volatile corrosion inhibitors capable of protecting steam-condensing and condensate return circuits--plus the inhibitors already needed for cooling system corrosion control.

Most internal combusion engines include fan-cooled radiators in their cooling circuits. Figure 7 is part of a typical radiator section. The complete radiator section had 212 rectangular tubes about one inch by 1/8 inch inside diameter, with tube metal thickness about 0.005 inch. The tube metal generally was Admiralty brass, a 70/30 brass with 1% tin. The header also is Admiralty, covered with a 1/8 inch layer 60/40 lead-tin solder. The tubes first are locked in place with 90/10 solder before applying the sealing layer of 60/40 solder. The radiator tubes of Admiralty brass also were tin plated. This combination presents a complex corrosion couple of Admiralty brass with tin plating in combination with two solders and subject to intense stresses in the header areas.

Some diesel locomotives must work under extreme cold weather conditions with alternate periods of idling and maximum loading. This can create extreme radiator stresses which contribute to corrosion. One such location is deep pit open cut iron mines of Northern Minnesota. When engines were idling, radiator sections were bypassed and would reach ambient temperature, as low as -40 degrees F. Under heavy load, radiators would be hit by sudden flows of cooling water at temperatures of 220-240 degrees F. The resulting stress loads created corrosion failures of the tin-coated tube-solder joint at the header. Water leaks and radiator failures resulted. Figure 8 is a closeup of one tube end from a failed radiator section. Indications of separation of the tube from its surrounding solder layer can be seen at the right and left tube sides.

Many years ago, certain Arctic explorers carried food in cans sealed with pure tin solder. Under Arctic temperatures this tin solder bond failed completely. Apparently the tin changed from a crystalline form to an amorphous, powdered solid which destroyed the seal integrity. Resulting food spoilage caused deaths by poisoning. This type corrosion failure of pure tin, called "tin pest," or "tin disease," also had been observed many years ago in Russia. Russian cathedrals usually were not heated, and in the winter would reach extremely low temperatures. Pipe organs in some cathedrals had pipes made of pure block tin. Under extreme cold temperatures vibrating organ pipes were known

In Corrosion Chemistry; Brubaker, G., et al.;
ACS Symposium Series; American Chemical Society: Washington, DC, 1979.

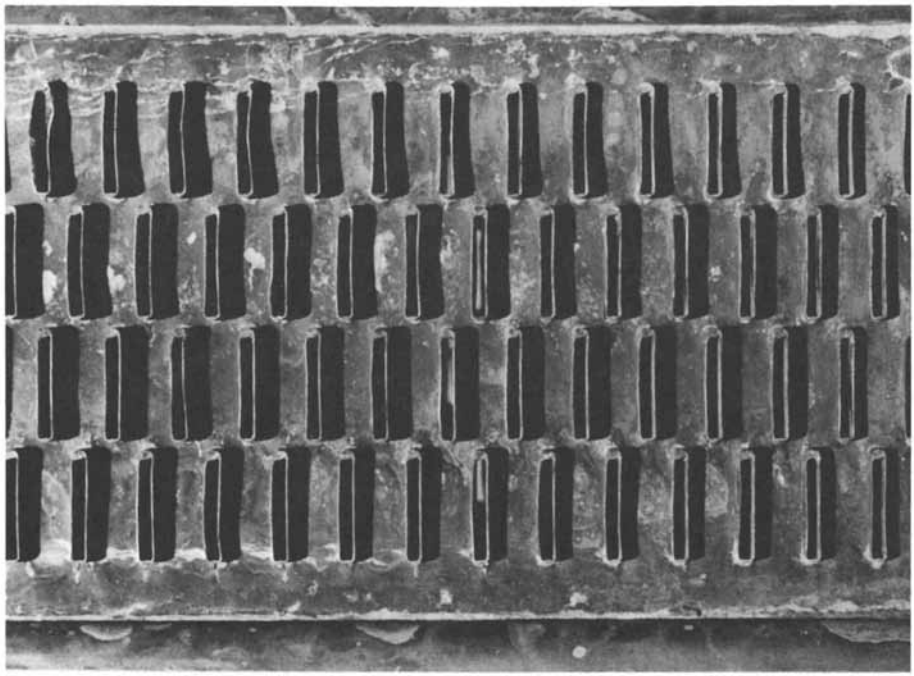

Figure 7. Typical air-cooled radiator section for closed-engine cooling system

In Corrosion Chemistry; Brubaker, G., et al.;
ACS Symposium Series; American Chemical Society: Washington, DC, 1979.

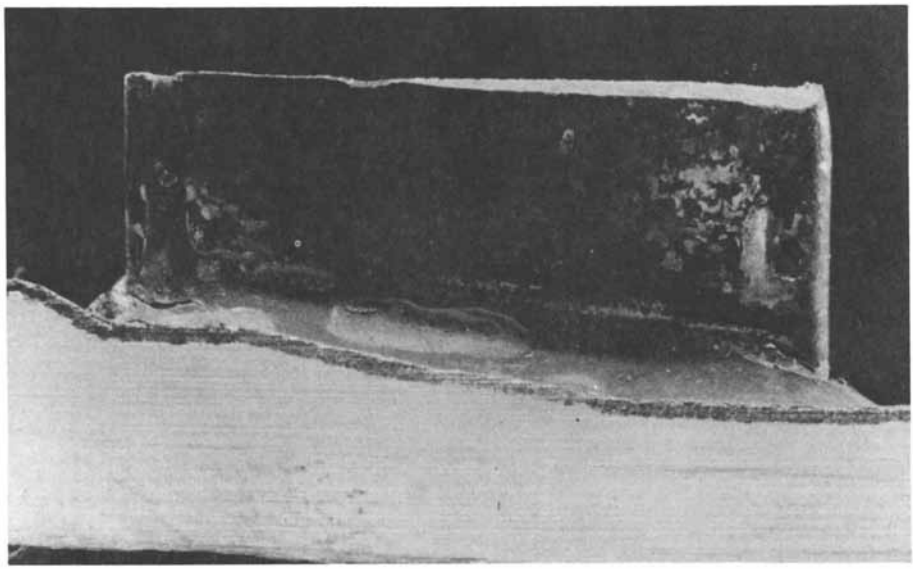

Figure 8. Top of individual tube, closed-system radiator section, where solder failure caused leakage

In Corrosion Chemistry; Brubaker, G., et al.;
ACS Symposium Series; American Chemical Society: Washington, DC, 1979.

to develop areas of "tin pest" and fail mechanically.

Under extreme low temperature operations of Diesel engines the radiator failures occurring seemed to involve very similar corrosion reactions. Apparently the tin layer on the tube surface converted to an amorphous, powder form, breaking the bond between tube, solder and header. Figure 8 also shows evidence of surface attack on the solder layer, by conversion of tin to amorphous form. The corrosion inhibitor used in these systems was a borate-nitrite-mercaptobenzothiazole proprietary composition.

Clean radiator tubes are readily protected by conventional alkaline chromate or borate-nitrite corrosion inhibitors in cooling water. Partially clogged tubes, however, create both heat transfer and corrosion problems. Figure 9 shows a radiator section with 90% of the tubes partly clogged by corrosion products, silt and oily particulate matter. Designed to handle flows of about 250 gpm, the section's 212 tubes each should conduct about 1 gpm, corresponding with a flow velocity of 4-5 ft./sec. If 40% of tubes are clogged, flow velocity in remaining open tubes may approach 15 to 20 ft./sec. From practical experience and research, the upper limits of flow velocity for Admiralty brass tubes are in the range of 5-7 ft./sec. With higher flow velociies, they are subject to impingement failures.

Impingement Attack. This is an electrochemical phenomenon in which part of the surface oxide is removed locally, leaving bare metal which becomes anodic. Metal loss begins at anodic spots; as the pit deepens, cavitation and scouring take over. The pits tend to undercut in the direction of flow. Looking down from the top they look like hoof tracks going in an upstream direction. As undercutting areas enlarge, small pieces break away to produce large holes or penetration failures. Looking down into tubes where impingement failures have occurred, one can see bright spots that look like tiny drilled holes.

How much cooling would one expect to accomplish in the heat exchanger shown in Figure 10? This is the result obtained when using dirty makeup water with silt and corrosion products, with no preventive maintenance. Cooling systems must be designed to permit mechanical cleaning and other preventive maintenance, or effective corrosion control becomes impossible.

Concentration Cells. Locations encouraging such attack are common in closed cooling systems. Consider metals riveted together, as in Figure 11. In the crevice,

In Corrosion Chemistry; Brubaker, G., et al.;
ACS Symposium Series; American Chemical Society: Washington, DC, 1979.

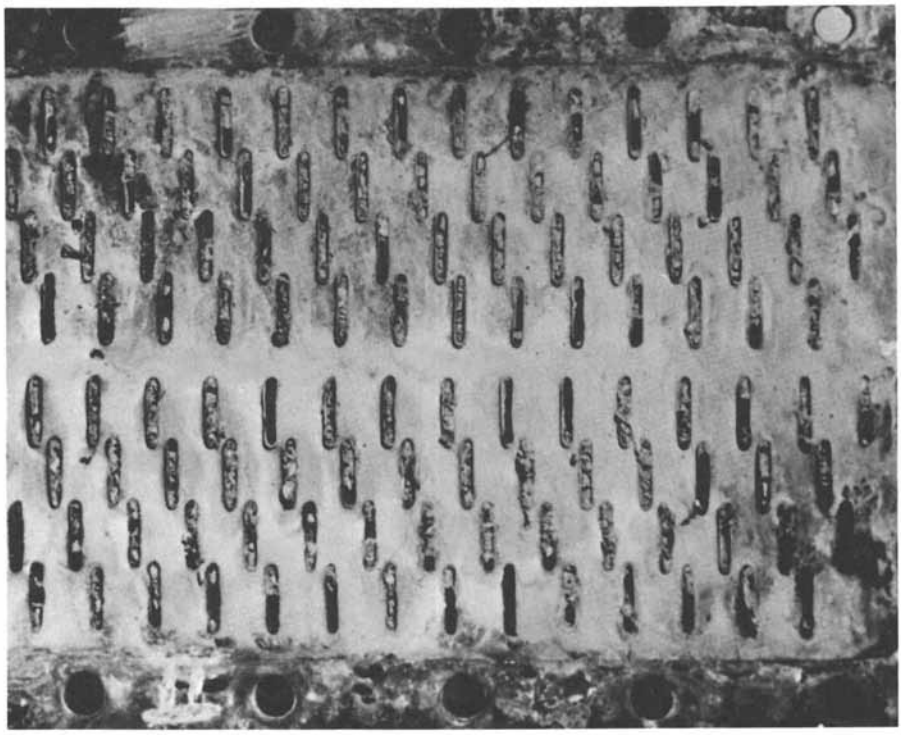

Figure 9. High coolant velocities in unclogged tubes of radiator section caused impingement attack and penetrating failures.

In Corrosion Chemistry; Brubaker, G., et al.;
ACS Symposium Series; American Chemical Society: Washington, DC, 1979.

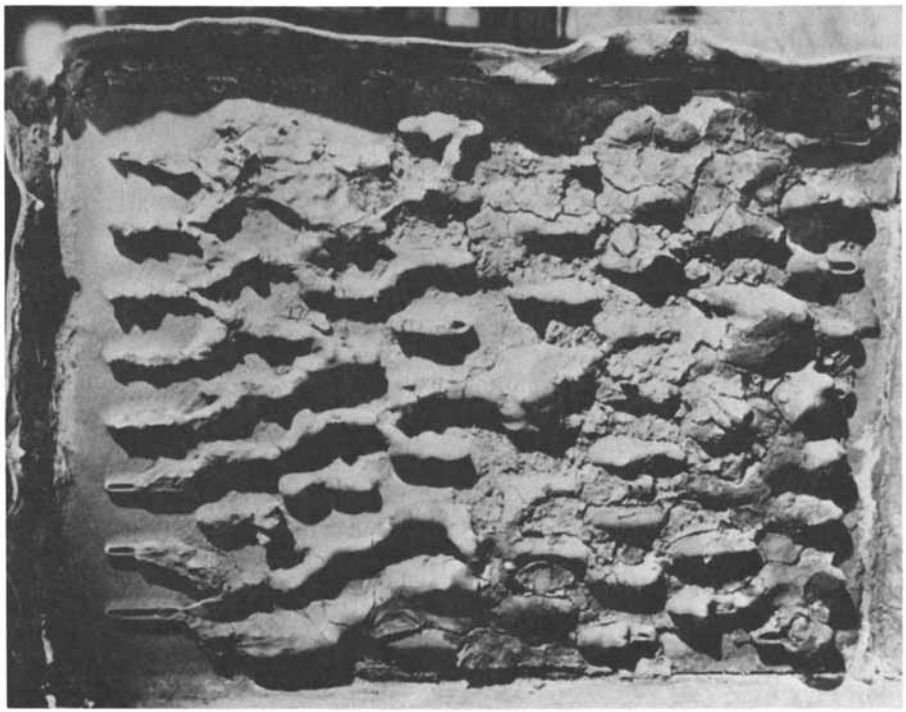

Figure 10. Poorly maintained heat exchanger; water passages clogged by silt, corrosion products, and other insoluble impurities

In Corrosion Chemistry; Brubaker, G., et al.;
ACS Symposium Series; American Chemical Society: Washington, DC, 1979.

cooling water would have a slightly lower oxygen content. Corrosion occurs in the low oxygen space, the locus of corrosion in an oxygen concentration cell. In contrast, in a somewhat similar construction, corrosion may be intensified at the open end of a crevice, away from the area of high metal ion concentration. The corrosion current flows from the metal towards the low metal ion concentration as shown in Figure 12. In cooling systems many components are poorly designed to prevent crevice corrosion.

An example of concentration cell corrosion is shown in Figures 13 and 14. This is a bronze circulating pump from an engine cooling system. Normally this alloy should be resistant to impingement attack caused by high flow velocity or peripheral speeds, particularly in a well inhibited cooling water. Yet both the alloy and rotational speed must be considered; in this case, speed of rotation was too high. The local attack on the outer edge of the impeller resembles impingement attack. However, on the reverse side (Figure 14) there is a well defined zone of pitting extending inward about 2 inches from the outer rim. This indicates a metal ion concentration problem. It has been suggested that if we could cut through the impeller and separate the outer 1/3 from the inner portion by an annular insulating bushing, it would be possible to detect current flowing from one zone to the other, when the impeller is turning. Correction of this type attack usually requires either a change of alloy to a more resistant material, or reduction in rotation rate. In this case, a sharply increased concentration of chromate corrosion inhibitor did not arrest the attack.

Man-failures in maintenance of inhibitor concentrations often contribute to corrosion failures. Figures 15 and 16 illustrate a failed cast iron impeller from a switcher locomotive cooling system. Penetrating corrosion, and corrosion product deposits in well-defined patterns can be seen on the inner face. On the outer side behind the vanes are deep corrosion zones resembling cavitation corrosion. A chromate corrosion inhibitor was used in the cooling water. Investigation disclosed that nightly overfilling with untreated make-up water was overflowing the cooling system, and diluting the inhibitor to a non-protective level. After completing repairs, the system was refilled and inhibitor level adjusted. The filling connection then was sealed and locked to prevent further untreated water addition. This eliminated the pump corrosion problem.

Dezincification of Brass. Two forms of dezincification

In Corrosion Chemistry; Brubaker, G., et al.;
ACS Symposium Series; American Chemical Society: Washington, DC, 1979.

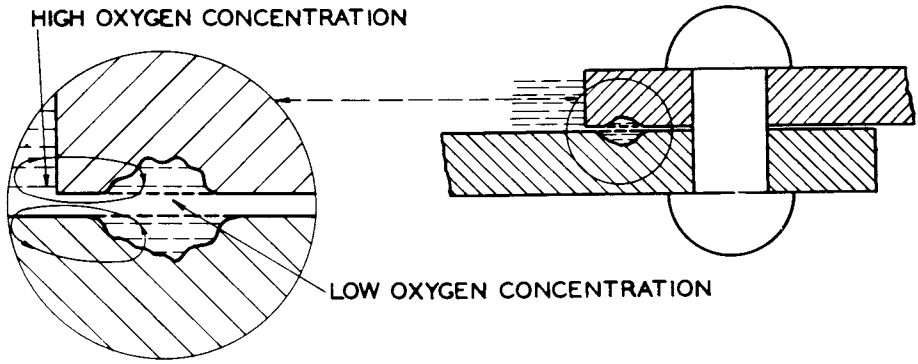

Figure 11. Typical attack location, oxygen concentration cell

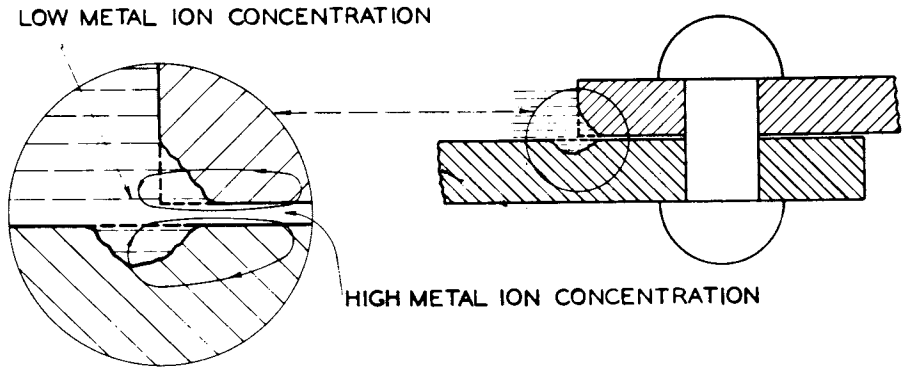

Figure 12. Typical attack location, metal-ion concentration cell

In Corrosion Chemistry; Brubaker, G., et al.;
ACS Symposium Series; American Chemical Society: Washington, DC, 1979.

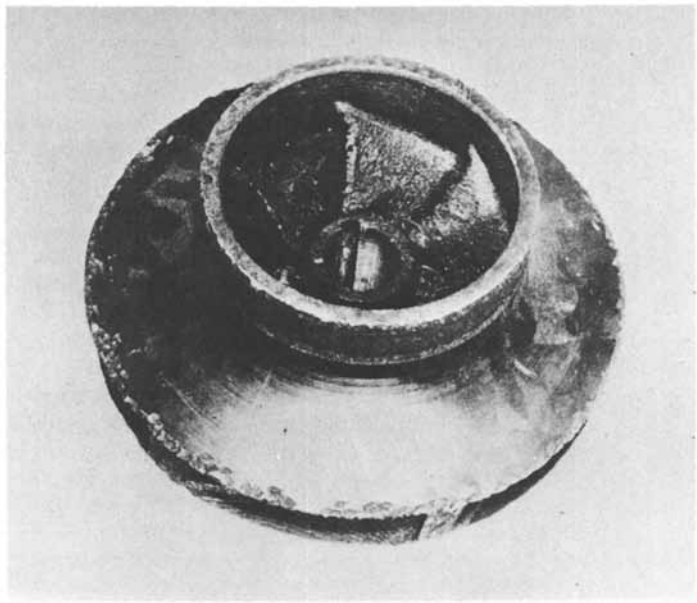

Figure 13. Bronze impeller of circulating pump damaged by impingement attack and concentration cells

In Corrosion Chemistry; Brubaker, G., et al.;
ACS Symposium Series; American Chemical Society: Washington, DC, 1979.

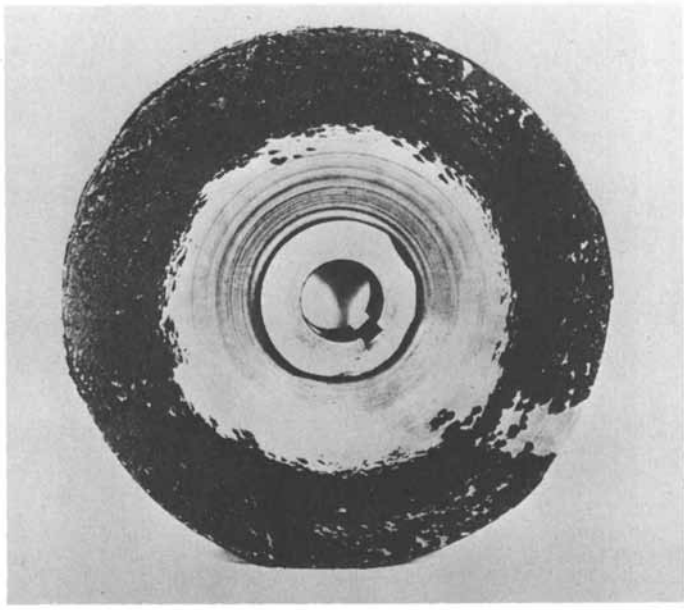

Figure 14. Band of concentration cell corrosion damage on bronze pump impeller

In Corrosion Chemistry; Brubaker, G., et al.;
ACS Symposium Series; American Chemical Society: Washington, DC, 1979.

Figure 15. Cast-iron pump impeller with cavitation corrosion damage

In Corrosion Chemistry; Brubaker, G., et al.;
ACS Symposium Series; American Chemical Society: Washington, DC, 1979.

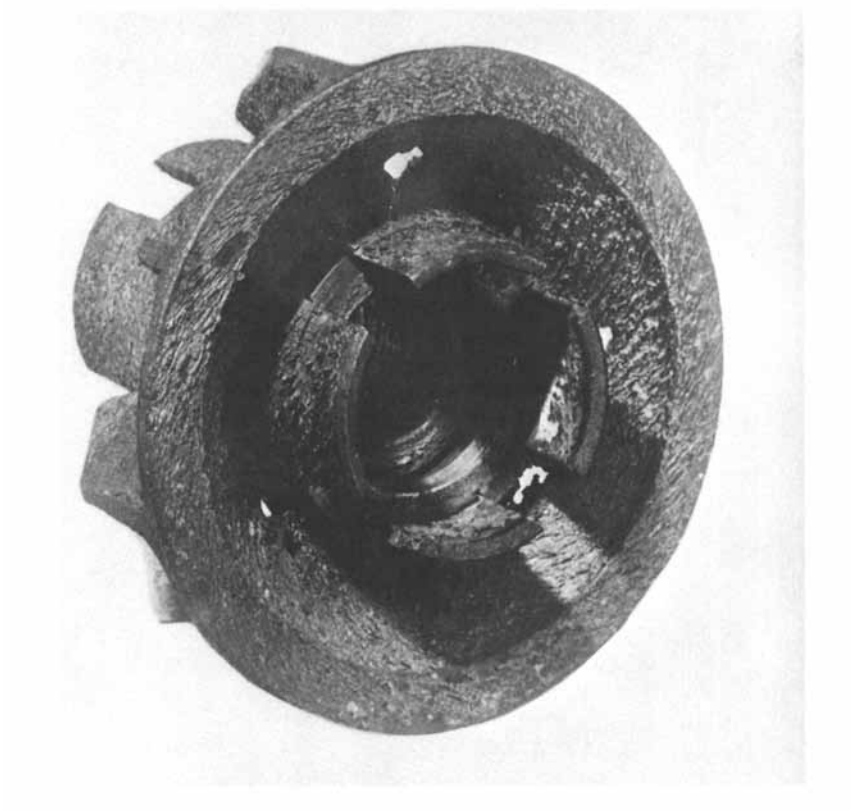

Figure 16. Opposite face of cast-iron impeller penetrated by cavitation corrosion. Note pattern of corrosion products deposition.

In Corrosion Chemistry; Brubaker, G., et al.;
ACS Symposium Series; American Chemical Society: Washington, DC, 1979.

are encountered in heat exchanger tubes, piping and brass headers. In layer type dezincification, attack proceeds relatively uniformly from the water side. Affected areas can be distinguished by the dull red color of the copper-rich areas where zinc has dissolved away. Layer dezincification usually proceeds until loss of strength or penetration to the root of threaded areas allows the component to fail mechanically. It generally occurs in low hardness, low pH cooling water, in the absence of proper corrosion inhibition, and is accelerated by chlorides and sulfates.

A more dangerous form of dezincification, known as Plug type, causes penetration failures and serious leaks. In plug type attack, zinc is selectively dissolved, with copper being left behind. In some cases it appears that both zinc and copper dissolve, with copper being redeposited as a spongy, porous plug in the corrosion spot. Plug dezincification is easily identified by the distinctive red spots of spongy copper which show up on the yellow brass surface. It is dangerous because of the speed with which leaks can occur. Layer type dezincification usually takes longer to reach failure. Figure 17 shows zones of plug type attack in the wall of a brass pipe. Figure 18 shows a failed Admiralty brass tube wall, both unetched and etched. The spongy copper plug is easily seen. In the etched specimen the normal grain pattern of Alpha brass and the porous copper plug in the pitted area are shown. In color, the undamaged brass is yellow-gold, while the dezincified plug is dull red. Properly maintained chromate concentrations in cooling water are specifically effective in prevention of dezincification. But the best long term protection involves redesign to eliminate zinc, or at least, to replace high-zinc brasses (such as 60-40 yellow brass) with low-zinc copper alloys; (80-10-10 or 85-5-5-5 red brass are good). Inhibited brass (containing 1/2% arsenic or 0.1% antimony) also are excellent in prevention of dezincification.

Aluminum Failures. Many Diesel engine cooling systems were first constructed with aluminum headers and other components directly coupled to cast iron blocks, with copper connections, bronze screens and other dangerous multi-metal couples. These dangerous combinations proved almost impossible to protect, even with high concentrations of chromate corrosion inhibitors. In these aluminum-copper and aluminum-iron couples, failure by complete penetration of 5/8 inch aluminum header plates occurred in three months of service.

In Corrosion Chemistry; Brubaker, G., et al.;
ACS Symposium Series; American Chemical Society: Washington, DC, 1979.

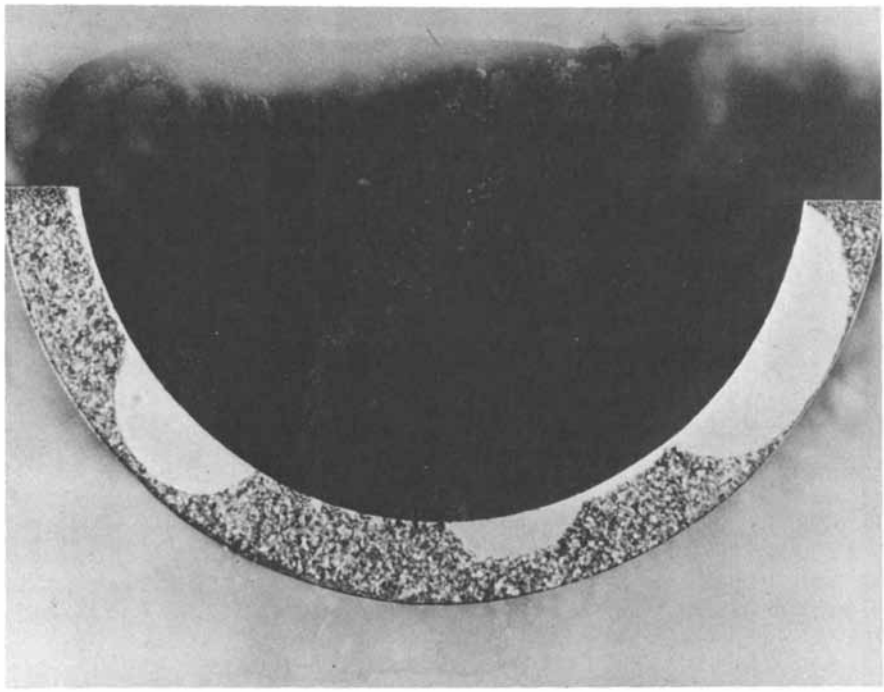

Figure 17. Light colored areas show plug-type dezincification in section of brass pipe

In Corrosion Chemistry; Brubaker, G., et al.;
ACS Symposium Series; American Chemical Society: Washington, DC, 1979.

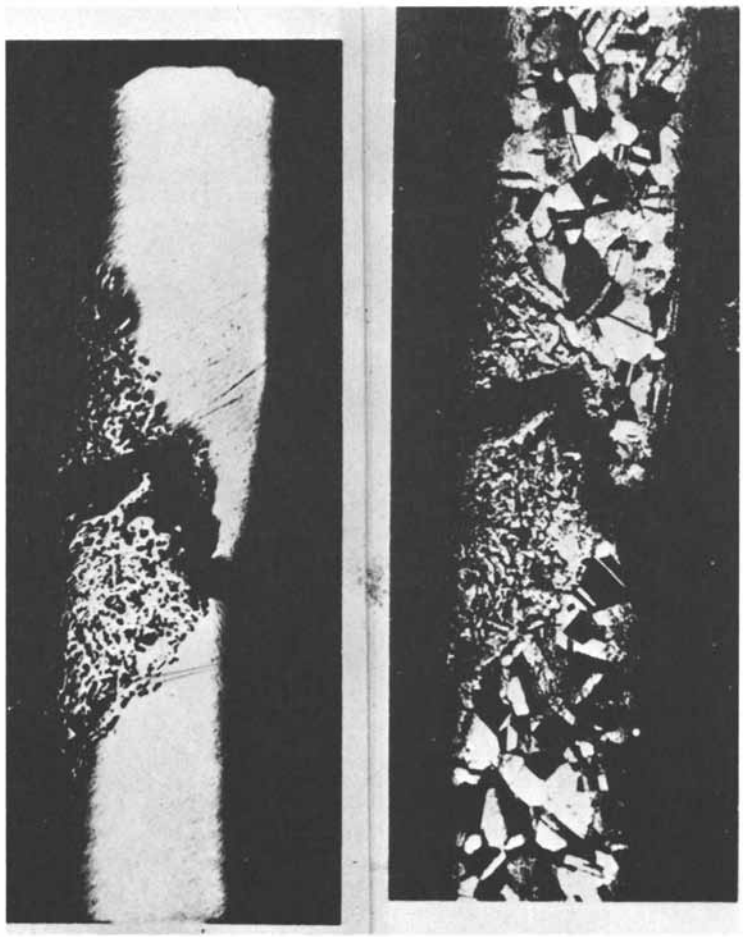

Figure 18. Thin cross-section of admiralty brass tube wall penetrated by plug-type dezincification. (Upper section) *specimen polished, unetched.* (Lower section) *same specimen polished and etched. Magnification about 170 diameters.*

In Corrosion Chemistry; Brubaker, G., et al.;
ACS Symposium Series; American Chemical Society: Washington, DC, 1979.

Figure 19 is an example of an aluminum header plate damaged by contact with high alkalinity, high pH cooling water. Figure 20 is a photomicrograph of one section of the plate, illustrating the cracking and exfoliation which occurred. Hydrogen released during corrosion reactions causes internal pressure in fissures, accelerating swelling and separation of this rolled plate. Under magnification of 250 diameters, the cracking and swelling are clearly visible. A few small nodules of copper were found suggesting that presence of copper also was involved in this corrosion failure.

In Canada, a number of mine sweepers were built using all non-magnetic materials. The entire engine block was constructed of a clad aluminum alloy. For corrosion inhibition in the closed cooling system, an inhibitor containing a high orthophosphate content was applied. The phosphate-based inhibitor caused severe corrosion of the engine blocks, resulting in penetration failures. Deep pitting leading to penetration of the cast aluminum block is shown in Figure 21. Many of the pits served as stress raisers, causing cracking. At the base of the pits where reducing action accompanies corrosion, copper deposition can be seen. Copper comes from corrosion of bronze circulating pumps, phosphor-bronze fittings and copper alloy lines. These cooling systems could have been well protected by a chromate inhibitor, or by a borate-nitrite-MBT product, but experienced accelerated attack when using the improper phosphate-silicate inhibitor.

Fretting Attack. This is a type of corrosive action in which metal transfers from one bearing surface to another, when vibration or other mechanical forces cause slight relative movement. In Figure 22 we are looking down into the opening of a Diesel engine cylinder block into which a ribbed cylinder liner is seated. Where the ribs are in contact with the engine block, transfer of metal by fretting has occurred. Cooling water circulates between the block and the liner. To prevent crevice attack between liner ribs and engine block, and avoid initiation of fretting damage, both engine block and liner surfaces should have been pretreated ("pickled") with a strong concentration of alkaline chromate inhibitor (1% to 5% strength), before attempting to seat the liner. Figure 23 shows the ribbed area at top of the liner. Absence of adequate corrosion control of this cooling system is shown by severe crevice corrosion and fretting damage on the contact faces of liner ribs, and also by the extensive

In Corrosion Chemistry; Brubaker, G., et al.;
ACS Symposium Series; American Chemical Society: Washington, DC, 1979.

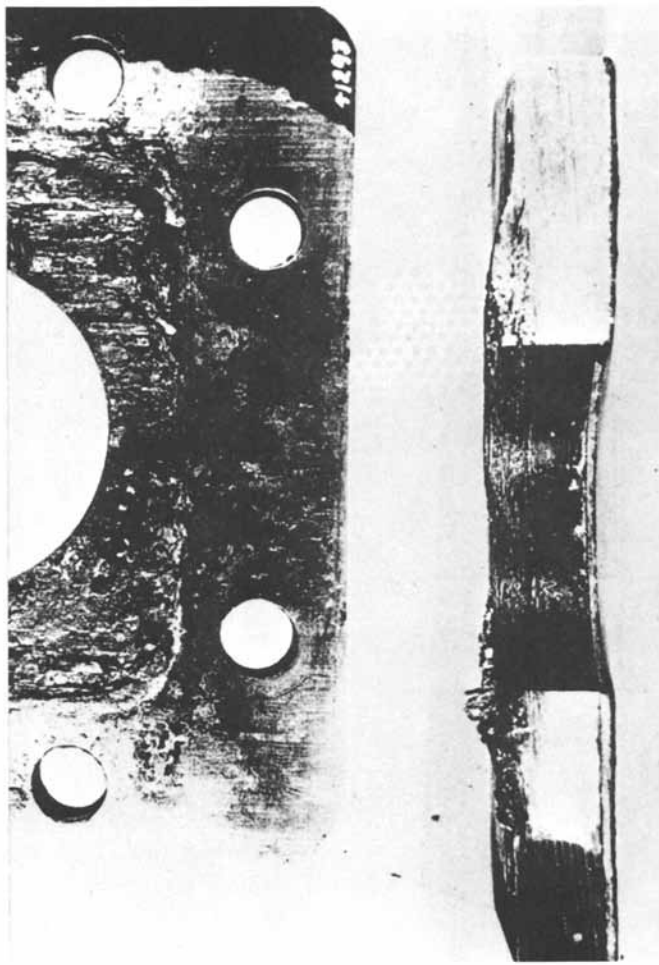

Figure 19. Wrought-aluminum header plate failed by exfoliation corrosion and cracking

In Corrosion Chemistry; Brubaker, G., et al.;
ACS Symposium Series; American Chemical Society: Washington, DC, 1979.

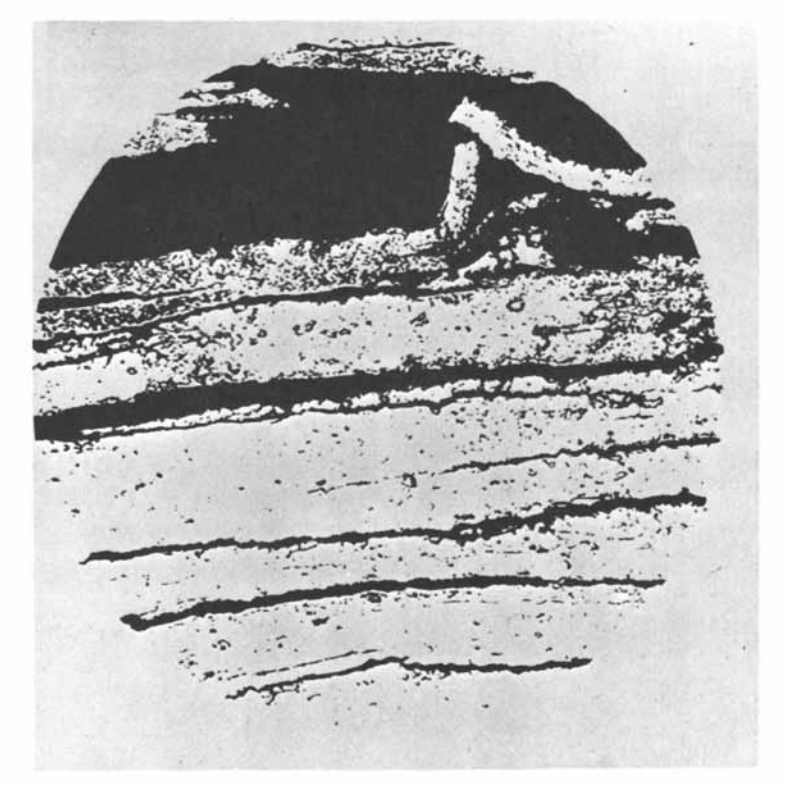

Figure 20. Section of failed aluminum plate showing cracking and exfoliation (magnification 215 diameters)

In Corrosion Chemistry; Brubaker, G., et al.;
ACS Symposium Series; American Chemical Society: Washington, DC, 1979.

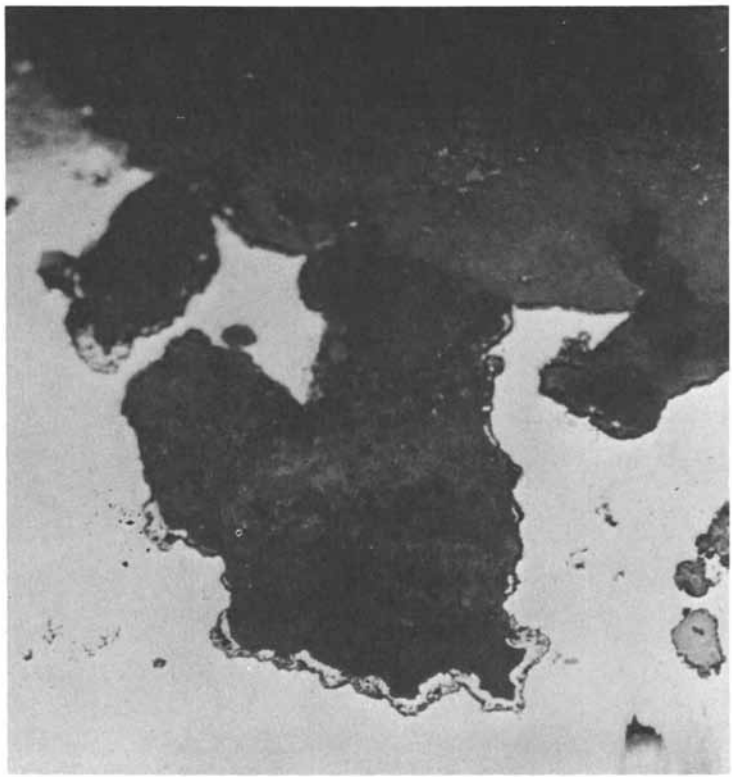

Figure 21. Section of clad-aluminum engine block which failed by pitting during use of improper inhibitor in coolant

In Corrosion Chemistry; Brubaker, G., et al.;
ACS Symposium Series; American Chemical Society: Washington, DC, 1979.

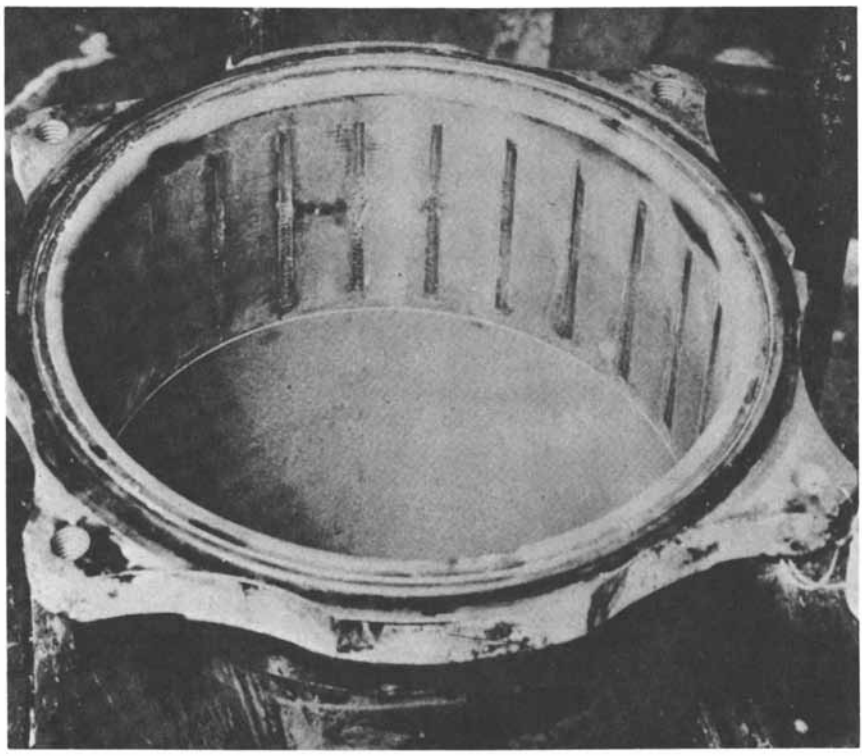

Figure 22. Fretting attack inside engine jacket at contact points with ribbed cylinder liner

In Corrosion Chemistry; Brubaker, G., et al.;
ACS Symposium Series; American Chemical Society: Washington, DC, 1979.

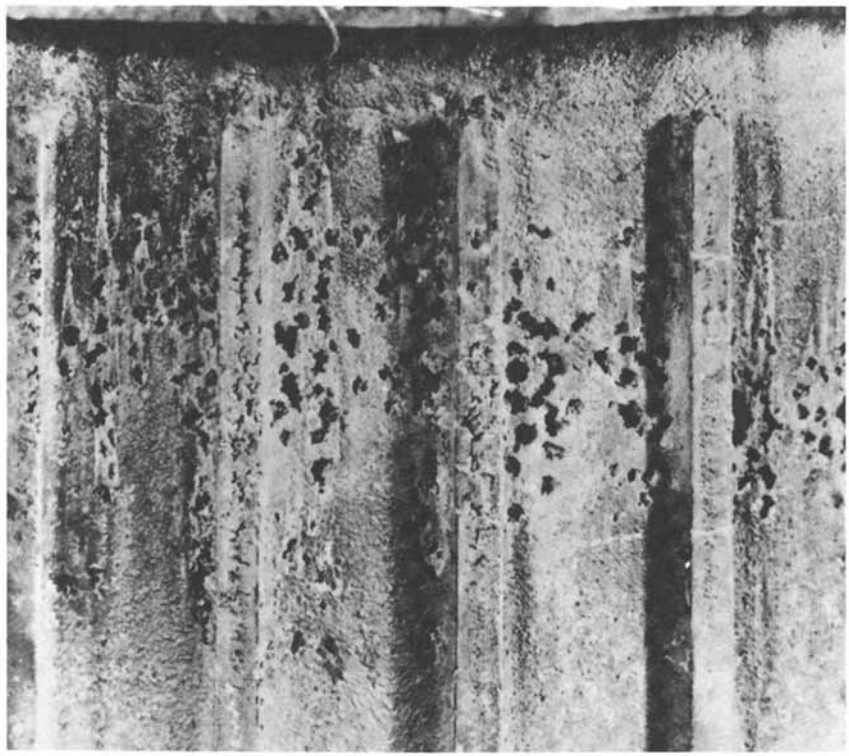

Figure 23. Cylinder-liner ribs show metal loss by fretting attack and crevice corrosion plus "worm holing" attack on liner at base of ribs

In Corrosion Chemistry; Brubaker, G., et al.;
ACS Symposium Series; American Chemical Society: Washington, DC, 1979.

'worm hole' corrosion in liner walls, in the severely stressed region at the base of liner ribs.

Cavitation-Corrosion. This form of corrosion attack, which causes localized failures of cylinder liners in Diesel engines, has been responsible for serious maintenance problems in power units of trucks, buses, railway locomotives and marine transport. The concentrated area of attack, and severity of corrosion are clearly shown in Figure 24. The areas of greatest attack occur 90 degrees from the crankshaft center line on the thrust or compression side; a lighter attack may appear on the opposite side. Other characteristics shown in Figure 25 include: 1) Honeycombed appearance of corroded metal. 2) Corroded surfaces substantially free of corrosion products. 3) Attack occurs in sharply defined areas, irregular in outline but with abrupt boundaries between affected and unaffected areas.

Cavitation corrosion of cylinder liners is not caused by high velocity water flow, nor by impingement of coolant streams. Rather, it appears that vibratory effects are primarily responsible. Under the tremendous stresses of fuel compression and combustion in the Diesel cycle, these 3/4 inch thick cylinder liners vibrate or "ring" at frequencies estimated to be in the range of 7,000 to 8,000 cycles per second, and higher.

In vibrating at such high frequencies, the liner metal is "jerked" away from cooling water contacting the surface so rapidly as to reduce local coolant pressure below the vapor pressure of the coolant fluid, forming minute vapor-filled cavities, or "bubbles." When the reverse vibration cycle occurs, the vapor-filled cavities instantly implode or collapse. The recurring collapse and reformation of vapor-filled cavities occurs in microseconds. Because the "bubbles" form and collapse so rapidly, the energy they release is measured in hundreds of tons per square inch. From study of photomicrographs of failed metal, it also appears that when these vapor cavities implode or collapse, they drive water and water vapor right into the grain structure. When the vapor cavities form again, and pressure is relieved trapped water vapor explodes upward. Photomicrographs show that crystalline structure has been distorted and rearranged by the tension effects of escaping water vapor.

The unwanted engine vibration is related to crankshaft rotational speed, but is caused by engine imbalance, crankshaft misalignment, or excessive wear of cylinder liners and pistons on the thrust side. In

In Corrosion Chemistry; Brubaker, G., et al.;
ACS Symposium Series; American Chemical Society: Washington, DC, 1979.

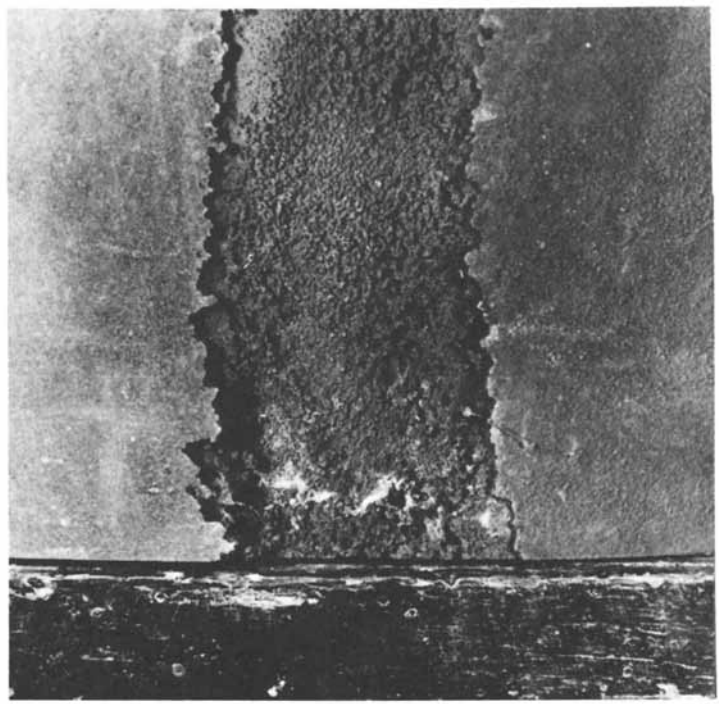

Figure 24. Vibratory cavitation corrosion of large diesel engine cylinder which progressed to perforation (7)

In Corrosion Chemistry; Brubaker, G., et al.;
ACS Symposium Series; American Chemical Society: Washington, DC, 1979.

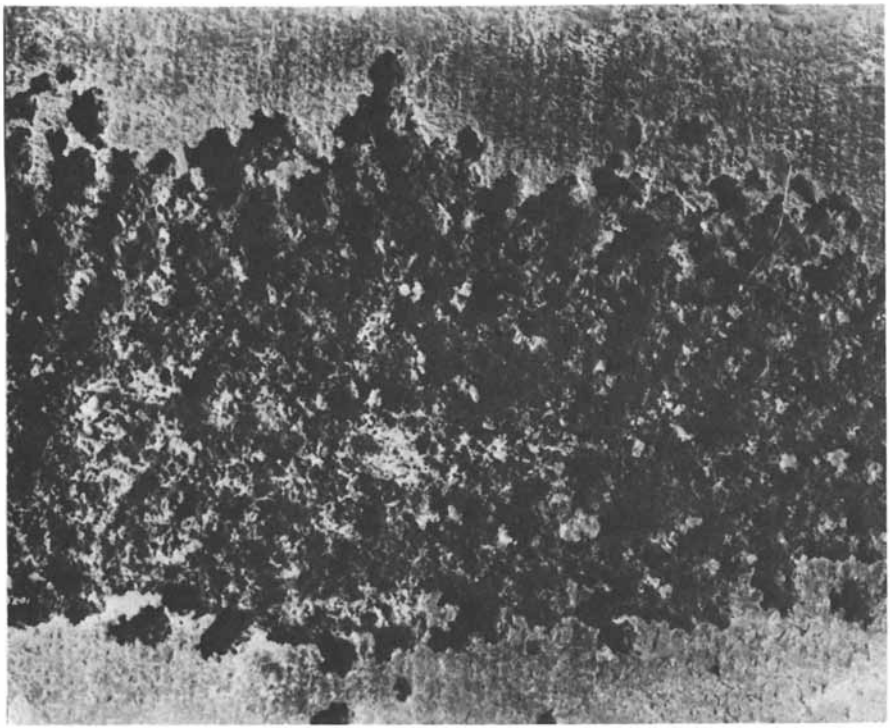

Figure 25. Concentrated zone of loss, absence of corrosion products, and sharply defined boundaries identify cavitation-corrosion attack on cylinder liner

In Corrosion Chemistry; Brubaker, G., et al.;
ACS Symposium Series; American Chemical Society: Washington, DC, 1979.

discussing mechanical/physical factors contributing to cavitation-corrosion of cylinder liners, Speller and LaQue (7) made the following suggestions:
1) Reduce liner vibration by any practicable means; i.e., redesigning liner supports to introduce dampening effects, or providing cushioning.
2) Develop and use harder, more resistant liner metals. (Hard alloy cast iron liners respond better to corrosion inhibition than do soft cast iron liners.)
3) Reduce opportunity for development of vapor cavities by operating at higher pressures and temperatures in cooling systems, and possibly by introduction of air bubbles as cushions against vapor-cavity collapse.
4) Maintain chromate corrosion inhibitors in cooling water at concentrations above 2,000 mg/l (as CrO_4), and hold coolant pH within the range of 8.5-9.5.
5) Include suitable wetting agents to improve contact between corrosion inhibitors and metal surfaces.

Field experience showed that cylinder liners could not be protected against cavitation-corrosion by plating with chromium or harder metals, or by plastic coatings. Both would explode off at the same rate as did the original liner metal. But tests showed that since corrosion factors were involved, as well as mechanical/physical factors, new cylinder liners could be protected against cavitation corrosion by proper concentrations of alkaline chromate inhibitors. Cavitation attack in progress might not be arrested on older liners of engines with severe vibrational problems, even when using chromates. But on newer engines, properly inhibited with chromate from the first day of service, cavitation corrosion could be completely prevented.

One other inhibitor type that will prevent cavitation-corrosion is the soluble oil type, which incorporates a light mineral oil plus emulsifiers and adsorption-type inhibitors, such as organic amines. Unfortunately, although effective in controlling cavitation, (possibly by cushioning effects of the adsorbed oil reinforced film) they soften and damage rubber connectors and seals, cause leakage and water loss. When emulsifiers are exhausted, the oil emulsion breaks, and allows oily films to form on heat transfer surfaces. Some of the amine type emulsifiers and inhibitors are potentially destructive to copper alloys in the circulating system, also. One other type inhibitor that has been used effectively for many years in closed cooling systems is generically identified as "borate-nitrate." These combinations use sodium nitrite, buffered by alkaline borates, and silicates with supplemental inhibitors such as mercaptobenzothiazole, thiazole or benzo-

In Corrosion Chemistry; Brubaker, G., et al.;
ACS Symposium Series; American Chemical Society: Washington, DC, 1979.

triazole to protect copper alloys in the system. The working concentration is about twice as high as that required for chromate inhibitors. Borate-nitrites are not always effective in suppression of cavitation-corrosion in affected systems, but otherwise have given excellent protection of closed cooling systems.

For control of deposits and scale, closed systems require hardness-free (or preferably mineral-free) makeup water. Microbicides are not required for closed systems, but dispersants to keep metal oxides and other insoluble contaminants in suspension are useful. They aid in preserving clean heat transfer surfaces, which provide maximum response to corrosion inhibition. Long chain ethylene oxide polymers also are being used to improve "wetting" properties of cooling water and minimize turbulence, where impingement and cavitation problems are observed.

Literature Cited

1. Langelier, W. F., Journal American Water Works Association, (1936), 28, (No. 10), 1500-1521.
2. Langelier, W. F., Journal American Water Works Association, (1946), 38, (No.2), 169-178 and 179-185.
3. Crum, Ferris B., and Wilkes, John F., U.S. Patent No. 2 783 200, (February 26, 1957).
4. Denman, Wayne L. and Hwa, Chih M., Canadian Patent No. 580 658, (August 4, 1959). Reissued as Canadian Patent No. 717 433, (March 28, 1961).
5. Zimmie, William E. and Bloecher, Frederick W., Jr., U.S. Patent No. 3 080 264, (March 5, 1963).
6. Zimmie, William E. and Bloecher, Frederick W., Jr., U.S. Patent No. 3 085 916, (April 16, 1963).
7. Speller, Frank N. and LaQue, Francis L., Corrosion, (1950), 6, (No. 7), 209-215.

RECEIVED September 1, 1978.

12

High-Temperature Corrosion in Coal Gasification Plants

V. L. HILL, D. YATES, and B. A. HUMPHREYS

IIT Research Institute, 10 West 35 Street, Chicago, IL 60616

Coal represents the greatest domestic reservoir of fossil energy available at the present time. Thus, it is likely in the near term that coal utilization will supply increasingly greater amounts of domestically consumed energy. While greater usage of coal for direct combustion is being projected, gasification of coal is an alternative to dwindling natural gas supplies. Gas produced by gasification can vary from low to high heating value depending on the gasification process employed. Low- and medium-Btu gas could be used for electric power generation, space heating, and industrial applications. High-Btu gas produced by gasification can be used as a replacement for natural gas.

Gasification of coal producing low- to medium-Btu gas is not a new process. However, several new gasification processes designed for greater conversion efficiency are under development. The second and third generation processes generally operate at higher temperatures and pressures than current gasification plants. In addition, the current non-domestic processes are based on use of low-sulfur European coals. Accordingly, the construction materials currently employed in these plants may not be suitable for conversion of high-sulfur eastern coals. The combination of higher plant operating temperatures and pressures and high sulfur concentration may reduce the available materials for plant construction.

Materials problems in newer coal gasification processes accrue generally from operating temperatures of 1500°-2800°F and pressures of 150-1200 psi. Added to these conditions are low oxygen activity and high sulfur activity in the product gas atmosphere. Finally, coal ash and sulfur sorbents present in the system can cause materials failure by corrosion and/or erosion-corrosion. Current metallic alloys that were developed

0-8412-0471-3/79/47-089-391$05.75/0

for high oxygen and low sulfur activity environments are subject to oxidation-corrosion or erosion-corrosion in the gasifier environment.

Background

Prior to 1972, no information existed on the behavior of high-temperature materials in gasification environments. Materials data were available for high-pressure equipment at low operating temperatures, or for low-pressure equipment at high operating temperatures. The emerging coal gasification processes, therefore, represented a new environment for high-temperature materials. Behavior of materials, both metallic and refractory, could not be predicted based on their performance on then-existing equipment.

During 1972 the Metal Properties Council, supported by the American Gas Association, initiated efforts in coal gasification materials research. Since 1975 the major support for the program has been supplied by the Department of Energy in cooperation with AGA. Five phases of effort have been defined,with work in progress. These areas are: Phase I - Laboratory High Temperature Oxidation-Corrosion; Phase II - Pilot Plant Corrosion Studies; Phase III - Quench System Aqueous Corrosion; Phase IV - High Temperature Erosion-Corrosion; and Phase V - Mechanical Property Measurements. The first four phases are being conducted at the IIT Research Institute.

A major potential problem for coal gasification materials due to high-sulfur coals is indicated by Table I. The table compares the melting points of sulfides and eutectic temperatures of the metal-metal sulfide systems for iron, nickel, cobalt, and chromium (1). It may be seen that the metal-metal sulfide eutectic temperatures vary from 1193°F for nickel to 2462°F for chromium. All three elemental bases of high-temperature alloys, iron, nickel, and cobalt, exhibit eutectic temperatures of 1810°F or less. The nickel-nickel sulfide eutectic is 1193°F.

The significance of the eutectic temperatures shown in Table I is that in high-sulfur gases melting of corrosion products of high-temperature alloys can occur within their normal operating range. Molten corrosion products are not developed during air oxidation. Furthermore, nickel-chromium alloys are generally employed in air environments at higher operating temperatures because of their higher strength and oxidation resistance. In sulfur-containing atmospheres these alloys are most susceptible to melting. Iron-base

In Corrosion Chemistry; Brubaker, G., et al.;
ACS Symposium Series; American Chemical Society: Washington, DC, 1979.

alloys would be expected to have the highest melting temperatures, but are generally less oxidation resistant and/or have lower strength. Thus, alloy selection for high-temperature coal gasification service tends to be the inverse of that applicable to high-temperature air oxidation.

Oxidation-corrosion data included in this paper were generated in Phases I and II of the program. Other phases of the IITRI work have been described in current literature (2-9).

Metal loss in this program has generally resulted from the combined effects of oxygen and sulfur. Thus, the term oxidation-corrosion is used in this paper to define metal loss. No attempt is made to separate the individual effects of the corrodent species since chemical analysis of the corrosion products was not conducted.

Results

Phase I - Laboratory High-Temperature Corrosion Testing. The Phase I corrosion program began in 1973 with design and fabrication of two reactors capable of operating to 2000°F at 1000 psi. Testing in a typical coal gasification atmosphere began in 1973. To date, over 40,000 hrs of testing have been completed in the 2 reactors involving 57 commercial and developmental alloys and coatings. Details of the test equipment have been reported elsewhere (2) and will, therefore, not be discussed in this paper.

The gasifier atmosphere used for most Phase I corrosion tests is given in Table II. During testing, only the inlet gas composition shown was controlled. The temperature-pressure dependent equilibrium gas compositions shown represent the actual test gas composition at each test temperature. Generally, the equilibrium gas composition was obtained in the reactor by interaction of the inlet gas species. This was verified by analyses of the reactor exit gas in a gas chromatograph.

The compositions of the alloys evaluated in Phase I are summarized in Table III. These alloys represent most classes of high-temperature iron-, nickel-, and cobalt-base alloys that could be considered for coal gasification service. Pack aluminized and chromized coatings on AISI 310 and IN-800 were also evaluated in the test program.

Corrosion data contained in this paper are not intended to summarize the results for the 57 alloys and coatings exposed for periods of up to 5000 hr. Rather,

In Corrosion Chemistry; Brubaker, G., et al.;
ACS Symposium Series; American Chemical Society: Washington, DC, 1979.

Table I

EUTECTIC TEMPERATURES OF SELECTED METAL-METAL SULFIDE SYSTEMS[a]

Eutectic	MP of Sulfide °C	MP of Sulfide °F	Eutectic Temperature °C	Eutectic Temperature °F	Sulfur Concentration at Eutectic a/o	Sulfur Concentration at Eutectic w/o
Ni-Ni_3S_2	810[b]	1490	645	1193	33.4	21.5
Co-Co_4S_3	932[b]	1710	877	1611	40	26.6
Fe-FeS	1190	2174	988	1810	44	31
Cr-CrS	1565	2849	1350	2462	43.9	32.5

[a]Reference 1.

[b]Formed peritectically.

Table II

INLET AND EQUILIBRIUM GAS COMPOSITION OF PHASE I CORROSION TESTS

Component	Gas Composition, v/o Gasifier Inlet[a]	Equilibrium[a] 900°F	Equilibrium[a] 1500°F	Equilibrium[a] 1800°F
H_2	24	4	23	31
CO	18	5	11	17
CO_2	12	25	19	15
CH_4	5	19	9	3
NH_3	1	1	1	1
H_2S	0-1.0	0-1.0	0-1.0	0-1.0
H_2O	Bal	Bal	Bal	Bal
N_2	-	-	-	-

[a]Inlet gas composition constant for all tests in gasifier gas.

[b]At 1000 psi and indicated temperature.

In Corrosion Chemistry; Brubaker, G., et al.;
ACS Symposium Series; American Chemical Society: Washington, DC, 1979.

Table III

CHEMICAL COMPOSITION OF ALLOYS SELECTED FOR TESTING IN PHASE I

Alloy	Composition, w/o									
	C	Mn	Si	Fe	Ni	Cr	Co	Al	Mo	Other
					Series 1					
302	0.05	0.64	0.55	71.02	9.24	18.18	-	-		
304	0.05	1.45	0.54	70.04	9.10	18.76	-	-		
316	0.05	1.65	0.43	65.23	13.18	17.14	-	-	2.5	
309	0.11	0.54	0.74	60.46	14 70	22.97	-	-		
314	0.06	1.90	2.21	51.64	20.00	24.00	-	-		
310	0.06	1.71	0.63	52.16	20.20	25.00	-	-		
310(Al)										
310(Cr)										
446	0.10	0.45	0.38	74.55	0.37	24.00				
IN-600	0.05	0.15	0.20	6.99	76.48	15.82	0.03	-		
IN-601	0.04	0.24	0.19	15.86	59.52	22.50	0.03	1.19		
IN-800	0.03	0.80	0.33	47.08	30.84	20.60	0.10	0.32		0.42Ti
IN-800(Al)										
IN-800(Cr)										
IN-793	0.03	0.72	0.40	43.22	32.22	21.40	0.02	1.76		
IN-671 (50/50)	0.03	0.03	0.03	0.30	48.40	50.00	0.01	-		0.35Ti
					Series 2					
HC 250	3.03	0.5	0.7	68.1	0.1	27.5	-	-	0.1	
HD 45	0.48	0.7	1.5	62.1	5.2	29.9	-	-	0.1	
HL 40	0.47	0.6	1.4	47.1	19.4	30.9	-	-	0.1	
HL 40-3Si	0.42	0.7	2.4	45.8	19 3	31.4	-	-	0.1	
RA-333	0.05	1.5	1.4	15.5	47.5	26.2	3.0	-	3.8	2.7W
Crutemp 25	0.07	1.5	0.6	47.2	24.8	25.4	-	-	0.4	
Multimet N155	0.11	1.4	0.7	29.1	19.8	21.8	19.5	-	3.0	1.1 Cb+Ta, 3.9W
Haynes 150	0.06	0.5	0.2	16.5	1.7	27.9	49.6	-	0.1	
Haynes 188	0.08	0.7	0.4	1.4	23.3	23.4	35.7	0.22	0.6	.051La, 14.6 W
Stellite 6B	1.0	1.4	0.6	2.0	2.4	28.5	56.4	-	1.1	6.5W
VE 441	0.03	0.1	0.1	81.5	0.01	0.01	-	15.1	3.2	0.04Zr
Nl	0.004	0.2	2.3	0.20	90.0	2.8	-	4.4	0.1	
Armco 21-6-9	0.04	8.2	0.7	62.9	6.8	20.7	-	-	0.22	
					Series 3a					
312	0.15	2.0	0.5	Bal	9	30	-	-	-	
329	0.05	0.5	0.4	Bal	4.3	27.1	-	-	1.4	
AL 29-4-4	0.005	-	-	Bal	4.0	29	-	-	4	
AL EX-20	1.0	20	-	Bal	3	5	-	10	-	
Co-Cr-W No. 1	2.5	-	-	-	-	30	Bal	-	-	12W
Thermalloy 63WC	0.4	-	-	Bal	35	26	15	-	-	5W
Wiscalloy 30/50N	0.55	-	-	Bal	47	27	-	-	-	4W
Armco 18SR	0.05	-	1.0	Bal	-	18.0	-	2.0	-	0.40Ti
Armco 22-13-5	0.06	5.0	-	Bal	12.5	22.0	-	-	2.0	0.20Cb, 0.20V, 0.3N
Hastelloy X	0.15	1.0	1.0	18.5	Bal	21.8	2.5	-	9.0	0.6W
Inconel 625	0.05	0.25	0.25	2.5	Bal	21.5	-	0.2	9.0	0.2Ti, 3.65Cb
Sanicro 32X	0.08	-	-	Bal	31	21	-	0.35	-	0.35Ti, 3W
Incoloy 825	0.03	0.50	0.25	30	41	21.5	-	0.10	3.0	2.25Cu, 0.9Ti

In Corrosion Chemistry; Brubaker, G., et al.;
ACS Symposium Series; American Chemical Society: Washington, DC, 1979.

Table III (cont.)

Alloy	Composition, w/o									
	C	Mn	Si	Fe	Ni	Cr	Co	Al	Mo	Other
					Series 3b					
FSX-414	0.25	1.0	1.0	2.0	10.5	29.5	Bal	-	-	7.0W
HK 40	0.4	2.0	2.0	Bal	20	28	-	-	0.5	
HK 40-3Si	0.35/ 0.45	2.0	3.0	Bal	18/22	24/28	-	-	0.5	
Thermalloy 63	0.4	-	-	Bal	35	26	-	-	-	
Thermalloy 63W	0.40	-	-	Bal	35	26	-	-	-	5W
RA-330	0.05	1.5	1.25	43	35.0	19.0	-	-	-	
IN-657	-	-	-	-	50	48	-	-	-	1.5Cb
IN-738	0.17	0.2	0.3	0.5	Bal	16.0	8.5	3.4	1.75	3.4Ti,0.1Z-, 2.6W,0.9Cb
556	0.1	1.5	0.4	Bal	20	22	20	0.3	3.0	2.5W,0.02La, 1.0Cb+Ta
617	0.07	-	-	-	54	22	12.5	1.0	9	
AL-16-5-Y	0.006	0.2	0.2	Bal	-	15.8	-	5.4	-	0.41Y

In Corrosion Chemistry; Brubaker, G., et al.;
ACS Symposium Series; American Chemical Society: Washington, DC, 1979.

results are presented to indicate significant trends in oxidation-corrosion data produced by variation of high temperature and H_2S concentrations for selected alloys.

Corrosion in Phase I was assessed by metallographic measurements of metal loss due to both scaling and internal corrosion. Gravimetric analysis was employed only to augment scaling loss measurements. Scaling and internal corrosion were combined to obtain a corrosion parameter defined as total corrosion, or sound metal loss. Total corrosion was then extrapolated to metal loss rates in mils/yr (mpy) only as a means of comparing the alloys exposed for various times. As will be seen subsequently, linear extrapolation, intended to be conservative, resulted in serious underestimation of yearly metal loss rates for some alloys. Often kinetically controlled transitions to higher corrosion rates, usually with melting, occurred during longer exposures of 1000-5000 hr at 1800°F.

Both the H_2S concentration over the range of 0-1.0 v/o of the CGA gas and the temperature controlled the measured corrosion rates. Figure 1 illustrates the effect of temperature on corrosion rates of several alloys and coatings in the CGA gas containing 1 v/o H_2S. Alloys AISI 309, AISI 310, and IN-800 demonstrate a clear temperature dependence of total oxidation-corrosion in 1000 hr. The 309 alloy had a scatter band of 5 to 125 mils total metal loss for four specimens at 1650°F. This is typical of borderline alloys that undergo time-dependent transitions to accelerated corrosion rates. Total corrosion of aluminized 310 and 800 was relatively unaffected by temperature over the range of 1500°-1800°F for 1000 hr exposures.

The effect of H_2S concentration on total corrosion of selected alloys in 1000 hr at 1800°F is illustrated in Fig. 2. A variety of different oxidation-corrosion behaviors were observed. Ferritic alloys, like AISI 446, generally showed increased corrosion rate with decreasing H_2S concentration, whereas 300 series austenitics typified by AISI 310 generally exhibited maxima at both 0.1 and 1.0 v/o H_2S. IN-800 had high corrosion only above 0.5 v/o H_2S. Aluminized AISI 310 and IN-800, IN-671, and several high-chromium alloys did not indicate a strong dependence of H_2S concentration in 1000 hr total corrosion. Cobalt-base alloys also generally performed as shown for the aluminized AISI 310 and IN-671 specimen.

Weight change of corrosion-resistant Series 1 alloys during a 5000 hr exposure at 1800°F in the CGA atmosphere containing 0.5 v/o H_2S is shown in Fig. 3. The AISI 446 and 314 stainless steels indicated

In Corrosion Chemistry; Brubaker, G., et al.;
ACS Symposium Series; American Chemical Society: Washington, DC, 1979.

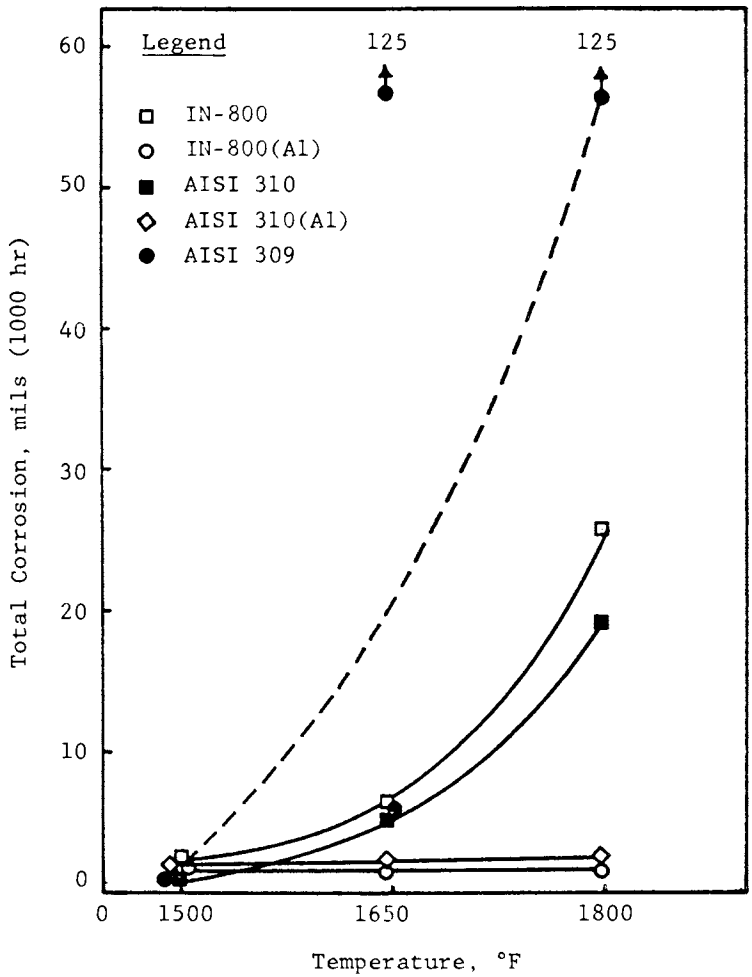

Figure 1. Effect of temperature on 1000-hour total corrosion of selected alloys in CGA environment containing 1 v/o H_2S

In Corrosion Chemistry; Brubaker, G., et al.;
ACS Symposium Series; American Chemical Society: Washington, DC, 1979.

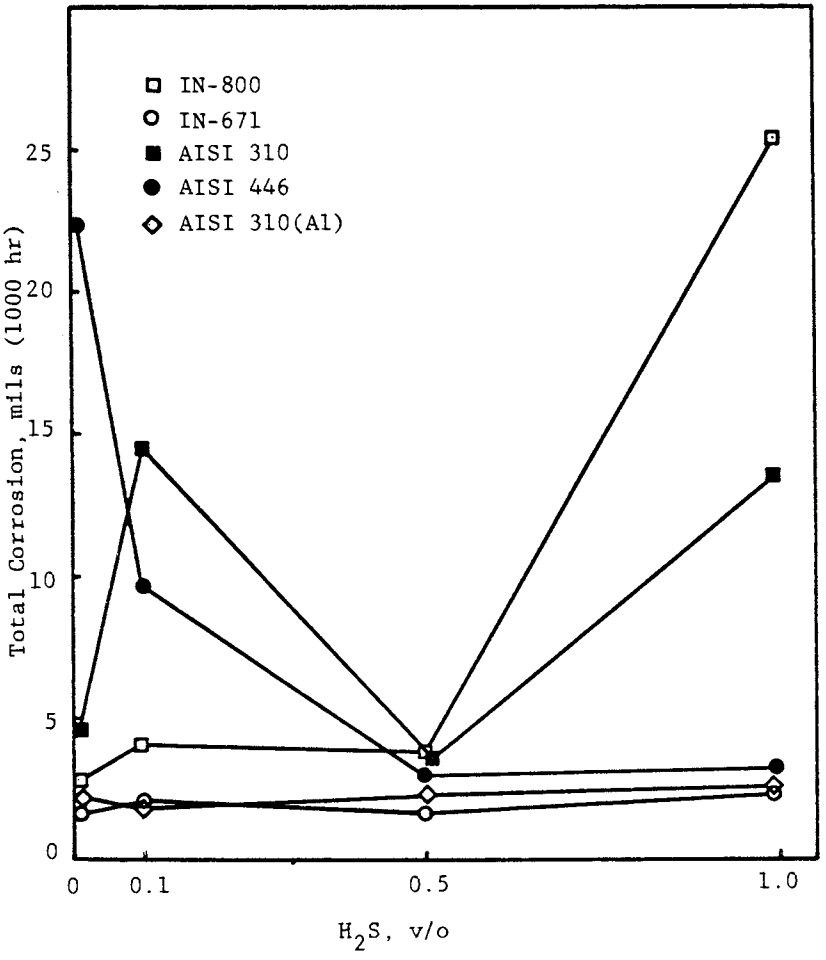

Figure 2. Effect of H_2S concentration on 1000-hour total corrosion of selected alloys in CGA environment at 1800°F

In Corrosion Chemistry; Brubaker, G., et al.;
ACS Symposium Series; American Chemical Society: Washington, DC, 1979.

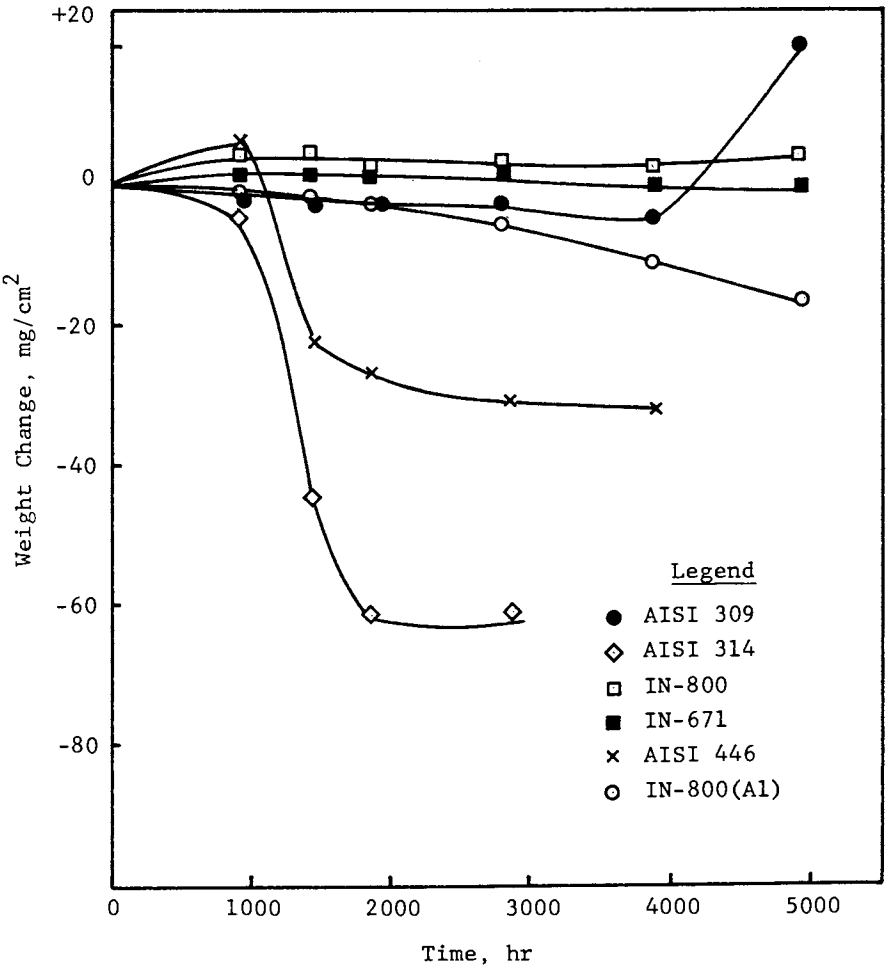

Figure 3. Weight change of selected alloys during 5000-hour exposure at 1800°F in CGA atmosphere containing 0.5 v/o H_2S

In Corrosion Chemistry; Brubaker, G., et al.;
ACS Symposium Series; American Chemical Society: Washington, DC, 1979.

transitions to higher oxidation-corrosion (weight loss) after 1000 hr. Although not shown, similar behavior was observed for AISI 310 stainless steel. AISI 309 demonstrated a transition to weight gain after 4000 hr. Rapid transition in the weight change curves generally was coincident with the development of localized and/or general melting of the corrosion products. These results suggest the errors that could occur if 1000 hr data were extrapolated to yearly oxidation-corrosion rates. To date, testing for 5000 hr has been completed only at 1800°F in the CGA atmosphere containing 0.5 v/o H_2S.

The current results of 5000 hr tests at 1800°F in the CGA gas containing 0.5 v/o H_2S are summarized in Table IV. Here the 1000, 3000, and 5000 hr total corrosion data have been linearly extrapolated to mpy corrosion rates. Several alloys--for example, AISI 309, AISI 310, and AISI 314--that had extrapolated corrosion rates of 20-40 mpy after 1000 hr indicated transitions to higher rates in 1000-2000 hr. As a result, the linearly extrapolated rates at 3000 hr were greater than 80 mpy. Other alloys, such as HK-40 and IN-617, exhibited internal penetration at 1000 hr that did not increase significantly for the longer exposures. For these alloys, corrosion data obtained by linear extrapolation of 1000 hr data was maintained for 3000 and 5000 hr, respectively. The data shown in Table IV illustrate that 1000 hr corrosion data could not be linearly extrapolated to mpy corrosion rates for all alloys. It was necessary to conduct 5000 hr tests to verify the existence of incubation times of 1000-4000 hr for transitions to rapid corrosion.

Microstructures of two alloys exposed in the CGA atmosphere are presented in Figs. 4 and 5. The microstructure of AISI 314 exposed 1000 hr at 1800°F in the CGA gas containing 0 v/o H_2S is shown in Fig. 4. The adherent, layered scale on this alloy consisted of fourteen individual metal-oxide layers. Metal phase visible in the scale was nickel-rich containing some iron, but was free of chromium. Oxide phase was chromium-rich tending towards a chromium-iron spinel at the oxide-metal interface. This unusual microstructure was also observed on AISI 309 and 310 exposed under the same conditions, although fewer layers were present.

In contrast, the microstructure of IN-671 exposed 5000 hr in the CGA at 1800°F is shown in Fig. 5. Here, a thin, dense two-layered scale was observed with minor grain boundary internal corrosion. Total metal loss in 5000 hr was about 2 mils. The IN-671 (50Ni-50Cr) alloy along with aluminized AISI 310 and IN-800 generally

In Corrosion Chemistry; Brubaker, G., et al.;
ACS Symposium Series; American Chemical Society: Washington, DC, 1979.

Table IV

LINEARLY EXTRAPOLATED CORROSION RATES OF PHASE I ALLOYS EXPOSED 1000-5000 HR AT 1800°F IN CGA ENVIRONMENT (0.5 v/o H_2S)

<20 mpy	20-40 mpy	40-80 mpy	>80 mpy
	1000 hr		
IN-671, 310(Al), 800(Al), 188, 6B, T63WC, FSX-414, Alloy X, Co-Cr-W-No. 1, N155, 150, HL40, RA-333, Crutemp 25	309, 310, 446, HK40, IN-800, IN-617	IN-738, 556, 314	
	3000 hr		
310(Al), HL40, IN-617, IN-657, FSX-414, Co-Cr-W No. 1, 150[a]	IN-738	32X, 446	314,[a] 309, 310,[a] 556[a]
	5000 hr		
IN-800, IN-671 800(Al), N155, Alloy X, 188, 6B	HK40, Crutemp 25, T63WC	RA-333	

[a]2000 hr.

In Corrosion Chemistry; Brubaker, G., et al.;
ACS Symposium Series; American Chemical Society: Washington, DC, 1979.

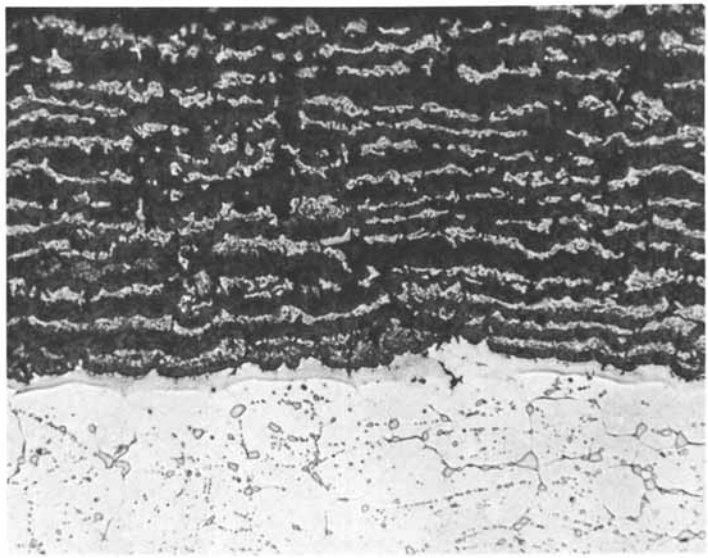

Figure 4. Surface microstructure of AISI 314 after 1000-hour exposure at 1800°F in CGA gas containing 0 v/o H_2S. Neg. No. 42225 (170×).

Figure 5. Surface microstructure of IN-671 after 5000-hour exposure at 1800°F in CGA gas containing 0.5 v/o H_2S. Neg. No. 44911 (170×)

In Corrosion Chemistry; Brubaker, G., et al.;
ACS Symposium Series; American Chemical Society: Washington, DC, 1979.

provided excellent oxidation-corrosion resistance in the CGA atmosphere at all H_2S concentrations.

Work in progress on Phase I will provide further information on the long-term corrosion behavior of commercial alloys in CGA environments. Significantly more 5000 hr data are required at 0.1 and 1.0 v/o H_2S concentrations at 1800°F. Data to 5000 hr are also desirable at 1500° and 1650°F, particularly for Series 2 and 3 alloys.

Phase II - Pilot Plant Testing. This phase of coal gasification materials evaluation involves exposure of metals and refractories in selected test locations in current pilot plants. Corrosion testing in this effort began during 1974 with four pilot plants and now involves six: HYGAS, CONOCO COAL, Synthane, BI-GAS, Steam-Iron, and Battelle.

Materials evaluation in pilot plants covers all phases of the coal gasification process. Test specimens are installed in the coal pretreatment, gasification, gas quench systems, and methanation equipment in the plants. Three exposures, nominally 1, 3, and 6 months, at plant operating conditions are scheduled for each test location. Post-exposure corrosion evaluation employed in Phase II are the same as those used in other phases of the IITRI program, i.e., metallography combined with gravimetric analysis.

A summary of the current status of the pilot plant testing program is presented in Table V. Testing in a total of 35 metal and 6 refractory locations in the HYGAS, CONOCO COAL, Synthane, and BI-GAS plants is in progress. Second and third exposures are in progress in the HYGAS and CONOCO COAL plants. First and second exposures are in progress in the Synthane, BI-GAS, Steam-Iron, and Battelle plants.

Post-exposure analyses have been completed, or are in progress, for 55 metal specimen racks primarily from the HYGAS and CONOCO COAL plants. Analyses of several installations from the first exposure at Synthane are in progress. Currently, 60% of the required racks for the three exposures in all plants have been shipped to the plants and installed.

Corrosion data have been generated for metals in the quench systems and refractories in the gasifier. However, specific oxidation-corrosion data in this paper will be limited to metals exposed in the high-temperature gas phase locations of the HYGAS and CONOCO COAL plants. Again, the results reported will emphasize trends indicated by the pilot plant exposures.

In Corrosion Chemistry; Brubaker, G., et al.;
ACS Symposium Series; American Chemical Society: Washington, DC, 1979.

Table V

CURRENT STATUS OF PHASE II PILOT PLANT TESTING PROGRAM

Plant	Total Locations		Specimen Racks						
			Total			Installed		Analyzed	
	Metals	Refr.	Required	Shipped	Exposure	Metals	Refr.	Metals	Refr
HYGAS	12	1	46	31	2,3	31	3	16	2
CONOCO COAL	4	2	58	58	1,3	28	30	23	25
Synthane	12	2	60	45	1,2	31	9	12	3
BI-GAS	7	1	43	12	1	11	1	4[a]	0
Steam-Iron[b]	12	2	42	8	1	8	--	--	--
Battelle[b]	6	2	24	4	1	2	--	--	--
Total	53	10	273	158		111	43	55	30

[a]Start-up racks.

[b]Added to test program December, 1976.

In Corrosion Chemistry; Brubaker, G., et al.;
ACS Symposium Series; American Chemical Society: Washington, DC, 1979.

A typical rack employed for installation of specimens in pilot plants is shown in Fig. 6. Both corrosion coupons, 2 x 1 x 0.35 in. thick, and bend specimens intended to determine stress-corrosion cracking susceptibility, are included in the installation for aqueous corrosion testing. Specimens are separated by high density alumina spacers to eliminate electrochemical effects. During exposure, the racks are welded to existing components in the pilot plant equipment.

High-temperature gas phase oxidation-corrosion data have been obtained for two exposures in the CONOCO COAL plant and one exposure in the HYGAS plant. Table VI summarizes the operating environments and in-plant times for these exposures. Since the pilot plants operate at variable temperatures, pressures, and gas compositions, weighted average values are given for the plant exposures.

Linearly extrapolated oxidation-corrosion data for the 1150 hr first exposure in the HYGAS gasifier off-gas are plotted in Fig. 7. In this location at 580°F (average) carbon steel, AISI 410, AISI 304, IN-800, and titanium exhibited very limited corrosion. Alloy IN-600 and Monel 400 had corrosion rates of 42 and 124 mpy, respectively.

Test exposure oxidation-corrosion data for selected alloys in the fluidized bed of the HYGAS gasifier are shown in Fig. 8. Alloys exposed in this location are different from those in the gasifier off-gas because of the higher operating temperature. The fluidized bed represents the highest operating temperature of the four test locations in the HYGAS gasifier. First-exposure data, however, indicate relatively minor corrosion of AISI 430, AISI 309, IN-600, Alloy X, and RA-333 of 4 to 18 mpy. Again, IN-600 showed extensive attack (complete corrosion of 0.250 in. thick specimens) in 1720 hr of plant operation during the first exposure. Thus, IN-600 (Ni-16Cr) exhibited severe corrosion over the entire operating temperature range of the HYGAS gasifier. Although not shown in Fig. 8, IN-601 (Ni-23Cr-1Al) had a corrosion rate of 12 mpy in the HYGAS fluidized bed.

Two exposures have been completed in both the CONOCO COAL gasifier and regenerator. Linearly extrapolated corrosion rates for selected alloys exposed in these CONOCO COAL test locations are presented in Figs. 9 and 10. The duration of exposure in these test locations was about 800 and 1600 hr in the first and second exposures, respectively.

Figure 9 shows that the corrosion rates in the CONOCO COAL gasifier were relatively low for both exposures. The apparent reduction in corrosion rate for

In Corrosion Chemistry; Brubaker, G., et al.;
ACS Symposium Series; American Chemical Society: Washington, DC, 1979.

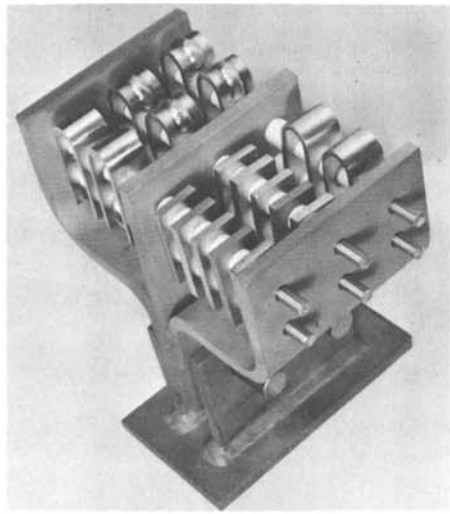

Figure 6. Typical corrosion specimen rack for Phase II pilot plant exposures

In Corrosion Chemistry; Brubaker, G., et al.;
ACS Symposium Series; American Chemical Society: Washington, DC, 1979.

Table VI

CORROSION CONDITIONS IN CONOCO COAL AND HYGAS PLANT EXPOSURES

Location	Exposure	Temp., °F	Press., psi	Time, hr
	CONOCO COAL Plant			
Gasifier, off-gas[a]	1	1425	150	800
	2	1425	150	1600
Regenerator[b]	1	1850	150	800
	2	1850	150	1600
	HYGAS Plant			
Gasifier, fluidized bed[c]	1	1340	980	1718
Gasifier, off-gas[d]	1	580	980	1150

[a]Gas composition: $48H_2$, $23H_2O$, $12CH_4$, $8.5CO$, $6CO_2$, $2.5N_2$, trace H_2S (v/o)

[b]Gas composition: $70N_2$, $25CO_2$, $5CO$, trace H_2S (v/o)

[c]Not analyzed.

[d]Gas composition: $20.4H_2$, $40.6H_2O$, $9.3CO_2$, $2.5CO$, $5.2CH_4$, $4.2N_2$, $0.1H_2S$, 17.7 oils (v/o)

In Corrosion Chemistry; Brubaker, G., et al.;
ACS Symposium Series; American Chemical Society: Washington, DC, 1979.

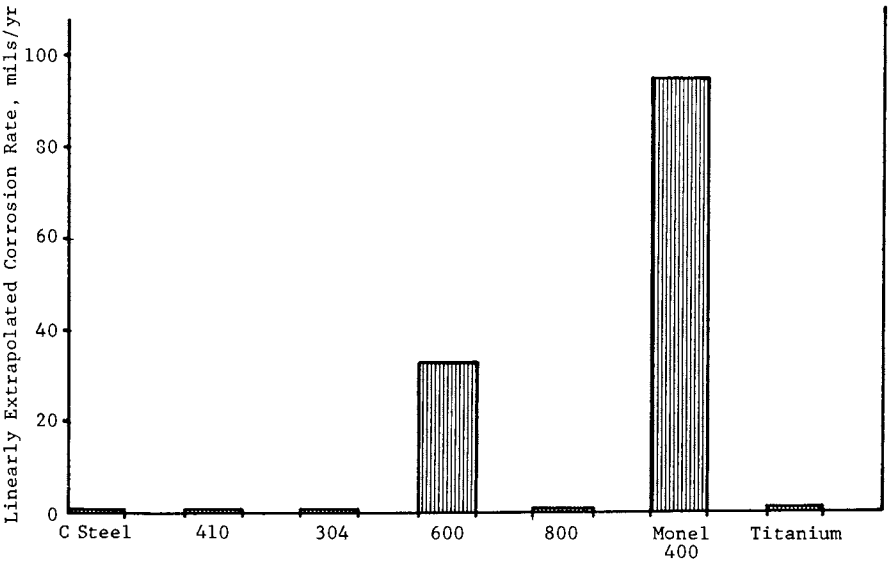

Figure 7. Linearly extrapolated corrosion rates of selected alloys in HYGAS gasifier, off-gas

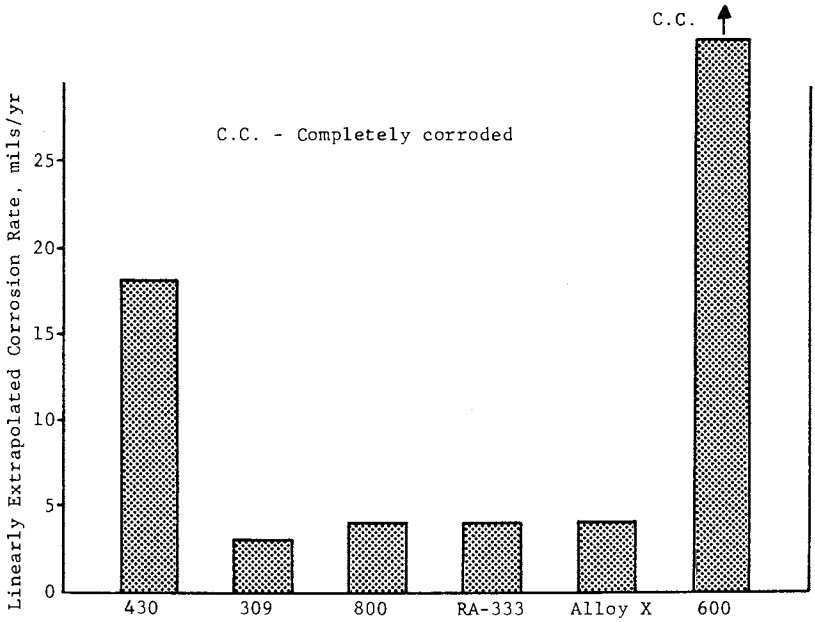

Figure 8. Linearly extrapolated corrosion rates of selected alloys in HYGAS gasifier, heat exchanger bed

In Corrosion Chemistry; Brubaker, G., et al.;
ACS Symposium Series; American Chemical Society: Washington, DC, 1979.

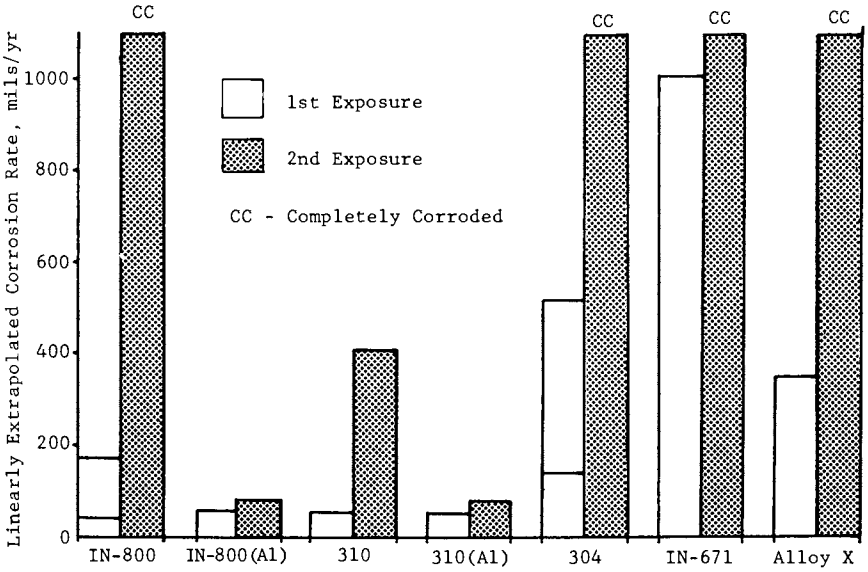

Figure 9. Linearly extrapolated corrosion rates of selected alloys in CONOCO COAL regenerator, off-gas

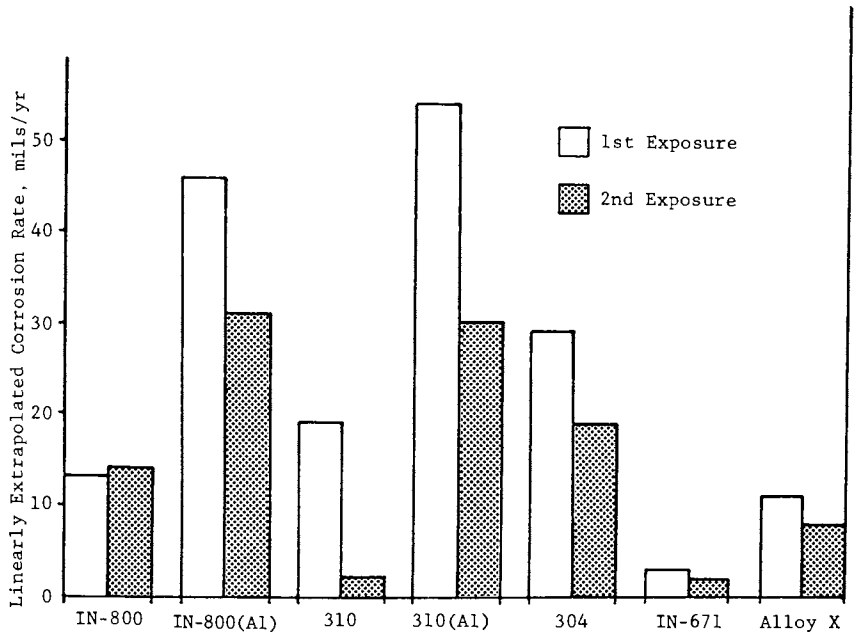

Figure 10. Linearly extrapolated corrosion rates of selected alloys in CONOCO COAL gasifier, off-gas

In Corrosion Chemistry; Brubaker, G., et al.;
ACS Symposium Series; American Chemical Society: Washington, DC, 1979.

the longer second exposure for most alloys was due to linear extrapolation of metallographically determined total corrosion. Apparently, the time dependence of total corrosion for most alloys tended to be parabolic rather than linear.

For both exposures in the gasifier, corrosion of pack diffusion aluminized AISI 310 and IN-800 was greater than the uncoated base alloys. Metallographically, the aluminized coatings appeared to be preferentially attacked; corrosion of the coated layers terminated at the base metal interface during both exposures. The coatings on IN-800 tended to be completely converted to scale, whereas those on AISI 310 were locally penetrated along short circuit diffusion paths.

Corrosion data for the CONOCO COAL regenerator in Fig. 10 indicate significantly higher corrosion during the longer second exposure. Several alloys including IN-800, IN-671, Alloy X, and AISI 309 stainless steel were completely corroded during the second exposure. IN-671 also completely corroded during the first exposure. In contrast to the gasifier, pack aluminized AISI 310 and IN-800 demonstrated the best corrosion resistance in the second exposure in the regenerator. Thus, aluminizing provided variable protection in the CONOCO COAL plant.

To date, very limited corrosion has been observed for dense refractories exposed in both the HYGAS and CONOCO COAL plants. Castables, brick, and ramming mix materials have resisted the CGA environments with limited attack. This was expected since the exposure temperatures of 1500°-1800°F are relatively low for refractory materials. Phosphate bonded materials, originally thought to be suspect for CGA service, have shown no significant deterioration. Some deterioration of low-density insulating materials has been observed. These materials, however, are not normally exposed to the CGA environment in pilot plant gasifiers. For this reason, testing of insulating materials has been terminated.

Severe corrosion of silicon nitride bonded silicon carbide brick did occur during the second exposure in the CONOCO COAL gasifier and during first exposure in the Synthane gasifier. Dense brick of this material nearly completely disintegrated in about 1600 hr at 1400°-1500°F. In contrast, the material survived both exposures at 1800°-1900°F in the regenerator without deterioration. These results are thought to be due to attack by water vapor in the gasifier.

Future corrosion data obtained from the Synthane, BI-GAS, Steam-Iron, and Battelle pilot plants will add

In Corrosion Chemistry; Brubaker, G., et al.;
ACS Symposium Series; American Chemical Society: Washington, DC, 1979.

significantly to the existing pilot plant information. Environmental conditions in these plants differ significantly from those of the HYGAS and CONOCO COAL plants. Accordingly, the new pilot plant information will provide oxidation-corrosion data for a wider range of gas compositions and operating temperatures.

Summary of Results

Since the effort described herein is an ongoing program, well-defined conclusions are, as yet, inappropriate. Some trends, however, are readily evident in oxidation-corrosion obtained to date in coal gasification atmosphere. It is clear that coal gasification environments are much more severe than air at the same temperatures. Furthermore, a chromium content of 20 weight percent, and preferably 25 weight percent, in high-temperature alloys is required for long-term resistance to CGA environments. The role of secondary additions, aluminum, titanium, silicon, molybdenum, tungsten, etc., and residuals such as manganese, has not been clearly established.

Oxidation-corrosion data obtained from the pilot plants generally compare well with laboratory data in ranking of high-temperature alloys. Pilot plant results, however, indicate more severe corrosion than laboratory oxidation-corrosion data. This should be expected because of cyclic operation of pilot plants and additional variables comprising the pilot plant environments. The contribution of erosion and erosion-corrosion by coal ash, char, and sulfur sorbents to the corrosion process in the pilot plants has not been defined.

Laboratory oxidation-corrosion data indicate that extrapolation of short-term oxidation-corrosion data to yearly rates is difficult. These extrapolations are necessary to provide a basis for comparing oxidation-corrosion data obtained from variable CGA exposure times. Extrapolated data, particularly at high H_2S concentrations in the CGA atmosphere, should be employed with caution. Long-term kinetics of the oxidation-corrosion process can result in transitions in corrosion behavior to high rates not predictable by short exposures. Similar behavior, breakaway oxidation, occurs in air primarily at temperatures above 2000°F.

Acknowledgments

The author would like to express his appreciation to A. O. Schaefer of the Metal Properties Council,

W. R. Hulsizer of the International Nickel Company, and H. E. Frankel, W. T. Bakker, and S. J. Dapkunas of the Department of Energy for their helpful suggestions. IITRI personnel who contributed significantly to this program include M. A. H. Howes, S. Bhattacharyya, C. Hales, and Y. Harada.

Literature Cited

1. Hansen, M., and Anderko, K., "Constitution of Binary Alloys," 2nd ed., McGraw-Hill Book Co., New York, 1958.
2. Howes, M. A. H., and Schaefer, A. O., "Selection of Materials Used in Coal Gasification Plants," American Gas Association, Sixth Synthetic Pipeline Gas Symposium, Chicago, Illinois, October 1975.
3. Parikh, N. M., Howes, M. A. H., Bangs, E. R., and Schaefer, A. O., "Materials in Coal Gasification Processes," Paper No. 173, NACE, Corrosion/75, April 1975.
4. Samans, C. H., and Hulsizer, W. R., "Current Progress in Materials Selection for Coal Conversion," ASME, Mexico City, September 24, 1976.
5. Hulsizer, W. R., "Developing a Data Base," American Gas Association, Eighth Synthetic Pipeline Gas Symposium, Chicago, Illinois, October 1976.
6. Hill, V. L., and Howes, M. A. H., "Metallic Corrosion in Coal Gasification Pilot Plants," Paper No. 50, NACE, Corrosion/77, March 1977.
7. Bhattacharyya, S., Bock, F. C., MacNab, A., and Cox, T. B., "Alloy Selection for Coal Gasification Quench Systems," Paper No. 51, NACE, Corrosion/77, March 1977.
8. Hill, V. L., "Corrosion and Erosion-Corrosion of Materials in Coal Gasification Environments," American Gas Association, Ninth Synthetic Pipeline Gas Symposium, Chicago, Illinois, October 1977.
9. Bhattacharyya, S., Hill, V. L., Humphreys, B. A., and Hamel, F. B., "Aqueous Corrosion in Coal Gasification Pilot Plants," American Gas Association, Ninth Synthetic Pipe Gas Symposium, Chicago, Illinois, October 1977.

RECEIVED September 1, 1978.

INDEX

In Corrosion Chemistry; Brubaker, G., et al.;
ACS Symposium Series; American Chemical Society: Washington, DC, 1979.

In Corrosion Chemistry; Brubaker, G., et al.;
ACS Symposium Series; American Chemical Society: Washington, DC, 1979.

In Corrosion Chemistry; Brubaker, G., et al.;
ACS Symposium Series; American Chemical Society: Washington, DC, 1979.

D

E

In Corrosion Chemistry; Brubaker, G., et al.;
ACS Symposium Series; American Chemical Society: Washington, DC, 1979.

F

In Corrosion Chemistry; Brubaker, G., et al.;
ACS Symposium Series; American Chemical Society: Washington, DC, 1979.

G

H

I

In Corrosion Chemistry; Brubaker, G., et al.;
ACS Symposium Series; American Chemical Society: Washington, DC, 1979.

In Corrosion Chemistry; Brubaker, G., et al.;
ACS Symposium Series; American Chemical Society: Washington, DC, 1979.

N

O

P

In Corrosion Chemistry; Brubaker, G., et al.;
ACS Symposium Series; American Chemical Society: Washington, DC, 1979.

Q

R

In Corrosion Chemistry; Brubaker, G., et al.;
ACS Symposium Series; American Chemical Society: Washington, DC, 1979.

S

In Corrosion Chemistry; Brubaker, G., et al.;
ACS Symposium Series; American Chemical Society: Washington, DC, 1979.

In Corrosion Chemistry; Brubaker, G., et al.;
ACS Symposium Series; American Chemical Society: Washington, DC, 1979.